

AD-A256 467

①



PHOTOLUMINESCENCE STUDY OF $Si_{1-x}Ge_x/Si$
 AND Si/Ge STRAINED LAYER SUPERLATTICES

DISSERTATION

Todd D. Steiner, Captain, USAF

AFIT/DS/ENP/92-002

DTIC
 ELECTE
 OCT 27 1992
 S E D

DEPARTMENT OF THE AIR FORCE
 AIR UNIVERSITY
AIR FORCE INSTITUTE OF TECHNOLOGY

Wright-Patterson Air Force Base, Ohio

DISTRIBUTION STATEMENT A
 Approved for public release
 Distribution Unlimited

1

AFIT/DS/ENP/92-002

PHOTOLUMINESCENCE STUDY OF $\text{Si}_{1-x}\text{Ge}_x/\text{Si}$
AND Si/Ge STRAINED LAYER SUPERLATTICES

DISSERTATION

Todd D. Steiner, Captain, USAF

AFIT/DS/ENP/92-002

Approved for public release; distribution unlimited

92-28249



AFIT/DS/ENP/92-002

PHOTOLUMINESCENCE STUDY OF $Si_{1-x}Ge/Si$ AND Si/Ge
STRAINED LAYER SUPERLATTICES

Todd D. Steiner, B.S., M.S.
Captain, USAF

Approved:	
Reviewed:	X
Checked:	
Dist:	
A-1	

Approved:

Robert L Hempstead 13 July '92
Jung Kee Lee 13 July '92
Patrick M. Henninger 13 July '92
John Jones Jr 13 July '92

Accepted:

DTIC QUALITY INSPECTED 3

Dean, School of Engineering

PHOTOLUMINESCENCE STUDY OF $\text{Si}_{1-x}\text{Ge}_x/\text{Si}$ AND Si/Ge
STRAINED LAYER SUPERLATTICES

DISSERTATION

Presented to the Faculty of the School of Engineering
of the Air Force Institute of Technology

Air University

In Partial Fulfillment of the
Requirements for the Degree of
Doctor of Philosophy

Todd D. Steiner, B.S., M.S.

Captain, USAF

July 1992

Approved for public release; distribution unlimited

PREFACE

The purpose of this dissertation was to characterize the photoluminescence from Si/Ge and $\text{Si}_{1-x}\text{Ge}_x/\text{Si}$ superlattices, with the goal of determining the conditions for maximum luminescence for subsequent incorporation into efficient light emitting devices.

This project could not have been undertaken without a reliable source of samples. I wish to thank Dr. David Godbey and Dr. Phil Thompson of the Naval Research Lab for providing the samples as well as helpful discussions and words of encouragement. Thanks also go to Lt. Col. Gernot Pomrenke for suggesting the general area of research, and for the insight to provide AFOSR funds for both AFIT and NRL. He also deserves credit for arranging the AFIT/NRL collaboration as well as the Special DOD Interest group on Silicon-Germanium.

I also wish to thank my advisory committee, Dr. Robert Hengehold and Dr. Yung Kee Yeo; Dave Elsaesser for annealing runs; the technical staff, especially Greg Smith, for invaluable support; and Dr. Tom Kennedy and Dr. Evan Glaser for helpful discussions of PL data. Finally, special thanks to my wife, Kimbree, and children, Westley and Madison, for their patience while I worked three years worth of sixteen hour days.

Todd D. Steiner

Table of Contents

	Page
Preface.....	iii
List of Figures.....	vii
List of Tables.....	xi
List of Symbols.....	xii
Abstract.....	xvi
I. Introduction.....	1
II. Background.....	4
Properties of Silicon, Germanium and $\text{Si}_{1-x}\text{Ge}_x$ alloys.....	4
Crystal Structure.....	4
Band Structure and Optical Properties.....	5
Comparison to III-V Semiconductors.....	7
Superlattices.....	8
Bandstructure.....	10
Applications.....	14
Growth.....	15
Si-Ge Growth Considerations.....	16
Silicon Molecular Beam Epitaxy.....	16
Critical Thickness.....	20
Doping.....	24
In-situ Characterization.....	25
Ex-situ Characterization.....	26
$\text{Si}_{1-x}\text{Ge}_x/\text{Si}$ and Si/Ge Superlattice Bandstructure.....	28
Band Offsets.....	28
Band Gap of Strained $\text{Si}_{1-x}\text{Ge}_x$	29
Theoretical Calculations.....	32
Requirements for Direct Band Gap Si/Ge SL.....	35
Kronig-Penney Model.....	37
Device Applications.....	39
Monolithic Optoelectronics.....	39
Heterojunction Bipolar Transistor.....	40
Modulation Doped Field Effect Transistor.....	42

Bipolar Inversion Channel FETs.....	44
Infrared Detectors.....	46
Quantum Well Infrared Detectors.....	47
Light Emitting Devices.....	47
Stability of Si _{1-x} Ge _x /Si and Si/Ge SLs.....	49
Photoluminescence.....	51
General Considerations.....	51
PL from Bulk and Epitaxial Silicon.....	52
Near-band-edge PL from Si.....	66
PL from Bulk Si _{1-x} Ge _x	67
PL from Si _{1-x} Ge _x /Si and Si/Ge Superlattices.....	68
Isoelectronic Bound Exciton Emission from Si and Si _{1-x} Ge _x	73
III. Experimental.....	75
Sample Growth.....	75
Post-Growth Annealing.....	75
Photoluminescence Experimental Setup.....	77
Photoluminescence Experimental Procedures.....	78
System Alignment and Calibration.....	78
Sample Preparation and Mounting.....	80
System Startup Procedures.....	80
PL Measurement Procedures.....	81
Choice of Laser Excitation.....	81
IV. Results and Discussions.....	82
Dependence of PL on Excitation.....	82
Near-Band-Edge PL.....	96
Temperature Dependence of Sharp Peaks.....	100
Experimental Determination of SL Band Gap.....	108
Effects of Alloy Fluctuations.....	109
Calculations of Band Gap in Si _{1-x} Ge _x /Si SLs Using a Kronig-Penney Model	112
40/20, x = 0.25 Samples	114
120/40, x = 0.25 Samples.....	117
140/70, x = 0.12-0.36 Samples.....	117
120/40, x = 0.36 Samples.....	122
80/40, x = 0.35 Sample	122
Annealing Studies.....	125
Annealing Effects on Sharp BE Lines.....	125
Dislocation Lines Brought Out by High Temperature RTA.....	131

Broad Band PL.....	132
Peak Positions.....	132
Model for Broad Band PL Mechanism.....	134
Annealing Effects on Broad Band PL	137
Temperature Dependence of Broad PL Band	143
Annealing Effects on Broad PL Band Activation	
Energies	143
Shifts of Broad PL Band with Sample Temperature	161
Shifts of Broad PL Band with Annealing Temperature..	166
Photoluminescence from Monolayer Si/Ge Superlattices.....	167
PL from Deep Centers.....	170
Sample Characterization vs. position in wafer.....	173
Peak shifts due to changes in SL band gap.....	173
Changes in peak intensity.....	175
New PL peaks.....	175
Changes due to growth temperature variations.....	179
V. Summary.....	181
Sharp Near-Band-Edge Bound Exciton Lines	181
Broad PL Band	181
Annealing Studies.....	183
Recommendations for Future Study.....	185
References.....	186
Vita.....	210

LIST OF FIGURES

1. Crystal Structure of Silicon and Germanium4

2. Band Structure of Silicon and Germanium5

3. Band Gap of Unstrained Bulk $\text{Si}_{1-x}\text{Ge}_x$ Alloys vs Alloy
Concentration6

4. Superlattice Band Offsets10

5. Superlattice Energy Bands as a Function of Well Width....12

6. Superlattice Minizones and Minibands.....13

7. Bandgap vs Lattice Constant for Important Semiconductor
Systems.....17

8. Schematic of Si-MBE System.....18

9. Critical Thickness of $\text{Si}_{1-x}\text{Ge}_x$ grown on Si vs. Alloy
Concentration22

10. Si/Ge Band Alignment29

11. Valence Band Offsets for $\text{Si}_{1-x}\text{Ge}_x/\text{Si}$ on $\text{Si}_{1-y}\text{Ge}_y$30

12. Band Gap of $\text{Si}_{1-x}\text{Ge}_x$ for Different Strain Conditions.....31

13. Zone-folding in a 10 Monolayer Period Superlattice.....33

14. Si_4Ge_4 Band Structure Calculation.....34

15. Requirements for Buffer Layer Composition in Direct Band
Gap Si/Ge Superlattices.....35

16. Si-Ge Heterojunction Bipolar Transistor.....40

17. Modulation Doping in Si-Ge.....43

18. Si-Ge Modulation-Doped FET.....44

19. Si-Ge BICFET.....45

20. $\text{Si}_{1-x}\text{Ge}_x/\text{Si}$ Superlattice Waveguide Avalanche
Photodetector.....46

21.	Si _{1-x} Ge _x Phonon Energies vs Alloy Concentration.....	67
22.	Photoluminescence Experimental Setup.....	77
23.	Response of System to 1000 °C Blackbody.....	79
24.	Comparison of Front vs Back PL, SL00405.1.....	84
25.	Dependence of PL on Excitation Wavelength - SL00201.1...	86
26.	Dependence of PL on Excitation Wavelength - SL00206.1...	88
27.	Dependence of PL on Excitation Wavelength - SL00405.1...	89
28.	Dependence of PL on Excitation Wavelength - SL10322.2...	91
29.	Dependence of PL on Excitation Wavelength - SL10206.1...	92
30.	Dependence of PL on Excitation Wavelength - SL00326.1...	93
31.	Dependence of PL on Excitation Wavelength - SL10531.2...	95
32.	PL from Sample # SL00201.1 at 1.6K.....	98
33.	Sharp Line Spectra for SL00201.1, SL00206.1, and SL1032.2	99
34.	Temperature Dependence of PL - SL00201.1.....	101
35.	Temperature Dependence of PL - SL00206.1.....	102
36.	Temperature Dependence of PL - SL10322.2.....	103
37.	Ln I vs 1/T - SL00201.1 BE(NP)	105
38.	Ln I vs 1/T - SL00206.1 BE(NP)	106
39.	Ln I vs 1/T - SL10322.2 BE(NP)	107
40.	Kronig-Penney Calculation - Si/Si _{0.75} Ge _{0.25} (40/20) SL Band Gap vs Si _{0.75} Ge _{0.25} Layer Thickness.....	115
41.	Kronig-Penney Calculation - Si/Si _{1-x} Ge _x (40/20) SL Band Gap vs x	116
42.	Kronig-Penney Calculation - Si/Si _{0.75} Ge _{0.25} (120/40) SL Band Gap vs Si _{0.75} Ge _{0.25} Layer Thickness.....	118
43.	Kronig-Penney Calculation - Si/Si _{0.75} Ge _{0.25} (120/40) SL	

Band Gap vs x	119
44. Kronig-Penney Calculation - Si/Si _{1-x} Ge _x (140/70) SL	
Band Gap vs Si _{1-x} Ge _x Layer Thickness for x=0.12,0.24, 0.30, and 0.36	120
45. Kronig-Penney Calculation - Si/Si _{1-x} Ge _x (140/70) SL	
Band Gap vs x	121
46. Kronig-Penney Calculation - Si/Si _{0.64} Ge _{0.36} (120/40) SL	
Band Gap vs Si _{0.64} Ge _{0.36} Layer Thickness	123
47. Kronig-Penney Calculation - Si/Si _{0.65} Ge _{0.35} (80/40) SL	
Band Gap vs Si _{0.65} Ge _{0.35} Layer Thickness	124
48. Annealing Study of SL00201.1.....	126
49. Annealing Study of SL00206.1.....	127
50. Annealing Study of SL10322.2.....	128
51. PL from SL10416.1 vs Anneal Temperature.....	130
52. Broad Peak Energy vs Alloy Concentration.....	133
53. Model for Broad Band Emission.....	135
54. Dependence of PL on Annealing Temperature - SL00405.1..	138
55. Dependence of PL on Annealing Temperature - SL10301.1..	139
56. Dependence of PL on Annealing Temperature - SL11105.1..	140
57. Dependence of PL on Annealing Temperature - SL10322.2..	141
58. Temperature Dependence of Broad Band PL - SL10206.1....	144
59. Temperature Dependence of Broad Band PL - SL00206.1....	145
60. Temperature Dependence of Broad Band PL - SL10322.2....	146
61. Temperature Dependence of Broad Band PL - SL00405.1....	147
62. Temperature Dependence of Broad Band PL - SL10531.1....	148
63. Temperature Dependence of Broad Band PL - SL10531.2....	149
64. Temperature Dependence of Broad Band PL - SL11105.1....	150

65.	Ln I vs 1/T, Broad Band PL - SL10206.1.....	151
66.	Ln I vs 1/T, Broad Band PL - SL00206.1.....	152
67.	Ln I vs 1/T, Broad Band PL - SL10322.2.....	153
68.	Ln I vs 1/T, Broad Band PL - SL00405.1.....	154
69.	Ln I vs 1/T, Broad Band PL - SL10531.1.....	155
70.	Ln I vs 1/T, Broad Band PL - SL10531.2.....	156
71.	Ln I vs 1/T, Broad Band PL - SL11105.1.....	157
72.	Hole Binding Energy vs Position in Si _{1-x} Ge _x layer	160
73.	Local Band Gap Fluctuations	163
74.	Dependence of PL on Annealing Temperature - SL11112.1..	168
75.	PL, SL00201.1 for portion containing "G" line at 969 meV.....	171
76.	PL - SL00201.1 vs sample position in wafer.....	174
77.	PL vs sample position in wafer - SL10531.1.....	176
78.	PL vs sample position in wafer - SL10322.2.....	177
79.	PL - SL00201.1.....	178

LIST OF TABLES

I.	Properties of Si and Ge and selected III-Vs.....	8
II.	PL lines in bulk and epitaxial silicon.....	55
III.	Sample Structures	76
IV.	Sharp line energies and phonon energies.....	97
V.	Sharp line energies and derived SL band gap.....	104
VI.	Linewidths and shifts of BE lines.....	110
VII.	Summary of Kronig-Penney parameters and results.....	113
VIII.	Broad PL Band vs. Anneal Temperature	142
IX.	Broad Band Activation Energy vs. Anneal Temperature ...	158
X.	Hole Binding Energy vs. well position	161
XI.	Shifts of Broad PL Band with Sample Temperature	162

List of Symbols

Γ	=	Brillouin zone center
a	=	lattice constant
a_0	=	Bohr radius
a_0^*	=	effective Bohr radius
Al	=	aluminum
Ar	=	argon
As	=	arsenic
B	=	boron
BE	=	Bound exciton
BICFET	=	Bipolar Inversion Channel Field Effect Transistor
BMEC	=	Bound multi-exciton complexes
CB	=	Conduction Band
CVD	=	Chemical Vapor Deposition
E_b	=	binding energy of bound exciton
E_c	=	conduction band minimum
E_{ex}	=	free exciton binding energy
E_g	=	energy gap, bandgap
EL	=	electroluminescence
E_v	=	valence band maximum
eV	=	Electron Volt
FE	=	Free exciton
FZ	=	Float zone
GaAs	=	Gallium Arsenide
Ge	=	Germanium
GSMBE	=	Gas Source Molecular Beam Epitaxy

h = Planck's constant
 HEMT = High Electron Mobility Transistor
 HBT = Heterojunction Bipolar Transistor
 hh = heavy hole
 HH = Heavy Hole (Band)
 HHMT = High Hole Mobility Transistor
 IBE = Isoelectronic Bound Exciton
 In = Indium
 k = Boltzmann's Constant
 K = degrees Kelvin
 Kr = Krypton
 L = Symmetry point defined as the center of hexagonal faces
 on the first Brillouin Zone of FCC structure
 LA = Longitudinal Acoustic
 LED = Light-Emitting Diode
 lh = light hole
 LH = Light Hole (Band)
 LN₂ = Liquid Nitrogen
 LO = Longitudinal Optical phonon
 LPE = Liquid Phase epitaxy
 m_e^* = effective mass of electron
 m_{hh}^* = effective mass of heavy hole
 m_{lh}^* = effective mass of light hole
 m_0 = mass of electron
 MBE = Molecular Beam Epitaxy
 meV = millielectron volts
 MOCVD = Metal Organic Chemical Vapor Deposition

MODFET = Modulation Doped Field Effect Transistor
 ML = Monolayer (The silicon unit cell contains four ML.)
 NP = No phonon (line)
 P = Phosphorus
 PL = Photoluminescence
 PLE = Photoluminescence Excitation (Spectroscopy)
 R_0^* = effective Rydberg
 RBS = Rutherford Backscattering Spectroscopy
 RHEED = Reflected High Energy Electron Diffraction
 RTA = Rapid Thermal Annealing
 RTCVD = Rapid Thermal Chemical Vapor Deposition
 SEM = Scanning Electron Microscopy
 Sb = Antimony
 Si = Silicon
 Si-Ge = refers to the general class including Si/Ge SLs,
 $Si_{1-x}Ge_x$ strained and bulk alloys, and $Si_{1-x}Ge_x/Si$ SL
 Si/Ge = Silicon-germanium superlattice alternating pure Ge with
 pure Si
 $Si_{1-x}Ge_x$ = A silicon-germanium alloy where x is the fraction of
 Ge
 $Si_{1-x}Ge_x/Si$ = A superlattice alternating Si layers with silicon-
 germanium alloy layers
 SL = Superlattice
 SLS = Strained-layer superlattice
 T = Temperature, usually in degrees Kelvin (K)
 TA = Transverse Acoustic
 TEM = Transmission Electron Microscopy

TO = Transverse Optical phonon
UHV = Ultra-High Vacuum
UV = ultraviolet
VB = Valence Band
VPE = Vapor Phase Epitaxy
x = germanium fraction in $\text{Si}_{1-x}\text{Ge}_x$ alloy
X = Symmetry point defined as the center of square faces on
the first Brillouin Zone boundary for the FCC structure
y = germanium fraction in $\text{Si}_{1-y}\text{Ge}_y$ alloy
buffer layer

ABSTRACT

In recent years, there has been interest in obtaining efficient photoluminescence (PL) and electroluminescence from $\text{Si}_{1-x}\text{Ge}_x/\text{Si}$ or Si/Ge superlattices. In this dissertation, long-period $\text{Si}_{1-x}\text{Ge}_x/\text{Si}$ superlattices grown by molecular beam epitaxy at 500 °C and annealed post-growth using rapid thermal annealing were investigated using photoluminescence (PL). The as-grown samples have broad PL bands from isoelectronic centers related to Ge complexes as well as sharp near-edge bound exciton lines. The broad PL band was found to be 120 meV below the band gap, after accounting for the effects of confinement of holes. Post-growth annealing resulted in a reduction in the broad PL band activation energies and a shift of the broad band to higher energies. The reduction in the activation energies of the broad band were found to be due to the position of the emission centers within the $\text{Si}_{1-x}\text{Ge}_x$ layers. The emission centers in the middle of the $\text{Si}_{1-x}\text{Ge}_x$ were deactivated at higher temperatures than those at the edges, which caused the shift of the broad band to lower energies as the sample temperature increased. The shifts of the broad PL band as the annealing temperature increased were found to be due to a net shift of the emission centers towards the interfaces. The effective local band gap at the interfaces was higher than the average in the $\text{Si}_{1-x}\text{Ge}_x$ layers, thus resulting in the shift of the broad PL band to higher energies for the annealed samples.

PHOTOLUMINESCENCE STUDY OF $\text{Si}_{1-x}\text{Ge}_x/\text{Si}$ AND Si/Ge
STRAINED LAYER SUPERLATTICES

I. Introduction

Silicon-germanium (Si-Ge) heterostructures, which includes $\text{Si}_{1-x}\text{Ge}_x$ strained layers, $\text{Si}_{1-x}\text{Ge}_x/\text{Si}$ superlattices, and monolayer Si/Ge superlattices, have become a major area of research since 1985. The reason for this interest falls into two general categories. First, Si-Ge heterostructures offer the possibility of enhancing the performance of silicon electronic devices to levels previously only achieved in the more exotic III-V semiconductors at costs typical of silicon devices. Second, Si-Ge offers possibilities for optoelectronic devices that could not have been imagined in bulk silicon, because of its indirect band gap. In the first category are the Heterojunction Bipolar Transistor (HBT), the High Electron Mobility Transistor (HEMT), and the High Hole Mobility Transistor (HHMT). Each of these has been implemented using Si-Ge technology, and their performance continues to be enhanced at commercial laboratories throughout the world. In the second category are the devices that have more risk involved, and as a result, have taken more time to develop. This includes emitting and detecting devices that operate in the

range from 1.3 to 1.8 microns. While the risk involved in developing these devices is higher, so is the potential payoff. The band gap of Si-Ge heterostructures is ideal for silicon based photonics, and since most work is done on silicon substrates, there is the potential for monolithic photonics and optoelectronics. Clearly, photonics and optoelectronics at costs comparable to present silicon electronics would be a major technological breakthrough.

In this dissertation, the optical properties of $\text{Si}_{1-x}\text{Ge}_x/\text{Si}$ and Si/Ge superlattices were examined using photoluminescence (PL). The emphasis was first on characterizing the different luminescence bands, then on maximizing the bands that have potential for electroluminescence. The PL characterization was done as a function of temperature, excitation power, and excitation wavelength for a variety of sample structures. The broad band luminescence with potential for electroluminescence was further examined and characterized by repeating the above experiments on samples annealed under different conditions.

This dissertation is organized as follows: Chapter I is an introduction; Chapter II gives background on previous research relevant to Si-Ge heterostructures and superlattices. Chapter III gives a description of the experimental setup used to make the PL measurements as well as a description of the sample growth procedures and parameters. Chapter IV describes the experimental

results and discussion thereof, and includes some theoretical calculations and modelling in the context of interpreting the data. Chapter V is the summary of the important results, and recommendations for future research.

II. BACKGROUND

Properties of Silicon, Germanium, and Bulk $Si_{1-x}Ge_x$ alloys

Crystal structure Both silicon and germanium crystallize in the diamond form, which

consists of two interpenetrating FCC lattices, as shown in Figure 1. A $Si_{1-x}Ge_x$ alloy consists of silicon and germanium atoms randomly dispersed on the diamond lattice. The lattice constant for silicon, a_{Si} , is 0.5431 nm and is 0.5657 nm for germanium, a_{Ge} . The lattice constant for

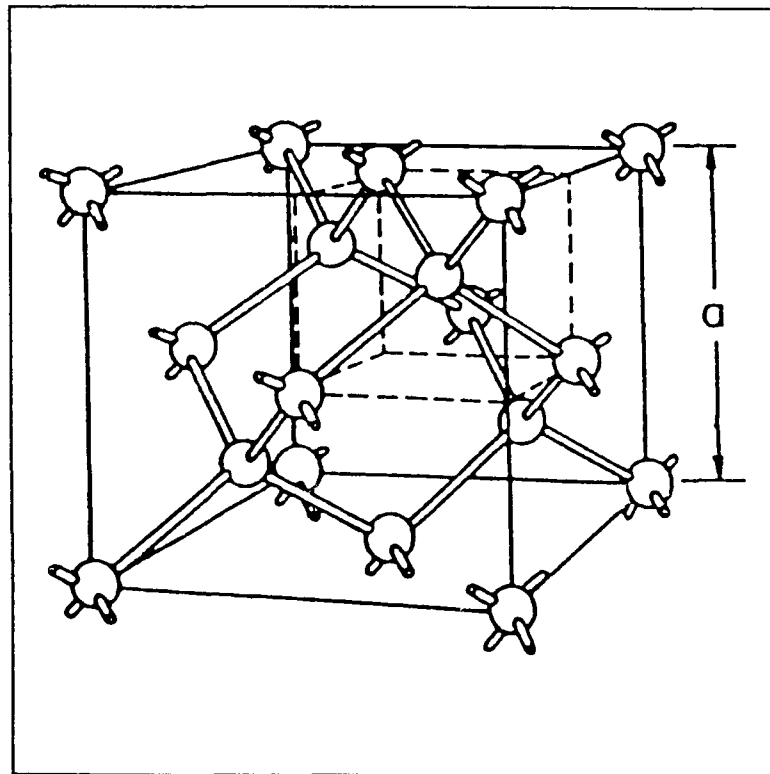


Figure 1: Crystal Structure of Silicon and Germanium (Sze 1981).

bulk $Si_{1-x}Ge_x$ has been found to obey Vegard's Law (Dismukes 1964, Aharoni 1978)

$$a_{SiGe} = a_{Si} + (a_{Ge} - a_{Si})x = a(x), \quad (1)$$

where x is the germanium fraction.

Bandstructure and Optical Properties Examination of the

bandstructures of silicon and germanium give clues to their optical and electrical properties; in fact most of the important information is contained in the electronic band structure in one form or another. Silicon and germanium are both indirect band gap semiconductors. As shown in Figure 2, the conduction band minimum in silicon is 4/5 of the distance from the zone center Γ to the X symmetry point, while for germanium the conduction band minimum is at the L symmetry point. The conduction band minimum in silicon is six-fold degenerate while the conduction band minimum in germanium is four-fold degenerate. Both silicon and germanium have heavy hole and light hole valence bands that are degenerate at the zone center

center, and a split-off hole band below the valence band maximum. The degeneracies of the conduction and valence band greatly affect the electrical properties of silicon and germanium. The degenerate bands result in lower mobilities for both electrons and holes.

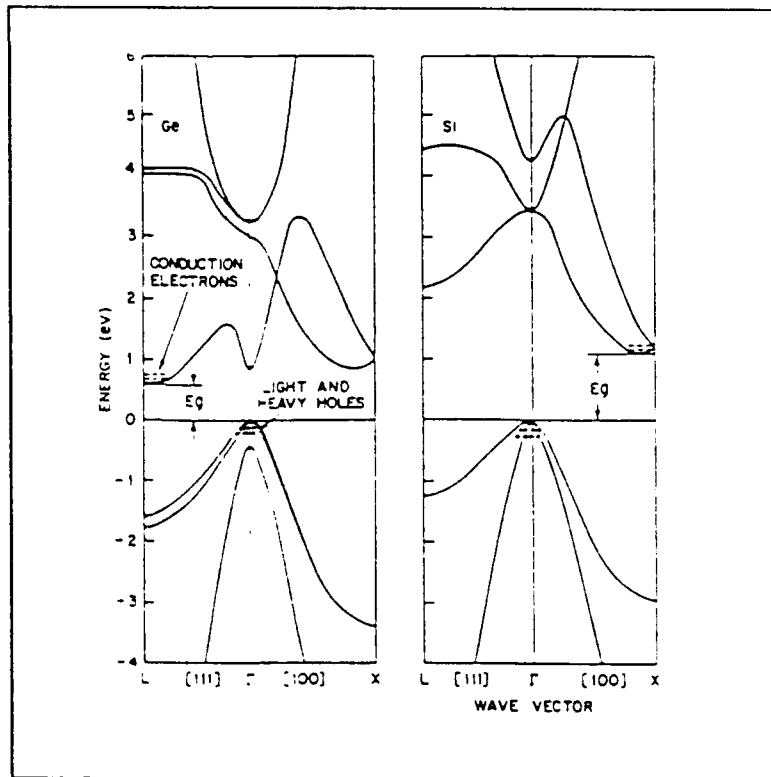


Figure 2: Band structure of silicon and germanium (Sze 1981)

The optical properties of bulk unstrained $\text{Si}_{1-x}\text{Ge}_x$ alloys have been extensively studied beginning in the 1950s (Johnson, 1954; Levitas, 1954; Braunstein, 1958). This early work found that the bandstructure depended greatly on ordering of the silicon and germanium atoms within the unit cell. For random unstrained alloys, the bandstructure has been determined to be an average of the silicon

and germanium bandstructures (Stroud and Ehrenreich 1970). For random alloys the bandstructure is silicon-like for $x < 0.85$ (with the conduction band minima at the Δ symmetry points which are between the Γ and X points (approximately 0.8 times the distance from Γ to X)). For $x >$

0.85 the bandstructure is germanium-like (with the conduction band minima at the L symmetry points). The resulting energy gap dependence as a function of alloy composition is shown in Figure 3. An analytical expression for the bandgap of bulk unstrained

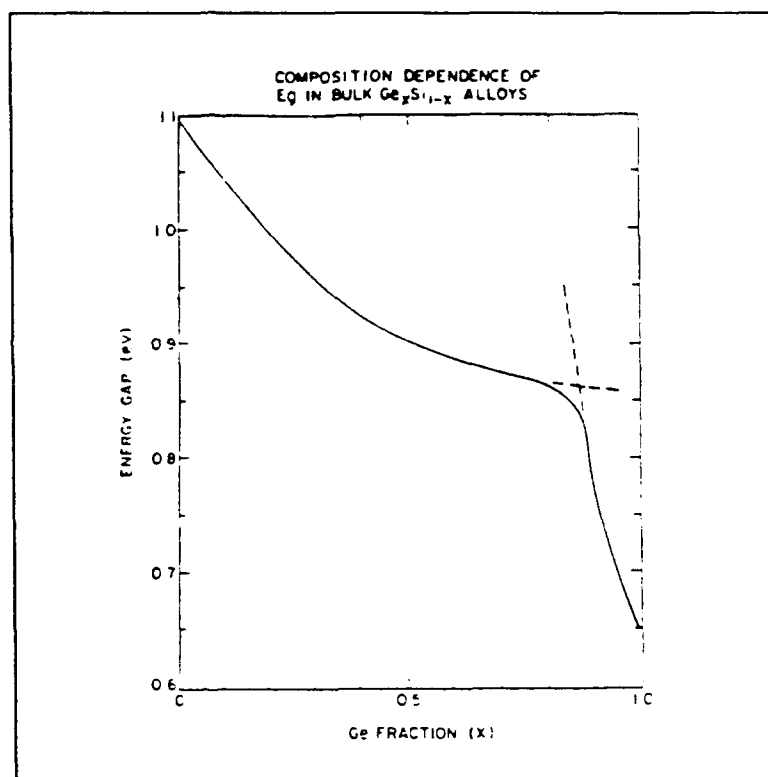


Figure 3: Bulk $\text{Si}_{1-x}\text{Ge}_x$ bandgap vs. alloy concentration (Bean 1988)

$\text{Si}_{1-x}\text{Ge}_x$ at room temperature over the full range of alloy concentration, x , has been found to be (Weber and Alonso 1989)

$$E_g = 1.155 - 0.43x + 0.206x^2 \text{ eV.} \quad (2)$$

Comparison to III-IV semiconductors. Silicon has dominated the semiconductor electronics market since the 1950s, even with its relatively poor electronic properties. Also, silicon, as well as germanium, and bulk silicon-germanium alloys are indirect semiconductors making efficient light emission impossible from bulk materials. The carrier mobilities are not spectacular compared to some of the III-V semiconductors (See Table I). Silicon has mechanical properties, though, that make it attractive and have contributed to its technological importance. It has a high value of Young's modulus and a tensile strength three times that of steel (Bean 1988). It also has a high thermal conductivity which has significance in device applications and aids growth with low defect concentrations. Most importantly, silicon possesses an inert oxide that is easily grown. These properties make silicon based semiconductor technologies attractive especially if the electronic properties can be enhanced by introducing $\text{Si}_{1-x}\text{Ge}_x/\text{Si}$ heterostructures and superlattices.

Table I: Properties of Si, Ge, and selected III-V's

(at room temperature)

	Si	Ge	GaAs	InP	GaSb	InAs	GaP
direct/indirect	i	i	d	d	d	d	i
lattice constant	5.431	5.646	5.653	5.869	6.096	6.058	5.451
E_g , 0 K (eV)	1.17	0.744	1.52	1.42	0.81	0.43	2.32
E_g , 300 K (eV)	1.12	0.66	1.43	1.27	0.68	0.36	2.25
Effective mass, electron, m_e/m	0.98 ^l	1.64 ^l	0.066	0.073	0.047	0.026	0.82
Effective mass, heavy hole, m_{hh}/m	0.49	0.28	0.5	0.4	0.3	0.41	0.60
Effective mass, light hole, m_{lh}/m	0.16	0.16	0.082	0.078	0.06	0.025	
Hole mobil. V-cm ² /s	430	1800	300	100	1000	450	75
Electron mobility	1350	3600	8000	4500	5000	30000	110
Exciton Binding Energy (eV)	14.7	4.15	4.2				

^l longitudinal ^t transverse

(Values from Kittel 1986; Sze 1981)

Superlattices

A superlattice is a periodic array of two or more materials that often has properties different from either of the bulk

constituents. While a superlattice can be composed of any materials, we are most concerned with semiconductor superlattices first proposed by Esaki and Tsu in 1969, in which the constituent semiconductors are alternated in a one-dimensional periodic structure where the period is less than the electron mean free path (Esaki and Tsu, 1969; Esaki and Tsu, 1970). Early studies of superlattices focused on the transport properties in the growth direction. Later, absorption, photoluminescence, magnetoabsorption, 2-D transport properties in the growth plane, and other studies led to discovery of the significant developments that have made superlattices one of the hottest research areas in physics over the last decade.

The periodic alternation of semiconductors in a compositional superlattice results in one-dimensional spatial variation of the conduction and valence band offsets, as shown in Figure 4. The periodic variation of the conduction and valence bands creates the superlattice potential which is responsible for most of the interesting properties of superlattices. The band alignment is determined by the difference between the constituent material energy gaps and the valence (or conduction) band offset, a fundamental property of the heterojunction, which can be estimated theoretically or measured using x-ray photoemission spectroscopy or other techniques.

It is also possible to fabricate doping superlattices, where

the superlattice potential is created from a periodic variation of the doping; n- and p-type layers in either a single or in different semiconductors are alternated on scales similar to compositional superlattices. (Dohler 1972a&b) While doping superlattices have many interesting properties, including some that cannot be duplicated in compositional superlattices, space and time limits their discussion here. Doping superlattices in Si-Ge or in Si have not been fabricated, although they have been studied theoretically. (Gallup 1990, Lee 1990)

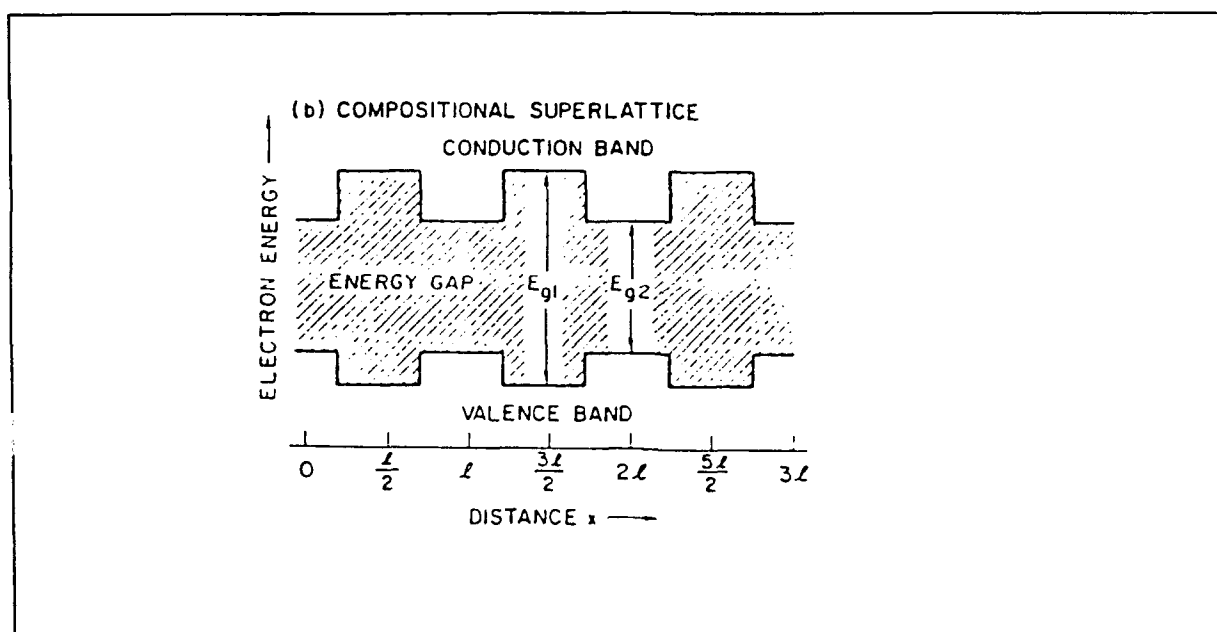


Figure 4: Superlattice Band Offsets (Esaki 1985b)

Bandstructure The electronic structure of a superlattice contains or predicts most of its interesting properties, so its determination is of fundamental importance. The starting point for most bandstructure calculations is the assumption that the

bulk properties of the individual layers are retained. The simplest model uses the effective mass approximation and writes the electronic wave function as a plane wave, just as in the Kronig-Penney problem. The Kronig-Penney model has been used extensively to analyze experimental data. It is accurate as long as the thicknesses of the alternating SL layers are greater than 20 angstroms and the lowest conduction band states and highest valence band states are nondegenerate. The Kronig-Penney model in its simplest form is a one band model and cannot describe interaction between bands, such as between light and heavy hole bands, but it does give an accurate determination of the superlattice band gap. More complicated theoretical bandstructure calculations take into account the interaction between the various bands, such as between light hole and heavy hole bands, which are important for states that are far in energy from the band edge.

The result of a Kronig-Penney or other effective mass calculation is a series of conduction and valence minibands, with the energies, bandwidths, and number of minibands dependent on the superlattice parameters - conduction and valence band offsets, layer thicknesses, and hole and electron effective masses. As the layer thickness decreases, the minibands are pushed to higher energies as shown in Figure 5, corresponding to an increase in the superlattice bandgap. In addition, the bandwidths increase as the well widths decrease. The bandwidths

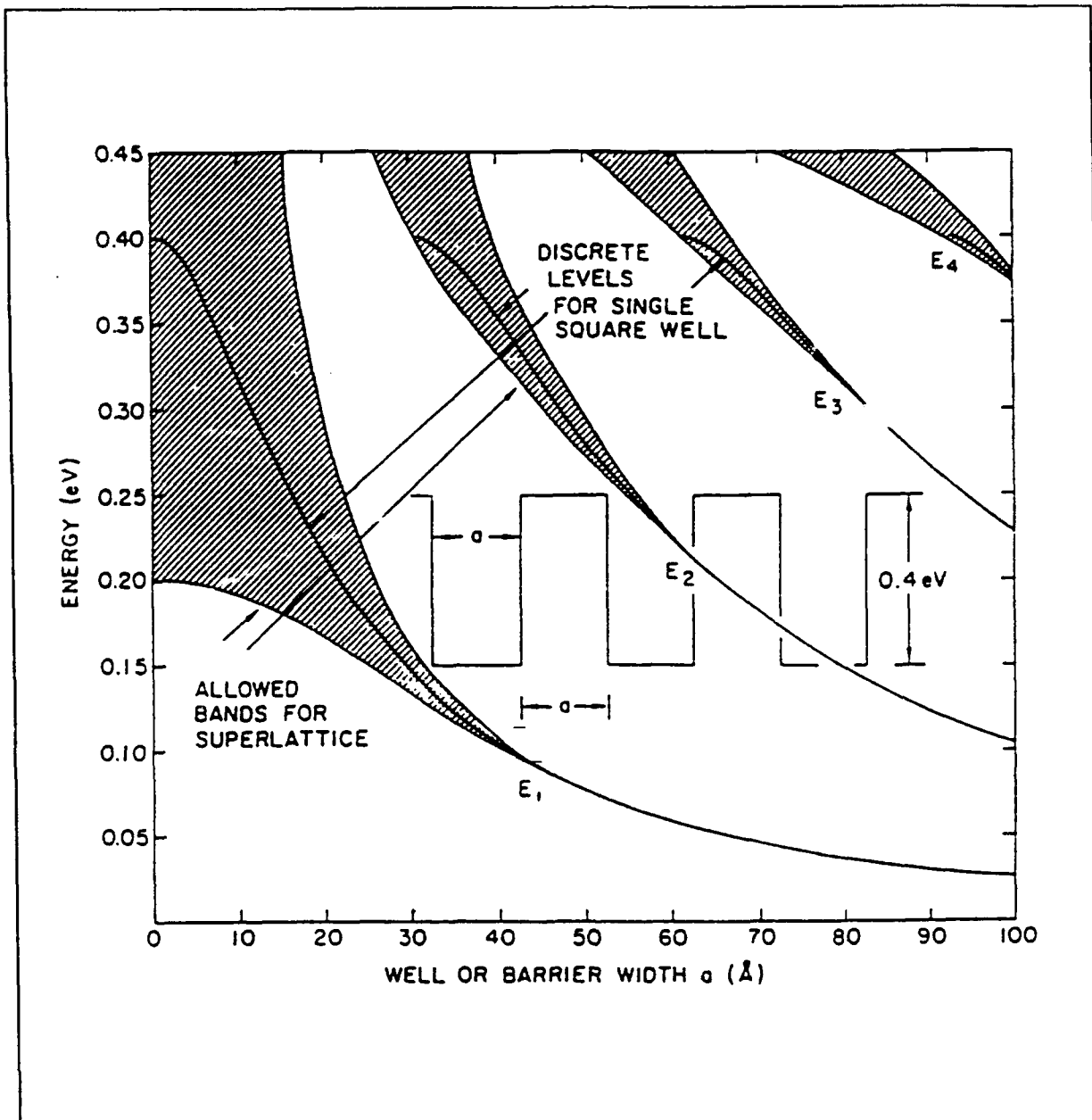


Figure 5: Superlattice energy bands as a function of well width. The bandwidth of SL bands increase as the well width decreases due to wavefunction overlap from adjacent well. (Esaki 1985b)

are due to overlap of wavefunctions from adjacent wells; where there is no overlap, as is the case for a single quantum well or for superlattices that have thick barriers, the bandwidths are small or nonexistent.

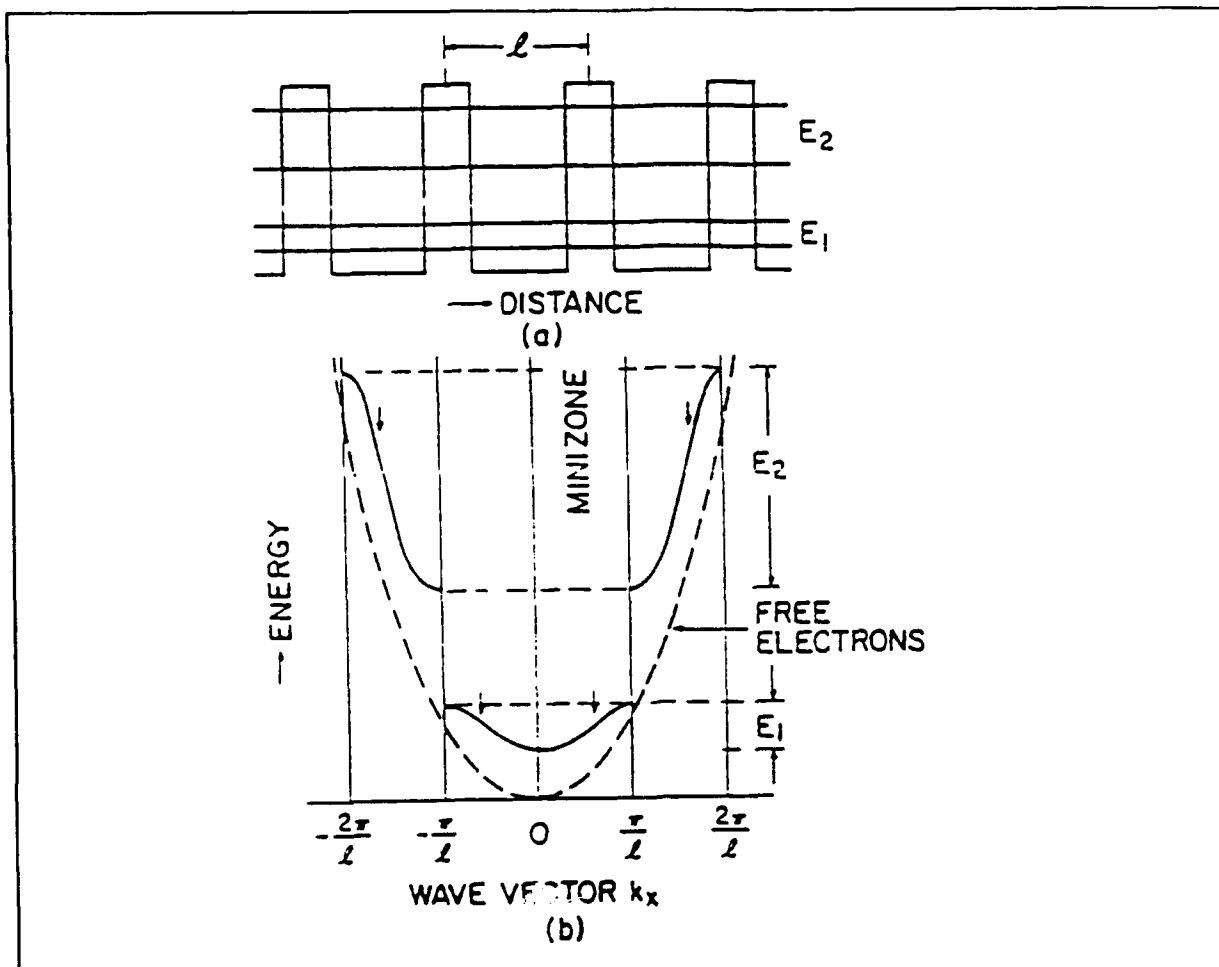


Figure 6: Superlattice minizones and minibands. (Esaki 1985b)

The superlattice potential can be thought of as a perturbation of the bulk bandstructure. The superlattice period is generally larger than the bulk lattice constant that determines the periodicity of the bulk crystal and thus its Brillouin zone boundaries. The superlattice periodicity causes the bulk Brillouin zone to be divided into minizones, the number of minizones equal to the ratio of the superlattice period to the bulk lattice constant. These minizones perturb the bulk bandstructure, creating minibands and minigaps as shown in Figure 6, analogous to the perturbations to free electron energy bands

in the nearly free electron approximation. These minibands are the same as those determined from a Kronig-Penney type model.

Applications Superlattices expand the available choices of semiconductors for device applications from a few to a nearly infinite array, because of the ability to tailor the band structure by varying the SL layer thicknesses, SL period, and the bandgap of the constituent materials if they are alloys. An additional degree of tailorability occurs when there is a lattice mismatch between the constituent layers. In this case, the amount of strain in each of the layers can be varied by the choice of substrate, and this variable strain causes shifts and splittings of the various conduction and valence bands. This degree of tailorability for each material system, when multiplied by the available choices for superlattice systems, gives the infinite array of material choices for nearly every energy and wavelength range from UV (380 nm) to far infrared (50 μm). This is especially useful in the areas of optical detectors and emitters. Varying amounts of quantum confinement by varying the superlattice structure can be used to change the band gap of the superlattice, thereby allowing each material system to have a range of accessible band gaps. Thus a device designer can pick the superlattice structure based on the energy range of device operation. For example GaAs/AlGaAs quantum well/superlattice lasers can be fabricated to emit anywhere from 700 to 850 nm.

Superlattices and quantum wells are extremely efficient optical emitters with quantum efficiencies near unity, (Weisbuch 1987) so high that the luminescence from SL and quantum wells is typically intrinsic rather than extrinsic or defect related that dominates typical bulk semiconductors. Intrinsic luminescence persists to higher temperature than extrinsic luminescence, which is of importance to devices that need to operate at room temperature (most practical devices). The high quantum efficiency, together with band gap tailorability, make quantum well and superlattice LED's and lasers one of the most important device applications of superlattices.

Another important class of device applications uses modulation doping to increase carrier mobilities, and hence the device speed. In modulation doping the barrier materials are doped, creating excess carriers in the well materials. (Gossard 1985) Since carriers are spatially removed from the impurity centers, impurity scattering, one of the major limitations on carrier mobility, is significantly reduced, resulting in high mobility devices. Both high hole mobility and high electron mobility devices have been made, primarily in the GaAs/AlGaAs system.

Growth Superlattices are now grown using a variety of techniques, including Molecular Beam Epitaxy (MBE), Liquid Phase Epitaxy (LPE), and Chemical Vapor Deposition (CVD). The MBE

technique has been found to be the most suitable technique for the growth of most semiconductor superlattices, because of its characteristic slow growth rate, low temperature deposition, and high degree of control of composition, doping, and layer thicknesses. (L.L. Chang, 1985) These characteristics provide high quality films with thin layers and abrupt, smooth interfaces required for good superlattices.

Si-Ge Growth Considerations

In order to bring the world of heterostructures and superlattices to silicon, another semiconductor is required that is chemically and crystallographically compatible. In addition, the other semiconductor must be lattice matched. The only semiconductor that meets these requirements is germanium (or a silicon-germanium alloy). As can be seen from Figure 7, there is a four percent lattice mismatch between pure Si and Ge, but the system does have a wide range of possible bandgaps, covering the technologically important 1.3 to 1.55 micron wavelength region.

Silicon Molecular Beam Epitaxy Molecular Beam Epitaxy (MBE) is the technique of choice for growth of $\text{Si}_{1-x}\text{Ge}_x/\text{Si}$ and Si/Ge superlattices, especially those used in research. As these structures become more well understood and the emphasis becomes the production of commercial devices, lower cost, higher

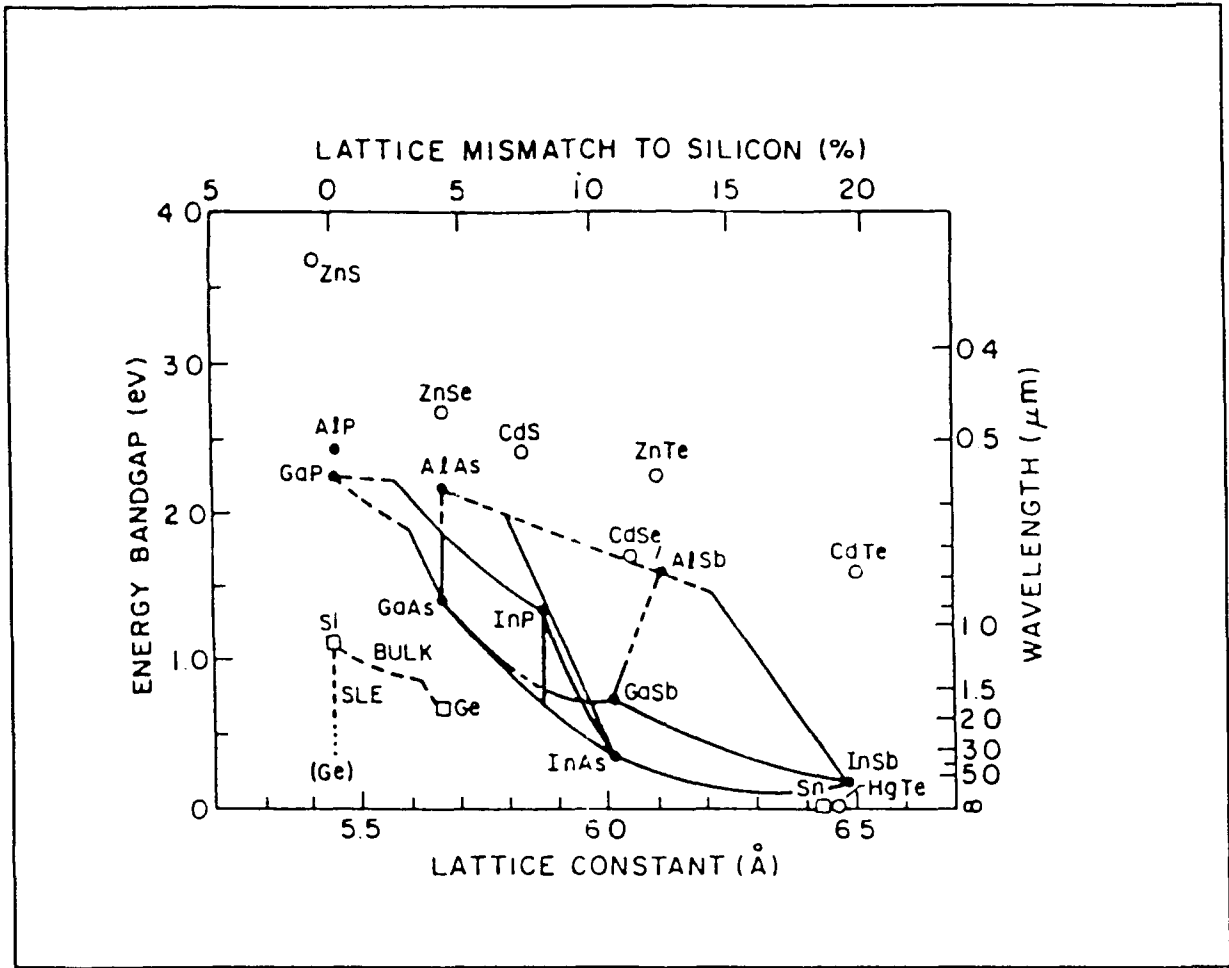


Figure 7: Bandgap vs. lattice parameter for important semiconductor systems. (Bean 1988)

throughput techniques such as chemical vapor deposition may overtake MBE. Currently only MBE provides the degree of control of sample structure, doping (of individual layers), and interface quality needed for good superlattices.

A schematic of a typical Si-MBE system is given in Figure 8. The essential elements of an MBE system include: (1) an ultrahigh vacuum (UHV) environment, (2) In-situ substrate heating and preparation, (3) Evaporation and ion sources, and (4)

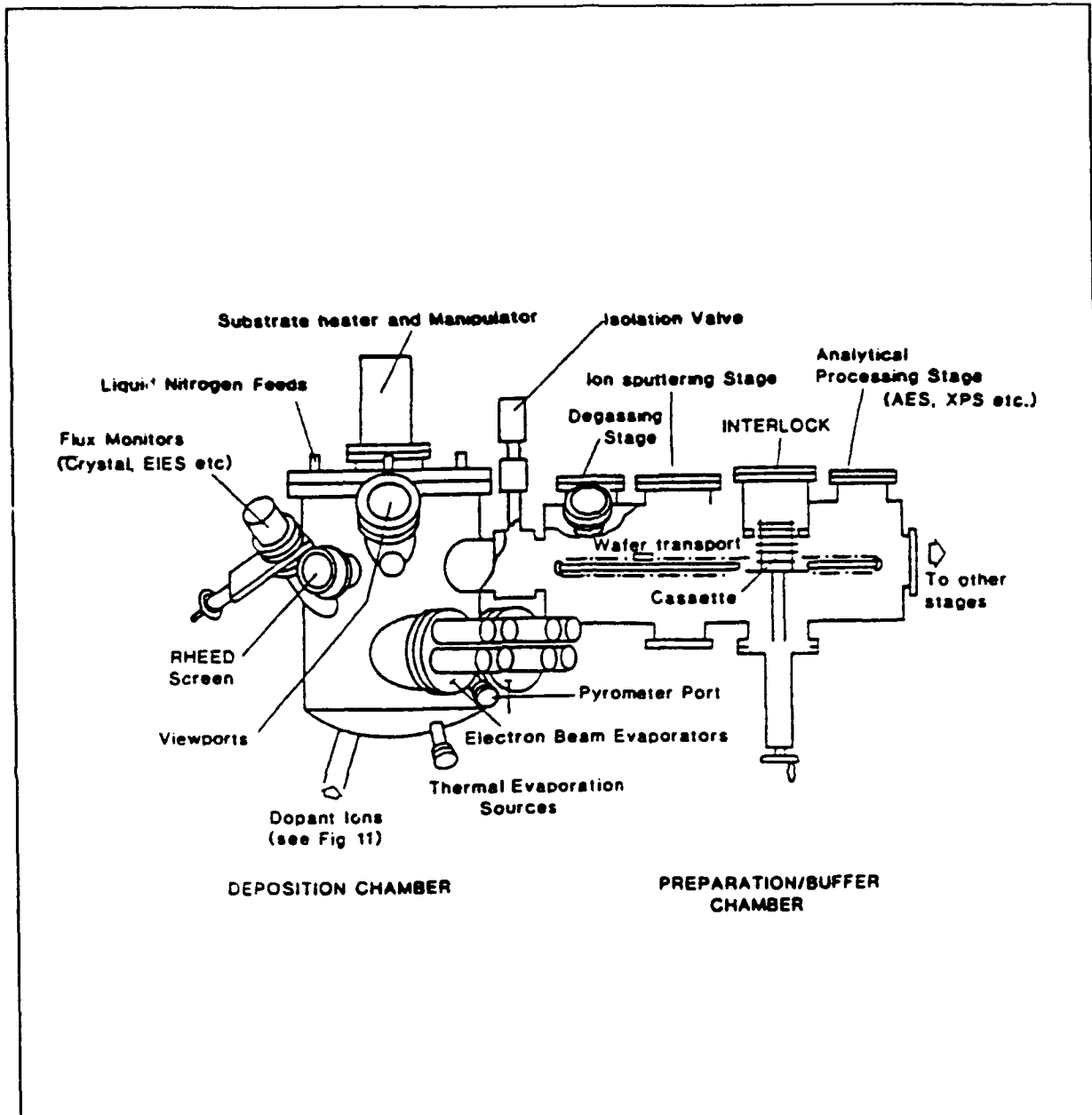


Figure 8: Schematic of Si-MBE system. (Kubiak 1988)

Analytical/diagnostic instrumentation. (Kubiak 1988)

Si-MBE growth requires a UHV environment in the range of 10^{-11} to 10^{-10} mbar which rises into 10^{-10} to 10^{-8} range during growth. This vacuum must be maintained in an oil-free

environment, in order to obtain low levels of contaminants. In order to keep contaminants to a minimum, wafers are loaded and unloaded in a buffer chamber separate from the growth chamber. The buffer chamber has separate pumps that can quickly reach UHV. The buffer chamber has a wafer transport mechanism for transferring the samples to the growth chamber and/or the characterization chamber.

After the wafers are loaded into the buffer chamber and the buffer chamber is evacuated, they are transferred to the growth chamber where they are mounted in a rotating mount that will help maintain uniform growth over the surface of the wafer. Below the sample mount is a sample heater and a thermocouple, which maintain growth temperature to within 10 °C. The heater is also used to heat substrates up to 900 °C for wafer preparation.

Si-MBE requires sources more complex than those for III-V semiconductors. Silicon and germanium are typically introduced with electron beam evaporators, in which the source material is heated with an electron beam. Electron beam evaporators avoid contamination problems associated with thermal heating in a crucible. (Pearce 1983) Typical dopants used in Si-MBE include B, Ga, In, Al, P, As, and Sb. These are introduced in a variety of ways, using E-beam sources, ion sources, thermal sources, and others.

It is necessary to have diagnostic equipment in-situ to monitor growth. Flux monitoring of E-beam sources is necessary to insure that growth is proceeding at the intended rate. Reflected High Energy Electron Diffraction (RHEED) can also be used to monitor growth, particularly the ratio of Ge to Si fluxes, but the varying electromagnetic fields associated with the E-beam sources must be neutralized before RHEED can be used.

Critical Thickness As can be seen in Figure 7, there is a 4 percent lattice mismatch between silicon and germanium that makes growth of Si-Ge heterostructures and superlattices more complicated than typical III-V systems that have lattice matched options available. The result is two types of growth of epitaxial layers of Ge or $\text{Si}_{1-x}\text{Ge}_x$ on Si (or Si or $\text{Si}_{1-x}\text{Ge}_x$ on Ge), commensurate and incommensurate. For commensurate, or pseudomorphic growth, the deposited epilayer takes on an in-plane lattice constant equal to that of the substrate. Germanium and $\text{Si}_{1-x}\text{Ge}_x$ have lattice constants greater than that of silicon, so that pseudomorphic Ge and $\text{Si}_{1-x}\text{Ge}_x$ grown on Si have biaxial in-plane compression and tension normal to the interface. Layers grown on Ge have the opposite strains. Above a critical thickness, the strain can no longer be accommodated within the epitaxial layer and incommensurate growth occurs. In this case misfit dislocations at the substrate/epilayer interface are generated to relax the strain in the epilayer. The critical

thickness is dependent on x , the alloy concentration, and has been found theoretically to be (Kasper 1977)

$$h_c = \frac{1.175 \times 10^{-2} \ln(8.9h_c)}{f_m} \quad \text{in nm,} \quad (3)$$

where

$$f_m(x) = \frac{a_{Si} - a(x)}{a_{Si}} = 0.042 x. \quad (4)$$

The experimental values for h_c have been found to much greater than those found theoretically, and have been found to obey the empirical relation (People 1985d)

$$h_c = \frac{1.9 \times 10^{-3}}{f_m^2} \ln(h_c/0.4) \quad (5)$$

The variation of critical thickness versus the germanium concentration is shown in Figure 9. The critical thickness of elemental Ge on Si is about 6 monolayers.

For a superlattice, the critical thickness applies to any single layer within the superlattice. In addition, there is a second critical thickness that applies to the overall thickness of the superlattices, that is equivalent to the critical thickness of a layer of $\text{Si}_{1-x}\text{Ge}_x$ with an alloy content that is the

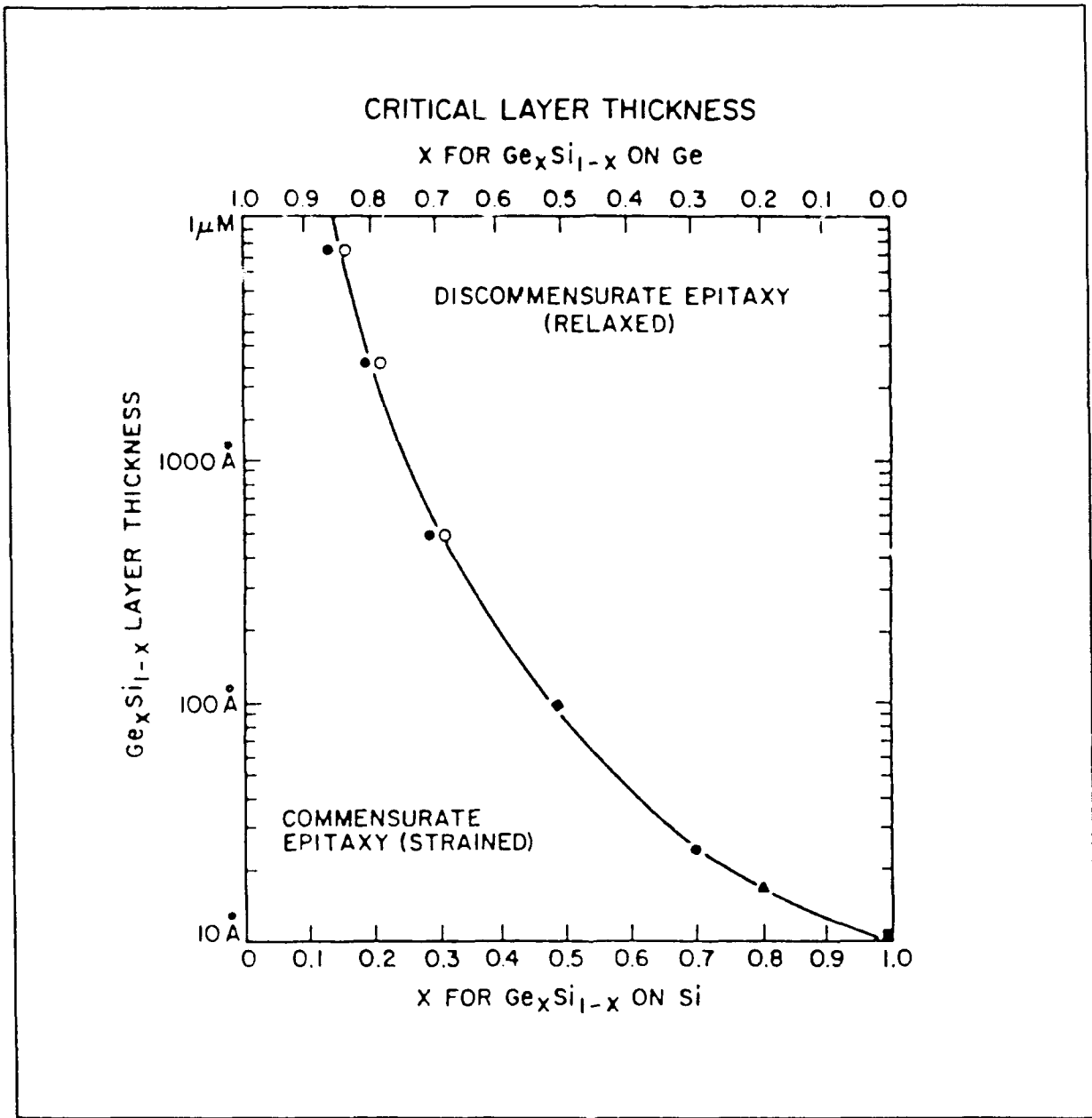


Figure 9: Critical Thickness of $\text{Si}_{1-x}\text{Ge}_x$ vs. Alloy Concentration. (Bean 1988)

average of the superlattice constituents. The average composition is given by (Jain 1991):

$$x_{av} = \frac{x_1 d_1 + x_2 d_2}{d_1 + d_2}, \quad (6)$$

and the lattice constant is

$$a_{av} = \frac{a_1 d_1 + a_2 d_2}{d_1 + d_2}, \quad (7)$$

where a_1 and a_2 are the unstrained lattice constants and d_1 and d_2 are the thicknesses of the two constituent layers. To calculate the overall critical thickness, we can use Equation (3) or (5) above, but we must substitute the misfit parameter f_m^{SL} for f_m , where

$$f_m^{SL} = \frac{a_{av} - a_{sub}}{a_{sub}}, \quad (8)$$

and a_{sub} is the in plane lattice constant of the substrate.

In a strained layer superlattice, there can be strain in each of the different types of layers, such that the overall strain in one period is partially or totally symmetrized. A strain symmetrized superlattice has a critical thickness greater than that of a superlattice where only one of the two layer types is strained. In principle it is possible to construct a strain symmetrized superlattice in which the compressive strain in one layer exactly cancels the tensile strain in the other so that the overall strain energy over each period is zero. In this case the critical thickness approaches infinity. The recipe for obtaining strain symmetrized superlattices is given by Kasper, et al.

(Kasper 1987b). The general idea is to grow the superlattice on a relaxed $\text{Si}_{1-x}\text{Ge}_x$ buffer that has a lattice constant between those of the constituent superlattice layers that results in equal strain in the two layers.

Doping Doping of Si-Ge structures is required for most device applications, so that the successful growth and characterization of doped Si-Ge heterostructures and superlattices is of fundamental importance.

Dopant incorporation into Si and Si-Ge heterostructures and superlattices has been studied extensively over the last several years. Dopants that have been successfully used in Si layers include B, Ga, In, P, As, and Sb. Doping is achieved by one of several methods. Coevaporation from elemental sources has been used to successfully incorporate boron into Si structures at low growth temperatures, compatible with Si-Ge epitaxy. (Mattey 1990, Parry 1991) Elemental boron sources have also been used to dope $\text{Si}_{1-x}\text{Ge}_x$ layers. (Kibbel 1990b, Jorke and Kibbel 1990) Boron has also been incorporated using HBO_2 or B_2O_3 sources, with concentrations as high as $3 \times 10^{20} \text{ cm}^{-3}$. (Tatsumi 1990, Lin 1989)

Successful pseudomorphic growth of Si-Ge structures by molecular beam epitaxy is usually done at low temperatures which leads to potential problems of dopant incorporation into Si-Ge heterostructures at high doping levels, since the doping

concentration achieved for co-evaporated dopants is dependent on the growth temperature. (Ni 1989) However, high growth temperatures result in poor quality Si-Ge heterostructures; misfit dislocations and defect concentrations are much higher for high temperature growth. This problem can be solved by the use of secondary ion implantation of dopants during growth for incorporation of some dopants. Gallium has been successfully incorporated into Si layers at low growth temperatures using this method. (Schaffler and Jorke 1990) Antimony (Sb) has been incorporated into Si for growth temperatures as low as 550 °C. (Ni 1989)

Deposition of an amorphous dopant layer and subsequent crystallization using solid phase epitaxy is a third method that has been used to dope epitaxial Si. However this method is most likely incompatible with Si-Ge MBE because of the thermal treatments necessary for crystallization.

In-situ characterization Several characterization techniques are available to Si-MBE that are performed in-situ, either during growth or in the MBE apparatus in a characterization chamber. All of the most useful methods are described for comparison and completeness; as will be seen in Chapter III, not all of the techniques described were used to examine or assist in the growth of the samples in this study.

Reflected High Energy Electron Diffraction (RHEED), a commonly used technique to monitor layer by layer growth in III-V MBE, is difficult to implement in Si-MBE, as mentioned above. It has been used successfully in some cases to monitor growth rate in Si-Ge heterostructures and superlattices. (Arbet 1989, Huang 1988, Sakamoto 1987)

Flux monitors are used to determine growth rates of Si and Ge. These are calibrated to deposition rates for the various growth temperatures used before SL growth so that flux measurements can be directly related to Si and Si-Ge deposition rates.

Ex-situ characterization As was the case with the in-situ characterization techniques, there are a variety of techniques available for characterization of Si-Ge heterostructures and superlattices. This section is intended only to introduce the most important techniques for comparison and to establish the degree of synergism between the various techniques.

It is common for superlattice samples to be examined using high resolution X-ray diffraction to determine the superlattice period and an estimate of the layer thicknesses.

Transmission Electron Microscopy (TEM) is a more sensitive technique for the measurement of individual layer thickness. TEM

can also be used to study defects that have been brought out using defect etching. Defect densities in Si/Ge superlattices as a function of critical thickness have been studied. (Kasper 1977, Kasper 1985)

Rutherford Backscattering Spectroscopy (RBS) is a technique that has been used to measure the composition of Si-Ge heterostructures and superlattices as well as the doping profiles and concentrations. It can measure with a high degree of accuracy the alloy concentration, x , in the $\text{Si}_{1-x}\text{Ge}_x$ layers. It can measure the concentration of most dopants, with the notable exceptions of P and B. (Pawlik 1988)

Raman spectroscopy has been used extensively in Si-Ge to determine both extrinsic and intrinsic properties. The vibrational modes of Si, Ge, and $\text{Si}_{1-x}\text{Ge}_x$ alloys with and without strain were determined by Raman spectroscopy. (Parker 1967, Cerdiera 1972, Brya 1973, Lannin 1973). With these vibrational modes for bulk materials known, $\text{Si}_{1-x}\text{Ge}_x$ strained layers as well as $\text{Si}_{1-x}\text{Ge}_x/\text{Si}$ and Si/Ge were examined to determine the effects of strain and quantum confinement on vibrational energies. (Cerdiera 1984, Kasper 1988) The result is that the optical phonon frequency is sensitive to the strain present in the Si, Ge, or $\text{Si}_{1-x}\text{Ge}_x$ layer, so that Raman spectroscopy can be used to determine the strain in a Si-Ge structure. In addition, folded acoustic phonons have been found in superlattice structures, in

agreement with zone-folding arguments and providing an additional probe of superlattice layer thicknesses. (Brugger 1986, Chang 1988a&b, and Lockwood 1987)

Si_{1-x}Ge_x/Si and Si/Ge Superlattice Bandstructure

Band Offsets Determination of the bandgap of Si_{1-x}Ge_x/Si and Si/Ge superlattices requires the accurate determination of the valence and conduction band offsets. The band offsets for Si-Ge have been studied extensively over the past several years, both theoretically and experimentally, for the full range of x and strain conditions.

Band offsets for Si-Ge heterostructures have been determined theoretically by first using deformation potential theory to obtain the conduction and valence band splittings and shifts due to strain. (Van de Walle and Martin 1986) Van de Walle and Martin estimated the valence band offset to be 0.84 eV for fully strained Ge on unstrained silicon and 0.31 eV for fully strained Si on unstrained Ge. These valence band offsets result in Type II band alignment for Si on Ge and Ge on Si as shown in Figure 10. Using a similar analysis, Bean determined valence band offsets for the Si_{1-x}Ge_x/Si heterojunction for various strain relaxed substrates, which are shown in Figure 11. (Bean 1988)

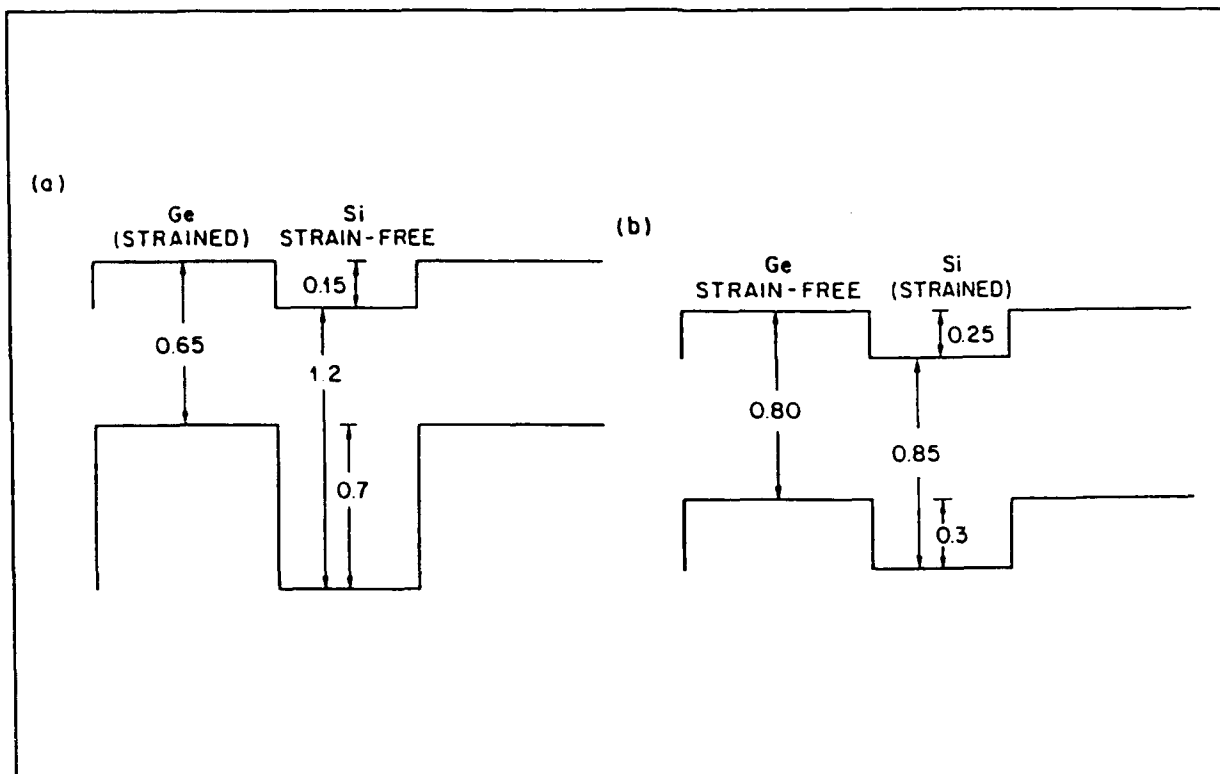


Figure 10: Band Alignments in Si/Ge. (Bean 1988)

X-ray photoemission has been used to experimentally determine the valence band offsets for Si-Ge heterostructures. (Ni 1987a 1987b) The measurement requires that the core level energies for the constituents of the heterojunction be known. This introduces a complication for strained layers, since known values for core levels of bulk materials must be corrected for strain. (Schwartz 1989) After correcting for strain, the valence band offsets have been found to be 0.74 eV for growth of fully strained germanium on unstrained silicon, and 0.17 eV for fully strained silicon on unstrained germanium. (Bevk 1990)

Band Gap of strained $Si_{1-x}Ge_x$ The band gap of $Si_{1-x}Ge_x$ depends upon the degree of strain in the layer, which is related to the

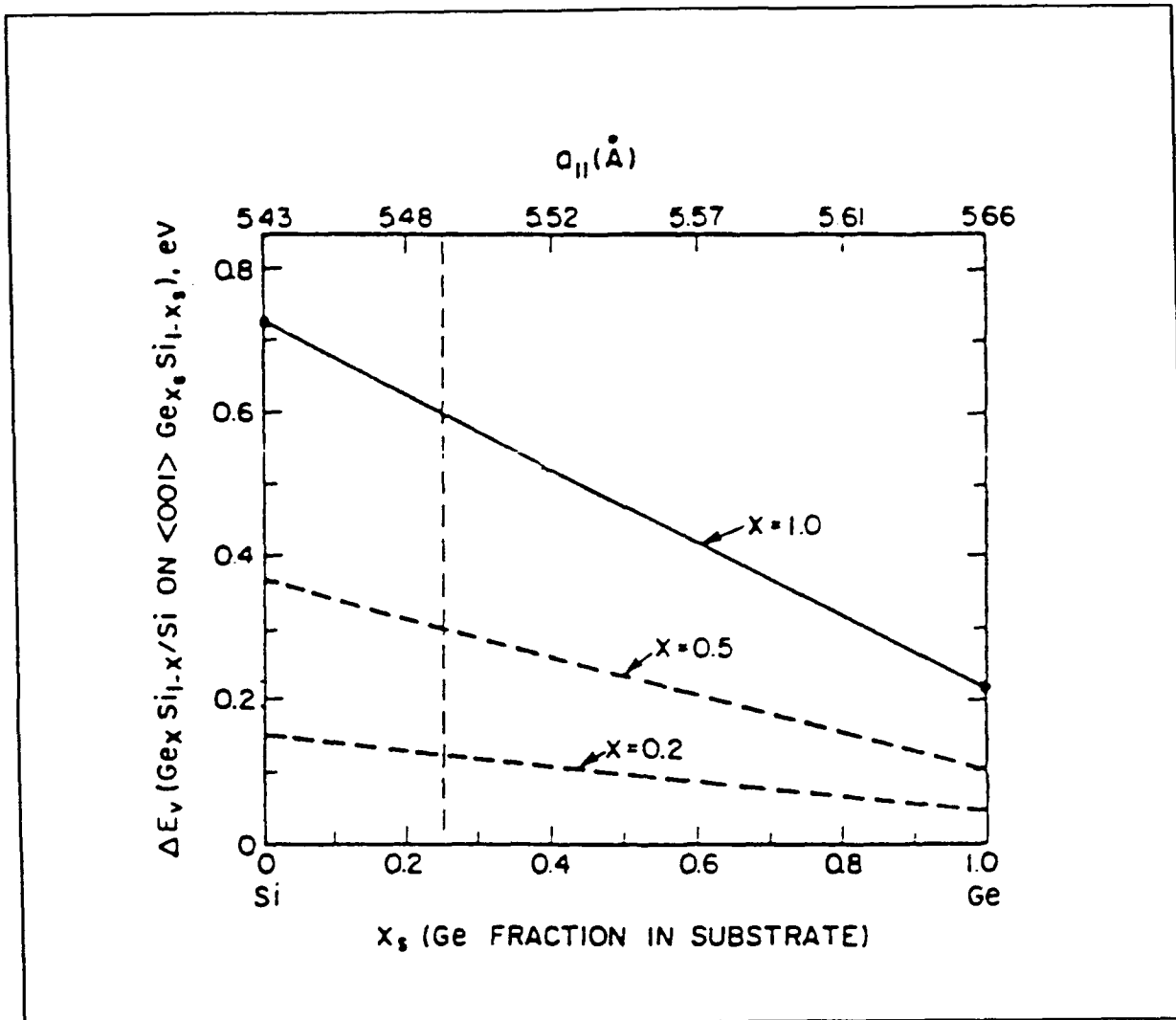


Figure 11: Valence Band Offsets for $\text{Si}_{1-x}\text{Ge}_x/\text{Si}$ Heterojunction Grown on a Strain Relaxed Substrate $\text{Si}_{1-y}\text{Ge}_y$. (Bean 1988)

in-plane lattice constant that is established from the growth parameters. Strain has been found to drastically alter the electronic band structure of $\text{Si}_{1-x}\text{Ge}_x$ due to splitting and shifting of valence and conduction bands. In Si or Si-rich unstressed $\text{Si}_{1-x}\text{Ge}_x$, the conduction band minimum is in the Γ -X-direction and is thus 6-fold degenerate. The valence band is two-fold degenerate, with a heavy hole component and a light hole component. When the $\text{Si}_{1-x}\text{Ge}_x$ becomes strained, the hydrostatic

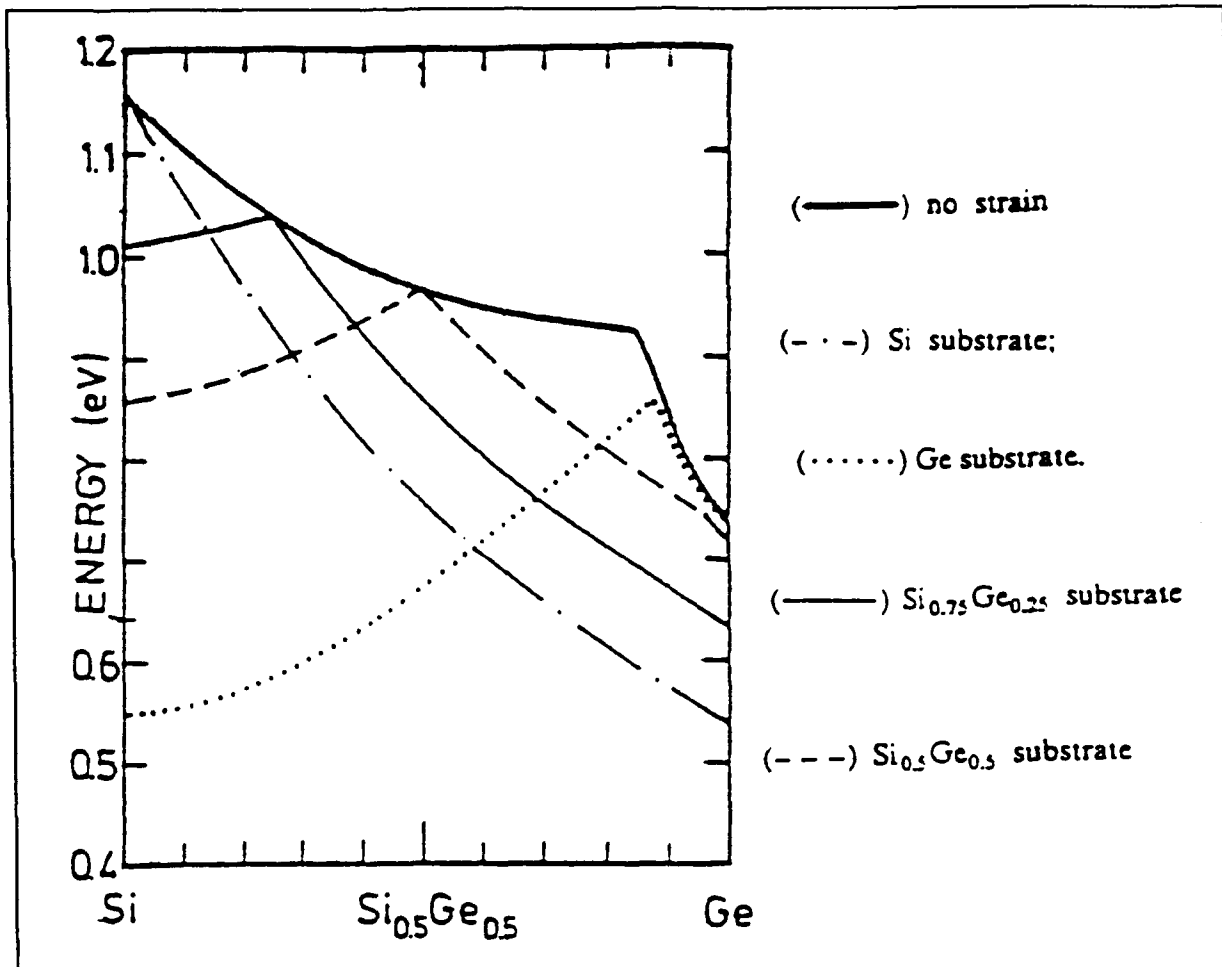


Figure 12: Band gap of $\text{Si}_{1-x}\text{Ge}_x$ for different strain conditions (Abstreiter 1989b)

part shifts the valence band up for compressive strain, and down for tensile strain. The uniaxial strain component results in a tetragonal distortion, lowering the symmetry of the crystal, which splits the degeneracy of the six-fold degenerate conduction band into a four-fold and a two-fold band, and splits the heavy and light hole bands. The shifts of valence and conduction bands, as well as the amounts of splitting for various strain conditions have been calculated by People using data for the unstrained band structure of $\text{Si}_{1-x}\text{Ge}_x$ and the known deformation

potentials for Si and Ge. (People 1986a, Abstreiter 1986)

As long as layers are grown below the critical thickness, such that there are a low density of misfit dislocations, we can assume that growth of $\text{Si}_{1-x}\text{Ge}_x$ on Si (or $\text{Si}_{1-y}\text{Ge}_y$) results in a fully strained layer, in which the in-plane lattice constant is equal to that of the substrate (or to $\text{Si}_{1-y}\text{Ge}_y$ in the case of growth on relaxed substrates with a lattice constant between Si and Ge). Once the lattice constant or strain in a $\text{Si}_{1-x}\text{Ge}_x$ layer is known along with the alloy concentration, x , the band gap can be determined from Figure 12, as determined by People and Abstreiter et al. (People 1986a, Abstreiter 1986) Note the huge differences in band gap for the different strain conditions, particularly between growth on Si substrates versus growth on Ge substrates. The bandgap of fully strained $\text{Si}_{1-x}\text{Ge}_x$ grown on Si has been determined experimentally to be (at 4.2 K)

$$E_g(x) = 1.170 - 0.89x + 0.369x^2 \text{ eV.} \quad (9)$$

(Robbins 1992)

Theoretical Calculations The first band structure calculations on Si-Ge heterostructures and superlattices concentrated on monolayer superlattices, largely because of the predictions that under appropriate conditions, it would be

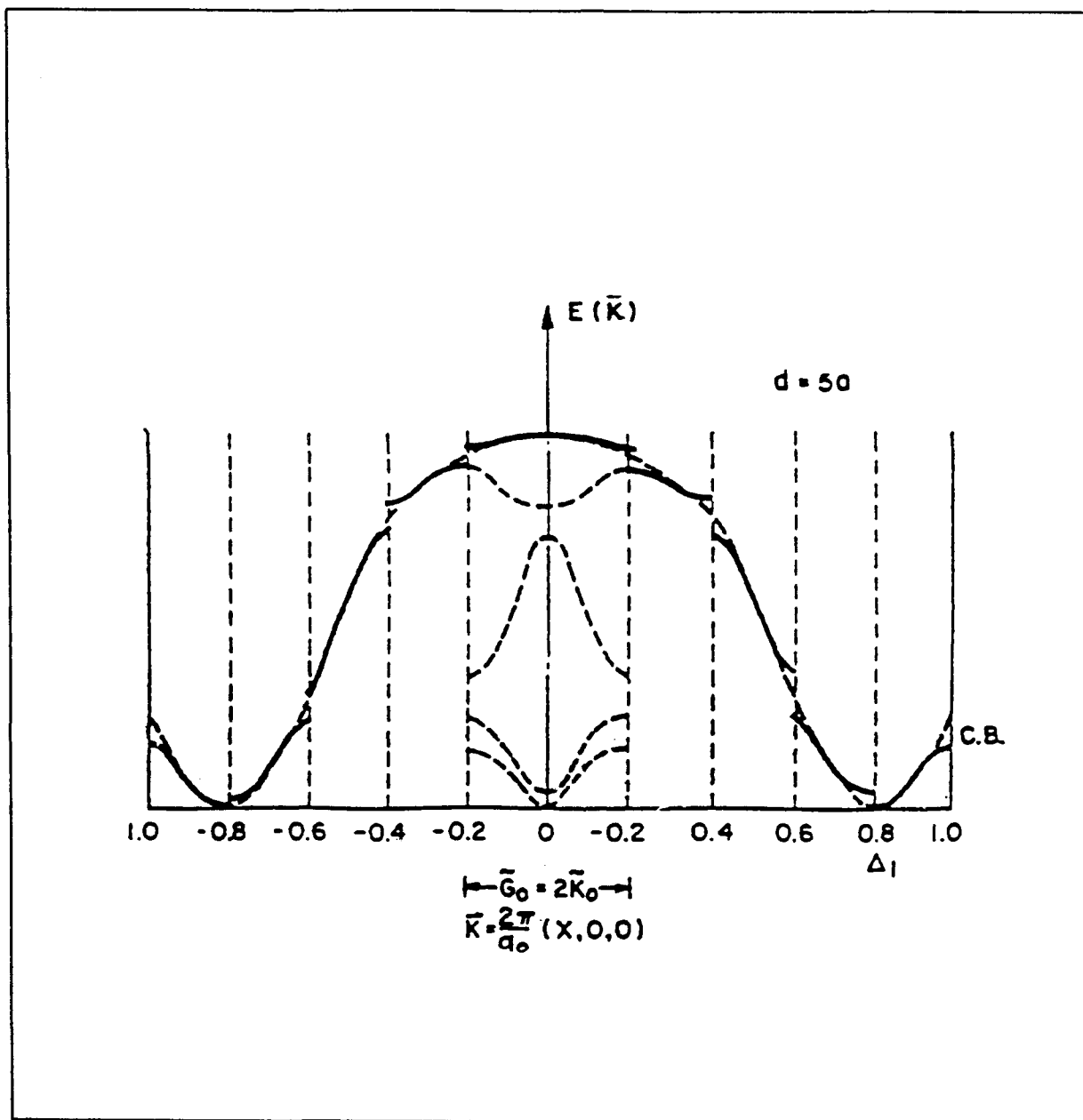


Figure 13: Zone-folding in a 10 monolayer period superlattice. (People 1986a)

possible to have a direct or pseudodirect band gap superlattice composed of layers that were indirect semiconductors. This idea originated with the work by Gnutzmann and Clausecker, which predicted that in short period superlattices, the additional periodicity imposed by the superlattice potential would fold

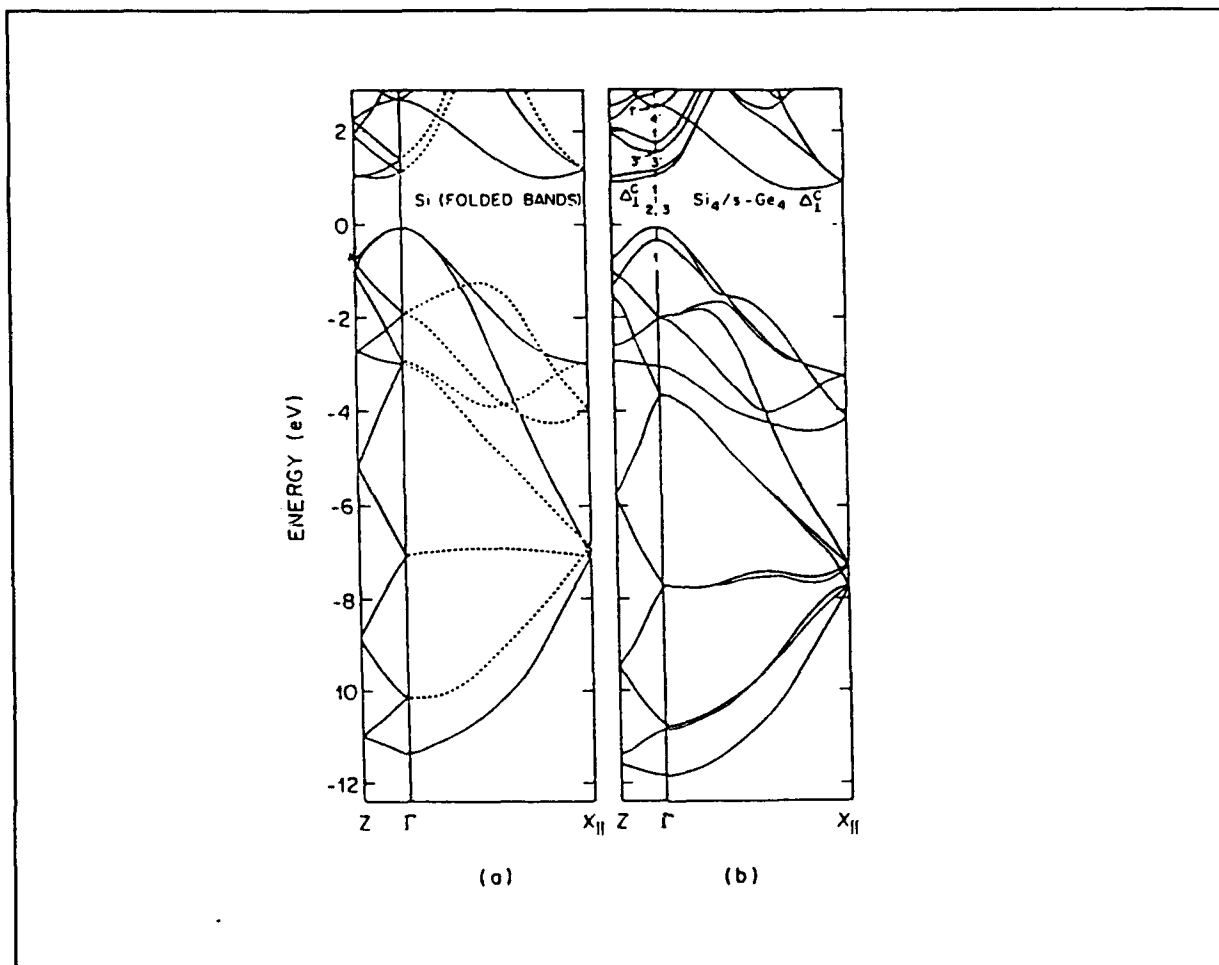


Figure 14: Si_4Ge_4 Band Structure Calculation (a) Si bands folded according to superlattice periodicity. (b) Calculated bands. In (a) the unfolded Si bands are solid while the folded bands are dotted. (Satpathy 1988)

bands back towards the zone center. (Gnutzmann and Clausecker 1974) In silicon the conduction band minimum lies approximately 4/5 of the distance from the zone center to the X zone boundary. In order to fold the conduction band minimum to the zone center, the bulk Si Brillouin zone needs to be folded in the z direction 5 times as shown in Figure 13. This can be accomplished with a Si_n/Ge_m superlattice where $n + m = 10, 20, 30$, etc. The 10 monolayer structure appears to be the best candidate to observe

zone folding. The zone-folding idea was proven in a local density pseudopotential calculation by Satpathy *et al* on Si_n/Ge_m superlattices for $n, m = 3-7$. (Satpathy 1988) In these calculations the folded Si bands look remarkably similar to the calculated superlattice bands, as shown in Figure 14. Hybertson and Schluter studied Si_2Ge_2 and Si_4Ge_4 superlattices using the pseudopotential technique. (Hybertson and Schluter 1987, 1988a & b) The lowest energy transitions in this case were found to be indirect.

Calculations by Froyen *et al* on Si_n/Ge_n for $n = 1, 2, 4, 6$ also found that in each the superlattice had an indirect band gap. (Froyen 1987, 1988) With the calculations by Ciraci and Batra for $n = 1-6$, all Si_n/Ge_n superlattices grown on Si for n less than or equal to 6 have been found to be indirect.

Requirements for Direct Band Gap Si/Ge SL. After the initial band structure calculations attention turned to the

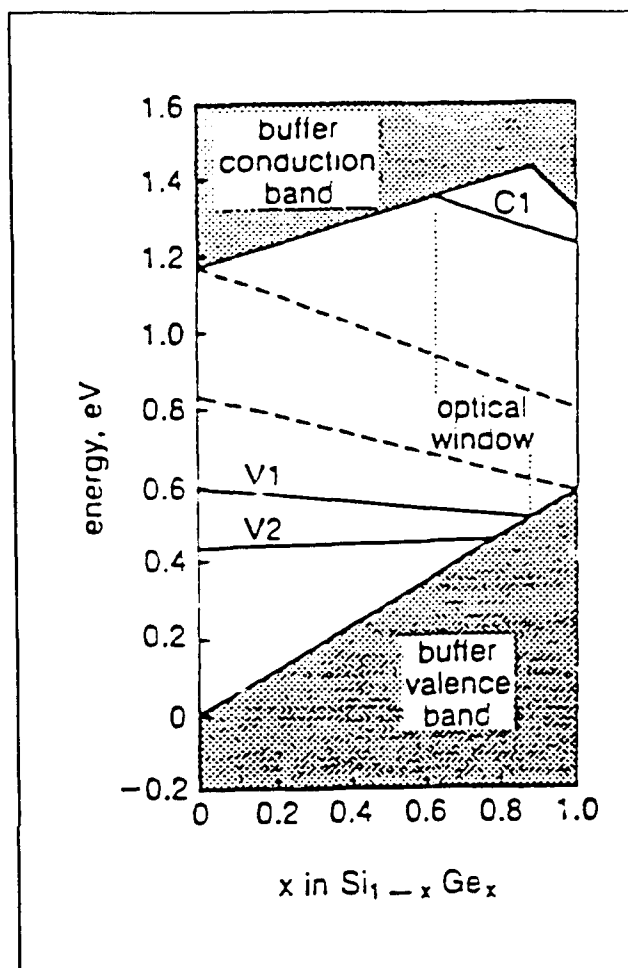


Figure 15: Requirements for buffer layer composition in direct band gap Si/Ge superlattices (Gell 1989)

conditions necessary for direct transitions in Si/Ge superlattices. Gell proposed that all Si/Ge superlattices grown on Silicon would be indirect because of the degeneracy in the conduction bands. (Gell 1989) The zone-folded conduction bands in the X_z direction for Si/Ge superlattices grown on Si are at same energy as the unfolded bands in the X_x and X_y directions. It is necessary to lower the X_z conduction bands relative to the X_y and X_x conduction bands. This can be accomplished by growing the superlattice on a substrate with an lattice constant larger than sil. The most practical method of achieving this is to grow a relaxed $\text{Si}_{1-x}\text{Ge}_x$ buffer layer on a Si substrate. The buffer layer composition must be chosen carefully, though, since the lattice constant that is forced upon the superlattice by the buffer layer composition affects the amount of strain in the Ge and Si layers. The strain in the individual Si and Ge layers determines the conduction and valence band offsets. The conduction and valence band offsets determine the positions of the zone-folded superlattice states. Thus there is a narrow range of buffer layer compositions, $x = 0.6$ to 0.83 , that result in direct band gap Si/Ge superlattices as shown in Figure 15. It turns out that buffer layers with this composition result in nearly equal strain in the Si and Ge layers, so that over each period the net strain is close to zero. Thus direct band gap Si/Ge superlattices can also be strain symmetrized so that there is, in principle, no critical thickness for the superlattice, which should help in the production of efficient light emitters.

Kronig-Penney Model The Kronig-Penney Model can be used to predict the band structure of superlattices with periods greater than 20 monolayers. (Pearsall 1989a) This is particularly useful to predict the superlattice band gaps for $\text{Si}_{1-x}\text{Ge}_x/\text{Si}$ superlattices, for which no full bandstructure calculations have been performed. The Kronig-Penney Model starts with a one-dimensional time-independent Schrodinger equation (Kittel 1986)

$$-\frac{\hbar^2}{8m\pi^2} \frac{d^2\psi(x)}{dx^2} + U(x) \psi(x) = E\psi(x) \quad (10)$$

where $U(x)$ = the periodic superlattice potential defined as the periodic extension of

$$U(x) = 0 , \text{ for } 0 < x < l_w \quad (11)$$

and

$$U(x) = U_0 , \text{ for } l_w < x < d \quad (12)$$

where

$$d = l_w + l_b = \text{superlattice period} = \text{well width} + \text{barrier width} \quad (13)$$

and

$$U_0 = \text{conduction or valence band offset} \quad (14)$$

The solution is assumed to be of the form

$$\psi(x) = Ae^{ik_v x} + Be^{-ik_v x} \text{ for } 0 < x < l_w \quad (15)$$

$$\psi(x) = C e^{k_b x} + D e^{-k_b x} \text{ for } l_w < x < d \quad (16)$$

where

$$k_w = \sqrt{\frac{8\pi^2 m_w E}{h^2}} \quad \text{and} \quad k_b = \sqrt{\frac{8\pi^2 m_b (U_0 - E)}{h^2}}, \quad (17)$$

and m_w and m_b are the effective masses in the well and barrier regions respectively. Using the boundary conditions of continuity of the wave function and its first derivative at the interfaces, and requiring that the solution be in the Bloch form

$$\psi(x + d) = \psi(x) e^{iqd}, \quad \text{where } q = \text{Bloch wave vector}. \quad (18)$$

The result is the dispersion relation

$$\cos(qd) = \cos(k_w l_w) \cosh(k_b l_b) + A \sin(k_w l_w) \sinh(k_b l_b), \quad (19)$$

where

$$A = \frac{m_b k_w}{m_w k_b}. \quad (20)$$

Equation [18] can be solved for $E(q)$ to determine the quantum confinement energies and the superlattice miniband structure for both the valence and conduction bands. The solutions to Equation [18] are a set of energy bands. The values at $q = 0$ are the

minimums, and define a set of quantum levels - a ground state and several excited states, the number depends on the superlattice parameters, the effective masses, etc. For $\text{Si}_{1-x}\text{Ge}_x$ on Si the heavy hole bands are well separated from the light hole bands so that only the heavy hole bands need to be considered for the determination of the band gap. The excited states, though, overlap with the light hole states, so that the resulting E vs. q band structure is not valid, since it does not consider interaction between the heavy and light hole bands. The effective superlattice band gap is determined from the energy difference between the conduction band ground state and the valence band ground state.

Device Applications

The silicon-germanium material system promises improvements in two areas. The Si-Ge based heterojunction bipolar transistor, bipolar inversion channel FET, and the modulation doped FETs provide higher speed electronic devices. The Si-Ge system also provides the opportunity to replace electronic devices on integrated circuits with optical devices, or to have optical and electronic devices on the same chip.

Monolithic Optoelectronics The largest potential payoff from Si-Ge heterostructures and superlattices would result if

photonic and electronic devices could be integrated onto the same integrated circuit chip. Electronic technology in silicon is well developed; Si-Ge offers the possibility for improvement of electronic devices. Photonics in silicon would require efficient detectors and emitters in the 1.3 to 1.5 micron wavelength range. Waveguides for light transmission could be $\text{Si}_{1-x}\text{Ge}_x$ channels possibly doped with erbium. Optical modulators would be needed as an optical analog for the transistor. The critical elements for monolithic optoelectronics are discussed below.

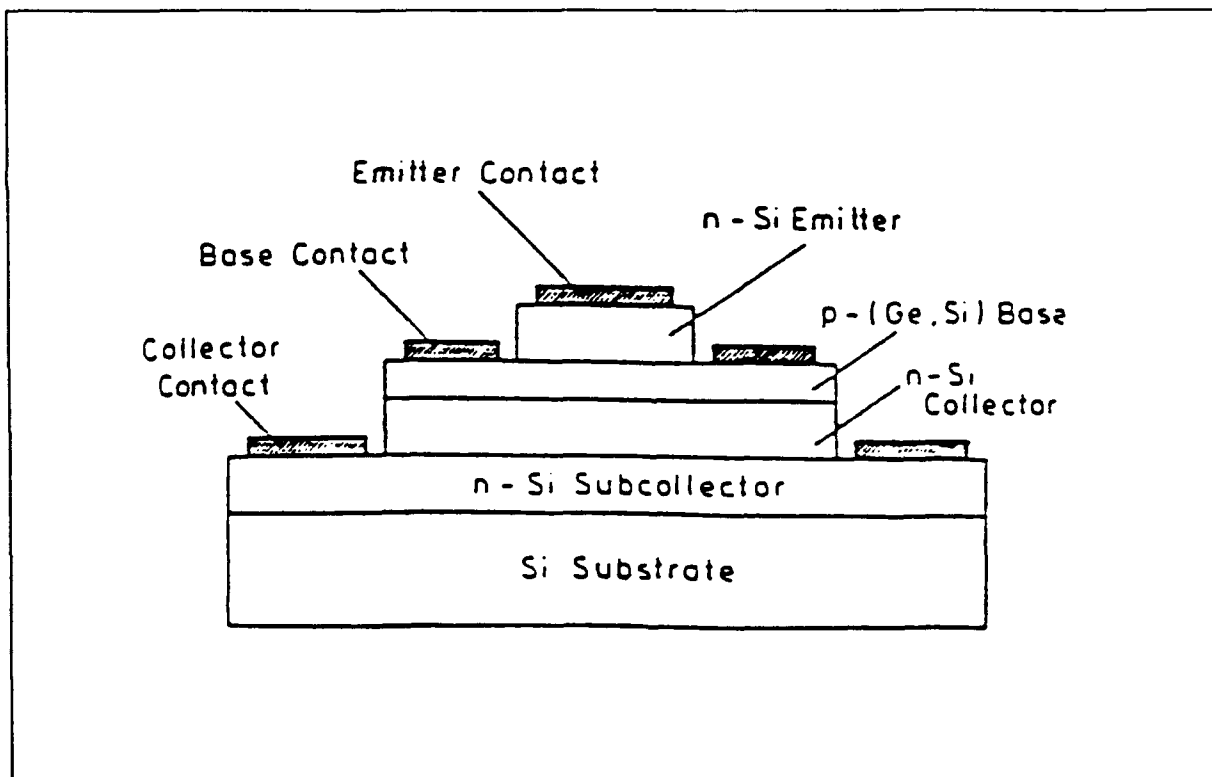


Figure 16: A Si-Ge Heterojunction Bipolar Transistor (Iyer 1987)

Heterojunction Bipolar Transistor The heterojunction bipolar transistor (HBT), an example which is shown in Figure 16, takes advantage of increased mobility in $\text{Si}_{1-x}\text{Ge}_x$ layers and

provides the single most successful device application to date in the Si-Ge system. Gain in an HBT is determined by the expression (Pearsall 1990)

$$G = A \frac{N_E}{P_B} e^{\frac{\Delta E_{E-B}}{kT}}, \quad (21)$$

where

$$N_E = \text{emitter doping, } P_B = \text{base doping, and} \quad (22)$$

$$\Delta E_{E-B} = \text{potential difference between emitter and base} \quad (23)$$

For high speed operation the base doping needs to be high. To maximize gain, the ratio N_E/P_B should be as high as possible. If the emitter and base are composed of the same material, as in a silicon HBT, increasing the emitter doping results in a negative value of ΔE , and thus a low gain. If the silicon base is replaced with a $\text{Si}_{1-x}\text{Ge}_x$ base with its lower bandgap, ΔE is high, allowing for high base doping (for high speed), without requiring high emitter doping necessary for high gain, since the exponential factor overwhelms the ratio of emitter doping to base doping. The high base doping results in a lower resistance base which reduces noise and degradation by injection effects. (Jain 1991) The base can be made thin, which decreases the transit time and increases the frequency response. Collector doping can also be increased, resulting in even higher frequency response.

The first Si-Ge HBT was fabricated by Iyer et al. (Iyer 1987). Since then, there have been numerous improvements to the original device. (Xu 1988, Tatsumi 1988, Patton 1988, Temkin 1988, Harame 1988, King 1989, Taft 1989a, Patton 1989, Kamins 1989, Kibbel 1990, Patton 1990). The device by Patton has the highest cutoff frequency to date, 75 GHz, that may be improved to over 100 GHz in the near future. (Patton 1990) This performance is comparable to the best III-V HBTs, but retains the fabrication advantages of Si-based technology.

Modulation Doped Field Effect Transistor (MODFET). The two types of modulation doping in Si-Ge are shown in Figure 17. In both cases, carriers are spatially removed from impurity centers, resulting in very low impurity scattering, which has a major effect on carrier mobilities. The first modulation doping of Si-Ge was demonstrated for holes (p-type) at Bell Laboratories, (People 1984, People 1985b, People 1985c) N-type modulation doping was first done at AEG and Munich Technical University. (Abstreiter 1985b, Jorke 1985) P-type modulation doping is achieved by doping the silicon layers in a Si/Si_{1-x}Ge_x heterostructure with acceptors. The resulting band bending then produces a two-dimensional hole gas in the Si_{1-x}Ge_x layers with mobilities as high as 5000 cm²/V-sec, ten times higher than bulk Si, and higher than any III-V bulk semiconductor. (People 1985c) N-type modulation doping is achieved by doping the Si_{1-x}Ge_x layers with donors. The result is a two-dimensional electron gas with

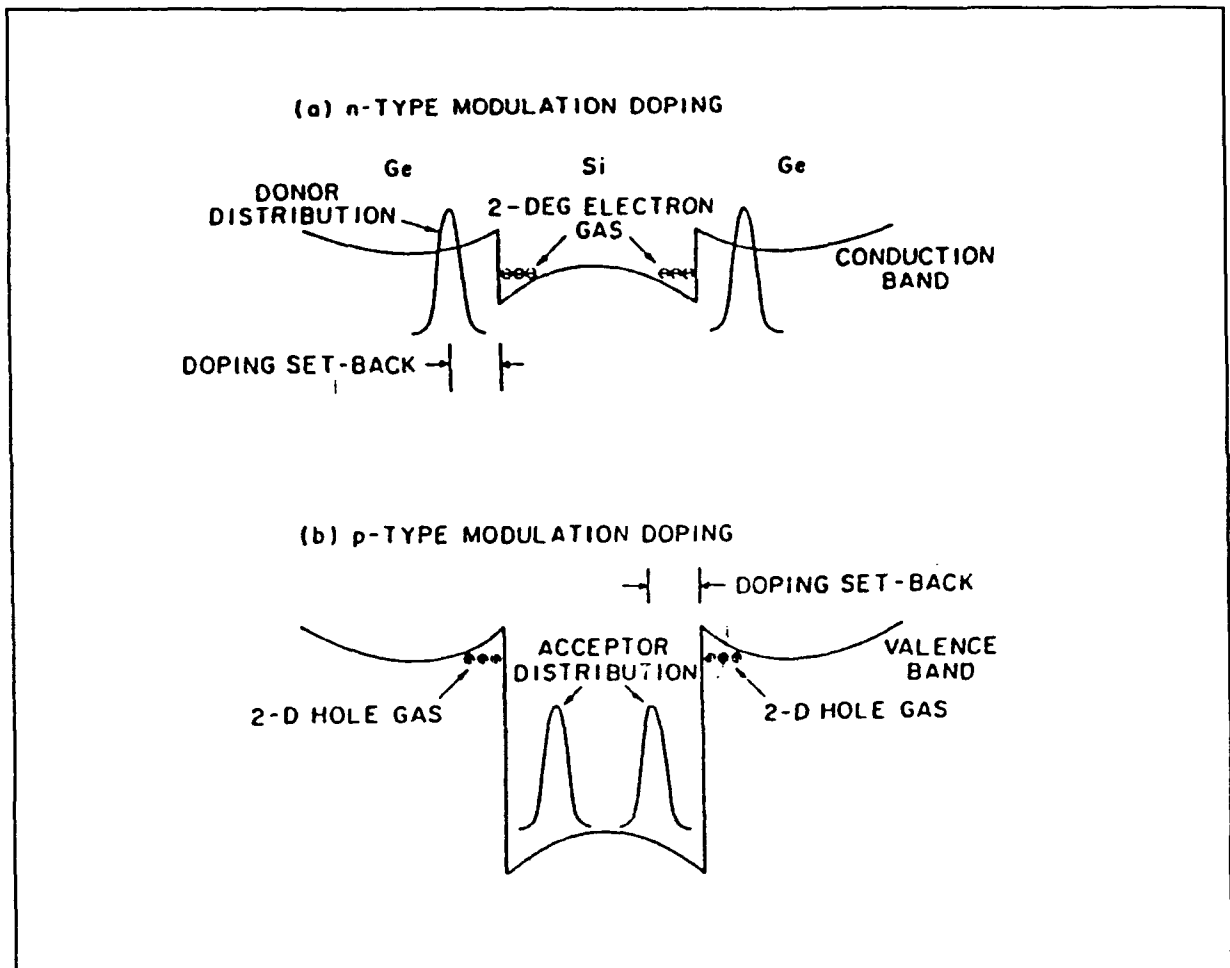


Figure 17: Modulation Doping in Si-Ge. (Pearsall 1989a)

mobilities as high as $180000 \text{ cm}^2/\text{V}\cdot\text{sec}$, more than 50 times higher than bulk Si, and higher than any other bulk semiconductor. (People 1985c, Abstreiter 1985b) Modulation doping in the fabrication of the modulation doped field effect transistor (MODFET) shown in Figure 18, also known as the high electron mobility transistor (HEMT) for the n-channel MODFET or the high hole mobility transistor (HHMT) is another class of electronic devices that benefits from the Si-Ge material system. As with the HBTs, the idea of the MODFET is borrowed from the GaAs/AlGaAs system. The two types of modulation doping in Si-Ge are shown

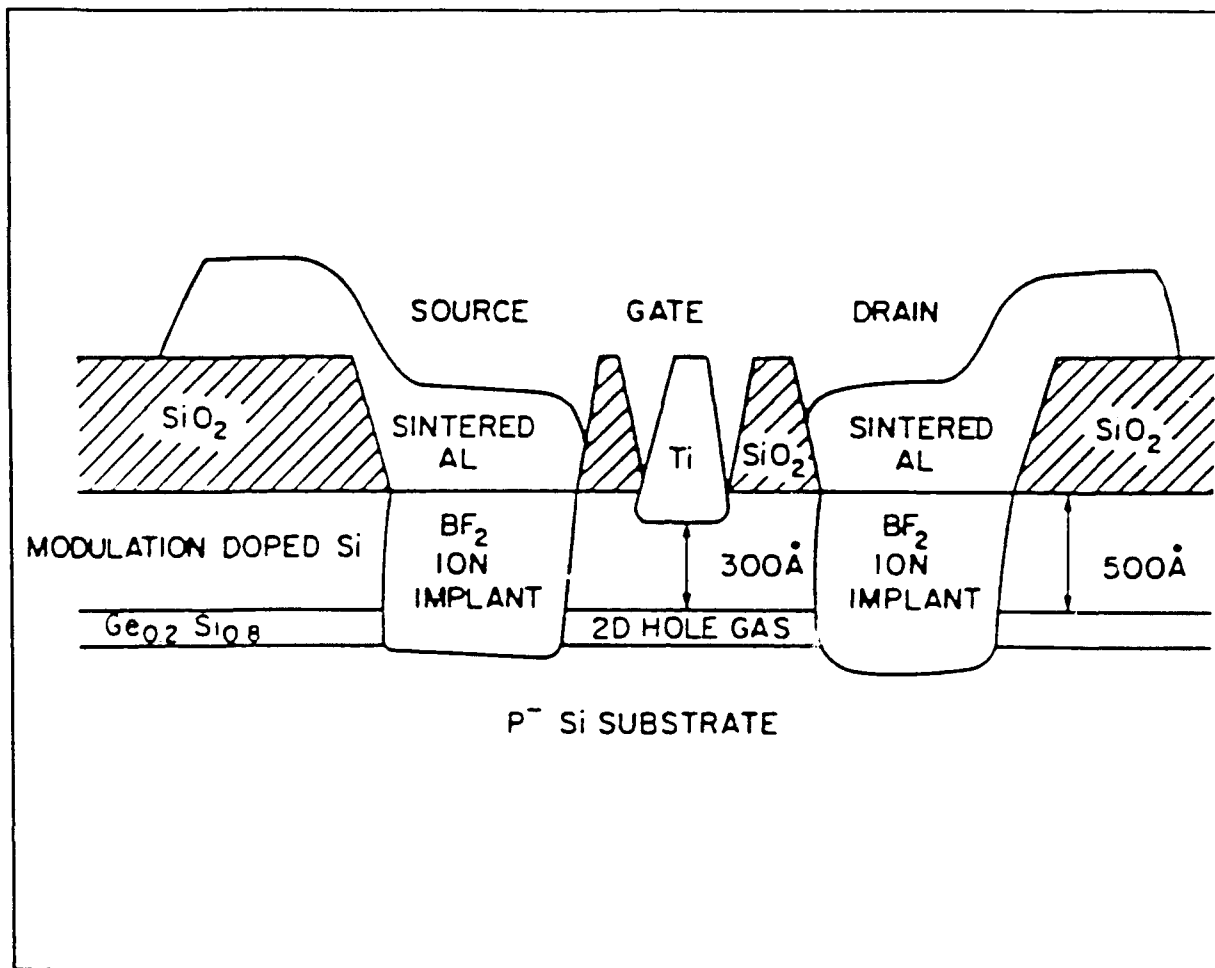


Figure 18: Si-Ge Modulation doped FET (Pearsall 1989)

in Figure 17. The hole and electron mobilities depend upon the doping profile and the doping setback, the distance of the delta doping layer from the heterojunction. N-type and p-type MODFETs have been fabricated with performance better than commercially available n- and p-type MOSFETs. (Pearsall 1985, Pearsall 1986b, Daembkes 1986)

Bipolar Inversion Channel FETs (BICFET) The BICFET was proposed in 1985 as a new device with improved switching

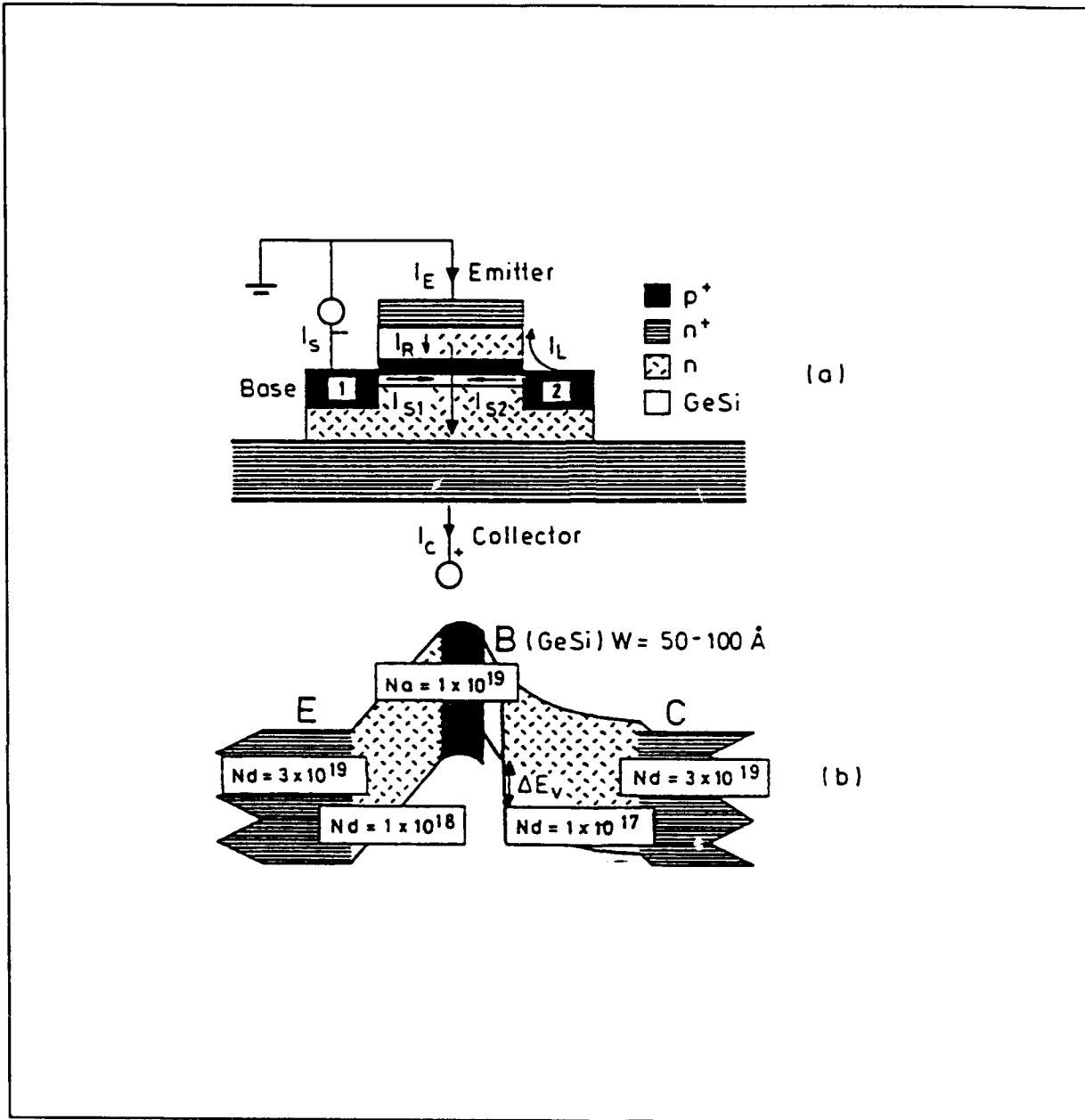


Figure 19: Si-Ge BICFET (a) Structure (b) band diagram (Jain 1991)

performance over conventional silicon bipolar transistors.

(Taylor and Simmons 1985) The BICFET uses an inversion channel rather than a charge neutral base region so it is a very attractive high-speed alternative to the HBT, since it avoids charge storage and carrier recombination problems inherent in the

base regions of HBTs. (Taylor 1988) The band alignment in Si-Ge favors p-channel operation, which is difficult to achieve in III-V heterostructures. A gain of 365 was measured in a p-channel Si-Ge BICFET (shown in Figure 19), the highest for any BICFET, and much higher than typical III-V BICFETS with gains of 8-15. (Taft 1989b).

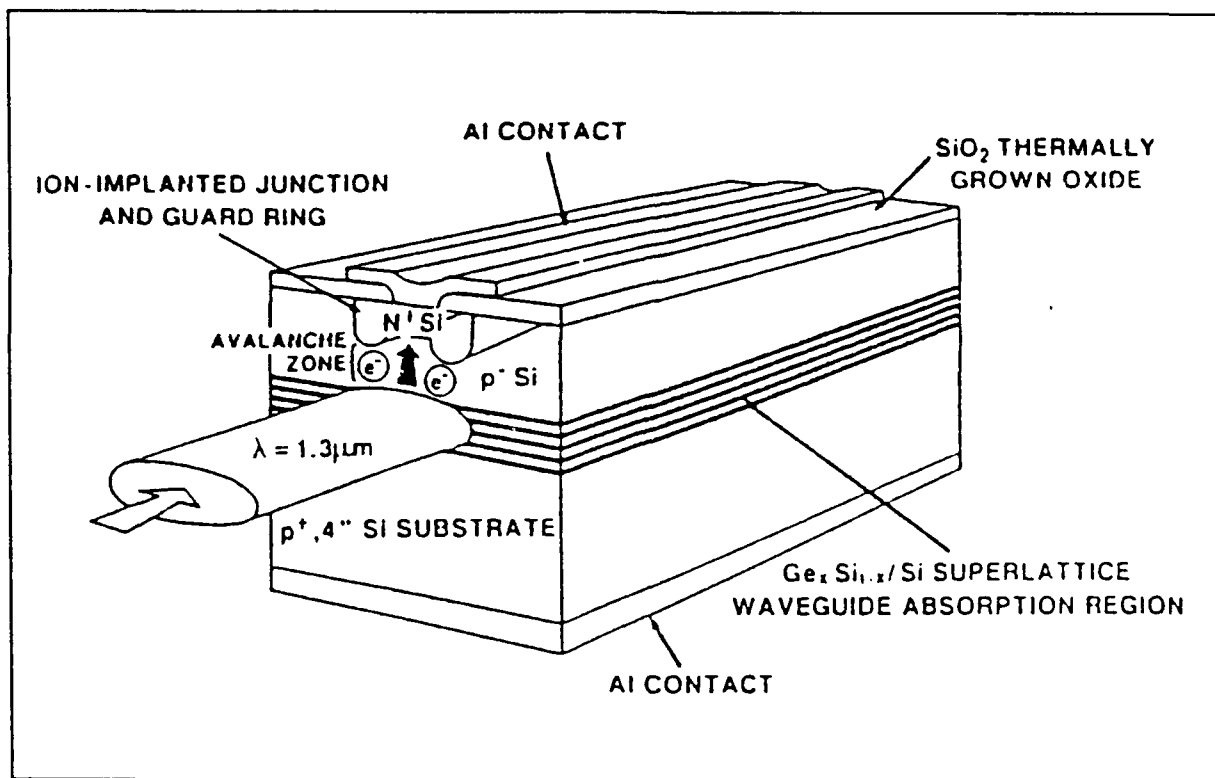


Figure 20: $\text{Si}_{1-x}\text{Ge}_x/\text{Si}$ superlattice waveguide avalanche photodetector. (Pearsall 1986c)

Infrared Detectors. Infrared detectors using Si-Ge have been fabricated with response in the critical 1.3 to 1.55 micron wavelength range. Luryi, et al, fabricated a Ge p-i-n photodetector on a silicon chip, that had a 40 percent quantum

efficiency, close to commercially available Ge detectors. (Luryi 1984) However, the structure was grown incommensurate, resulting in dislocations at the substrate buffer layer interface that caused high values of dark current and noise. Temkin, et al, fabricated a p-i-n superlattice waveguide photodetector in which the intrinsic region was a 20 period superlattice alternating 29 nm Si regions with 6 nm $\text{Si}_{0.4}\text{Ge}_{0.6}$. (Temkin 1986) An improved superlattice avalanche multiplication photodetector, shown in Figure 20, was fabricated later by the same group. (Pearsall 1986c)

Quantum Well Infrared Detectors. The quantum well infrared detector uses intersubband absorption, i.e., absorption between confined states, as its detection mechanism. In $\text{Si}_{1-x}\text{Ge}_x/\text{Si}$ superlattices the confined states (subbands) are in the valence band. The spacings between these states are small, no more than .3 eV for a practical case, so that $\text{Si}_{1-x}\text{Ge}_x/\text{Si}$ intersubband infrared detectors would be used for detection in the far infrared, from 4-50 μm , providing that charge can be conducted out of the wells.

Light emitting devices. To date, the goal of getting light out of silicon or silicon based structures has been reached with only limited success, particularly in the important infrared range (1.3 to 1.55 micron).

Luminescence related to deep levels in silicon was the primary mechanism for getting light out of silicon prior to the recent research into Si-Ge light-emitting structures. Most of the methods that have been attempted have involved isoelectronic centers in silicon. The first Light Emitting Diode (LED) using isoelectronic centers was from a carbon-related center created by irradiation damage. (Canham 1987) The most successful Si LED involved silicon doped with sulphur. (Bradfield 1989) There is some hope that these isoelectronic centers in Si or $\text{Si}_{1-x}\text{Ge}_x$ could have strong electroluminescence (EL) similar to that found in GaP:N, another indirect bandgap system. (Bergh 1976)

There has been some success getting EL from Si doped with erbium using ion implantation. (Ennen 1983, Ennen 1985) Recently, erbium has been used to dope $\text{Si}_{1-x}\text{Ge}_x$ epilayers and $\text{Si}_{1-x}\text{Ge}_x/\text{Si}$ superlattices. (Houghton 1991b) The photoluminescence from these structures is stronger than Si:Er and persists to high temperatures, but is still too weak for an efficient device, though there is hope for improvements. The data so far suggest that Er in $\text{Si}_{1-x}\text{Ge}_x$ has a large cross section for exciton capture, favorable for efficient light emission.

There have been several attempts to get PL from monolayer Si/Ge superlattices with a pseudodirect band structure, (Zachai 1988, 1990a&b) but none to date have exhibited EL, and the PL is most likely due to defect unrelated to the superlattice. (Schmid

1990b). The prospects for efficient EL from monolayer Si/Ge superlattices are not as good as some of the other possibilities at this time.

A LED with a 1 percent quantum efficiency and consisting of a single $\text{Si}_{1-x}\text{Ge}_x$ layer was fabricated by the NRC-Canada group. (Rowell 1991) The defect related luminescence was broad band (80 meV bandwidth) and at energies 120 meV below the $\text{Si}_{1-x}\text{Ge}_x$ band gap. It was proposed that the origin of the luminescence was isoelectronic centers related to Ge complexes. (Houghton 1991b)

Intense luminescence has also been obtained from porous silicon, i.e., silicon that has been electrochemically etched under closely controlled conditions such that the remaining structure consists of needlelike cones 10-20 nm in diameter. The emission from porous silicon is visible, ranging from yellow to deep red, and extending into the infrared in some cases. While porous silicon is interesting, it does not appear likely that emission in the 1.3-1.55 micron range can be obtained, so it does not directly compete with the structures above.

Stability of $\text{Si}_{1-x}\text{Ge}_x/\text{Si}$ and Si/Ge SLs

Stability of as grown Si-Ge structures with respect to critical layer thicknesses has already been commented on above.

All strained-layer superlattices are unstable in some respect because they are grown in a nonequilibrium situation. As a result, there are several effects which may cause the superlattices or heterostructures to attempt to relax to an equilibrium condition. The superlattices and heterostructures relax in two ways. First, the Ge or $\text{Si}_{1-x}\text{Ge}_x$ layers interdiffuse with the silicon layers, making the interfaces fuzzier than they may already have been (in the case of $\text{Si}_{1-x}\text{Ge}_x/\text{Si}$ interfaces). Second the strain may relax by the formation of misfit dislocations. The structural stability of Si/Ge and $\text{Si}_{1-x}\text{Ge}_x/\text{Si}$ superlattices when subjected to typical device fabrication or operating environments is important to future applications, as well as to fundamental material characterization.

Interdiffusion, strain relaxation, and misfit dislocation formation and propagation have all been investigated in recent years. (Prokes 1991a&b, Friess 1991, Kuan 1991) The studies by Prokes et al indicated that in initial stages of relaxation due to thermal treatments the relaxation is primarily through interdiffusion rather than formation of misfit dislocations. In addition it was found that a significant part of the interdiffusion is interstitial related, especially in the early stages of interdiffusion. Interdiffusion coefficients for Si and Ge in Si/Ge SLs have been determined using Raman spectroscopy. (Schorer 1991) The interdiffusion coefficient, D^* , has been shown to be related to the bulk interdiffusion coefficient, D_{∞} , according to

$$-2k^2 D_{\bullet} \left[1 + \frac{2\kappa k^2}{d^2 f/dx^2} \right] = -2k^2 D^*, \quad (24)$$

where κ = the gradient energy coefficient, f = Helmholtz free energy, $k = 2\pi/d$, where d = SL period. (Schorer 1991) The bulk interdiffusion coefficient of a Si-Ge alloy is

$$D_{\bullet} = [xD_{Ge} + (1-x)D_{Si}] F, \quad (25)$$

where

$$F = x(1-x) \frac{d^2 f/dx^2}{Nk_B T}. \quad (26)$$

In Eq [25-26] x is the Ge fraction, D_{Ge} and D_{Si} are the tracer diffusivities of Si and Ge atoms within the Si-Ge alloy, N is the atomic density, k_B is the Boltzmann constant, and T is the absolute temperature.

A complete study of misfit dislocation formation and propagation as a function of anneal temperature and anneal time was reported by Houghton. (Houghton 1991a)

Photoluminescence

General Considerations Photoluminescence (PL) is a useful technique for the nondestructive analysis of bulk and epitaxial semiconductors, as well as semiconductor superlattices. PL can

give semiquantitative information about impurity concentrations and other defects. PL can detect the presence of some defects at very low concentrations, depending on the efficiency of the optical emission associated with the defect. PL can give very accurate information about the bandgap of bulk materials as well as the effective band gap of superlattices. The temperature dependence of PL can be used to determine binding energies of defects, or combined with other data, can provide information about whether the emission is excitonic, or related to electron or hole traps, or other types of emission. The main limitation of PL is that it probes only the states below the energy gap of the semiconductor. For superlattices, only the lowest energy confined states that determine the effective superlattice band gap can be seen; the others are above the effective gap and can be probed using photoluminescence excitation spectroscopy (PLE).

PL from Bulk and Epitaxial Silicon Since the samples investigated in this dissertation have germanium concentrations less than 0.85, the bandstructure and optical properties are expected to be silicon-like. Thus previous studies of silicon by PL are very relevant to this research. It is to be expected that many of the luminescence features seen in Si-Ge structures are shifted or broadened peaks seen previously in bulk or epitaxial silicon. Prior to 1976, PL studies on silicon concentrated on near band edge features, primarily free exciton (FE) and shallow donor and acceptor bound exciton (BE) emission. The definitive

work was performed by Dean, *et al.* (Dean 1967). The introduction of the liquid nitrogen cooled intrinsic germanium detector in 1976 led to more detailed studies of deeper emission, as well as more highly resolved studies of the near band edge BE and FE features. Silicon, though deemed to be an "optically dead" material, has nevertheless become one of the most studied semiconductor materials by PL due to its technological importance to the electronics industry. As seen in Table 2, there have been multitudes of lines that have been identified in bulk Czochralski (CZ) or Float Zone (FZ) Si, and recently in epitaxial Si grown by MBE, MOCVD, Gaseous Source Molecular Beam Epitaxy (GSMBE), and others. PL has been able to detect the presence of a host of impurities, including those that are incorporated as shallow donors (As, P, Sb, Bi) and acceptors (B, Ga, In, Al), those forming isoelectronic centers, as well as those forming complexes with each other and with Si (C, N, H, O). Many of the centers have been found in FZ and CZ grown Si that have been subjected to specific irradiation and/or annealing conditions. Some of these have since been found in MBE grown Si (G, N1-N4, D1-D6, C, I1, I3), which indicates that these centers are characteristic Si defects, and not unique to the method of sample preparation.

In silicon, especially relatively pure silicon, most of the luminescence processes at low temperatures begin with the trapping of excitons that have been formed quickly (nanoseconds) by above bandgap photo-excitation of electron-hole pairs. This

is due to the long lifetime of free excitons, 60 μ sec, in pure Si. (Merle 1978)

Table II : Energies of Si PL lines at 4K (Unless otherwise specified, the information below is from Davies, 1989). All lines are zero phonon unless otherwise specified. The phonon column gives the principal phonon replicas. (TO = 58 meV, TA = 18 meV)

Energy (meV)	Phonons	Description
1170.0		Band gap at 0 K.
1155.7	TO,TA,TO+G	Free exciton (FE), no phonon (NP) line
1152.5		"1F" NP emission
1152		"2F" NP emission
1150.7	TO	Boron (B) BE, NP line
1150.1	TO	Antimony (Sb) BE, NP line
1150.1	TO	Phosphorus (P) BE, NP line. Multiexciton (m) lines at 1146.3, 1143.7, 1141.7, 1140.5, and 1139.3, for m = 2-6.
1149.6	TO	Aluminum (Al) BE, NP line. Multiexciton lines at 1146.3, 1147.7, 1141.5, and 1140.3.
1149.2	TO	Arsenic (As) BE, NP line
1149.0	TO	Gallium (Ga) BE, NP line
1148.8		"a1" and "a2" NP emission from P donor
1146.9	TA	Bismuth (Bi) BE, NP line
1143	TO, TA	"TD" produced in CZ Si by heating to 450 °C
1142.2		H ⁺ implantation and anneal 450-600 °C
1141.0	TO	Indium (In) BE, NP line

1137.3 FE with TA emission

1132.6 Li BE line with TA emission

1131 "Y"; radiation damage in Si:Li

1129.9 Multiexciton line involving two excitons bound to Li donor. Similar lines at 1127.8, 1125.9, 1124.5, and 1123.2 for $m = 3-6$.

1126 "Z"; radiation damage in Si:Li

1122.3 "A"; Line in MBE Si associated with N + Al (Alt 1985, Lightowers 1989b).

1122 "ABC"; Trigonal isoelectronic centre involving N + Al

1117.6 G = 66 "O1"; one of a series including "O2" = 1115.6, "O3"=1113.7, and "O4"=1111.8, Thermally induced in CZ silicon. Possibly bound to free or strain broadening.

1117.5 9.2 "PQR"; In related, associated lines at 1115.9 and 1108.5

1117 "X"; radiation damage of Si:Li

1117 Isoelectronic center involving Be + C

1116.9 "NL1"; associated lines at 1116.1 and 1119.3. Observed after B implantation and 10 min anneal at 450 C.

1108.3 "S"; associated lines at 1104.5, 1100.5,

1092.7, 1090.5, 1088.1, 1085.5, 1070.4,
1067.2, 1060.8, 1034.2, 1023.4, 1014.4,
formed in CZ Si by 100 hour anneal at 500
°C.

1108.1 Produced in CZ Si by neutron irradiation
and annealed at 250 C

1107.2 17 PL from Si after laser annealing.
Associated lines at 1108.2, 1108.7, and
1109.

1106.16 "k"; identified in MBE Si grown at 550
°C (Lightowers 1989b).

1100.6 Radiation damage center produced by He⁺,
H₂⁻, or proton bombardment.

1099.5 FE with LO emission

1097.7 FE with TO emission

1095 "3F"; Exciton bound to modified 1094.5 F
center. Multiexciton emission at 1092,
1090, and 1088.5 for m = 2-4.

1094.5 "F"; Emission of exciton bound to center
formed in CZ Si with [C] > 5x10¹⁶ cm⁻³.
Multiexciton emission at 1092.5, 1090,
1088.5, and 1087 for m = 2-5.

1093.2 Li BE with TO emission

1092.7 B BE with TO emission. Multiexciton lines
at 1090.4, 1088.1, and 1086.5 for m = 2-4.

1091.9 Sb BE with TO emission.

1091.8 P BE with TO emission. Multiexciton lines at 1088.2, 1085.6, and 1083.7 for $m = 2-4$.

1091 As BE with TO emission.

1090.0 Multi-BE with 2 excitons + TO. Similar lines at 1088.5, 1086.8, 1085, 1083.8, 1082.5, 1081.1, for $m = 3-8$.

1086.9 Tl related lines at $T < 20K$. Associated lines at 1081.5 and 1080.4.

1082 Radiation damage of Si:(C+Li); similar to "S" at 1045.

1081.1 Observed in B implanted Si after 400 °C anneal

1080 30.2 "I2"; Monoclinic I center produced by B implant or electron irradiation of Si:B, involves 2 B atoms.

1076 Si:Be isoelectronic center

1074.7 FE with TO + IV(a) emission (Dean 1967)

1067.2 One of S series; see 1108.3

1066.7 Associated with Fe-B pairs in MBE Si (Lightowers 1989b)

1062.5 Produced by n irradiation and 300 °C anneal of CZ Si

1060 Radiation damage at 100 K in high C, O

1052 "O1"; one of series of 3 lines produced

by heating CZ Si for 130 h at 500 °C; O2
1048; O3 at 1042

1051.7 FE with TO + IV(b) emission (Dean 1967)

1050.2 "Ge-2"; Ge-related radiation damage
center; associated line at 1047.2.

1050.1 "Tl PQR"; Tl related lines for T>15,
other lines at 1048, 1042.7.

1049 Radiation damage of Si:Ga and annealed
at 250 °C.

1045 32.2, 47.9 "Q"; Radiation damage of Si:Li;
55.1 associated lines at 1044 and 1048.

1039.8 "I3" or "X"; ion implantation, neutron
damage, and annealed at 500 to 800 K.
Also seen in ion beam doped Si:As grown
by MBE (Rowell 1990)

1037 Produced by ion bombardment

1034.2 One of the S series; see 1108.3 line

1033.2 FE with TO + G emission (Dean 1967)

1025 Produced in electron irradiated FZ Si:Li
and annealed at 450 C.

1023.4 One of the S series; see 1108.3 line.

1018.9 TA,22,51, "I1" or "W"; Ion implantation or similar
56,60,70.3 damage line. Trigonal center. Also seen
in low temp MBE Si_{1-x}Ge_x. (Noel 1990)

1014.8 Like 1018.9 "W" line but produced with Ne

implantation.

1014.7 7 "Cu"; Cu-related trigonal center

1014.4 One of the S series; see 1108.3 line

1012.6 "D6" dislocation related band (Sauer,
1985)

1012 Line like 1018.3 "W", but produced by He
implantation.

1011.7 FE with TO+G+IV emission (Dean 1967)

1010.3 15 Au related center

1009.7 Line like 1018.3 "W", but produced by Ar
implantation.

1004.8 Line like 1018.3 "W", but produced by Kr
implantation.

1003.7 Rhombic I center produced by neutron
irradiation and 400 °C anneal.

1000 Produced by Xe implantation.

997 "D4" dislocation related center (Sauer
1985)

990+/-10 Ion implantation damage and hydrogenation

996.8 Produced by neutron irradiation and
annealed at 150 °C

991.37 "j"; Observed in MBE Si grown at 550 °C;
annealed out at 300 °C (Lightowers
1989 a and b)

988.8 Produced by neutron irradiation and

annealed at 375 °C

977.8 Observed in Si:S

969.5 72 "G"; Monoclinic I center involving two
C and one Si atom

968.7 FE with TO+2G emission (Dean 1967)

967.4 Produced by neutron irradiation and
annealed at 150 °C

965.2 "I"; Produced by 450 °C heating of CZ Si

957 Produced in CZ Si by 180 h at 450 °C or
by irradiation damage below 200 °C

956.9 Perturbed form of 969 "G" line

953.9 Perturbed form of 969 "G" line

953 Perturbed form of 969 "G" line

953 "D5" dislocation related band (Sauer,
1985)

951.2 Perturbed form of 969 "G" line

949.9 "F"; C-related radiation damage center;
monoclinic I symmetry

947 Produced by radiation damage and 450 C
anneal

945.8 see 944.8

944.8 10.3,G,
6.4 Observed in Mn+Zn-doped Si;
luminescence from excited state at
945.8

943.7 6.4 "Cu^{*}"; Observed after Cu diffusion;
similar to 1014.7 Cu center; trigonal

center

939 "D3" dislocation related center (Sauer
1985)

935.2 Produced by radiation damage at 20 K in
C-doped FZ Si

935.1 29.4,66.3 "T"; Rhombic I center involving C
produced by radiation damage and annealed
at 450 °C

929.1 C-related radiation damage center

929 59.4 "Ga3", Gallium related defect

926 Radiation damage and anneal at 250 °C of
Si:Ga

925.5 TA,20,63 "H" or "K"; Radiation damage and annealed
at 450 °C in CZ grown Si; monoclinic I
center with C dependence

922.3 Produced by high temperature anneal
involving possibly C+Al

919.8 Radiation damage center involving C

903 "9"; Produced by 300-400 h at 450 °C
in CZ Si; monoclinic I center

900 "D5'" dislocation related band (Sauer,
1985)

897.9 Produced by radiation damage of CZ Si
and annealed at 350 °C

878 Produced by radiation damage and annealed
at 100 °C of Si:Li

875	55.8	"Ga1"; Radiation damage of Si:Ga involving C in a rhombic I center
874		"D2" dislocation related tetragonal center; associated lines at 807, 939, and 997 (Sauer 1985)
868.7		Seen in MBE Si:As (Rowell 1990)
°62.17		"i"; Found in MBE Si grown at 550 °C. Possibly C-N-H related (Lightowlers 1989b). Removed with 700 °C anneal.
861.68		"h"; Found in MBE Si grown at 550 °C. Possibly C-N-H related (Lightowlers 1989b). Removed with 700 °C anneal.
856		Rhombic I radiation damage center produced in Si:C at T<300 K; thermally destroyed at T>300 K
844	14,G	Observed after Cr diffusion into Si:B
836		"Al 1"; Rhombic I radiation damage center produced in Si:Al
829.8	15	Au-related center
812.91		"g"; found in MBE Si grown at 550 °C. Possibly C-N-H related. (Lightowlers 1989b)
812.30		"f"; found in MBE Si grown at 550 °C. Possible C-N-H related. (Lightowlers

1989b)

- 811.1 7.2,9.2,16.5 Rhombic I center produced by Pt
diffusion at 1150 °C
- 810.5 see 811.1
- 807 "D1"; dislocation related tetragonal
center (Sauer 185)
- 805.4 15 Tetrahedral center produced by Pt
diffusion at 1050 °C
- 793.4 3,7 Au-related
- 793.0 see 793.4
- 792.8 see 793.4
- 791.9 see 793.4
- 789.4 TA,65.5,72.5 "C"; Monoclinic I radiation damage
138.1,145 center involving C and O. Also seen
in Si_{1-x}Ge_x layers grown by low temp-
erature MBE. (Noel 1990)
- 785 Produced by radiation damage and
300 °C anneal of Si:Li
- 778.53 "e"; Found in MBE Si grown at 550
°C. Possibly C-N-H related
(Lightowers 1989b)
- 775.1 Room temperature irradiation product in
Si:Al
- 772.4 "N5"; see 745.6
- 768.6 C-related radiation damage center
- 767.4 "N4"; see 745.6. Seen in MBE Si

grown at 550 °C (Lightowlers 1989b).

767.3 TA,18,LA=43 "P"; Monoclinic I C-related center
65.6, 72 produced by radiation damage and
annealing at 450 °C in CZ Si

766.7 Produced by neutron irradiation and
annealing at 375 °C in CZ Si

761.5 "N3"; see 745.6

760.6 "M"; Radiation damage center involving
C

758 "N2"; see 745.6. Seen in MBE Si
(Lightowlers 1989b)

745.6 122.9,71.3 "N1"; Monoclinic I or trigonal center
involving N and C atoms. Seen in MBE
Si (Lightowlers 1989b)

744.9 Seen in MBE Si after irradiation with
2 MeV electrons (Lightowlers 1989b).

737.6 7.5, 10 Observed after Fe diffusion

735.1 see 737.6. Seen in MBE Si (Lightowlers
1989b)

734.7 see 737.6. Seen in MBE Si (Lightowlers
1989b)

707 15 Au-related center

698 TA "a"; Trigonal center in MBE Si (de Mello
1989).

677 Observed after Cr diffusion into Si:Ga

567.9 See 564.7

566.1		see 564.7
565.7		see 564.7
564.7	13, 60	Mn-related tetrahedral center
488		Monoclinic I radiation damage center involving C and O

Near-band-edge PL from Si. Most of the PL lines given above in Table II are from deep centers. Of most importance are the near-band-edge lines due to recombination of free excitons (FE) and excitons bound to shallow donors and acceptors (BE). The FE lines include the no phonon (NP) line at an energy 14.3 meV (the binding energy of a free exciton) below the bandgap plus the various phonon replicas of the NP line that result from phonons emitted along with photons for momentum conservation. The principal phonon replicas are the transverse acoustic (TA), longitudinal optical (LO), and transverse optical (TO) lines that are 18.4, 56.2, and 58.0 meV below the NP line, respectively. (Davies 1989) The ratio of the intensities of these three lines are 0.03: 0.1: 1 for TA: LO: TO. There are also several prominent two phonon and three phonon lines that are evident in PL from Si. These include lines at 1.08 eV and 1.04 eV, that are due to FE emission with one TO and one zone center G phonon, and FE emission with one TO, one G, and one zone edge IV phonon, respectively. Bound exciton lines (BE) and emission from bound

multi-exciton complexes (BMEC) include lines corresponding to each of the FE lines with energies below the FE components, the difference being the binding energy of the exciton to the shallow center, between 2.7 and 7 meV. (Thewalt 1982)

PL from Bulk $\text{Si}_{1-x}\text{Ge}_x$ The definitive works on PL from bulk $\text{Si}_{1-x}\text{Ge}_x$ alloys are those by Weber and Alonso and the earlier work of Mitchard and McGill. (Weber and Alonso 1989, Mitchard and McGill 1982) The Mitchard and McGill study was limited to samples with $x=0.1$, but these samples showed an important effect applicable to $\text{Si}_{1-x}\text{Ge}_x/\text{Si}$ superlattices - the bound exciton lines were broadened due to the effects of alloy fluctuations in the alloy layers. The Weber and Alonso study covered the full range of $0 < x < 1$, and presents several key pieces to the understanding of PL from $\text{Si}_{1-x}\text{Ge}_x/\text{Si}$ superlattices. It was shown that no phonon lines, which are forbidden in

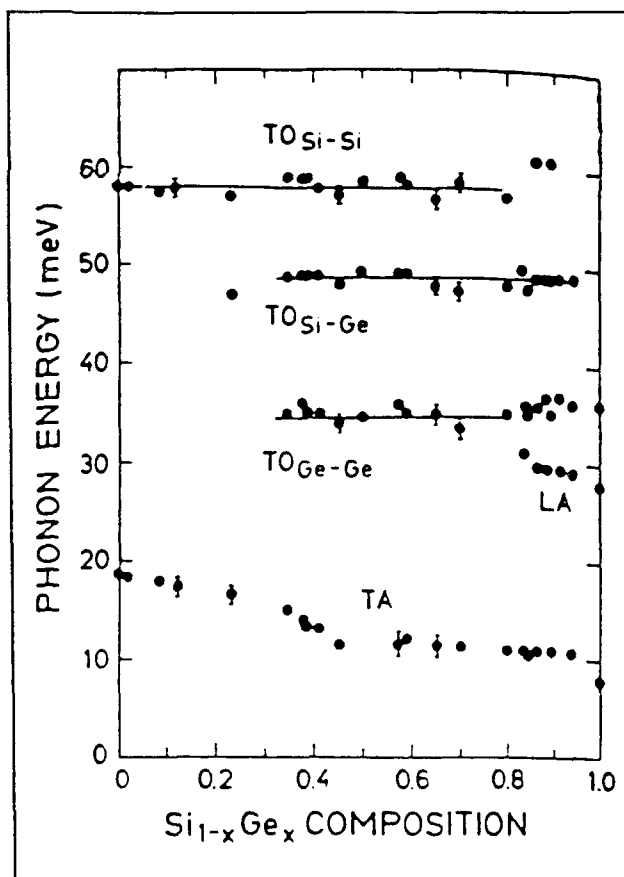


Figure 21: $\text{Si}_{1-x}\text{Ge}_x$ phonon energies vs. alloy concentration (Weber 1989)

pure Si samples, are quite strong in $\text{Si}_{1-x}\text{Ge}_x$, due to the statistical distribution of Si and Ge atoms acting as momentum conserving scattering centers. In addition, the phonon replicas of the no phonon lines were used to determine the phonon energies as a function of x ; these values are shown in Figure 21. For $x < 0.85$ the energies of $\text{TO}_{\text{Si-Si}}$, $\text{TO}_{\text{Si-Ge}}$, $\text{TO}_{\text{Ge-Ge}}$, and TA were found to be 58.0 meV, 49.0 meV, 34.5 meV, and 18.7 meV, respectively.

PL from $\text{Si}_{1-x}\text{Ge}_x/\text{Si}$ and Si/Ge superlattices PL from $\text{Si}_{1-x}\text{Ge}_x/\text{Si}$ and Si/Ge superlattices has been studied only recently, because of difficulty getting samples of sufficient quality to obtain usable signals. With the early theoretical predictions of the possibility of obtaining a direct band gap in monolayer Si/Ge superlattices, (Gnutzmann and Clausecker 1974, Gell 1988, Froyen 1987, Satpathy 1988) attention centered on obtaining PL from these structures. The first report of PL from Si/Ge superlattices was reported by Eberl, et al. (Eberl 1987) on strain symmetrized samples. Strain was symetrized by growing the Si/Ge superlattice on a thick partially relaxed $\text{Si}_{1-x}\text{Ge}_x$ buffer layer which resulted in growth of the superlattice at a lattice constant intermediate between that of silicon and germanium. Thus both the silicon and germanium layers were strained, but with the overall strain for each period close to zero. The same group continued to report results from similar structures. (Zachai 1988, Zachai 1990a&b) The strong PL at 0.85 eV obtained

from these samples was claimed to be due to direct or pseudodirect zone-folded free exciton transitions. However the similar intense broad features were later seen in $\text{Si}_{1-x}\text{Ge}_x$ layers that were too thick for zone-folding arguments to apply. (Noel 1990a) Thus it is believed that the strong luminescence seen by Zachai, *et al*, originated in the thick strain relaxed buffer layer, though the controversy has not yet been completely resolved. (Schmid 1990b, Zachai 1990a) The broad bands observed by Noel *et al* were found in samples grown by MBE at 400 °C and were substantially more intense with annealing. The typical annealing condition for the strongest luminescence was RTA for 30 sec at 625 °C. The broad bands were 120 meV below the strained $\text{Si}_{1-x}\text{Ge}_x$ band gap, and were reported not to depend on sample structure. The authors also determined from photoluminescence excitation spectroscopy (PLE) that the main luminescence peak did not involve phonons, though there may have been a TO phonon replica convoluted with the main peak in some cases. Later, the same group proposed that the origin of the broad luminescence was isoelectronic centers related to Ge complexes within the $\text{Si}_{1-x}\text{Ge}_x$ layers. (Houghton 1991b) The broad band emission was found only in MBE-grown Si-Ge.

Beginning with the first PL studies of Si/Ge and $\text{Si}_{1-x}\text{Ge}_x/\text{Si}$ superlattices and heterostructures, the goal has been to find identifiable near-band gap excitonic emission that could be used to verify theoretical determinations of band gap and other

properties such as phonon energies, similar to the results in bulk $\text{Si}_{1-x}\text{Ge}_x$. In MBE-grown Si/Ge and $\text{Si}_{1-x}\text{Ge}_x$ superlattices, near-bandgap excitonic emission has not been identified, though some claims have been made. The claims of excitonic emission from Si/Ge superlattices have been mentioned above. (Eberl 1987, Zachai 1988, Zachai 1990a&b) In addition to the above claims of the German group, there have been similar claims of superlattice band edge emission from MBE Si-Ge by several other groups. (Rowell 1987, Montie 1989b, Okumura 1989, Montie 1990, Glaser 1990a&b, Kallel 1990) In several cases, emission was similar to the broad band emission discussed above. In others there were sharp bands, but the peaks were at energies of known silicon dislocation-related bands, D1-D6. (Sauer 1985) In no cases did the authors show conclusive evidence of excitonic emission. Terashima *et al* reported near-bandgap PL from MBE-grown $\text{Si}_{1-x}\text{Ge}_x$ single epitaxial layers grown below the critical thickness for $x=0.04$ and $x=0.15$. (Terashima 1990) Radiative recombination of bound excitons and free excitons was found. In addition defect-related L bands, similar to those seen in bulk $\text{Si}_{1-x}\text{Ge}_x$ were identified. (Weber and Alonso 1989, Mitchard and McGill 1982).

There have been recent reports of near-band gap excitonic emission from Si-Ge structures, either from $\text{Si}_{1-x}\text{Ge}_x$ strained layers or $\text{Si}_{1-x}\text{Ge}_x/\text{Si}$ superlattices grown by techniques other than molecular beam epitaxy, such as chemical vapor deposition or liquid phase epitaxy. Sturm *et al* reported near-bandgap PL from

$\text{Si}_{1-x}\text{Ge}_x/\text{Si}$ superlattices grown by a combination of rapid thermal processing and chemical vapor deposition (RTCVD). (Sturm 1991) The emission consisted of a strong no phonon (NP) component and phonon replicas involving TA, $\text{TO}_{\text{Si-Si}}$, $\text{TO}_{\text{Si-Ge}}$, and $\text{TO}_{\text{Ge-Ge}}$ phonons. Recombination of free excitons (FE) and excitons bound to shallow impurities (BE) were identified. The BE emission had lifetimes between 375 and 420 ns, similar to BE lifetimes in Si. From PLE the BE binding energies were determined to be 5 meV, also in agreement with Si BE binding energies. A comprehensive study of PL from $\text{Si}_{1-x}\text{Ge}_x$ single layers grown by liquid phase epitaxy has recently been reported. (Robbins 1992) In this study near-bandgap features similar to those reported by Sturm *et al* were found, but in this case the FE and BE components were clearly resolved. From this study, an analytical expression for the exciton energy gap was determined to be (for $0 < x < 0.24$)

$$E_x(x) = 1.155 - 0.874x + 0.367x^2 \text{ eV.} \quad (27)$$

In addition an expression for the exciton binding energy that takes into account the effects of strain was derived.

Near-band gap emission from single $\text{Si}_{1-x}\text{Ge}_x$ layers was reported recently by another group. (Dutarte 1991) Once again the samples were grown by RTCVD. In this case the samples consisted of a single buried fully strained $\text{Si}_{1-x}\text{Ge}_x$ layer, with $x = 0$ to 0.22. The emission consisted of a NP line and phonon replicas similar to those found by Sturm *et al*. The buried

$\text{Si}_{1-x}\text{Ge}_x$ layer samples with cap layers were compared to samples without cap layers that did not show excitonic emission from the epitaxial $\text{Si}_{1-x}\text{Ge}_x$. This comparison indicates that nonradiative surface recombination is minimized by the use of Si capping layers and/or that exciton confinement is required to see excitonic features from Si-Ge structures.

In summary, the PL from $\text{Si}_{1-x}\text{Ge}_x$ layers or $\text{Si}_{1-x}\text{Ge}_x/\text{Si}$ superlattices grown by MBE seems to be different than that of samples grown by other methods. (Houghton 1991b) The MBE-grown samples are dominated by broad PL bands that are defect-related, while the CVD or LPE samples that are grown at higher temperatures do not have broad PL bands, but have FE and BE lines near the bandgap. This has led to some speculation that the broad bands in MBE-grown samples are a convolution of the narrow FE and BE lines and their phonon replicas that have been broadened by some mechanisms. (Rowell 1991) As mentioned above it has also been suggested that the broad bands are due to isoelectronic emission from Ge-complexes. (Houghton 1991b) In either case, it is clear that a better understanding of the broad PL bands and their relationship to the near-bandgap excitonic emission is required.

Isoelectronic bound exciton emission from Si and Si_{1-x}Ge_x

In indirect band gap semiconductors, the radiative decay of excitons bound to isoelectronic impurities and complexes is an important luminescence mechanism. The most celebrated of these has been GaP:N, (Thomas 1963) but isoelectronic bound exciton (IBE) emission has also been seen in Si, having first been identified in 1979 in an indium related complex. (Mitchard 1979) Since its first observation in Si, IBE emission has been seen in Si:Be, Si:Cu, Si:In, Si:Li, Si:S, Si:Se, Si:Zn, and Si:Tl. (Henry 1981, Weber 1982, Lightowlers 1984, Watkins 1984, Lightowlers 1985, Brown 1986a&b, Bradfield 1988, Modavis 1991, M.O. Henry 1989, Singh 1989) Isoelectronic centers in silicon are different in one respect than GaP or other indirect bandgap materials. A single group IV impurity does not create bound exciton states in silicon; multiatom states are required. (Bradfield 1988) IBE emission in silicon is characterized by a long radiative lifetime, from microseconds to milliseconds in some cases. This long lifetime is due to the very low probability of competing nonradiative Auger processes. Isoelectronic centers bind excitons by tightly binding one carrier, usually electrons, and loosely binding the other in a hydrogen-like orbit. Thus the center is usually an electron or hole trap, with a fairly high capture cross section for excitons (or electrons or holes). This high capture cross section, and the long radiative lifetime, combined with the absence of competing nonradiative processes

make IBE emission a promising method of obtaining light emission from silicon and silicon-like structures.

III. EXPERIMENTAL

Sample Growth

The samples were grown by molecular beam epitaxy (MBE) in a VG-V80 system. Silicon and germanium were evaporated by Temescal CV 14 electron beam evaporation sources. The Si(100) substrates were first chemically cleaned by a modified Shiraki procedure, the grown oxide was evaporated at 850-900 °C in the deposition system. A 100 nm silicon buffer layer was grown at 650 °C at a rate 1.5 Å/sec. The superlattices were grown at 500 °C, with the alloy deposition rate of 2 Å/sec. The superlattice structures were grown 500 nm thick with a final silicon capping layer of 30 nm. Table III lists the sample structures investigated, which were verified by X-ray diffraction.

Post-Growth Annealing

After cleaning the samples, as described below, the samples were annealed post-growth in N₂ gas environment using Rapid Thermal Annealing (RTA). The annealing temperatures ranged from 525 °C to 850 °C. The annealing times ranged from 15 seconds to 2 minutes. The RTA was performed at the Wright Laboratory Solid State Electronic Technology Directorate.

Photoluminescence Experimental Setup

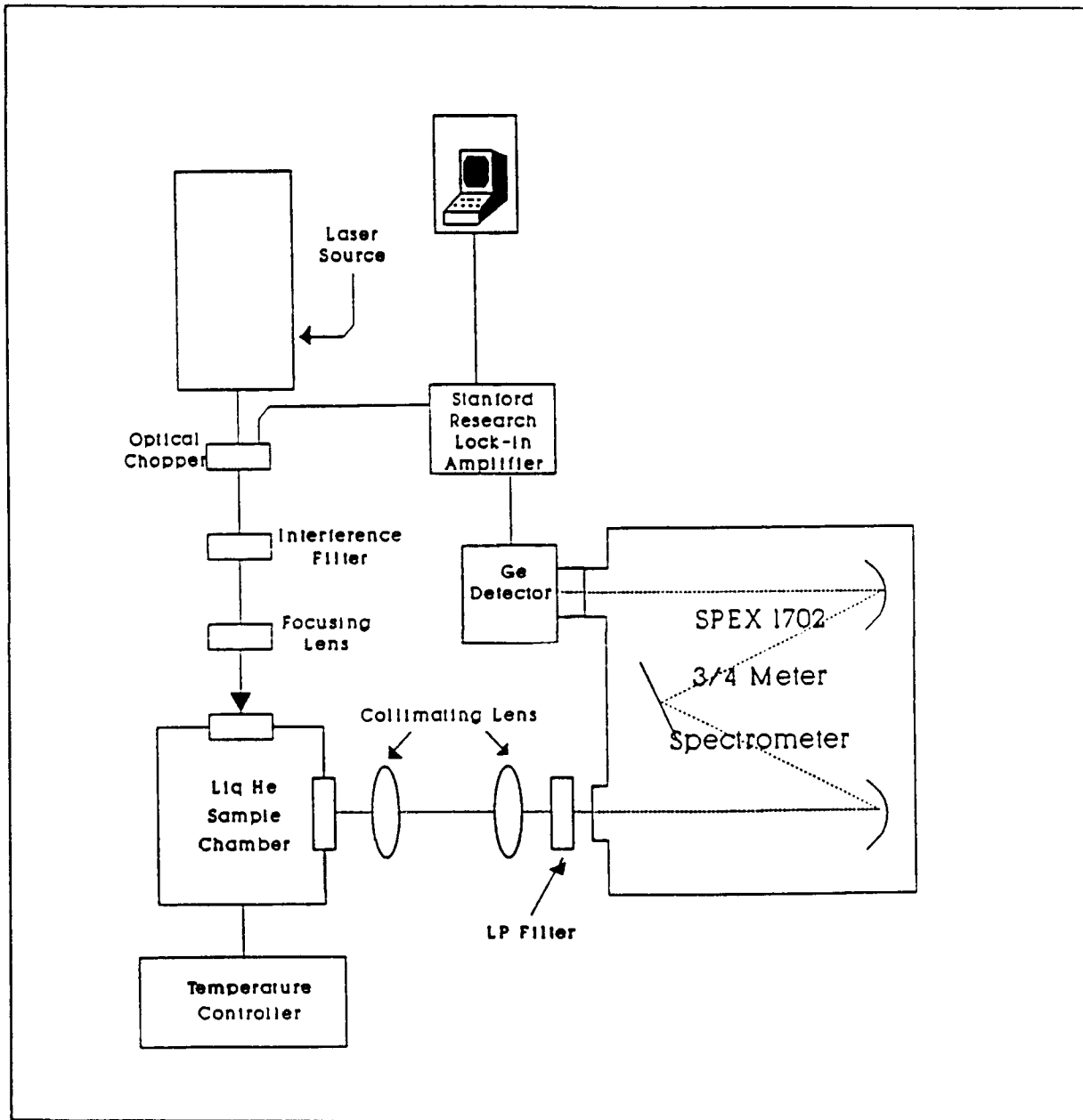


Figure 22: Photoluminescence Experimental Setup

The setup used for the photoluminescence measurements is given in Figure 22. The samples were mounted in a strain free manner using rubber cement on a copper cold finger inside a Janis

10DT optical cryostat. The liquid helium could be pumped by a mechanical pump to obtain sample temperatures below 4.2 K, and thus the cryostat allowed variation of the sample temperature from 1.6 K to room temperature using a heater. The sample temperature was monitored with Lakeshore 100DT silicon diode temperature sensors and controlled with a Lake Shore DRC-82C temperature controller. The PL was collected into a SPEX 1702 3/4 meter spectrometer and detected by a North Coast 817L(or S) liquid nitrogen cooled germanium detector. The entrance and exit slit widths of the spectrometer were nominally set at 1000 and 2000 microns, respectively so that the resolution was 2.5 meV at 1 eV. The signal was obtained using a Stanford Research SR530 lock-in amplifier and preamplifier and fed to a Zenith 248 (IBM AT compatible) PC using Labtech Notebook data acquisition software. Excitation was provided with either a Spectra Physics Series 2000 krypton or argon ion laser, that was chopped with a Stanford Research SR 540 optical chopper.

Photoluminescence Experimental Procedures

System Alignment and Calibration Before measurements could be taken, the spectrometer, detector, and optics had to be aligned. This was done using a He-Ne laser. Once the system was aligned two calibrations were performed. First, a krypton calibration lamp spectrum was taken to calibrate the spectrometer

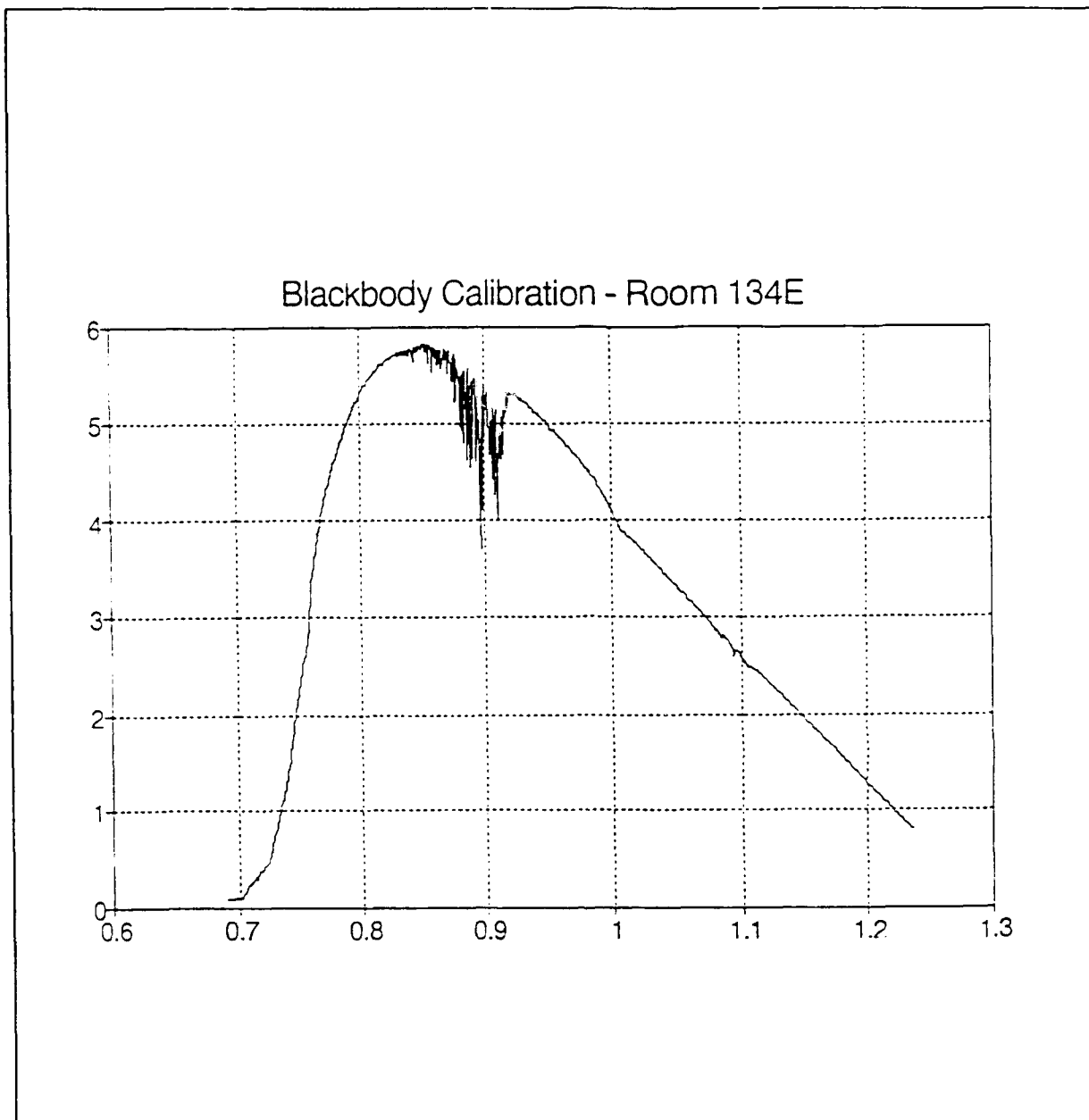


Figure 23: Response of System to 1000 °C Blackbody

dial setting to the known positions of the krypton lines. Krypton lines over the full range over which PL data was to be taken were used from 1.0 to 1.8 microns. Second, a blackbody source at 1000°C was used to determine the system response. The response of the system to the source is shown in Figure 23. The

system response was determined by dividing the blackbody output of the system by the known output from a blackbody source at 1000 °C. As can be seen in Figure 23, there is a strong absorption at 0.9 eV that is due to water vapor in the path between the sample chamber and the detector.

Sample Preparation and Mounting The samples were received from the Naval Research Lab in large pieces, usually 1/6 of a 3 inch wafer. These were cut into smaller 3-4 mm square pieces for mounting on the cold finger. After cutting but prior to mounting the samples were cleaned using a three step procedure: (1) clean in trichloroethylene, (2) clean in methanol (3) wash with deionized water. The cleaned samples were mounted, usually four at a time on the copper cold finger using a small amount of rubber cement on the upper edge of the sample. During data acquisition the laser spot was placed on the lower half of the sample, to avoid complications with the effects of strain on the PL.

System Start up Procedures To prepare the system for cool down and data acquisition, the jacket between the LN₂ and liquid helium dewars had to be evacuated to insure that helium could be held for long periods of time. The jacket was evacuated using an Alcatel turbomolecular pump backed by a mechanical pump. Care

had to be taken to insure that oil from the mechanical pump did not get inside the dewar. After pumpdown the system was cooled down by first adding LN₂, then adding liquid helium at least four hours after adding LN₂.

PL Measurement Procedures After the samples were mounted and the system was cooled down, the PL measurements were taken. The samples were typically arranged in a 135° geometry, which has been found to be the best arrangement for obtaining PL from the samples where the excitation is primarily near the surface (which applies to most PL measurements regardless of excitation). (Davies 1989) The PL signal, once found, was optimized by adjusting excitation beam position, optics between the sample and the spectrometer, chopper speed, and phase of the lock-in amplifier.

Choice of Laser Excitation The samples were excited with the 647 nm Kr line, 488 or 514 nm Ar line, or 337-357 nm Kr multiline, allowing the variation of penetration depth from 5 μm to .01 μm. Since the superlattice regions were 0.5 microns thick, PL features due to the superlattice region could be isolated from those due to the Si substrate or the buffer layer by using the UV excitation source.

IV. RESULTS AND DISCUSSION

Dependence of PL on excitation

The four laser excitation sources used, 647 nm krypton, 514 nm argon, 488 nm argon, and 337-357 nm krypton UV multiline, each had a different penetration depth. The penetration depth is determined from Beer's Law

$$I(x) = I(0) e^{-\alpha x} \quad (28)$$

where α = absorption coefficient at wavelength
of excitation beam

$I(x)$ = Intensity as a function of depth in sample,
and $I(0)$ = Intensity at surface.

The penetration depth is the depth at which $I(x)/I(0)=1/e$, and thus is the depth in which most of the electron-hole pairs are created. The penetration depths for 647, 514, 488, and 350 nm excitation are 5 μm , 1 μm , 0.9 μm , and 100 angstroms, respectively. Most of the electron-hole pairs created in the excitation region quickly form excitons. These free excitons can diffuse through the material depending on the concentration of defects or centers capable of trapping them, because of the long radiative lifetime for free excitons in indirect band gap materials, 60 μs for bulk Si. The long lifetime of free excitons results in a long diffusion length for free excitons, as high as 430 μm in material with a low defect

concentration (Davies 1989). To estimate the free exciton diffusion length in silicon, the PL from the back of several samples was compared to the PL from the front, using UV excitation, and the results are shown in Figure 24. The excitation of the back was absorbed in the silicon substrate, while excitation of the front was absorbed in the 0.5 micron thick superlattice region. The PL from the front contained broad bands from the superlattice region and little or no substrate or cap layer luminescence. The PL from the back contained strong substrate related luminescence as expected, but also contained a reduced broad band from the superlattice region which indicated that excitons created in the substrate had diffused to the superlattice region where they subsequently recombined via the center responsible for the broad band. The thickness of the substrate was 0.5 mm, or 500 microns, which is close to the previous estimates for the free exciton diffusion length in Si. Diffusion through the superlattice, becomes a more complicated issue, even ignoring capture of excitons by defects, because of the potential barriers imposed by the superlattice potential. The free exciton Bohr radius, about 40 angstroms in Si, gives a relative measure of the exciton diffusion through the superlattice. For wells (Ge or $\text{Si}_{1-x}\text{Ge}_x$) of the same dimensions or less than the free exciton Bohr radius, it is expected that there will be significant diffusion of excitons through the superlattice and the resulting PL will be from the upper superlattice layers. For wells larger than the Bohr radius, it is expected that the free excitons will become confined to the

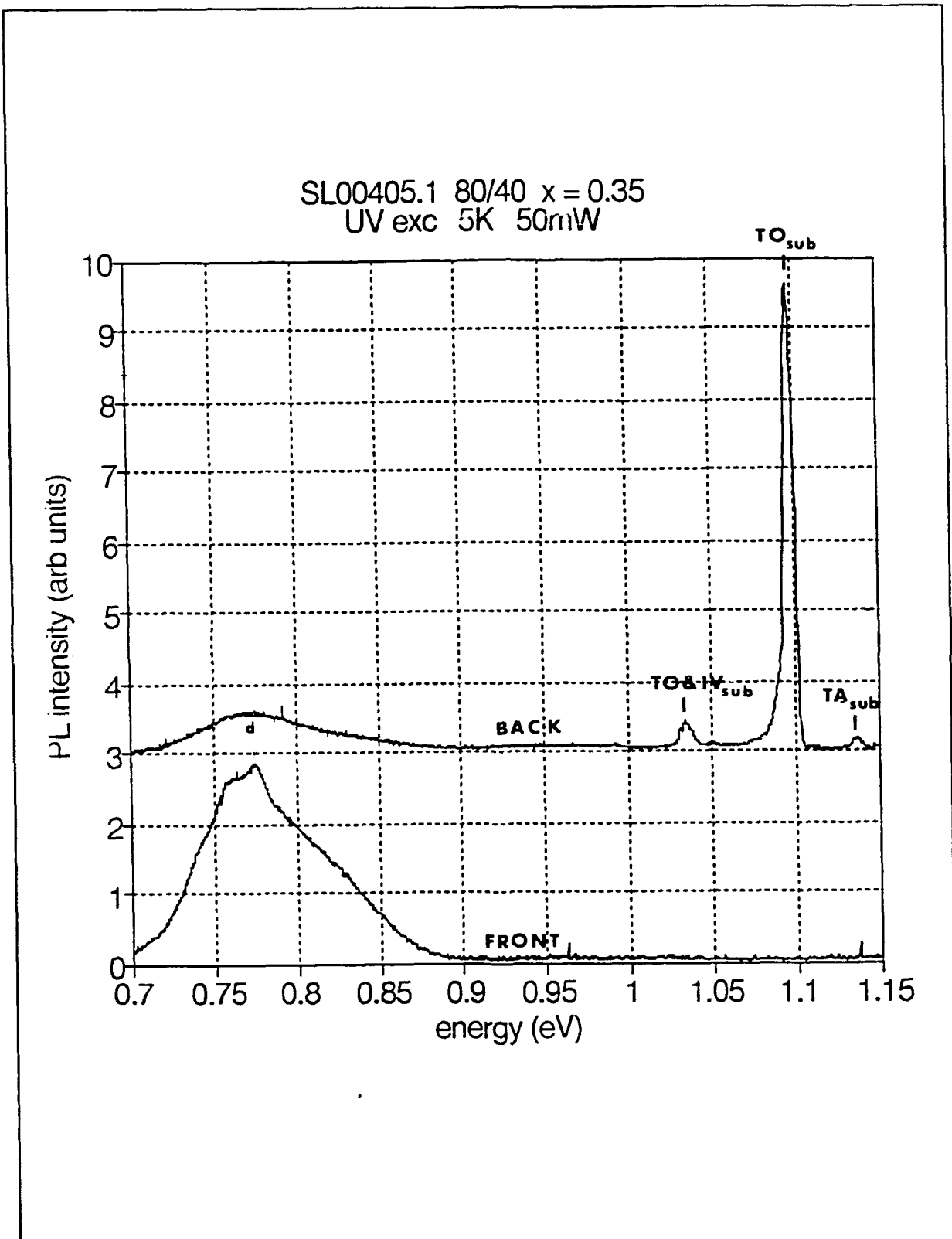


Figure 24: Comparison of front vs. back PL, SL00405.1

first few wells and the resulting PL will only be from the upper layers of the superlattice.

Since it is well-known that interfaces in superlattices are an effective getterer for impurities and other defects, it is expected that the superlattices layers closest to the surface to have a lower concentration of defects than the layers closest to the superlattice/substrate interface. Visible laser excitation, either 647, 514, or 488 nm is absorbed by both the superlattice and substrate areas and exciton diffusion is not a significant issue since all areas (substrate, buffer, superlattice, and cap) are excited. However, UV excitation is nearly fully absorbed in the silicon cap region, and requires exciton diffusion in order to look at recombination in the superlattice region. The advantage of UV excitation is that nearly all of the excitons created in the excitation region would be captured in the superlattice region. As long as there are centers capable of radiative recombination in the superlattice region, it is assured that there will be a high density of excitons to supply those recombination processes. This is more favorable than the case in which excitons are created throughout the superlattice and substrate regions resulting in a lower relative exciton density in the superlattice region.

In Figures 25-31 the PL for various excitation wavelengths are compared. In sample SL00201.1 (Figure 25), the PL from UV excitation does not contain the same structure as the PL from the

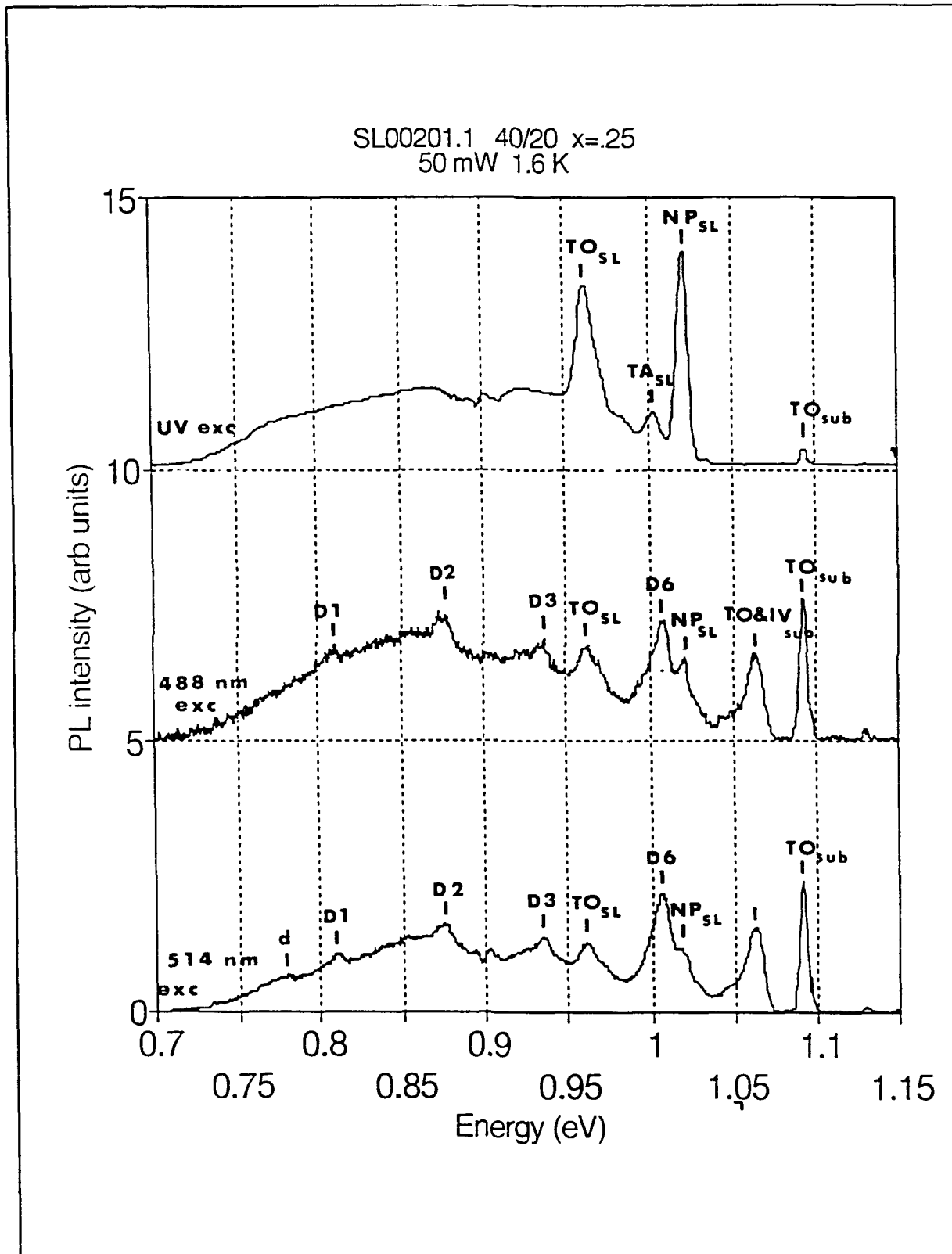


Figure 25: Dependence of PL on excitation wavelength - SL00201.1

more deeply penetrating 488 nm (blue) and 514 nm (green), although a broad band emission is seen in all three samples. The additional lines from blue and green excitation are D-lines (D1-D5) seen previously in highly dislocated bulk and epitaxial silicon. It is apparent from these excitation dependent spectra showing D-lines for the more deeply penetrating excitation that the dislocation dependent D-lines originate from deep within the sample structure, most likely at the substrate/buffer interface or in the buffer itself. The substrate related peaks, $TO_{\text{substrate}}$ and $TO+IV_{\text{substrate}}$, are much stronger in the 514 and 488 nm excitation cases than the UV excitation case. The spectrum from UV excitation has much stronger superlattice related sharp peaks, NP_{SL} , TA_{SL} , and TO_{SL} , that will be discussed in more detail later. The 514 nm excitation also produces a d line at 770 meV that will be discussed later.

In Figure 26 (SL00206.1), UV excitation produces sharp superlattice related peaks, TO_{SL} , TA_{SL} and NP_{SL} , that are not seen with 488 or 514 nm excitation. The broad PL band is seen for all three excitations. In addition, d line luminescence is seen at 770 meV for UV excitation. Substrate related peaks near 1.1 eV, $TO_{\text{substrate}}$, are seen in all three spectra, but are stronger for optical excitation.

In Figure 27 (SL00405.1), all three spectra have a broad band from 0.7 to 0.9 eV, with a d line at 770 meV on top of the broad

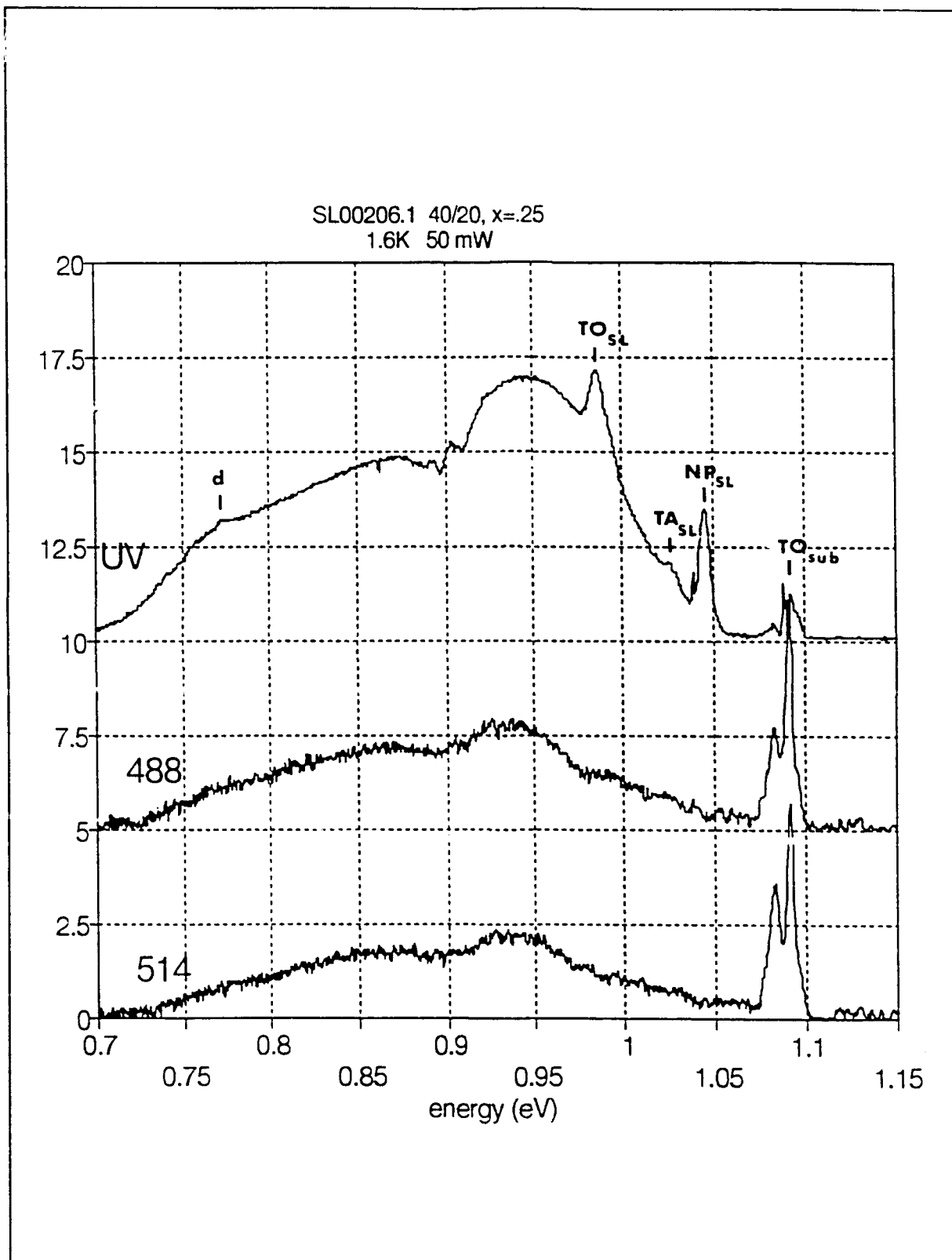


Figure 26: Dependence of PL on excitation wavelength - SL00206.1

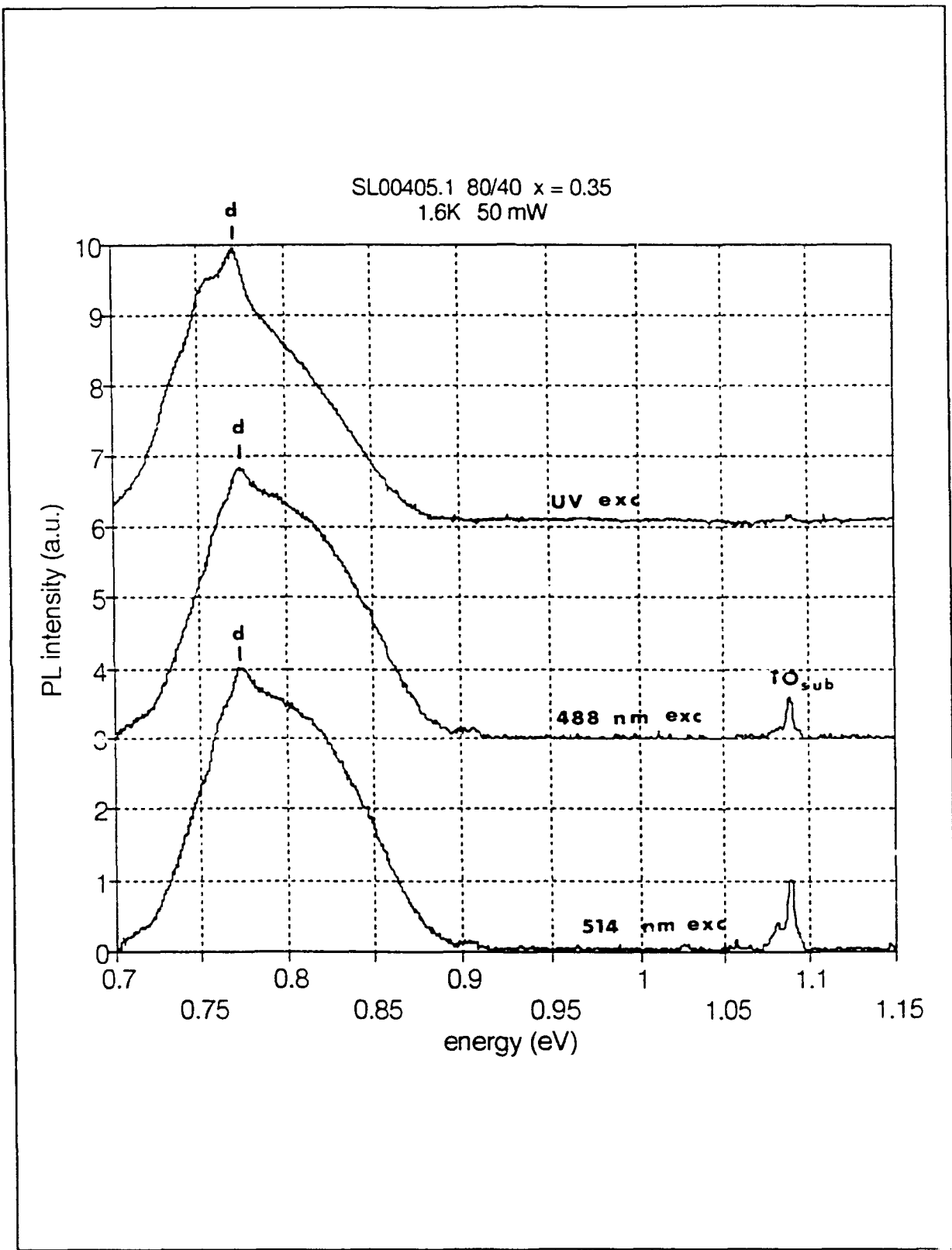


Figure 27: Dependence of PL on excitation wavelength - SL00405.1

band. There are slight differences in the shape of the broad band for the three different excitations, but these may be due to differences in the system response between the UV and the optical excitation spectra. The UV spectrum was taken in Room 134E while the 514 and 488 nm spectra were taken in Room 134C.

In Figure 28 (SL10322.2), the broad band is also dependent upon the excitation. The UV excitation spectrum has its peak at 870 meV with perhaps a second peak at 940 meV. The 514 nm excitation spectrum has the 940 meV peak is dominant, with the 870 peak reduced. Superlattice related sharp peaks, TO_{SL} and NP_{SL} , are seen in both spectra, but are much stronger compared with the broad PL band using UV excitation.

In Figure 29 (SL10206.1), the broad band at 860 meV has the same shape for UV, 514 nm, and 488 nm excitation. Substrate related peaks between 1 and 1.1 eV, are seen for 488 nm and 514 nm excitation, but not for UV excitation. The substrate for this sample was heavily-doped, which is the reason for the broad substrate related peaks that are different than most of the other samples investigated.

In Figure 30 (SL00326.1), the spectrum for UV excitation is dominated by a broad band from 0.7 to 1.1 eV, while the 514 and 488 nm excitation spectra are dominated by the peaks near 1.1 eV, $TO_{substrate}$, from FE and BE emission with TO phonon emission. Peaks

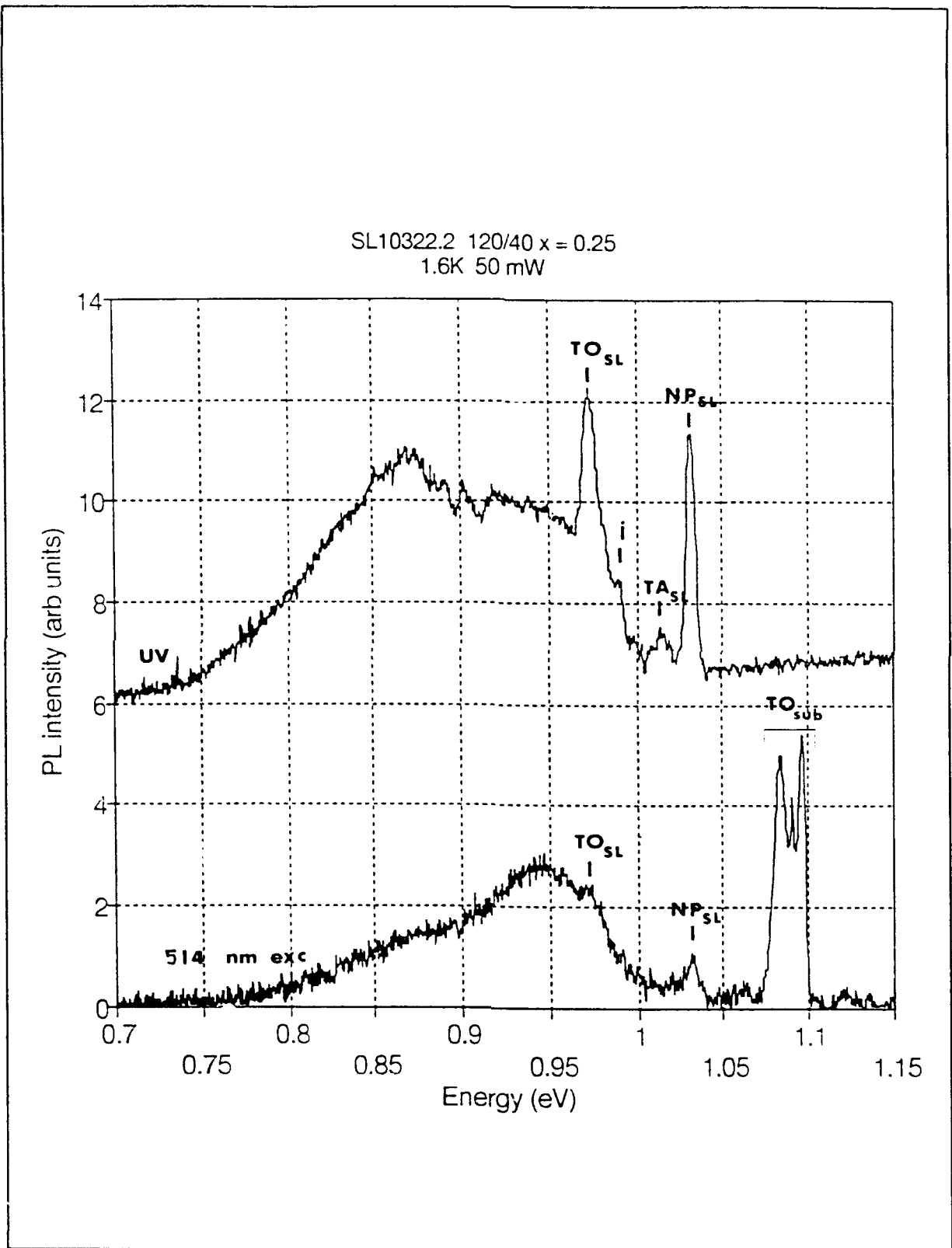


Figure 28: Dependence of PL on excitation wavelength - SL10322.2

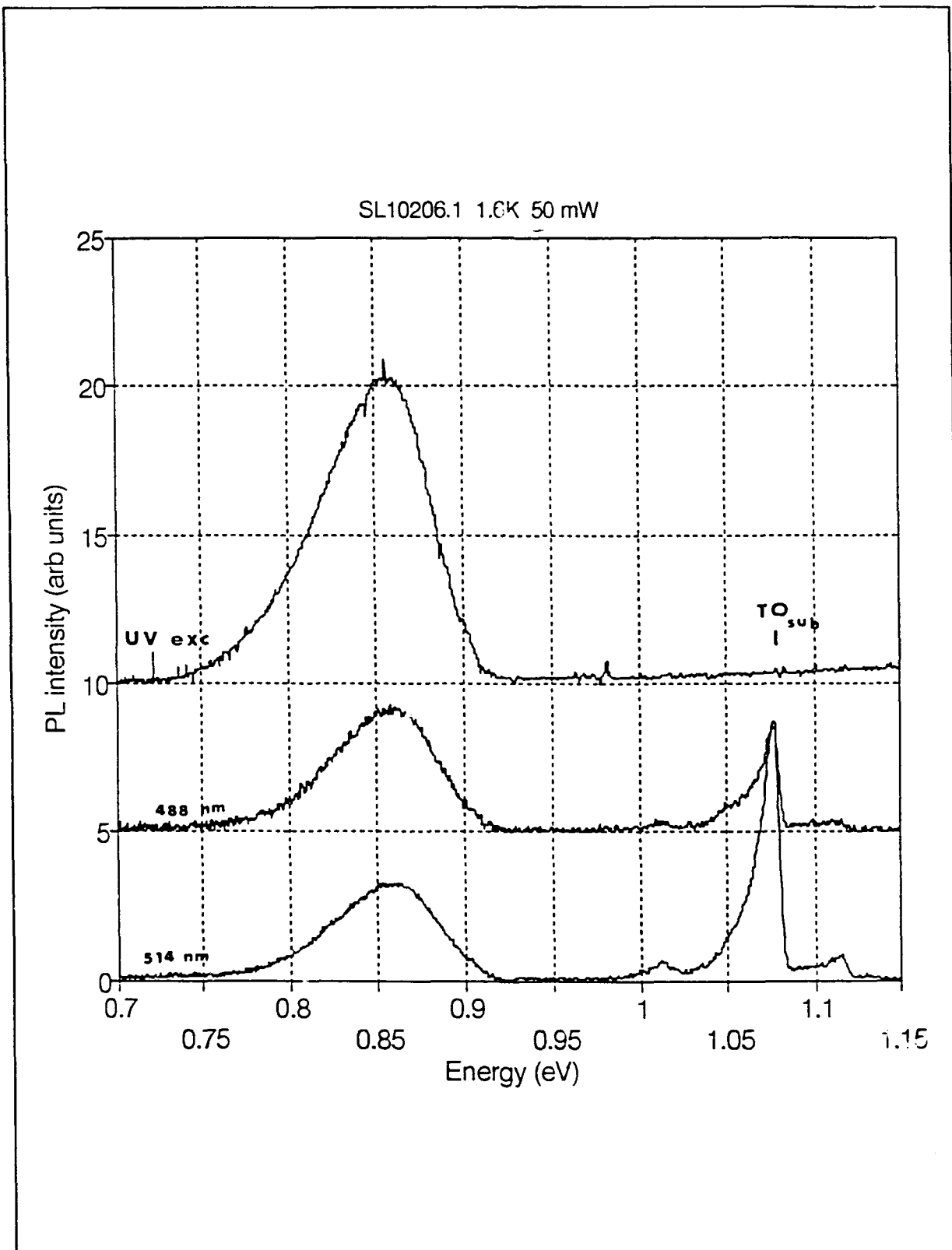


Figure 29: Dependence of PL on excitation wavelength - SL10206.1

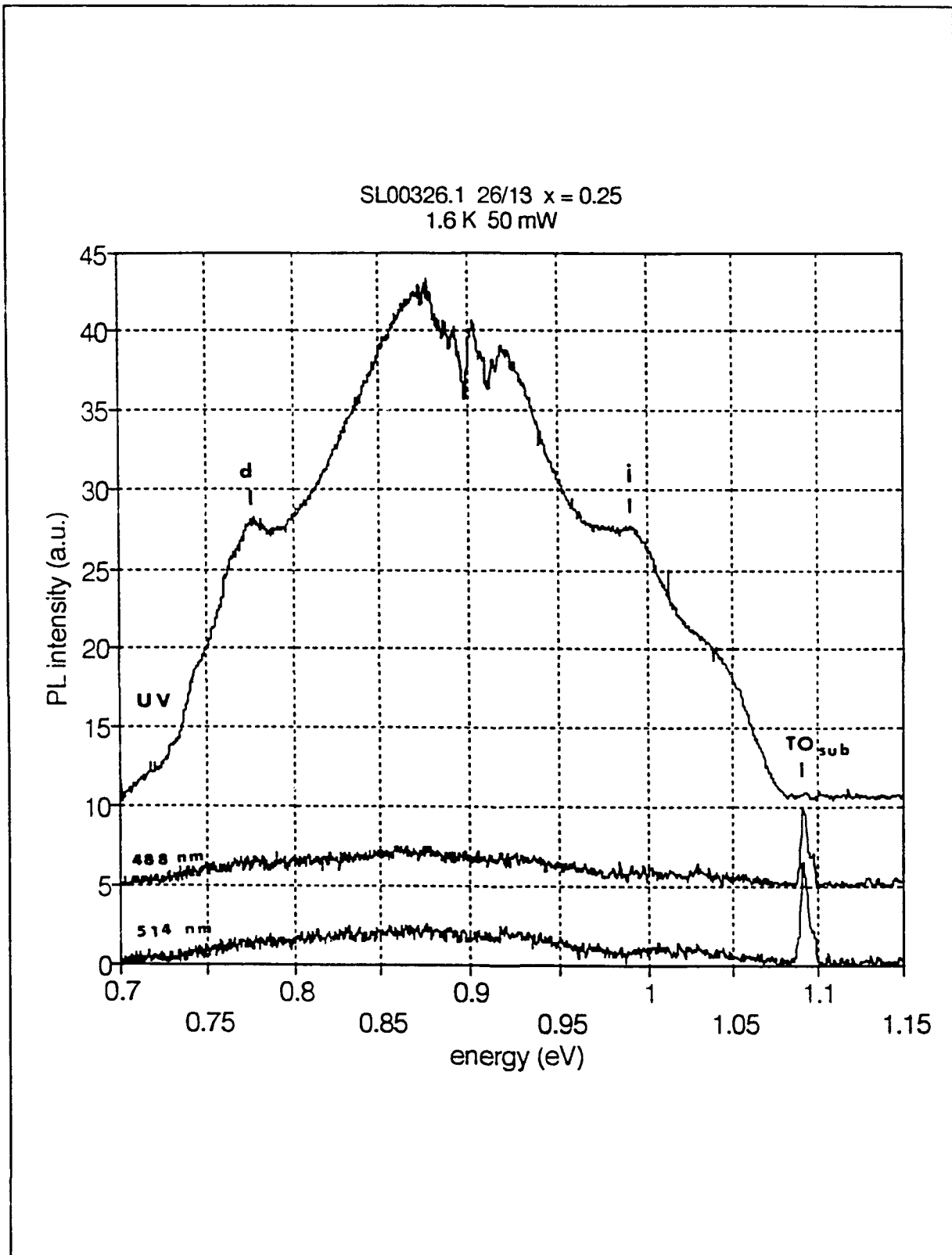


Figure 30: Dependence of PL on excitation wavelength - SL00326.1

at 775 meV (d) and 990 meV (j) are also seen for UV excitation.

In Figure 31, SL10531.2, all three spectra have the broad PL band near 0.8eV, but the spectra for 488 and 514 nm excitation have dislocation lines D1 and D2 on top of this broad band which appears to shift the broad band peak position. The substrate related peaks, $TO_{\text{substrate}}$ are seen only with 488 or 514 nm excitation.

In every case in Figures 25-31, the substrate peaks are strong for 514 or 488 nm excitation, but are weak or nonexistent for UV excitation, showing that in the UV excitation case, most of the recombination is occurring in the superlattice region. The spectra obtained with UV excitation that contain substrate peaks are most likely due to part of the excitation beam hitting the edge of the sample and exciting substrate PL that is collected inefficiently due to the collection geometry. It was difficult to insure that the invisible UV beam hit the center of the samples, which were cut small because of practical limitations. It was necessary to take samples from the center area of the wafer for direct comparisons of samples within the same wafer, which limited the size of the pieces cut, in order to have enough samples available.

The luminescence at energies below the characteristic substrate luminescence is mostly due to recombination in the superlattice. The exceptions to this are the D-line luminescence in samples SL00201.1 and SL10531.2 (Figures 25 and 31), and

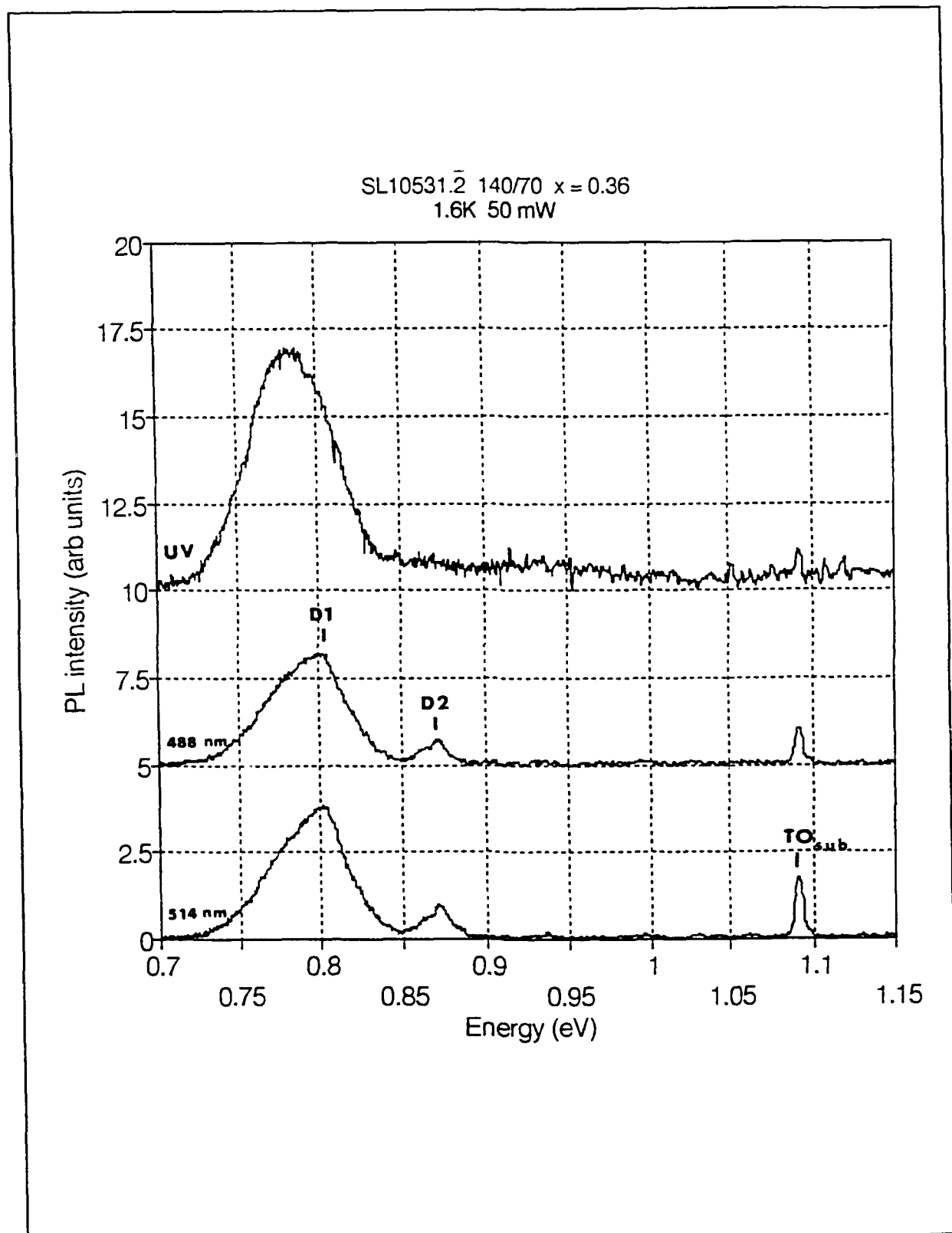


Figure 31: Dependence of PL on excitation wavelength - SL10531.2

possibly the 770 meV PL luminescence in SL00206.1, SL00405.1, and SL00326.1 (Figures 26, 27, and 30 respectively). Note that in each case the superlattice luminescence for the UV excitation is of the same intensity or greater than that for visible (514 or 488 nm) excitation. All of the intensities are roughly comparable. The laser power in all cases was 50 mW and the spot sizes were roughly comparable. Thus the total energies absorbed by the samples were roughly the same for all three excitations. In the UV excitation case, all of the energy is absorbed in the upper cap layer where excitons are formed; in the visible excitation case, the excitation energy is absorbed over the entire superlattice region and into the buffer and substrate regions.

Near-Band-Edge PL

Three samples, SL00201.1 (40/20, $x = 0.25$), SL00206.1 (40/20, $x = 0.25$), and SL10322.2 (120/40, $x = 0.25$), contained sharp PL features consistent with near band-edge emission. The sharp PL is due to shallow bound excitons (BE), and consists of a no phonon (NP) line as well as phonon assisted lines. The exciton binding energies obtained from the temperature dependence of the BE(NP) lines are in the range of 1.4 to 4.2 meV.

The sharp lines in Figure 32, expanded in Figure 33 for the three samples, show a strong no phonon (NP) line as the highest SL

Table IV: Sharp Line positions and phonon energies

Sample Number	NP	TA	Phonon Energies (meV)		
			TO _{Si-Si}	TO _{Si-Ge}	TO _{Ge-Ge}
SL00201.1	1017	17.7	58.1	48.8	34.8
SL00206.1	1047	18.7	58.0	50.7	33.7
SL10322.2	1032	18.0	58.5	----	----
Average		18.3	58.3	49.7	34.3
Bulk Si-Ge alloys (Weber and Alonso 1989)		18.0	58.0	49.0	34.5

energy feature. The NP line, not allowed in pure silicon but still weakly present due to momentum transfer from the impurity associated with the transition, occurs strongly in $\text{Si}_{1-x}\text{Ge}_x$ because of momentum conservation due to the statistical distribution of Si and Ge atoms within the alloy. The NP line is accompanied by four phonon assisted lines with average energies of 18.3 ± 0.4 , 34.3 ± 0.8 , 49.7 ± 1.0 , and 58.3 ± 0.6 meV below the NP line, as given in Table IV. These phonon lines correspond to emissions with momentum conserving transverse acoustic (TA), transverse optical (TO) (Ge-Ge), TO (Si-Ge), and TO (Si-Si) phonons, respectively, and the phonon energies agree well with those found by Weber and Alonso for bulk $\text{Si}_{1-x}\text{Ge}_x$ alloys. (Weber and Alonso 1989) The PL spectra look very similar to the results for bulk samples, except for shifts in peak energies due to the dependence of the $\text{Si}_{1-x}\text{Ge}_x$ band gap on strain and to quantum confinement. As discussed in Chapter II the band gap of $\text{Si}_{1-x}\text{Ge}_x$ depends on the degree of strain in the layer (see Figure 12). Since these samples were grown on Si substrates and were grown well below the critical thickness, it is expected that the

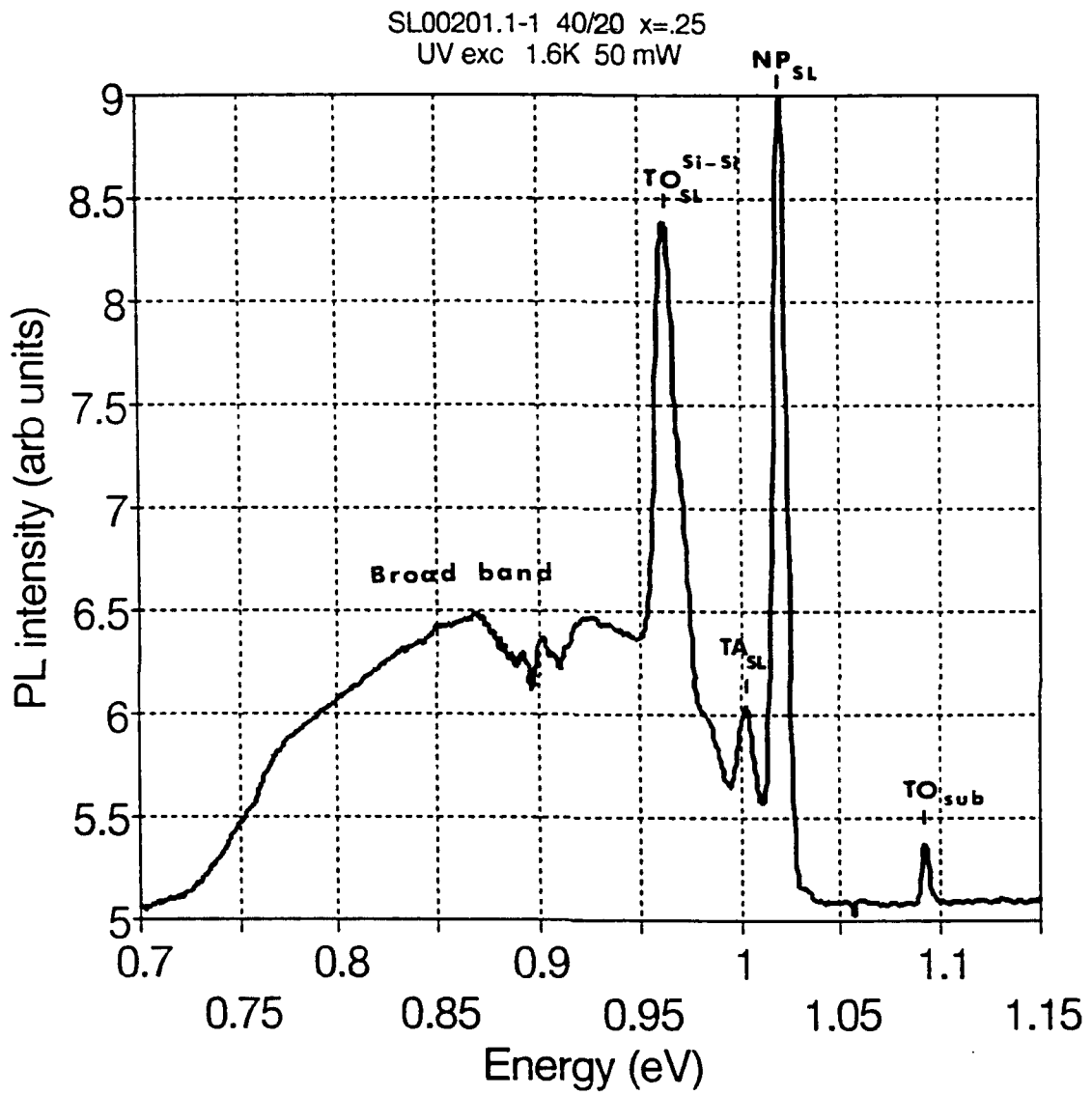


Figure 32: PL - Sample SL00201.1 at 1.6K. The highest energy feature is the no phonon (NP) line preceded by the TA, TO(Si-Si, TO(Si-Ge), and TO(Ge-Ge) phonon replicas

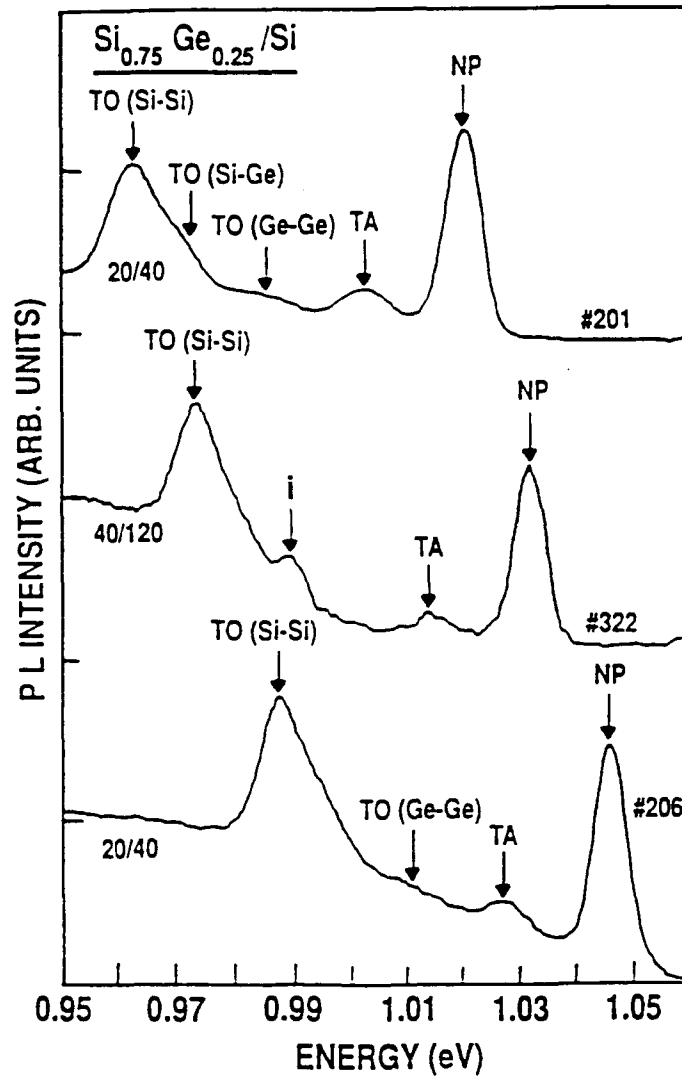


Figure 33: Sharp line spectra for three samples, SL00201.1, SL00206.1, SL10322.2.

$\text{Si}_{1-x}\text{Ge}_x$ layers are fully strained and thus have a band gap quite different from unstrained bulk $\text{Si}_{1-x}\text{Ge}_x$ layers. Quantum confinement is due to the superlattice structure that creates valence band wells, resulting in a shift of the effective superlattice band gap to higher energies.

Temperature dependence of sharp peaks. In order to determine the nature of these sharp features, the study of PL spectrum dependence on sample temperature has been made. Figures 34-36 show the near band-edge PL for samples SL00201.1, SL00206.1, and SL10322.2, respectively, measured at various temperatures from 1.6 to 12 K. It can be seen that the PL intensity decreases very rapidly as the sample temperature increases. This rapid decrease of the lines and their symmetric shape are characteristic of bound exciton (BE) emission. As the temperature increases above 1.6 K, the excitons are dissociated from the binding center, decreasing the population of bound excitons and increasing the population of free excitons, and consequently decreasing the BE emission intensity with a temperature dependence given by (Bimberg 1971)

$$I(T) = \frac{I_0}{1 + C e^{-\frac{E_b}{kT}}}, \quad (29)$$

where E_b is the binding energy of the exciton. By fitting the NP line integrated intensities obtained at various temperatures to Eq (29), the binding energy of the exciton to the defect for each

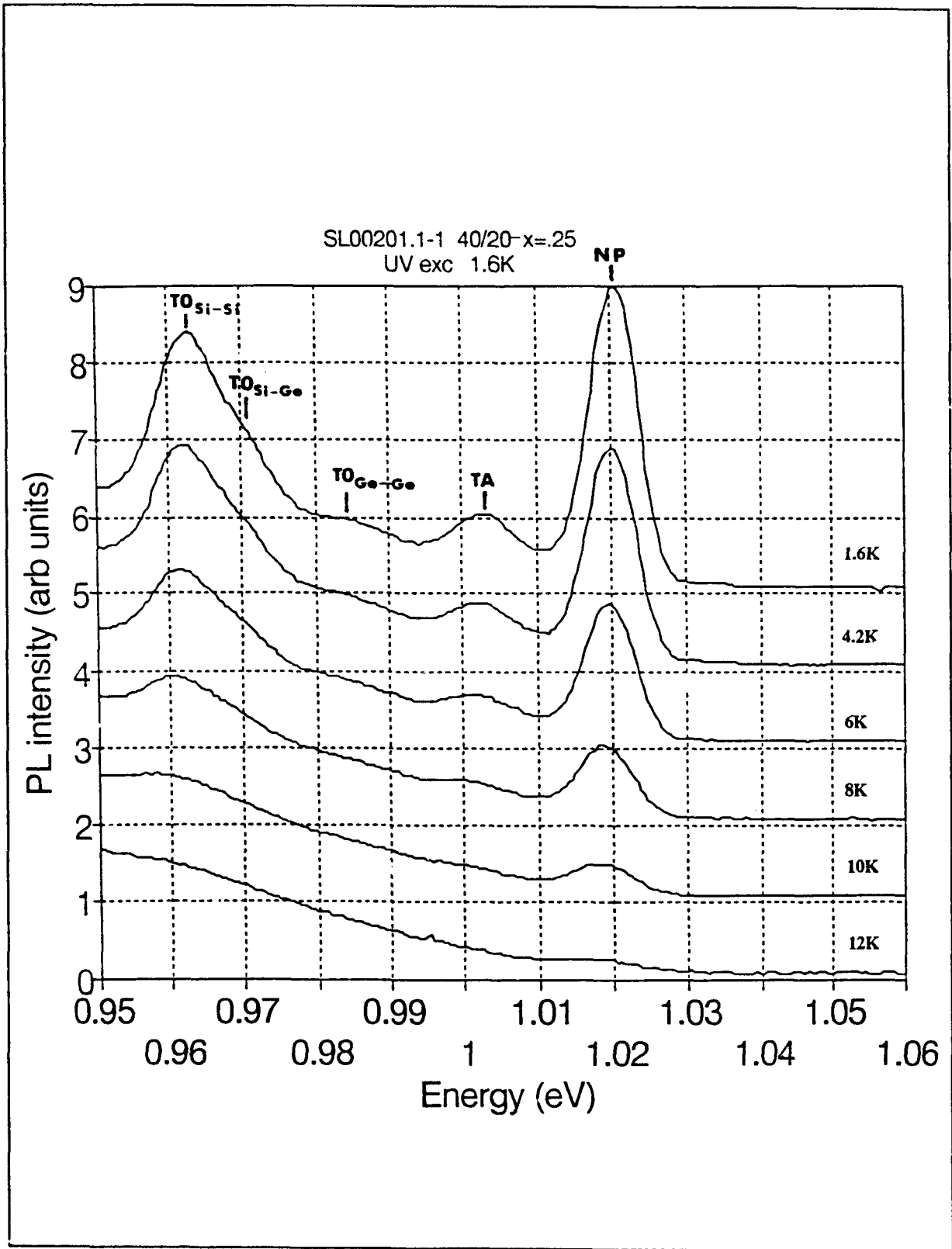


Figure 34: Temperature Dependence of PL - SL00201.1

SL00206.1 40/20 x=.25
UV excitation 25 mW

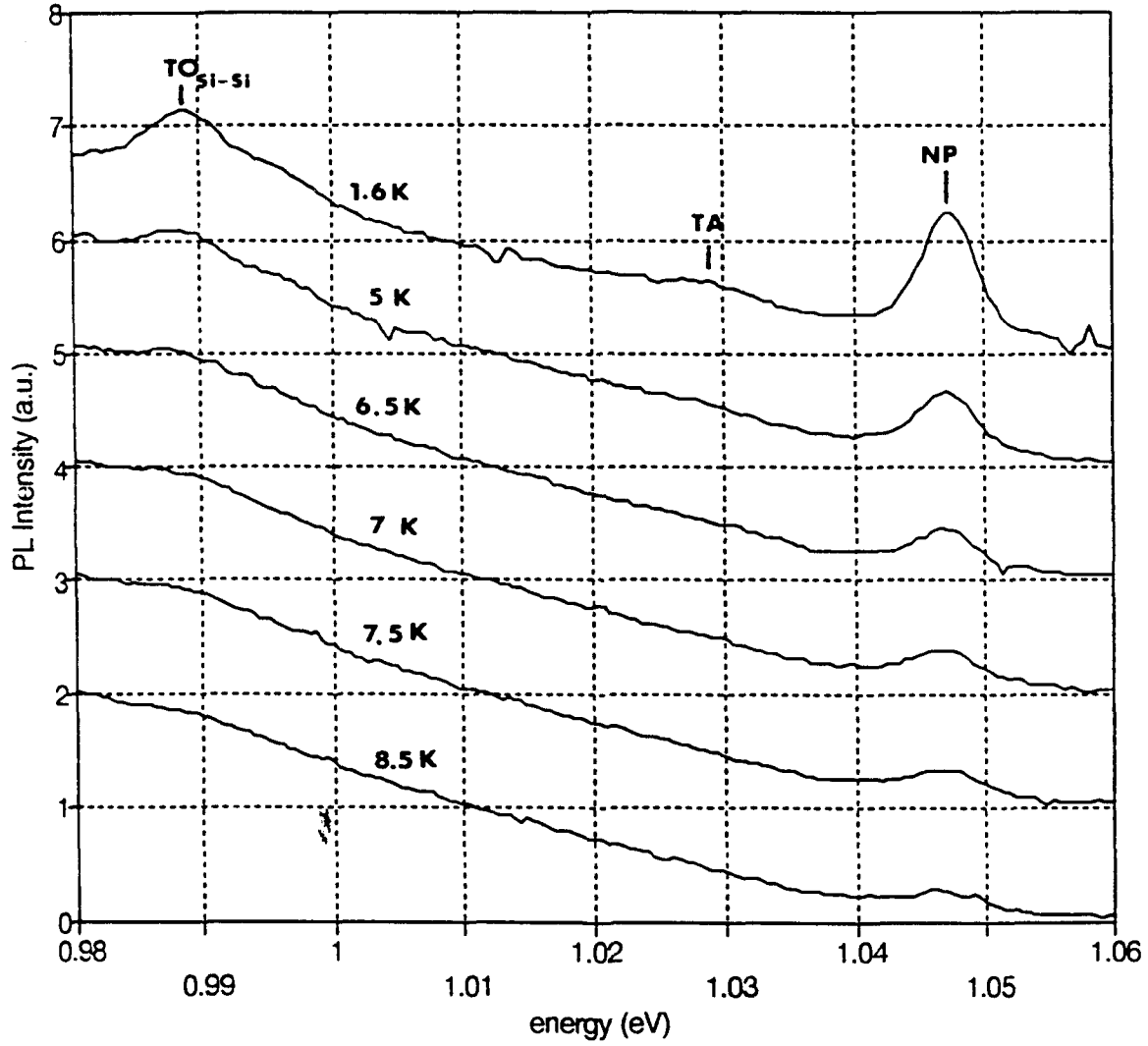


Figure 35: Temperature Dependence of PL - SL00206.1

SL10322.2 120/40 $x = 0.25$
UV exc 50 mW

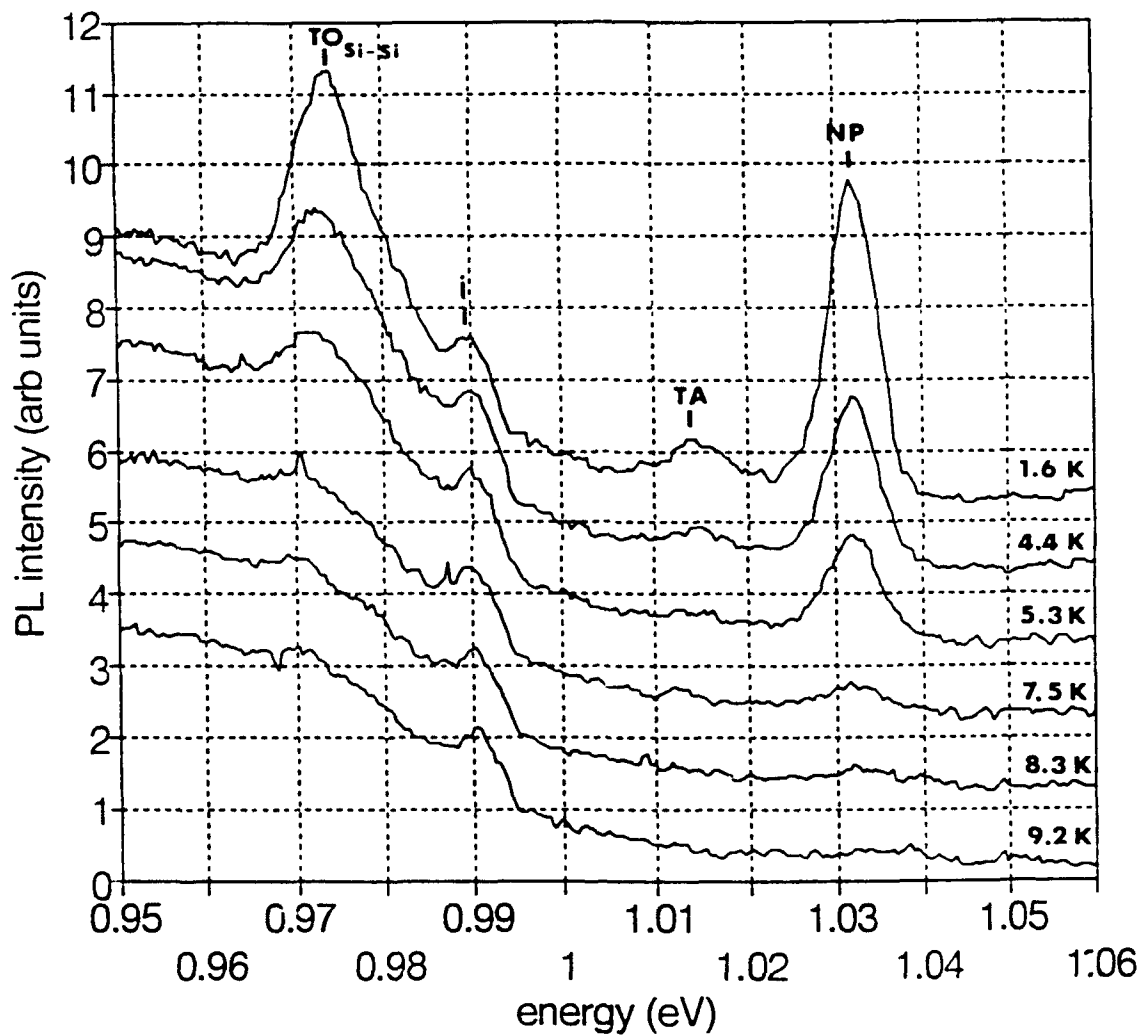


Figure 36: Temperature dependence of PL - SL10322.2

sample can be determined. The fitting is complicated by the constant factor C, which is related to the degeneracy of the initial and final states of the bound and free exciton. For silicon the constant C is around 20. (Davies 1989) Thus at high temperatures, the 1 in the denominator becomes overwhelmed by the constant C times the exponential factor and the intensity is given by:

$$I(T) = C' I_0 e^{\frac{E_b}{kT}}. \quad (30)$$

If we plot the natural logarithm of the integrated intensity versus $1/T$, then the slope of the best fit through the high temperature points is the binding energy divided by k , Boltzmann's constant. The temperature dependent PL fits are shown in Figures 37-39, and the results are summarized in Table V. These values, between 1.4 and 4.2 meV, agree with previous results for shallow bound excitons in CVD grown $\text{Si}_{1-x}\text{Ge}_x/\text{Si}$ superlattices, (Sturm 1990) bulk $\text{Si}_{1-x}\text{Ge}_x$

Table V: Sharp line energies and derived SL band gap

Sample No.	E_{NP}	(in meV)		E_j^{SL}	E_j^{SL} (calculated)
		E_b	E_{ex}		
SL00201.1	1017	2.2	11.9	1031.1	1065
SL00206.1	1047	4.15	11.9	1053.25	1065
SL10322.2	1032	1.4	11.9	1045.3	975

$$E_g = E_{NP} - E_b - E_{ex}$$

alloys, (Weber and Alonso 1989; Mitchard and McGill 1982) and bulk

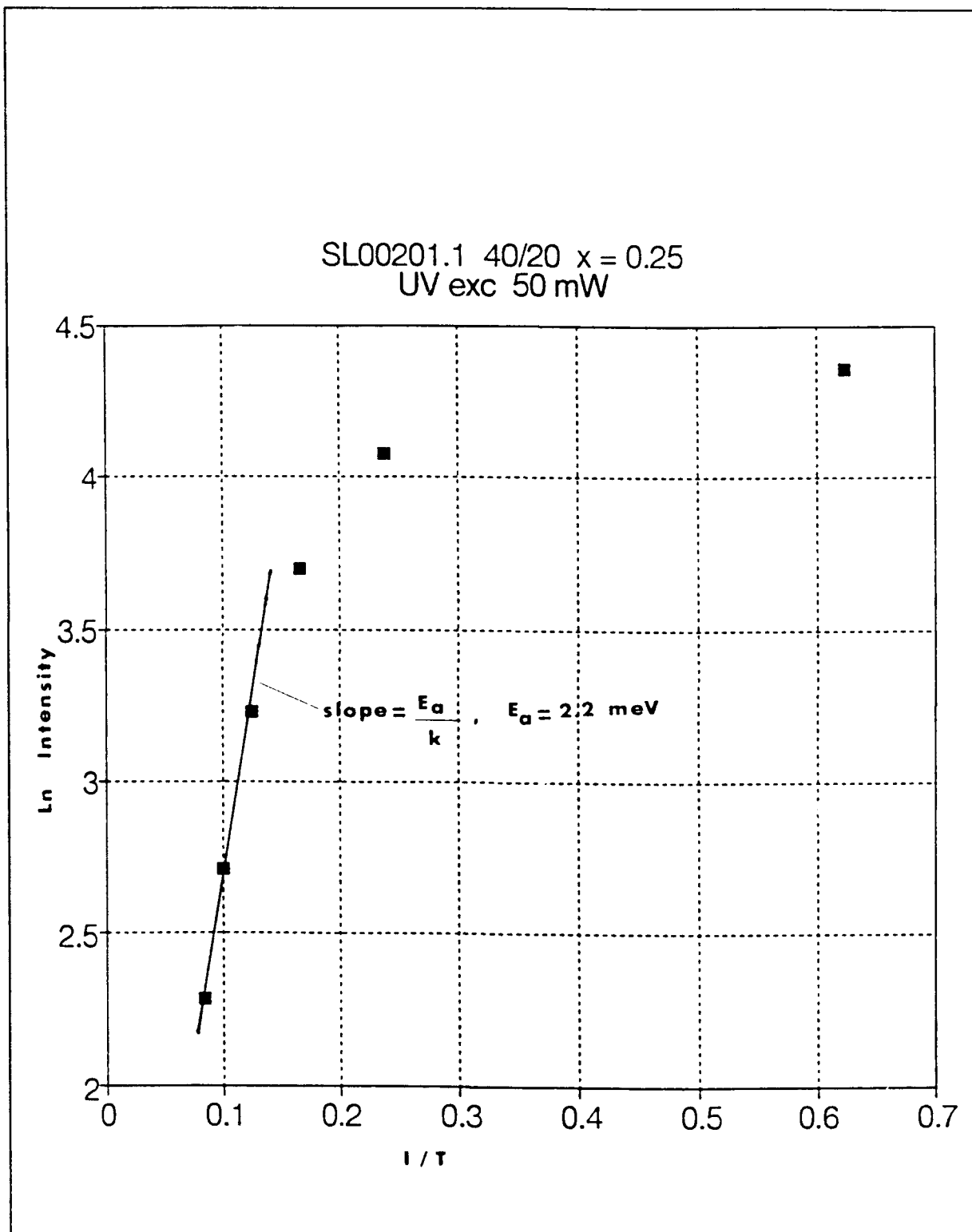


Figure 37: Ln I vs 1/T for the sample SL00201.1. Note the asymptotic approach to the linear fit shown. The slope is the activation energy divided by Boltzmann's constant

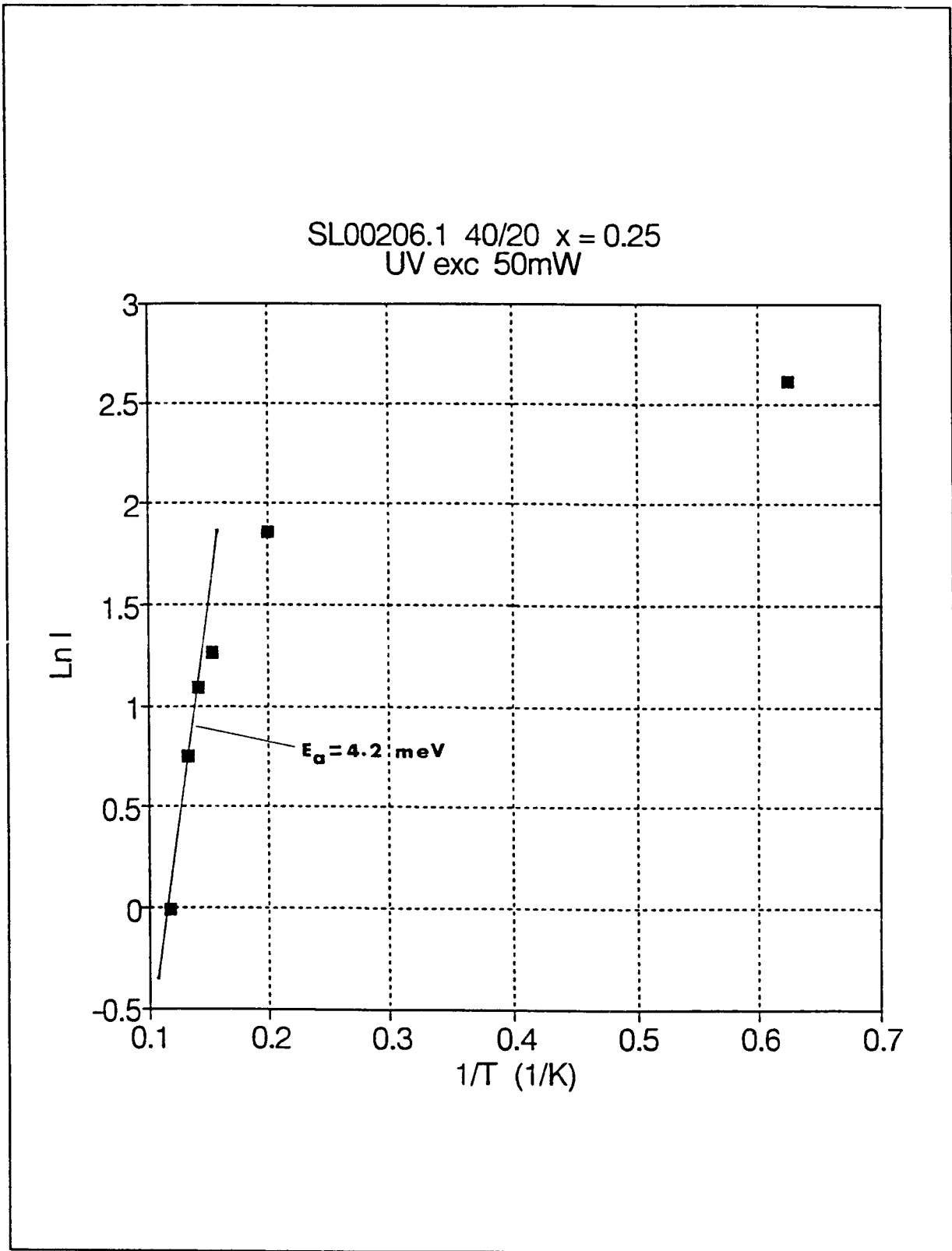


Figure 38: Ln I vs. 1/T - SL00206.1

SL10322.2 120/40 $x = 0.25$
UV exc 50 mW

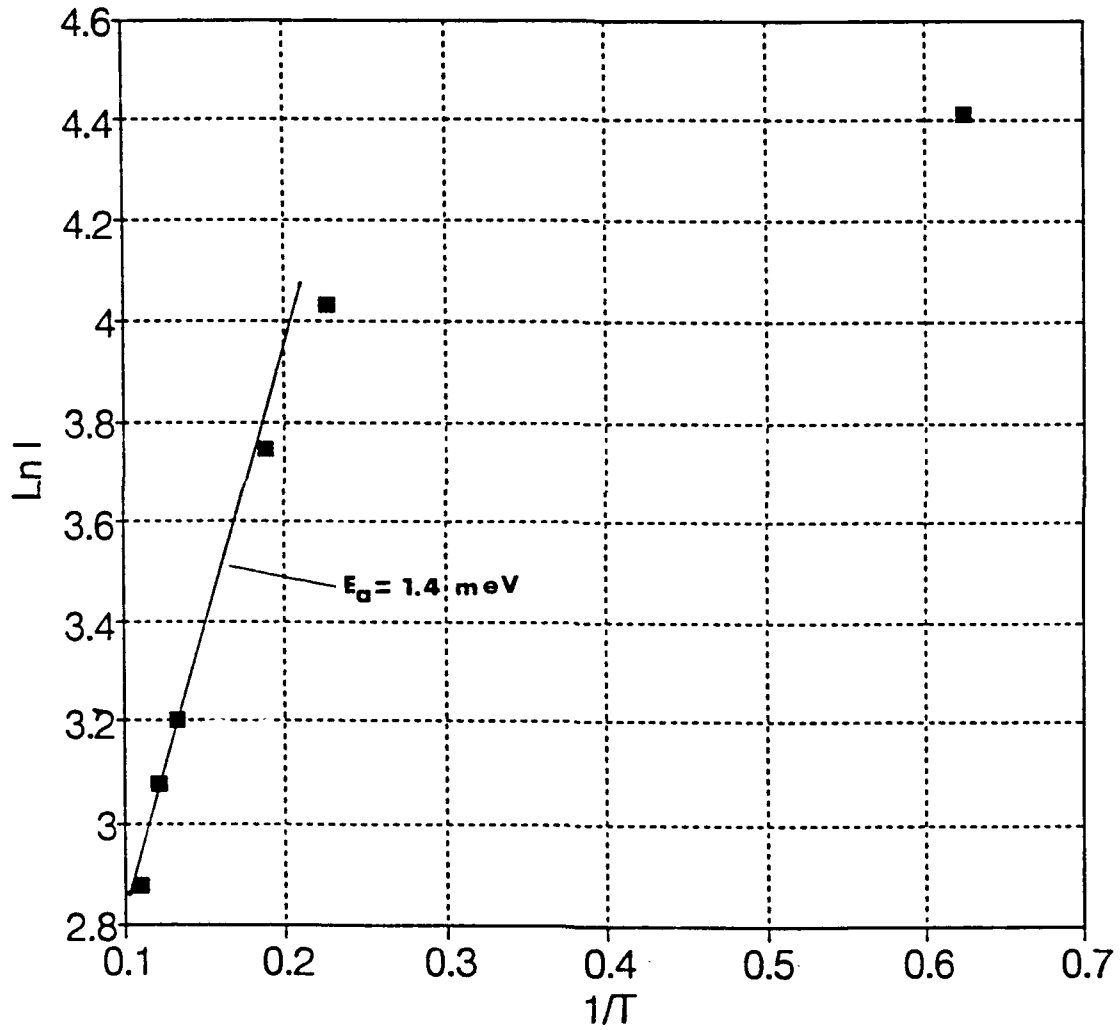


Figure 39: $\ln I$ vs. $1/T$ - SL10322.2

Si. (Thewalt 1982).

For our samples, shifts in the BE lines to higher energy as the sample temperature increases are not observed as was seen in the RTCVD samples, (Sturm 1990) which might have indicated free exciton (FE) luminescence. In fact, the BE lines shift slightly to lower energy with increasing temperature, which will be discussed later. It is likely that the FE lines were not observed because of the high concentration of centers leading to the short lifetime nonradiative recombination inherent in MBE samples grown at low temperatures. (Houghton 1991b) The long lifetime free excitons can be captured by non-radiative recombination centers where they are lost to nonradiative processes before they recombine radiatively. BE emission would be affected less because of its lower radiative lifetime, typically 1 μ sec for BE in Si (Thewalt 1982) compared to 60 μ sec for FE. (Davies 1989) It is proposed that the lifetime of nonradiative processes is on the order of 1 μ sec, so that nonradiative processes overwhelm FE emission but BE emission is still observable.

Experimental determination of SL band gap. From the peak energy positions of the NP lines, E_{NP} , and the binding energies obtained from temperature dependence of NP lines, E_b , the effective band gap of the superlattices, E_g , in Table V were determined using:

$$E_{NP} = E_g - E_b - E_{ex}. \quad (31)$$

The free exciton binding energy, E_{ex} , was assumed to be equal to a linear interpolation of the values for silicon and germanium, 14.3 and 4.7 meV, respectively. The superlattice band gaps deduced from PL data differ from those calculated using a Kronig-Penney model (shown below), although SL00206.1 is in close agreement. These differences, along with the apparent differences between the samples SL00201.1 and SL00206.1, which were designed to have the same sample structure, are mainly due to actual superlattice layer thicknesses different from the designed values. Sample SL00201.1 was found to have a superlattice period three angstroms longer than SL00206.1 using X-ray diffraction. The 30 meV difference in the NP line energy can be explained by attributing this three angstrom difference to 23 angstrom $Si_{1-x}Ge_x$ layers rather than the designed 20 angstroms. It is apparent that the band gaps deduced from the PL data are higher than the band gaps of strained $Si_{0.75}Ge_{0.25}$ layers, determined to 0.95 eV by Lang, et al, and 0.96 eV by Robbins, et al. (Robbins 1991, Lang 1985) This is an expected superlattice effect due to quantum confinement of holes resulting from the large valence band offset. The confinement energies, between 50 and 110 meV, are reasonable when compared to the Kronig-Penney calculations in the next section.

Effects of alloy fluctuations. Variation in the alloy concentration, x , in the $Si_{1-x}Ge_x$ layers is responsible for two effects apparent in PL data. First, the BE lines shift to lower

Table VI: Linewidths and shifts of BE lines

Sample No.	Linewidth	meV		Shift(1.6-12K)	Δx
		$E_{NP}(1.6K)$	$E_{NP}(12K)$		
SL00201.1	7.7	1021	1017	4	0.009
SL00206.1	5.9	1047	1046	1	0.007
SL10322.2	6.5	1032	1032	0	0.010

The alloy fluctuation, Δx , is calculated assuming all of the NP BE linewidth is due to variations in x .

energy as the sample temperature is increased. These shifts are summarized in Table VI. The binding energy of a shallow donor or acceptor depends on the local environment; an environment with silicon content greater than the average results in a higher binding energy than one with a silicon content lower than average, because E_b is greater in Si than it is in Ge. Thus at low temperatures BEs from environments with both low and high Si content are present equally, but as temperature is increased the luminescence from BEs in Si depleted environments dissociate faster than those in Si-rich environments, and thus the BEs in Si-rich environments dominate. Second, the linewidths of the BE lines, ranging from 5.9 to 7.6 meV (shown in Table VI), are similar to the linewidths found in bulk $Si_{1-x}Ge_x$, (Weber and Alonso 1989) which were 10 times greater than those found in Si, 0.4 meV. (Davies 1989) The linewidths in the bulk $Si_{1-x}Ge_x$ alloys studied by Weber and Alonso were due to fluctuations in the alloy concentration, x . The authors found that the BE linewidths followed the expression

$$\Delta E_{BE} = 2.36 \left[\frac{dE_g}{dx} \frac{x(1-x)}{\frac{4}{3}\pi a_B^3 N} \right]^{1/2} \quad (32)$$

For $x=0.25$, the case for these three samples, ΔE should be 7 meV, in excellent agreement with the observed linewidths. Thus the alloys fluctuations evident from the linewidths of the the BE lines are statistical in nature; there is no additional clustering of Ge atoms producing fluctuations outside of a normal distribution.

One obvious question that remains is - why are near-edge BE lines seen in some samples grown by MBE and not in others? In fact, 26 samples of various sample configurations have been examined in this study and perhaps hundreds by other groups. Only these three samples contain the identifiable near-edge FE or BE lines seen to date. It is reasonable to expect that near-edge lines should be present in all samples and not only in these three samples. The fact that they are not is the real problem requiring resolution. It is known, from Figures 25-26 and Figure 28, that the BE emission originates in the upper superlattice layers, but it is unclear if this is due to the distribution of shallow bound impurities in the superlattice, the distribution of competing broad band emission centers, or some other mechanism. It is clear, though, that BE emission is strongest in the upper layer of the superlattice and that this strength is related to the high exciton density created by the use of UV excitation.

It is proposed that the broad band centers, which dominate most MBE grown samples, are very efficient at trapping excitons, more efficient than shallow impurities responsible for BE emission. This has found to be the case for other isoelectronic centers in Si. They also capture free excitons at a much faster rate than the FE recombination process. In the three samples that have BE emission, it is likely that there is a nonuniform distribution of the centers responsible for the broad PL band, or a nonuniform distribution of the impurities associated with the BE emission (high impurity concentration in the upper superlattice layers), so that there is enough trapping and recombination of excitons at BE centers that these features can be seen in PL spectra.

Calculations of Band gap in $Si_{1-x}Ge_x/Si$ SLs using a Kronig-Penney Model

The effective superlattice band gaps for all of the structures investigated experimentally were determined using the Kronig-Penney Model described in Chapter II. The bandgap for Si used was 1.169 eV and for the $Si_{1-x}Ge_x$ band gap the values determined by Robbins et al in Equation (27) in Chapter II were used. (Robbins 1992) For the valence band, heavy hole effective masses were used, since the light hole bands are 100 meV below the heavy hole bands due to strain-induced splitting as discussed in Chapter II. For the conduction band an average of the longitudinal and transverse

Table VII: Summary of Kronig-Penney results and paramters used.

(angstroms)			(eV)		(in units of m0)		(eV)	
t_{Si}	t_{Si-Ge}	x	ΔE_v	ΔE_c	m_{hh}^*	m_c^*	E_g^{Si-Ge}	E_g^{SL}
40	20	0.25	0.19	0.02	0.5325	0.2846	0.959	1.065
120	40	0.25	0.19	0.02	0.5325	0.2846	0.959	0.990
120	40	0.36	0.27	0.01	0.5072	0.2687	0.888	0.904
140	70	0.36	0.27	0.01	0.5072	0.2687	0.888	0.893
140	70	0.30	0.225	0.02	0.5210	0.2775	0.926	0.931
140	70	0.24	0.18	0.02	0.5348	0.2859	0.966	0.971
140	70	0.12	0.085	0.03	0.5624	0.3014	1.055	1.059
80	40	0.35	0.26	0.02	0.5095	0.2702	0.894	0.910

effective masses applicable to the four-fold degenerate conduction band was used as given by

$$\frac{2}{m_e^*} = \frac{1}{m_t^*} + \frac{1}{m_l^*}, \quad (33)$$

where

$$m_t^* = \text{transverse effective and } m_l^* = \text{longitudinal effective mass.} \quad (34)$$

The band offsets were obtained from results by Bean shown in Figure 11. (Bean 1988) A summary of the parameters used in the Kronig-Penney model are given in Table VII. The parameters in Table VII were used to calculate valence band confinement of holes. The superlattice band gap was determined by adding the confinement

energies to the $\text{Si}_{1-x}\text{Ge}_x$ band gap. In all cases the band alignment was Type I, but the conduction band offsets were all very small so that the conduction band offsets are too small to produce electron confinement. In these cases the electron states are delocalized and not significantly affected by the superlattice potential. Thus the electron energy bands take on the characteristics of the bulk bands of each layer.

40/20 Samples. Samples SL00201.1, SL00206.1, and SL10415.2 were all nominally an 83 period, 40 angstroms silicon/20 angstroms, $\text{Si}_{0.75}\text{Ge}_{0.25}$ superlattice. The Kronig-Penney model was used to determine the bandgap of this structure. In addition, since it is expected that there may be small deviations from this structure, the bandgap was determined as a function of the well width, keeping the barrier width constant (Figure 40), and as a function of the alloy concentration x , keeping the layer thicknesses constant (Figure 41). As can be seen from these calculations the band gap of the 40/20 samples with $x = 0.25$ is much more sensitive to deviations in the superlattice layer thicknesses rather than the Ge fraction in the $\text{Si}_{1-x}\text{Ge}_x$ layers. For example if the actual well thickness were 18 angstroms (10 percent reduction) the superlattice band gap would change from 1.065 to 1.13 eV (a 6.1 percent increase). On the other hand a ten percent reduction in the Ge fraction, from .25 to .225, would result in an increase in the superlattice band gap from 1.065 to 1.088 (a 2 percent increase).

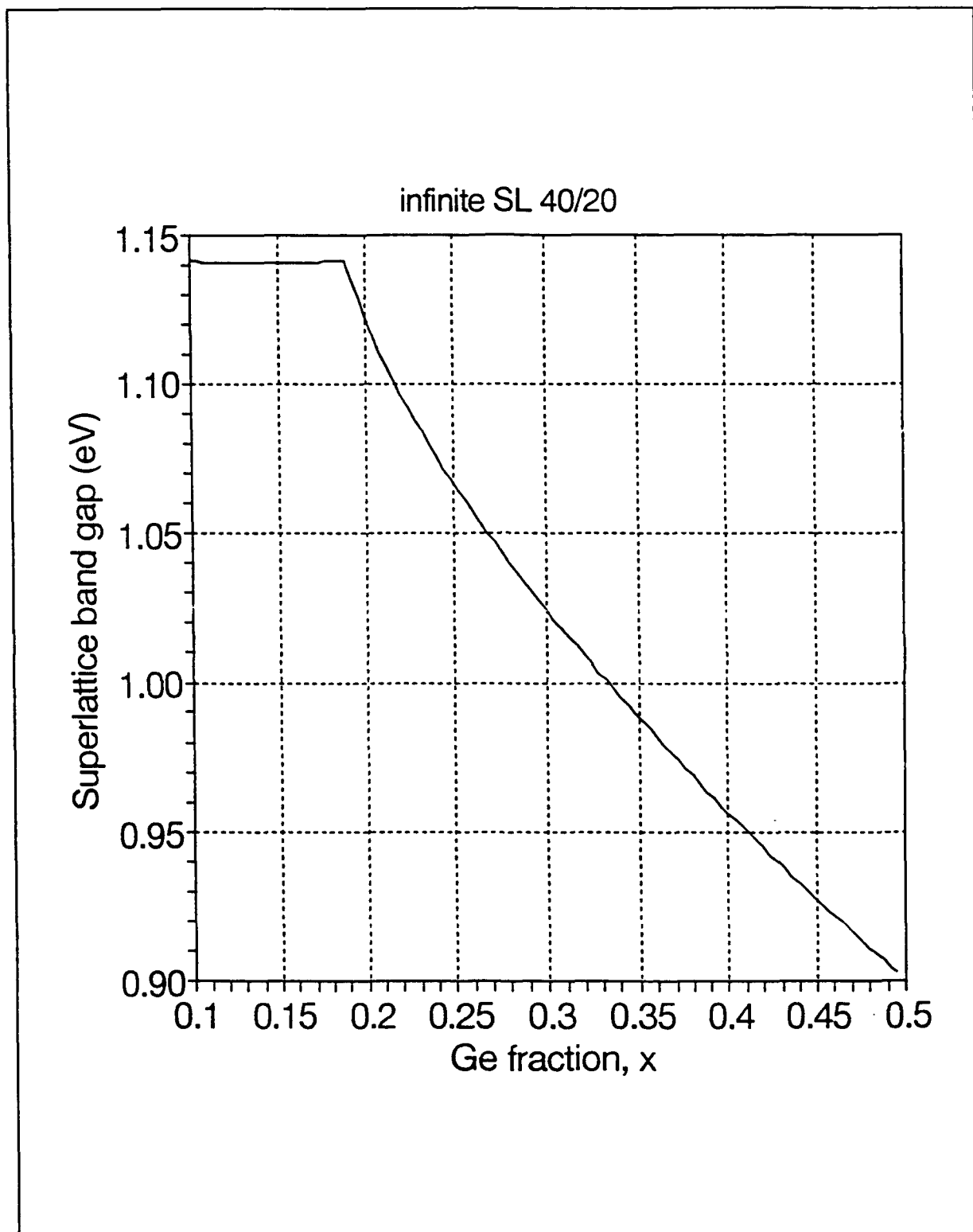


Figure 40: Kronig-Penney calculation - Si/Si_{1-x}Ge_x (40/20) SL bandgap as a function of x

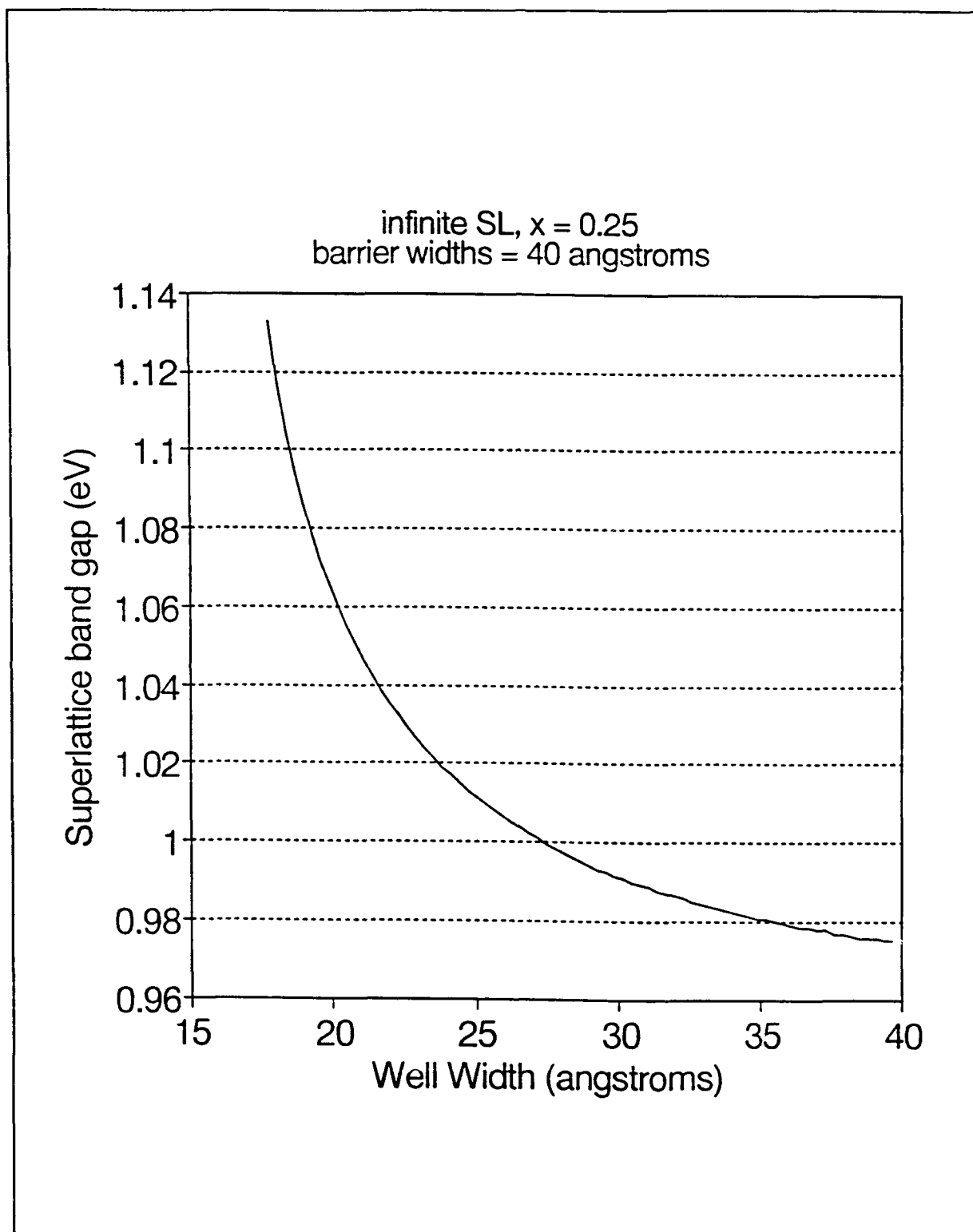


Figure 41: Kronig-Penney calculation - Si/Si_{0.75}Ge_{0.25} SL bandgap as a function of Si_{0.75}Ge_{0.25} layer thickness for a nominal 40/20 SL (SL00201.1, SL00206.1, and SL10415.2).

Using these calculations, if it is assumed that the differences in the experimentally determined band gap were due to variations in the actual layer thicknesses or alloy composition, the actual structure of SL00201.1 was either 40/20, $x=0.29$, or 40/22.5, $x=0.25$, or some combination in between. Similarly, SL00206 was either 40/20, $x=0.255$, or 40/20.2, $x=0.25$, or a combination in between.

120/40, $x = 0.25$ Samples. Samples SL10322.2, CH93, and SL10301.1 were all nominally a 30 period 120 angstrom Si/40 angstrom $\text{Si}_{0.75}\text{Ge}_{0.25}$ superlattice. The Kronig-Penney model was used to calculate the superlattice band gap as a function of well width (Figure 42), and as a function of alloy concentration (Figure 43). For this sample the SL band gap is slightly more sensitive to layer thickness deviations as opposed to changes in the Ge fraction in the $\text{Si}_{1-x}\text{Ge}_x$ layers. Using these calculation, the actual structure of SL10322.2, using the experimental determination of band gap from Table V, was either 120/40, $x=0.16$, or 120/32, $x=0.25$, or a combination in between.

140/70 Samples. Samples SL10531.2, SL10531.1, SL10206.1, and SL10530.1 were 70 angstrom $\text{Si}_{1-x}\text{Ge}_x$ /140 angstrom Si SLs, 0.5 microns thick with $x= 0.36$, 0.30, 0.24, and 0.12, respectively. In Figure 44 the bandgap for these structures are calculated along with the

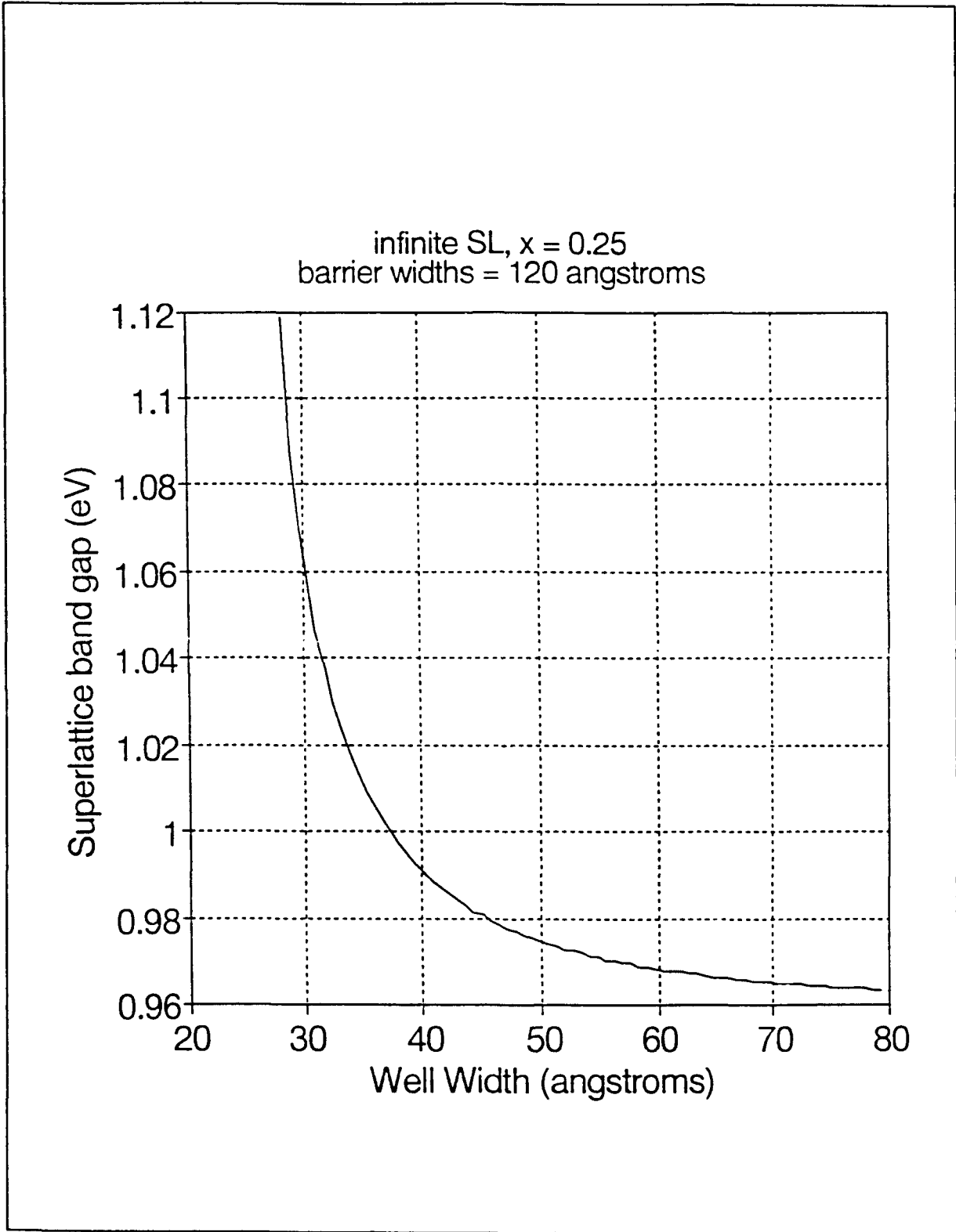


Figure 42: Kronig-Penney calculation - Si/Si_{0.75}Ge_{0.25} (120/40) SL bandgap as a function of Si_{0.75}Ge_{0.25} layer thickness

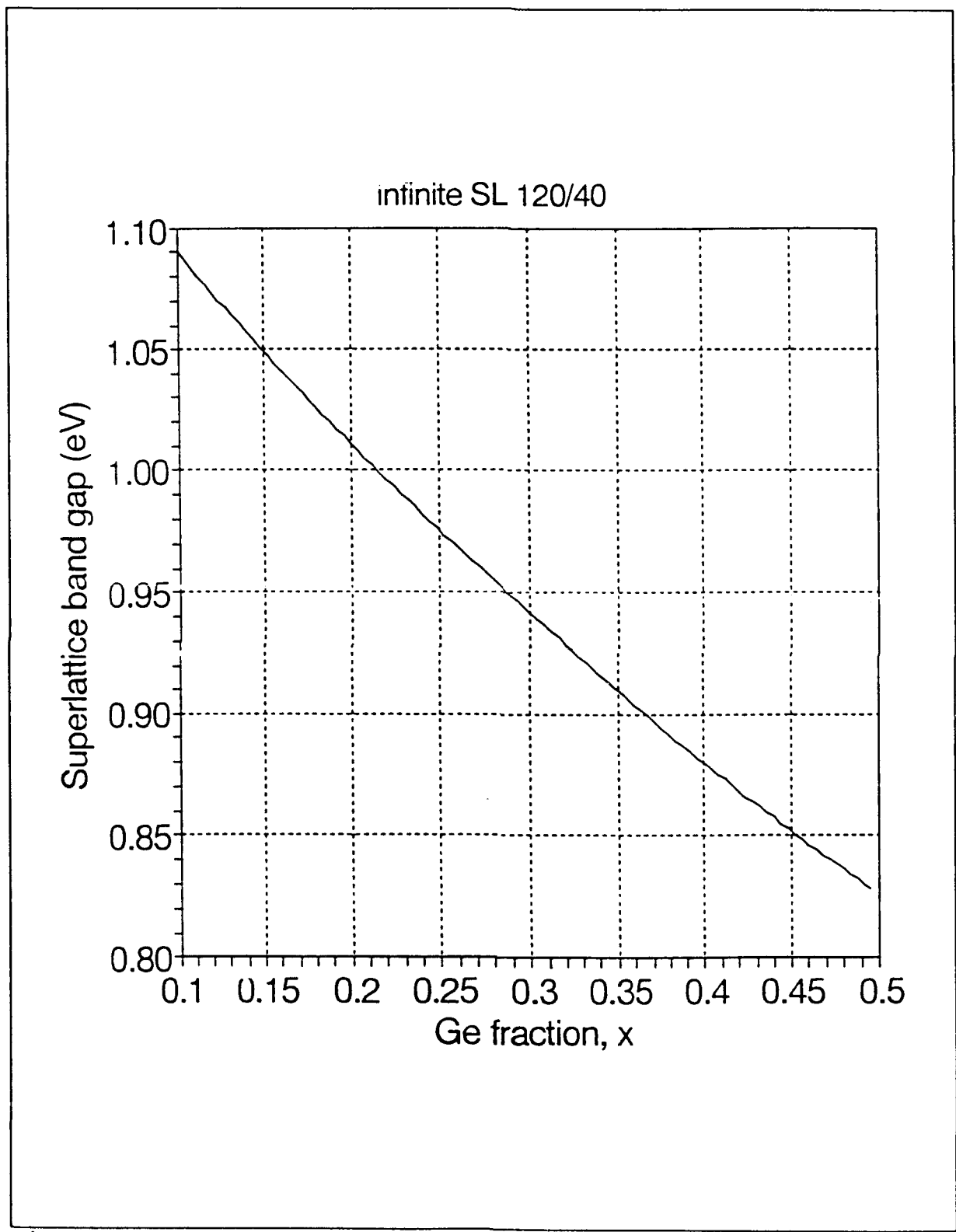


Figure 43: Kronig-Penney calculation - Si/Si_{0.75}Ge_{0.25} (120/40) SL bandgap as a function of x

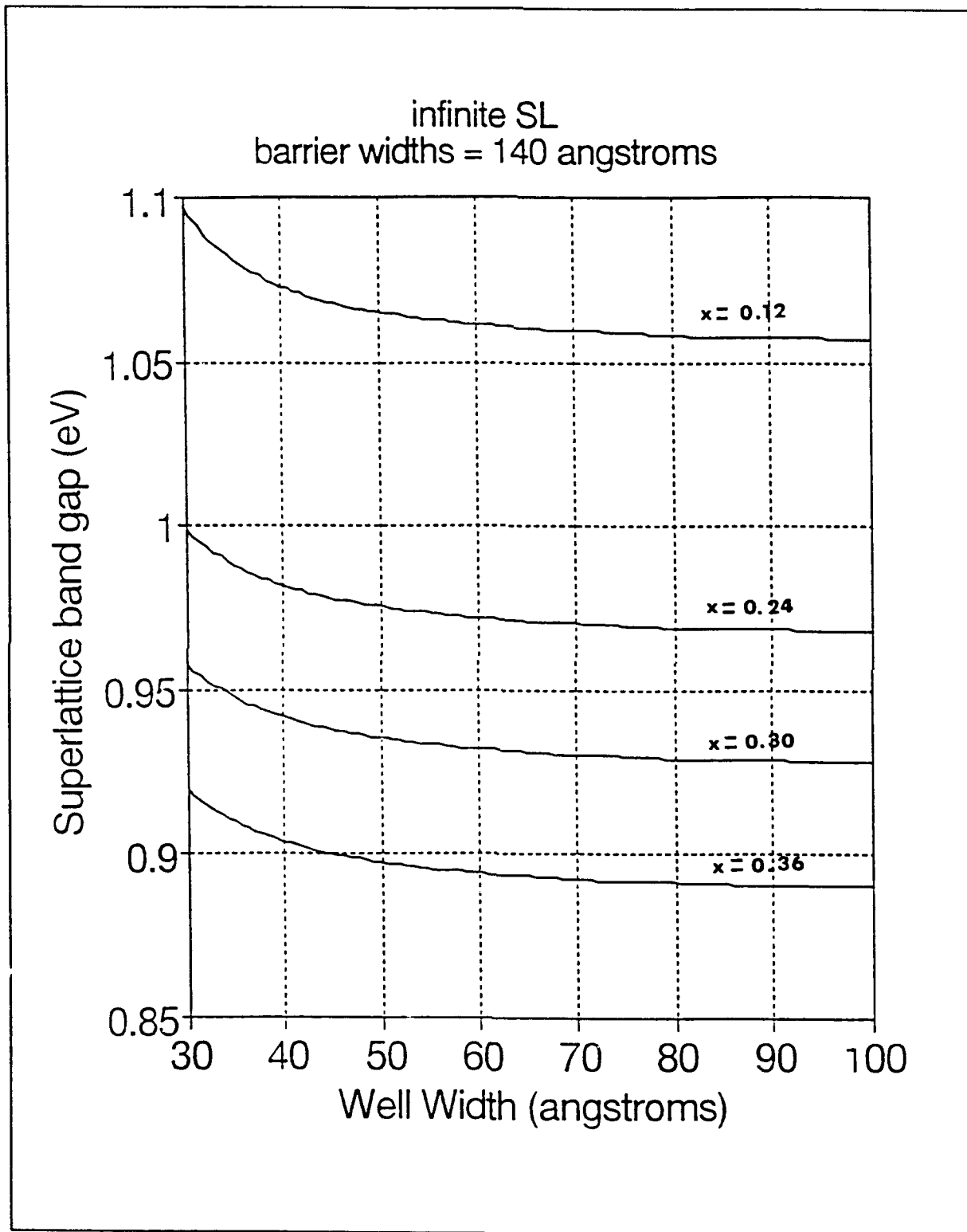


Figure 44: Kronig-Penney calculation - Si/Si_{1-x}Ge_x (140/70) SL bandgap as a function of Si_{1-x}Ge_x layer thickness for x = 0.12, 0.24, 0.30, 0.36.

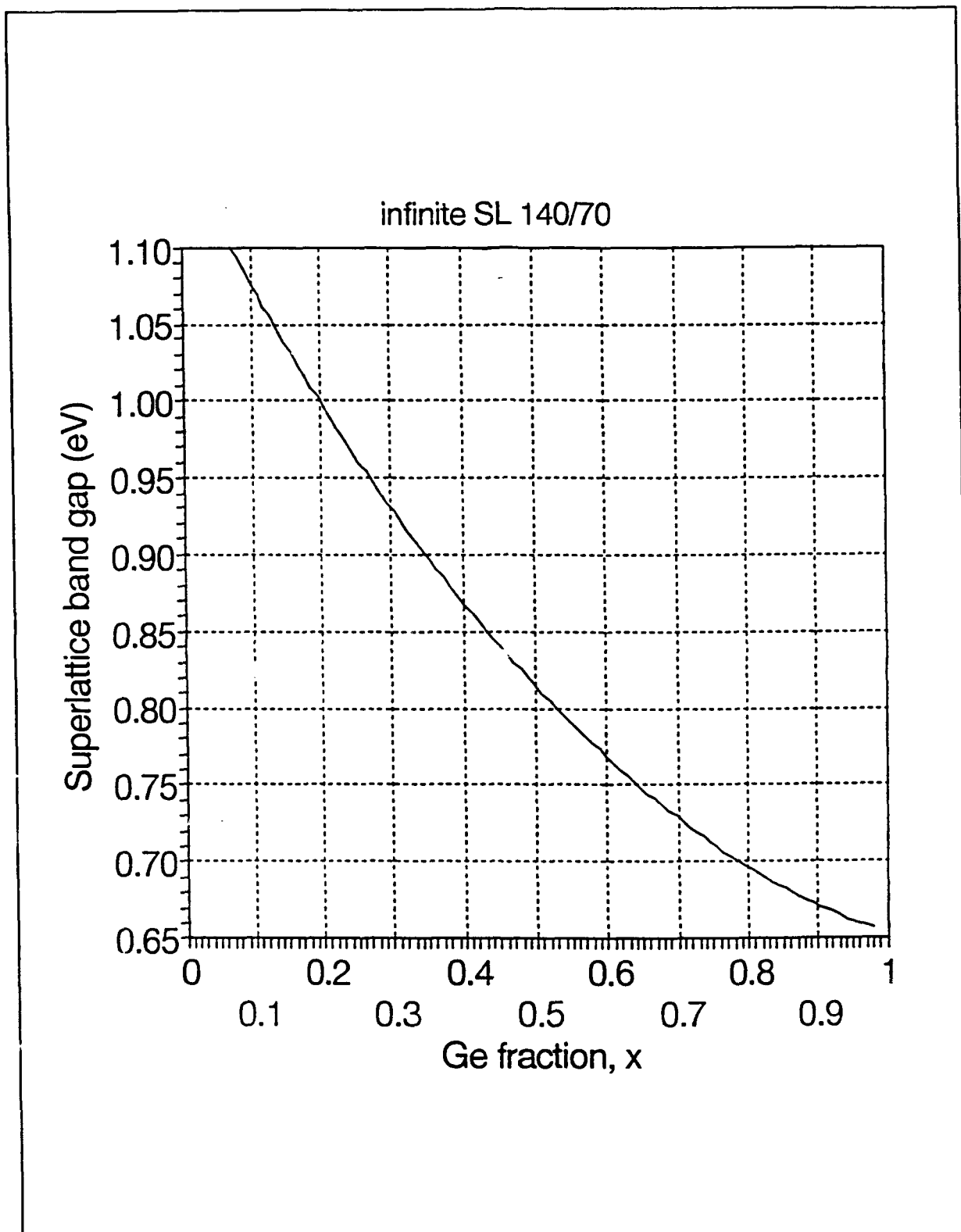


Figure 45: Kronig-Penney calculation - Si/Si_{1-x}Ge_x (140/70) SL bandgap as a function of x

variations due to different well widths. In Figure 45, the results of the Kronig-Penney calculation of the SL bandgap for the 140/70 structure is shown. In all of these structures there is very little quantum confinement so that the SL band gap is very close to the fully strained $\text{Si}_{1-x}\text{Ge}_x$ band gap.

120/40, $x=0.36$ Samples. Samples SL11105.1, SL11105.2, SL11105.3, SL11203.1, and SL11202.3 were all 120 angstrom Si/40 angstrom $\text{Si}_{0.64}\text{Ge}_{0.36}$. The calculated bandgap for this structure as a function of well width is shown in Figure 46.

80/40 Sample. The Kronig-Penney calculation for the 80 angstrom Si/40 angstrom $\text{Si}_{0.65}\text{Ge}_{0.35}$ superlattice, SL00405.1, as a function of well width is given in Figure 47.

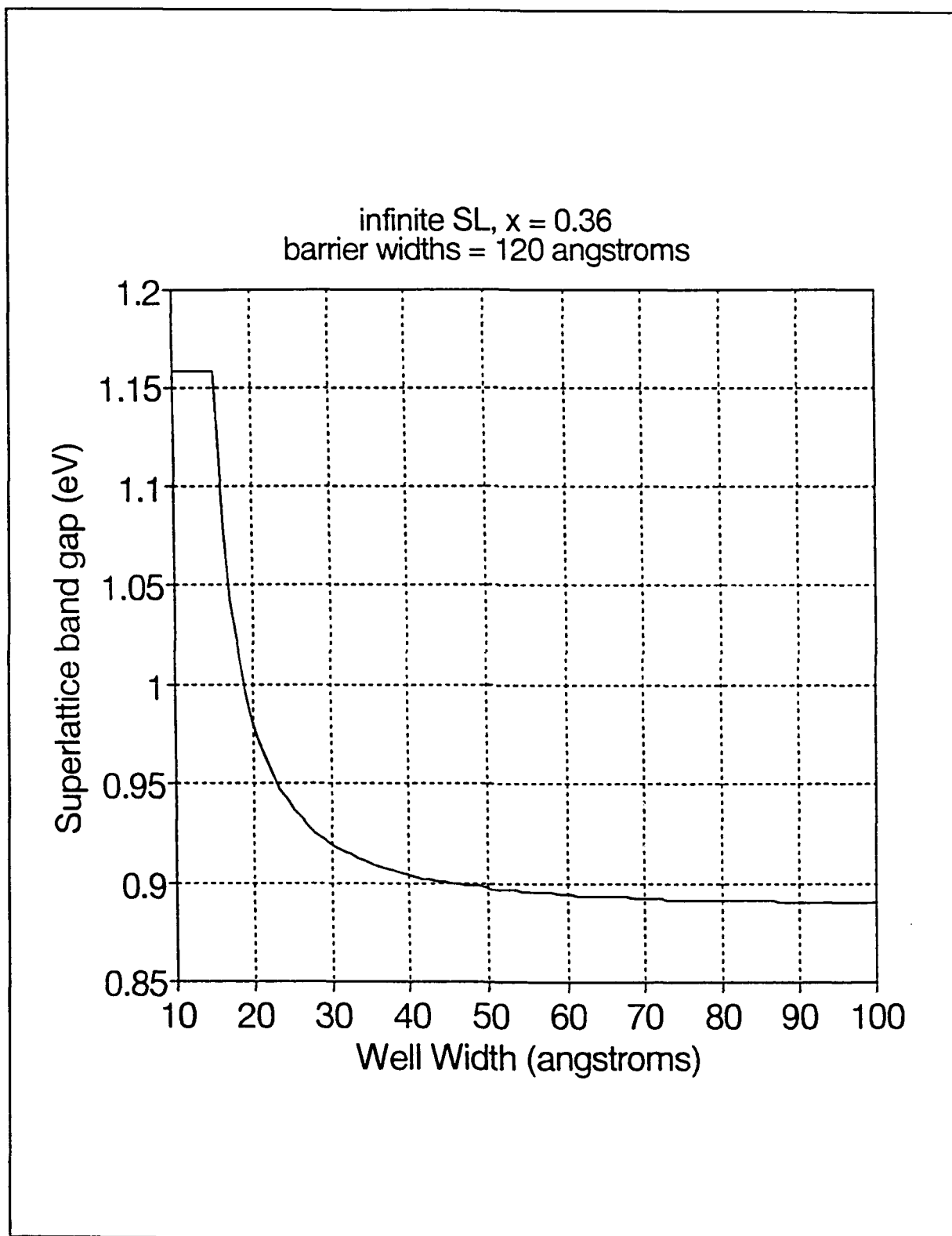


Figure 46: Kronig-Penney calculation - Si/Si_{0.64}Ge_{0.36} (120/40) SL bandgap as a function of Si_{0.64}Ge_{0.36} layer thickness

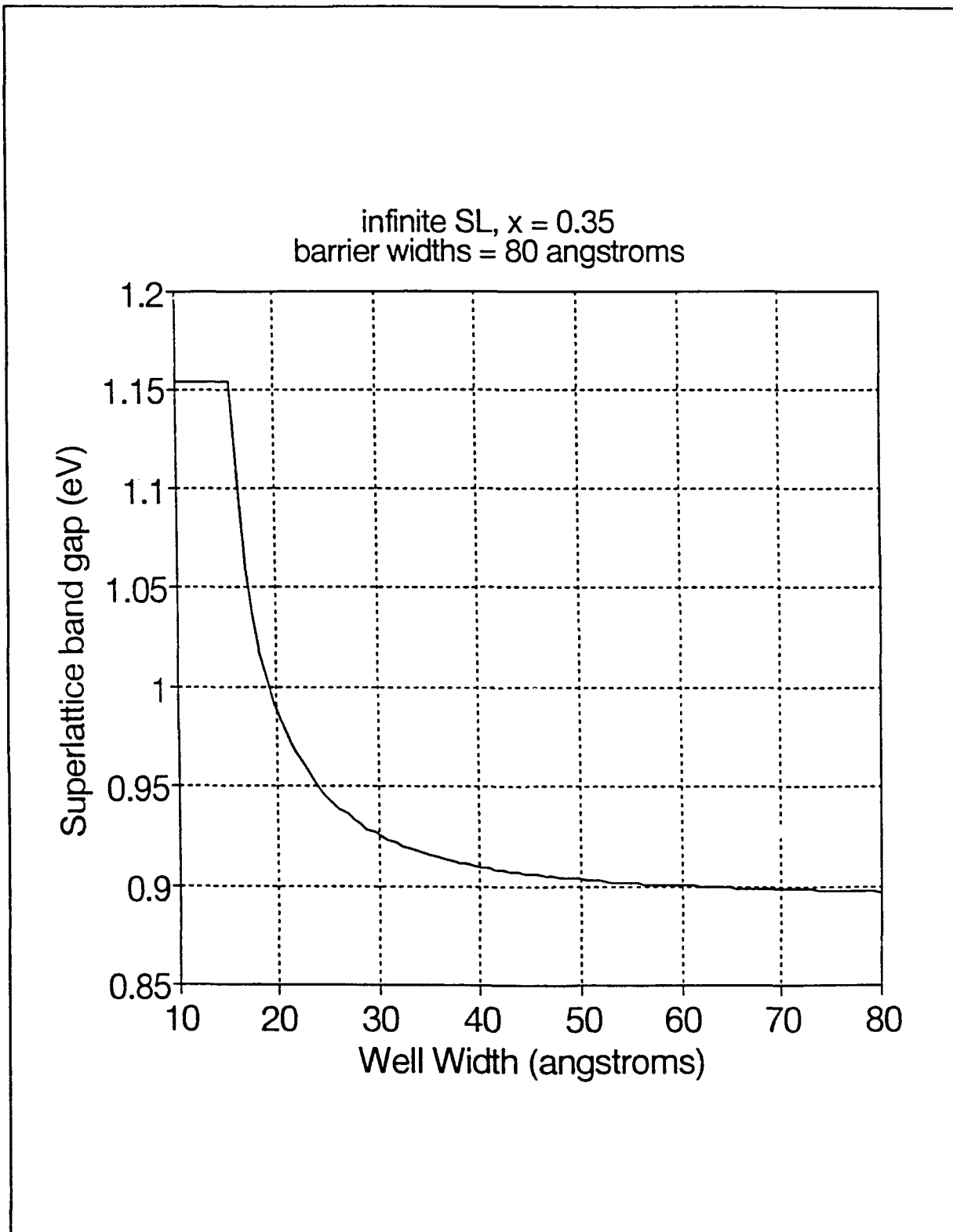


Figure 47: Kronig-Penney calculation - Si/Si_{0.65}Ge_{0.35} (80/40) SL bandgap as a function of Si_{0.65}Ge_{0.35} layer thickness

Annealing Studies

The annealing studies produced three main categories of results. First, the intensities and energies of the sharp BE lines depend upon the annealing condition. Second, the intensities and energies of the broad band PL depend upon the annealing condition. Third, annealing at high temperatures produces dislocation related lines that are similar to D lines in bulk and epitaxial silicon. In this section the first and last of these results will be discussed. The effects of annealing on the broad band PL will be discussed in the next section in the context of the luminescent mechanism responsible for the broad band emission.

Annealing effects on sharp BE lines. The effects of annealing on the sharp bound exciton lines were necessarily limited to three samples, SL00201.1, SL00206.1, and SL10322.2. The spectra for these three samples for annealing temperatures from 550 °C to 850 °C is shown in Figures 48-50. For all three samples, there is no shift in the position of the sharp bound exciton lines from the as-grown position for annealing temperatures below 650 °C. For annealing temperatures above 650 °C the bound exciton lines shift to higher energies. These shifts are due to interdiffusion and strain relaxation in the $\text{Si}_{1-x}\text{Ge}_x$ layers. Interdiffusion results in a net flow of Ge atoms from the $\text{Si}_{1-x}\text{Ge}_x$ layers to the Si layers. This results in wider $\text{Si}_{1-x}\text{Ge}_x$ wells with a lower value of alloy

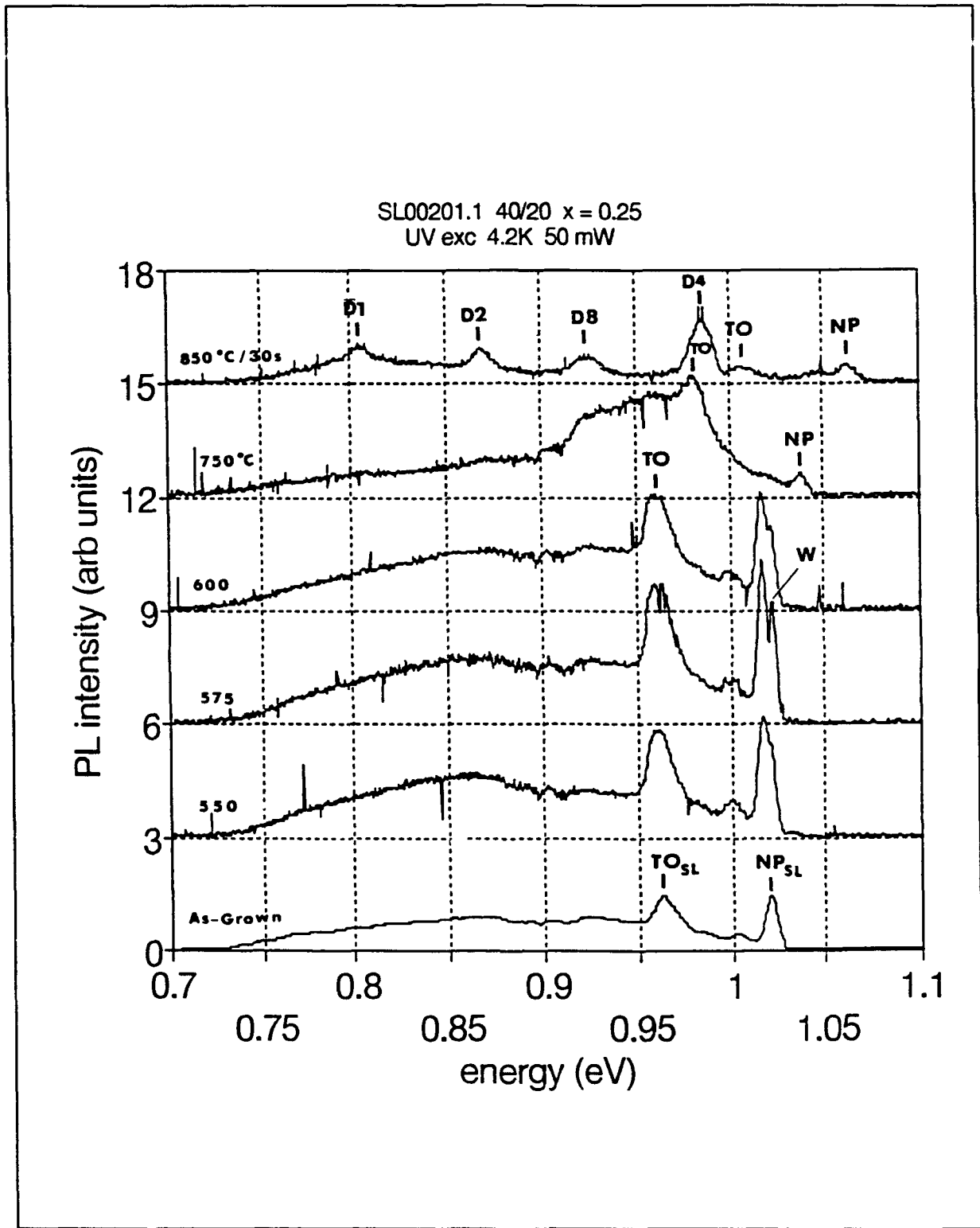


Figure 48: Annealing Study, SL00201.1. D1-D3 are dislocation related lines. "W" is a deep center. NP and TO lines are bound exciton lines from the superlattice.

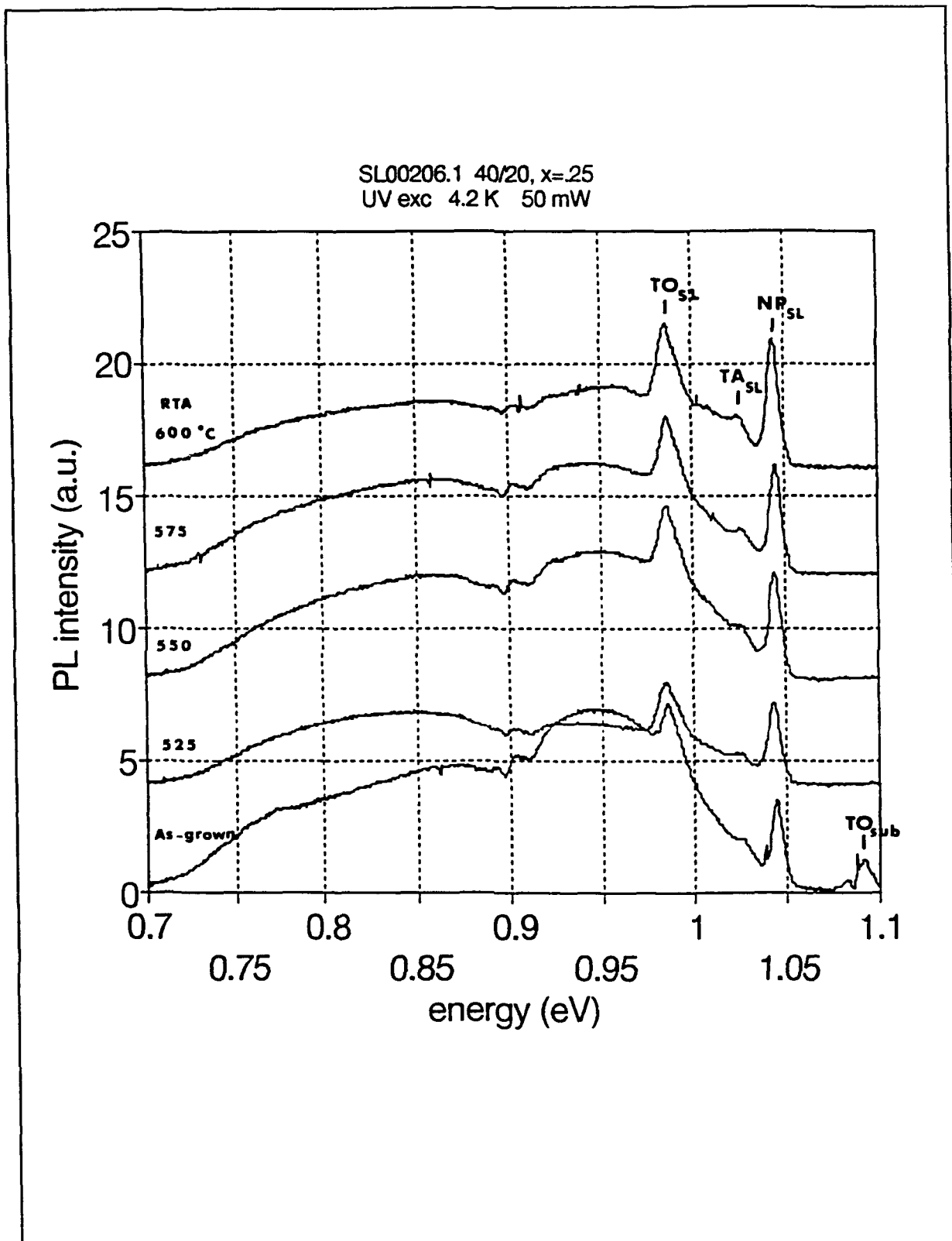


Figure 49: Annealing Study - SL00206.1

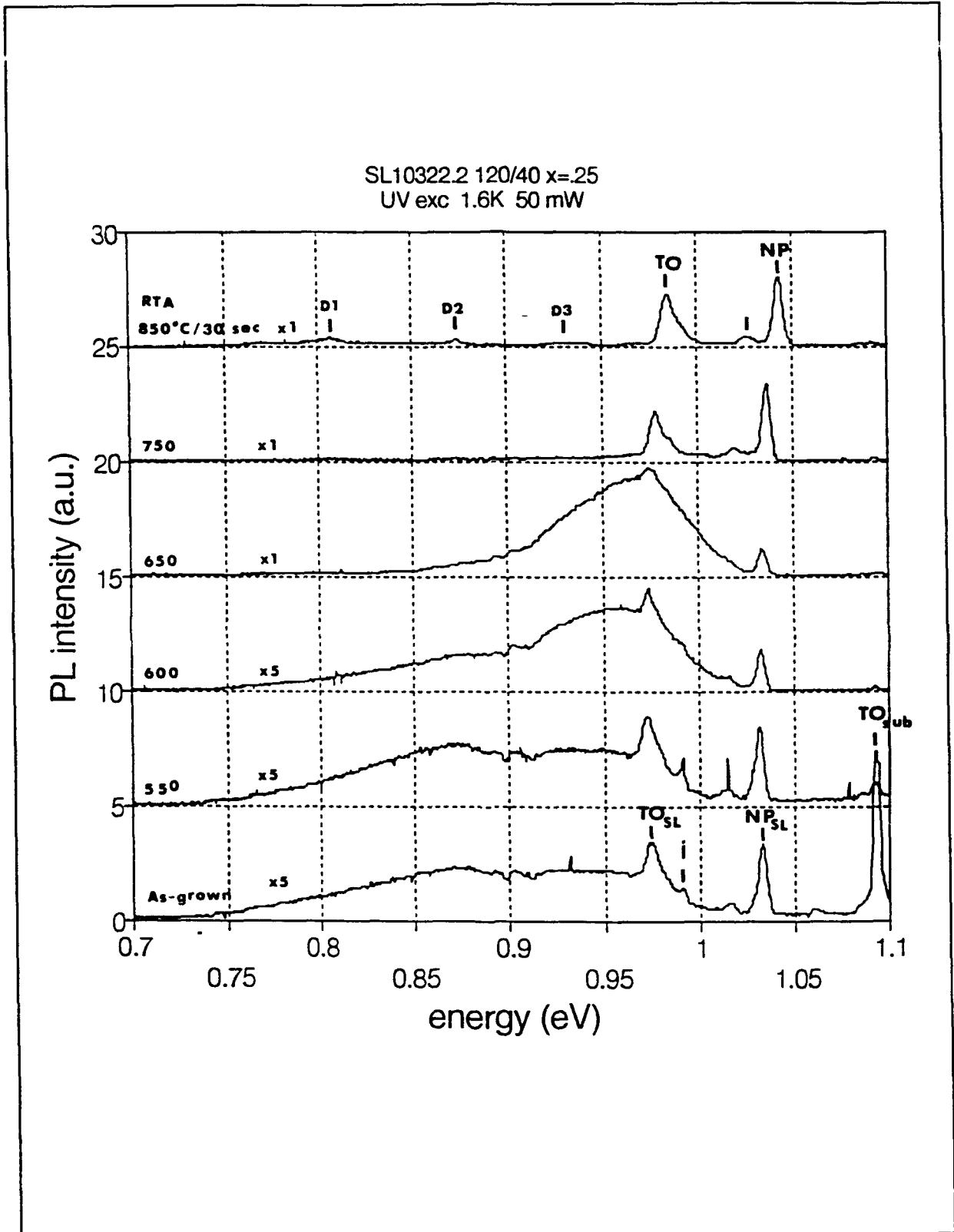


Figure 50: Annealing Study - SL10322.2

concentration, x . The widening of wells would result in a lower hole confinement energy and a lower effective superlattice band gap. The lower value of x in the wells would result in a higher effective superlattice band gap. In addition relaxation of the strain in the $\text{Si}_{1-x}\text{Ge}_x$ layers causes a shift to higher energy, corresponding to the dependence of $\text{Si}_{1-x}\text{Ge}_x$ band gap on strain. These three competing effects make the correlation of PL data to interdiffusion and strain relaxation for intermediate temperatures difficult. In the limit of very high temperatures, possibly at 850 °C, the superlattice structure is completely destroyed; the remaining superlattice region becomes a 0.5 micron thick strain relaxed epilayer with an alloy concentration determined by a weighted average of the layers of the superlattice. For SL00201.1, the completely interdiffused/relaxed superlattice results in an alloy layer with $x=0.083$. The bandgap for this layer would be 1.12 eV so that the NP line would be at 1.10 eV ($E_{\text{NP}} = E_{\text{ex}} - E_{\text{b}}$, where E_{ex} =free exciton binding energy = 14.3 meV and E_{b} =5 meV binding energy of exciton to shallow impurity). Since the NP line appears at 1.07 eV for the SL00201.1 850 °C sample, 30 meV lower than where it should appear for a fully relaxed and interdiffused superlattice, it is likely that the superlattice has not been fully relaxed for 850 °C/30 sec annealing. For sample SL10322.2, the completely relaxed alloy concentration would be 0.063, with a band gap of 1.13 eV. The NP line should appear at 1.11 eV, but instead appears at 1.04 eV.

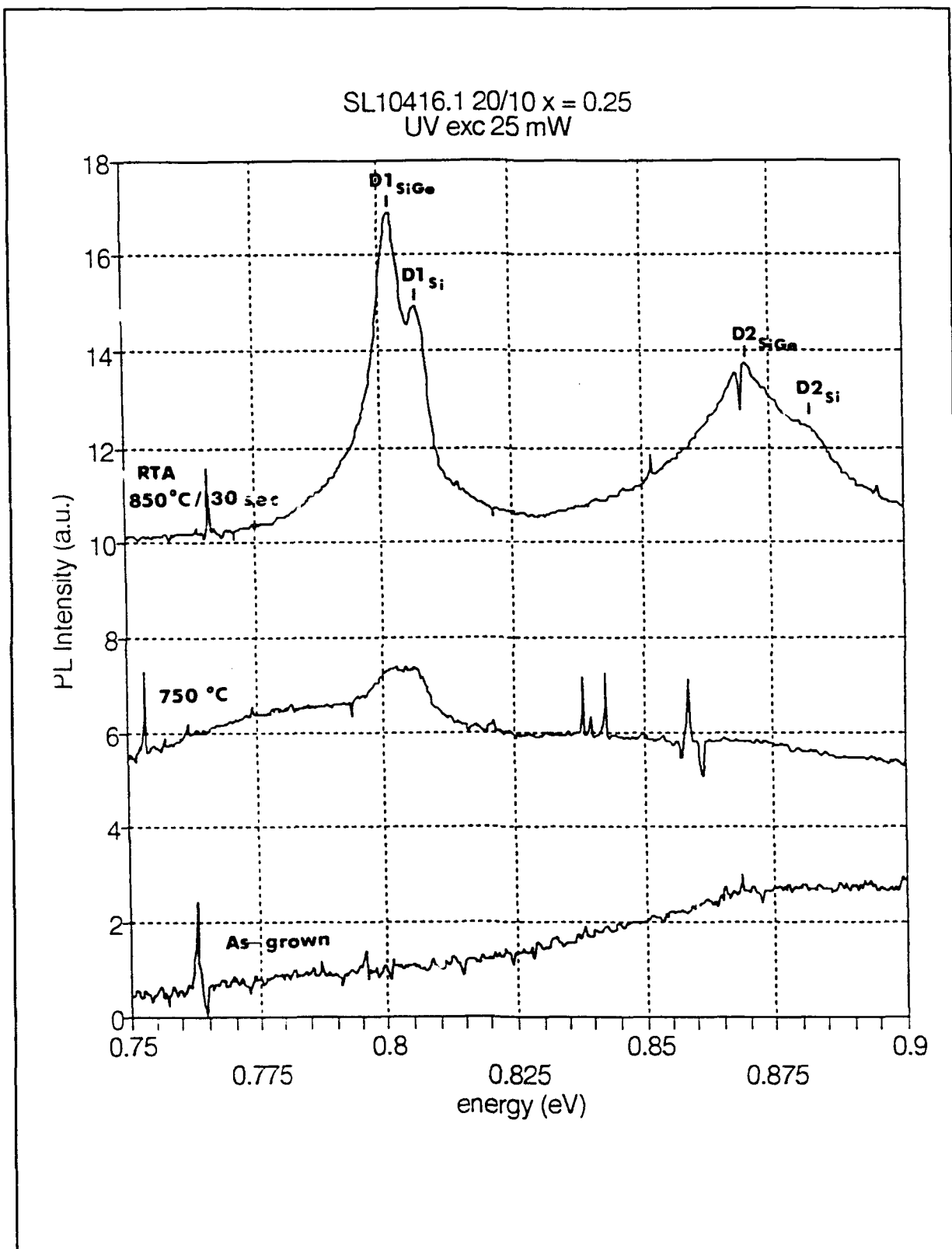


Figure 51: PL from SL10416.1 vs Anneal Temperature

Dislocation-lines brought out by high temperature RTA.

Annealing at high temperatures, usually above 650 °C, results in the formation of strong sharp PL lines at energies of Si dislocation-related D-lines. These are seen in Figures 48 and 50 as well as Figures 54-57 in the next section. These D-lines originated from dislocations created when misfit dislocations formed when the superlattice relaxed during heat treatment. In sample SL10416.1 (Figure 51) the D-lines created by high temperature annealing at 850°C are split into two components 5 meV apart. It is believed that the lower energy component of this doublet is related to dislocation-luminescence in the $\text{Si}_{1-x}\text{Ge}_x$ layers while the higher energy component is the Si dislocation luminescence. This is the first observation of D-lines in $\text{Si}_{1-x}\text{Ge}_x$.

Broad PL Band

Peak Positions. Nearly all of the samples examined have exhibited a broad PL band similar to the results of Noel, et al. (Noel 1990a). However our peak positions are not 120 meV below the strained $\text{Si}_{1-x}\text{Ge}_x$ bandgap as they found, but vary from 60 to 110 meV below the $\text{Si}_{1-x}\text{Ge}_x$ bandgap. This range of values is primarily due to varying amounts of quantum confinement of holes in the valence band. In Figure 52 the broad band PL peaks are plotted vs the germanium fraction, x , after subtracting from the PL peak position the calculated quantum confinement energy for holes determined from the Kronig-Penney model. In this way we can directly compare our peak positions relative to the band gap vs those of Noel et al. As can be seen in Figure 52, our broad band peaks after correcting for quantum confinement of holes, agree with Noel data that shows the peak emission is 120 meV below the band gap, but that in our case the correct band gap is the effective superlattice band gap. Our samples with sharp BE spectra, that precisely give the effective superlattice band gap, can be used as a confirmation of the 120 meV difference. Using the band gaps determined from the positions of the bound exciton NP lines in Table V, the positions of the broad band relative to the band gap can be determined as exactly as we can identify the broad peak position. The result is that the broad band peak position is 131, 113, and 145 meV below the band gap for SL00201.1, SL00206.1, and SL10322.2, respectively for an average of 130 meV. The slight

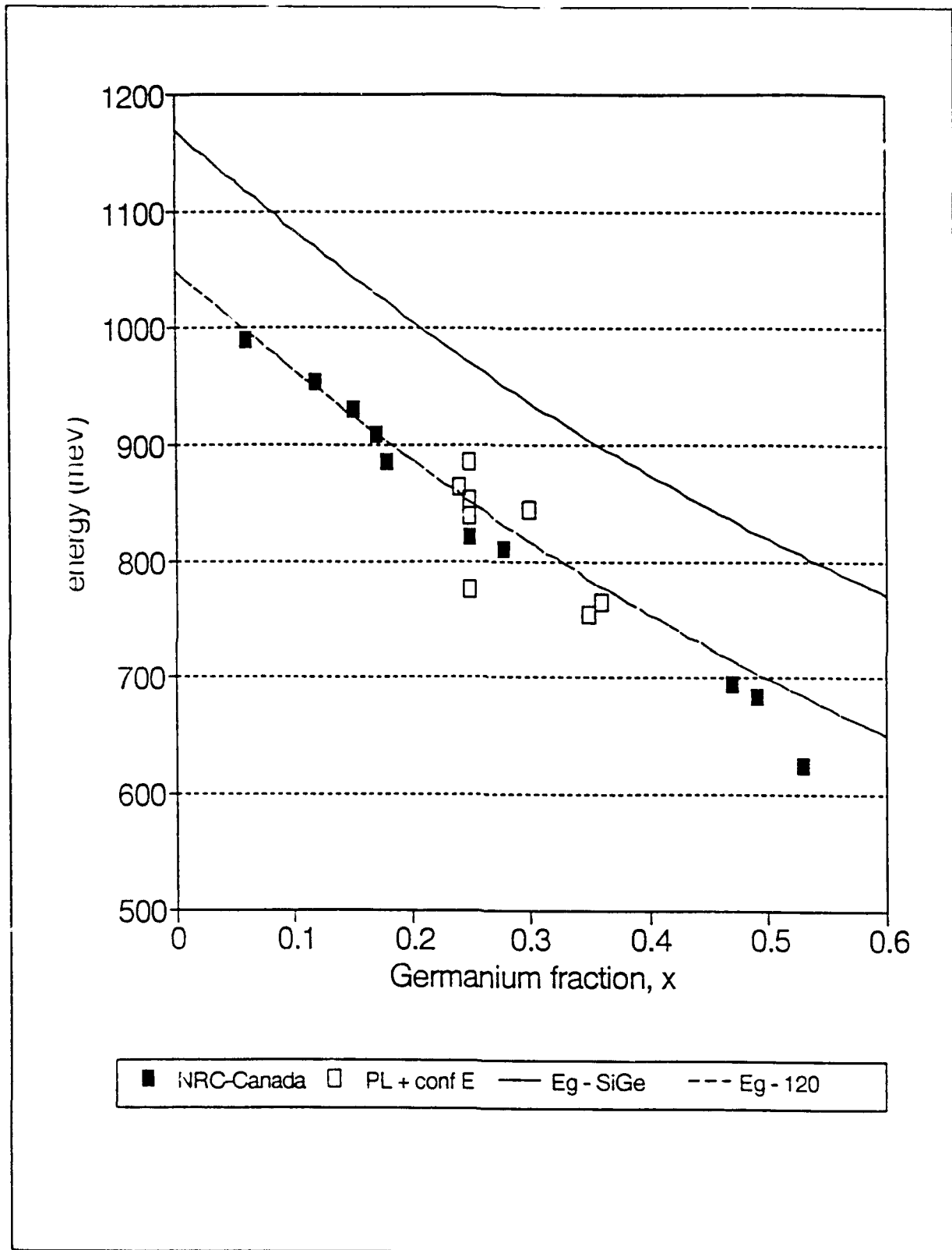


Figure 52: Broad Peak Energy vs. Alloy concentration

discrepancy here may be due to the difficulty in establishing the broad peak position in the samples that had both broad band and sharp BE emission.

Identification of the 120 meV difference between broad peak energy and the effective band gap is important for two reasons. First, the broad band emission in Si/Si_{1-x}Ge_x is due to deep centers that emit 120 meV below the band gap. Second, the broad band emission, even though it is deep, is affected by the superlattice potential and the emission energy moves with the amount of quantum confinement of holes.

Model for Broad PL Mechanism. There are several possible models or mechanisms to account for the broad band PL. The most likely mechanisms are the donor-acceptor pair model and the isoelectronic bound exciton complex model.

It has been proposed that the broad band emission is due to donor-acceptor pair recombination. (Kennedy 1992) Donor-acceptor pair emission has previously been seen in intentionally doped Si. (Enck and Honig 1969, Ziemelis and Parsons 1981, Ziemelis 1982) Donor-acceptor pair emission in Si is characterized by a long radiative lifetime, and a broad emission band that includes recombination from distant pairs. The emission energy for a given donor-acceptor pair is given by

$$E_{PL} = E_g - (E_A + E_D) + e^2/\epsilon R + E_{phonon} \quad (35)$$

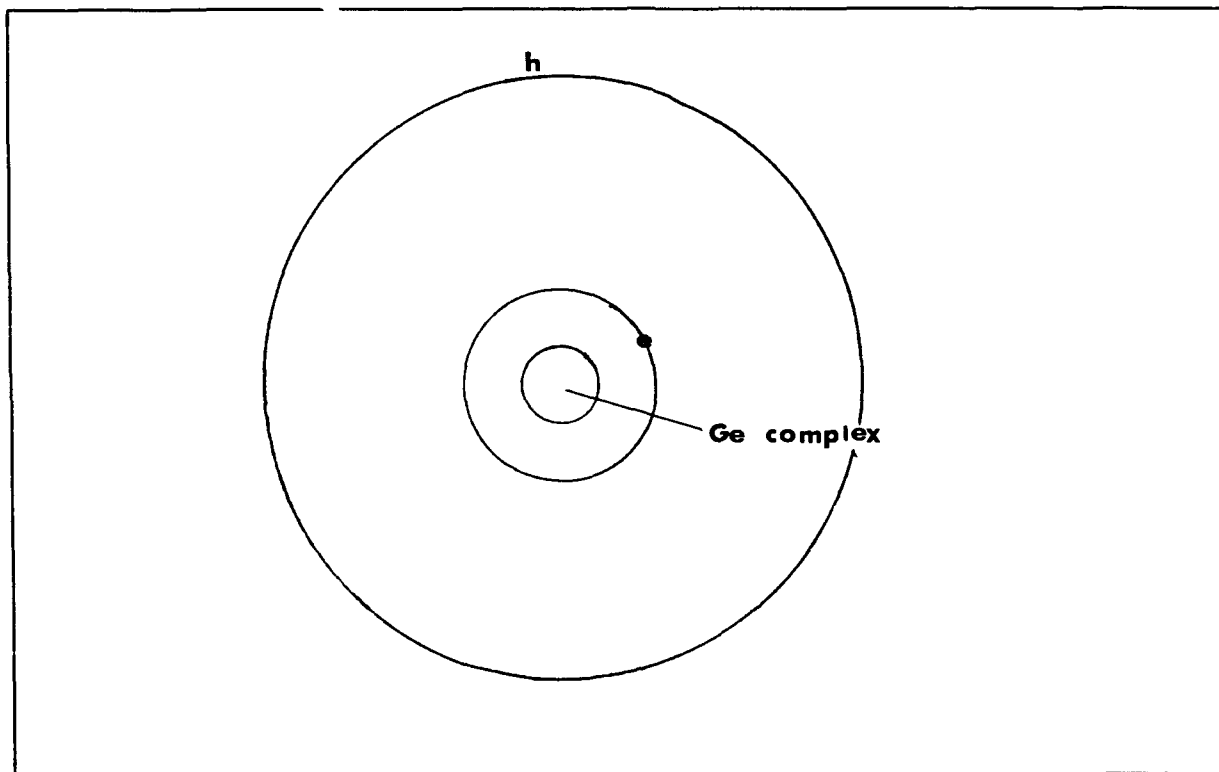


Figure 53: Model for Broad Band Emission. The center first tightly binds an electron; the charged center then loosely binds a hole.

where E_{PL} is the emission energy, E_A and E_D are the acceptor and donor ionization energies, and R is the distance between the donor and acceptor. For Si, the acceptor and donor ionization energies are 40 meV or higher, depending on the impurity. (Sze 1981) Thus, the donor-acceptor pair emission has a temperature dependence characterized by a 40 meV or higher activation energy, from the ionization of either donors or acceptors (whichever has a lower ionization energy, usually donors).

The other model for the broad band PL mechanism was first suggested by Houghton *et al.* They proposed that the broad PL seen in Si/Ge and $Si_{1-x}Ge_x$ /Si superlattices and heterostructures was due

to isoelectronic centers related to Ge complexes. (Houghton 1991) The complexes necessarily include Ge interstitials in order to differentiate the optically active Ge atoms from the lattice Ge. The complexes also must contain two or more atoms or vacancies. Isoelectronic centers have very strong emission in indirect band gap materials, the most notable example being GaP:N. Isoelectronic centers are characterized by a long radiative lifetime and are very efficient at trapping excitons. As is the case with most isoelectronic centers, it is proposed that the centers responsible for the broad emission first tightly bind an electron through an electron trap, and the hole is more loosely bound in a hydrogen-like orbit, as shown in Figure 53. This type of configuration is typical of excitons bound to isoelectronic centers including isoelectronic complexes. In this configuration, the hole, having a large effective Bohr radius of approximately 30 angstroms, would be affected more by the superlattice potential, due to the overlap of the hole wave function with the superlattice potential barriers. The electron, being tightly bound and having a smaller effective Bohr radius, would be affected less by the superlattice potential. Furthermore, the band alignment in Si/Si_{1-x}Ge_x has a conduction band offset of 50 meV or less, too little for any confinement effects on electrons.

Other models have been proposed that rely on fluctuations in the Si_{1-x}Ge_x alloy concentration or in layer thicknesses that produce regions within the superlattice with a lower band gap. (Chi 1991,

Rowell 1991) It has been proposed that these regions could confine excitons forming a high density exciton phase, resulting in broad band emission below the $\text{Si}_{1-x}\text{Ge}_x$ band gap similar to electron-hole droplet emission in bulk Si or Ge. In fact, this is the model used previously to explain similar broad band L-band emission in bulk $\text{Si}_{1-x}\text{Ge}_x$ alloys. (Weber and Alonso 1989) The problem with these models is that they can not explain the 120 meV difference between the peak emission and the band gap. However, it is possible that fluctuations in either the alloy concentration or the layer thicknesses, or both, could have an effect on the linewidth and peak position of the broad band, which will be discussed further below.

Annealing effects on broad band PL. The effects of annealing on the broad band PL were in three categories. First, similar to the Noel results, PL intensity increases with annealing temperature up to approximately 650 °C, then decreases at higher annealing temperatures as interdiffusion and strain relaxation commences. Second, the PL peaks shift to higher energies as the annealing temperature increases, even for annealing at 550 °C (see Figures 54-57). At annealing temperatures below 650 °C for samples grown at 500 °C, interdiffusion and strain relaxation should be minor and is not expected to produce a shift in superlattice band gap corresponding to the shifts in the broad band peak positions that we have seen. (Houghton 1991a) The positions of the sharp BE lines, which are very sensitive to sample structure (as shown by

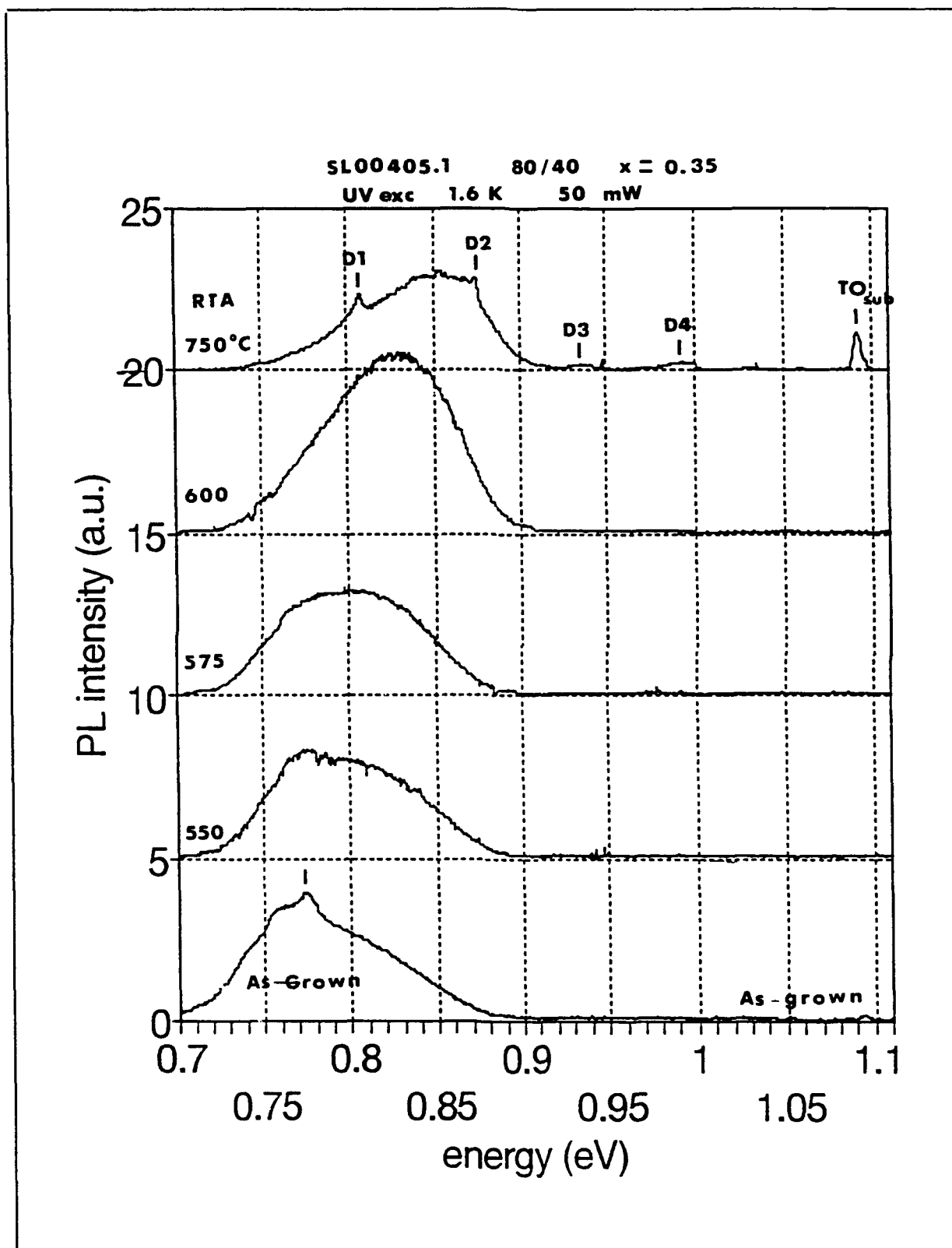


Figure 54: Dependence of PL on annealing temperature - SL00405.1

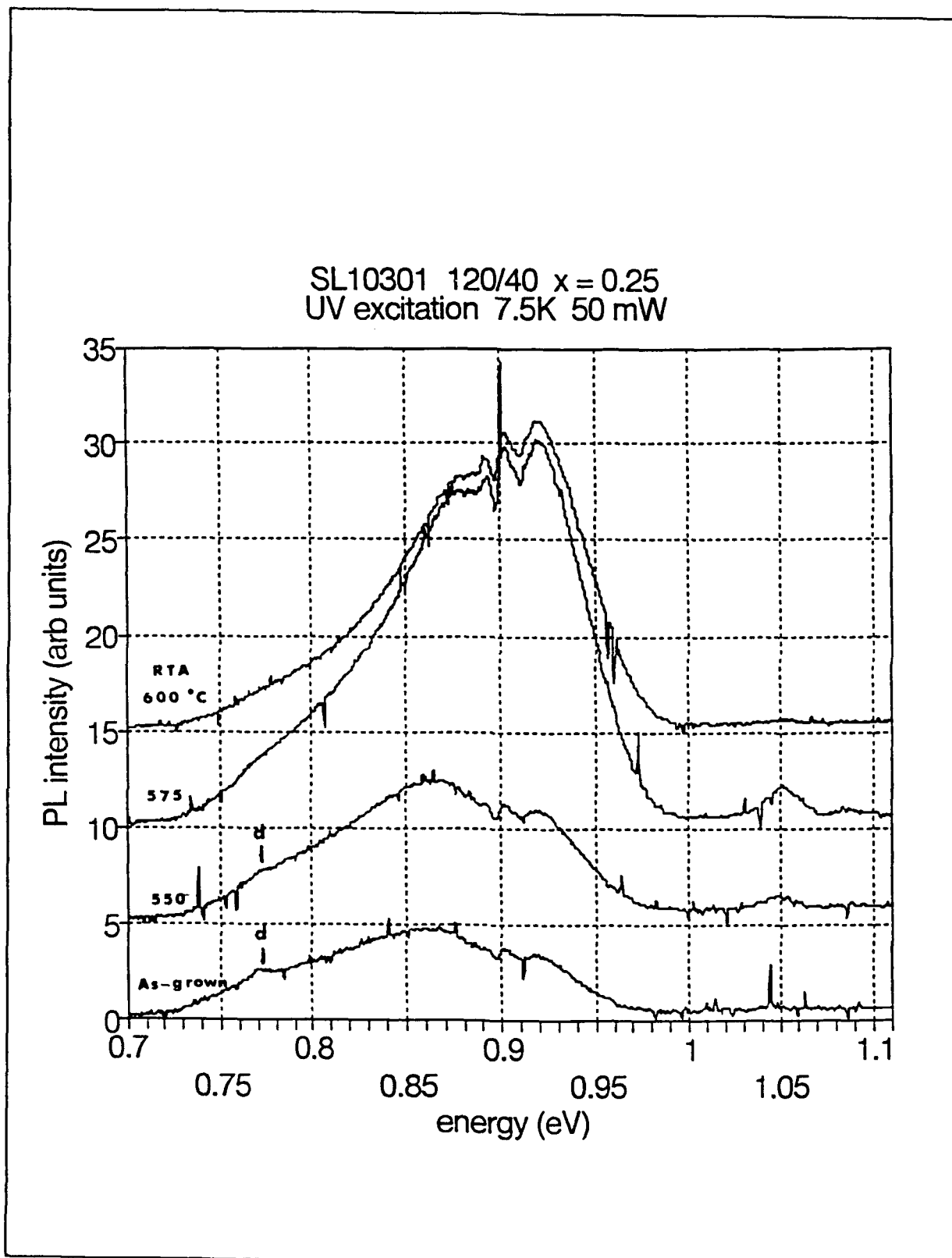


Figure 55: Dependence of PL on annealing temperature - SL10301.1

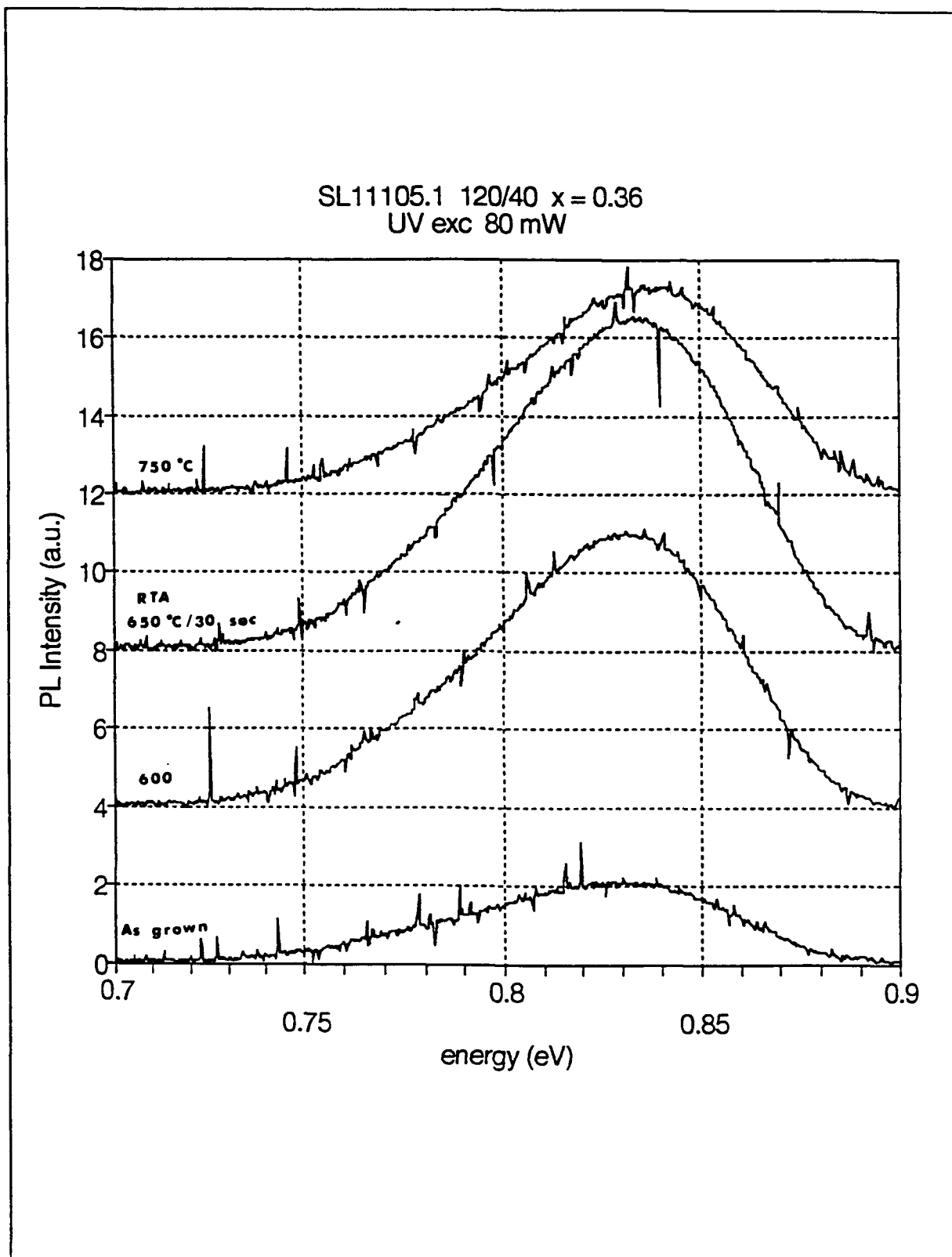


Figure 56: Dependence of PL on annealing temperature - SL11105.1

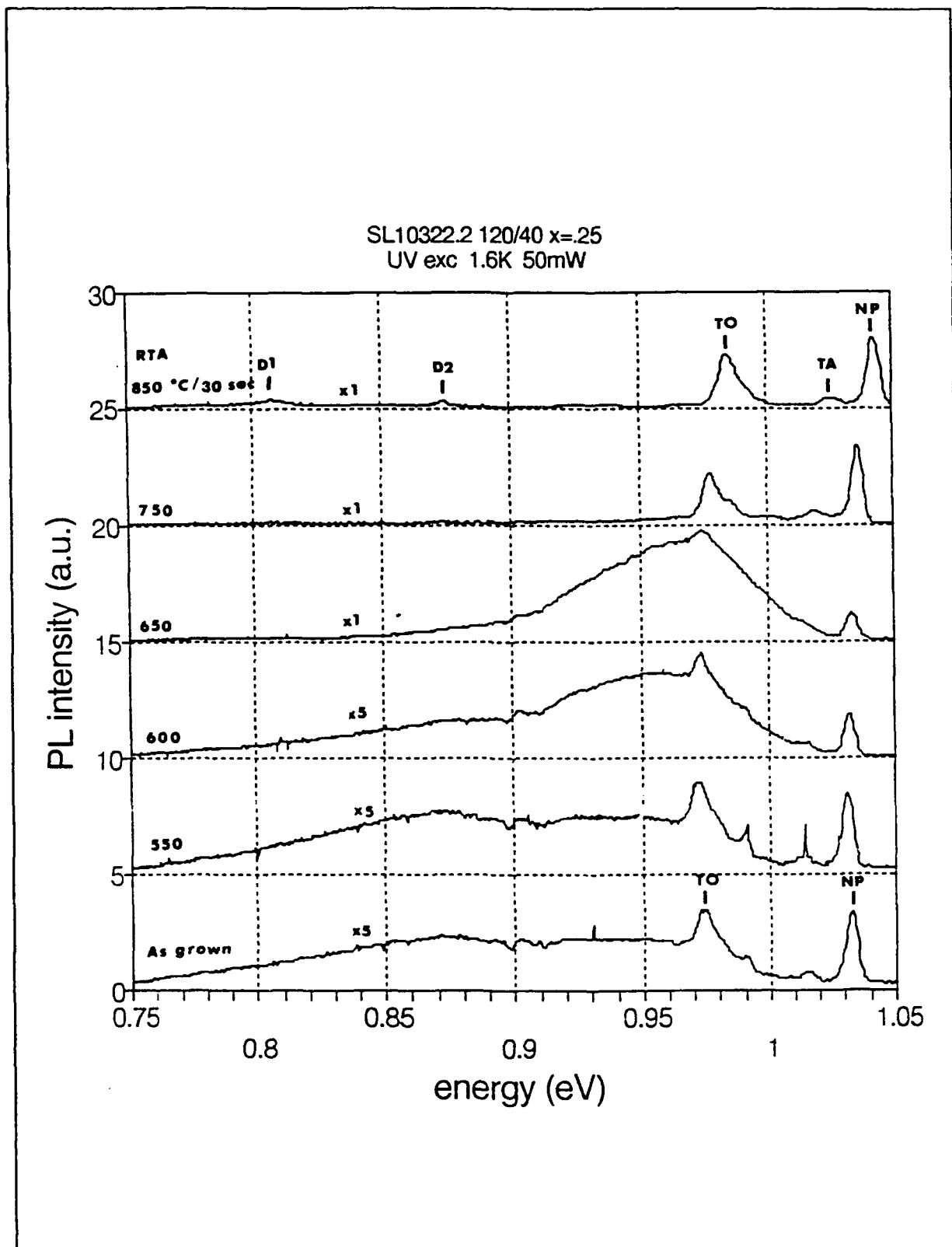


Figure 57: Dependence of PL on annealing temperature - SL10322.2

Table VIII: PL Peaks positions vs. Anneal Temperature

Sample No.	t_{Si}/t_{SiGe}	PL Peak Positions (meV)				
		As Grown	550/30	600/30	650/30	750/30
SL00405.1	80/40	770	775	826	827	850
SL10206.1	140/70	860	863	867	---	874
SL11105.1	120/40	825	825	830	840	---
SL10531.1	140/70	880	885	---	---	---
SL10531.2	140/70	776	788	792	790	800
SL10322.2	120/40	930	930	960	970	---

the Kronig-Penney calculations in the previous section) that would be altered by interdiffusion and strain relaxation, do not shift until the samples are annealed above 650 °C (see Figures 48-51). Thus, the shifts in the broad band peak for anneal temperatures below 650 °C cannot be due to substitutional interdiffusion. It is proposed that the shifts are due to diffusion of Ge interstitials that are part of the Ge complex that produces the broad PL band. Since interfaces are efficient at trapping impurities, the result is a net diffusion of Ge interstitials from the center of the $Si_{1-x}Ge_x$ layer to the edges, and thus a shift of the PL peak. The details of the peak shift will be discussed below. Third, the activation energies determined from the PL temperature dependence decreased as the anneal temperature increased. These three effects will be discussed more below.

Temperature Dependence of Broad Peak. The broad PL band was examined as a function of sample temperature for each of the samples; the results are shown in Figures 58-64. The PL signal in each case increases from 1.6 K to 20 K, then falls off for higher temperatures with an activation energy in the range of 7.5 to 27 meV. The activation energies were determined by plotting the natural log of the integrated broad peak intensity versus $1/T$, similar to the analysis done in the case of the sharp BE peaks. At the higher temperatures this plot approaches a linear fit with the slope equal to the activation energy divided by Boltzmann's constant, as in the previous section. The fits for each sample are shown in Figures 65-71, and the activation energies for the as-grown as well as the annealed samples are summarized in Table IX. These activation energies rule out the donor-acceptor pair model as the emission mechanism, which should have activation energies greater than 40 meV. The broad PL bands also shift to lower energy with increasing temperature.

Annealing Effects on Broad PL Band Activation Energies. As shown in Table IX, the activation energies of the broad PL band depend upon the annealing temperature. The activation energies decrease from the as-grown case, and are a minimum at the highest anneal temperature for which the broad band peak is observed for each sample. This shift in the activation energies can be explained in terms of the isoelectronic bound exciton complex model. We start with the assumption that in the as-grown samples,

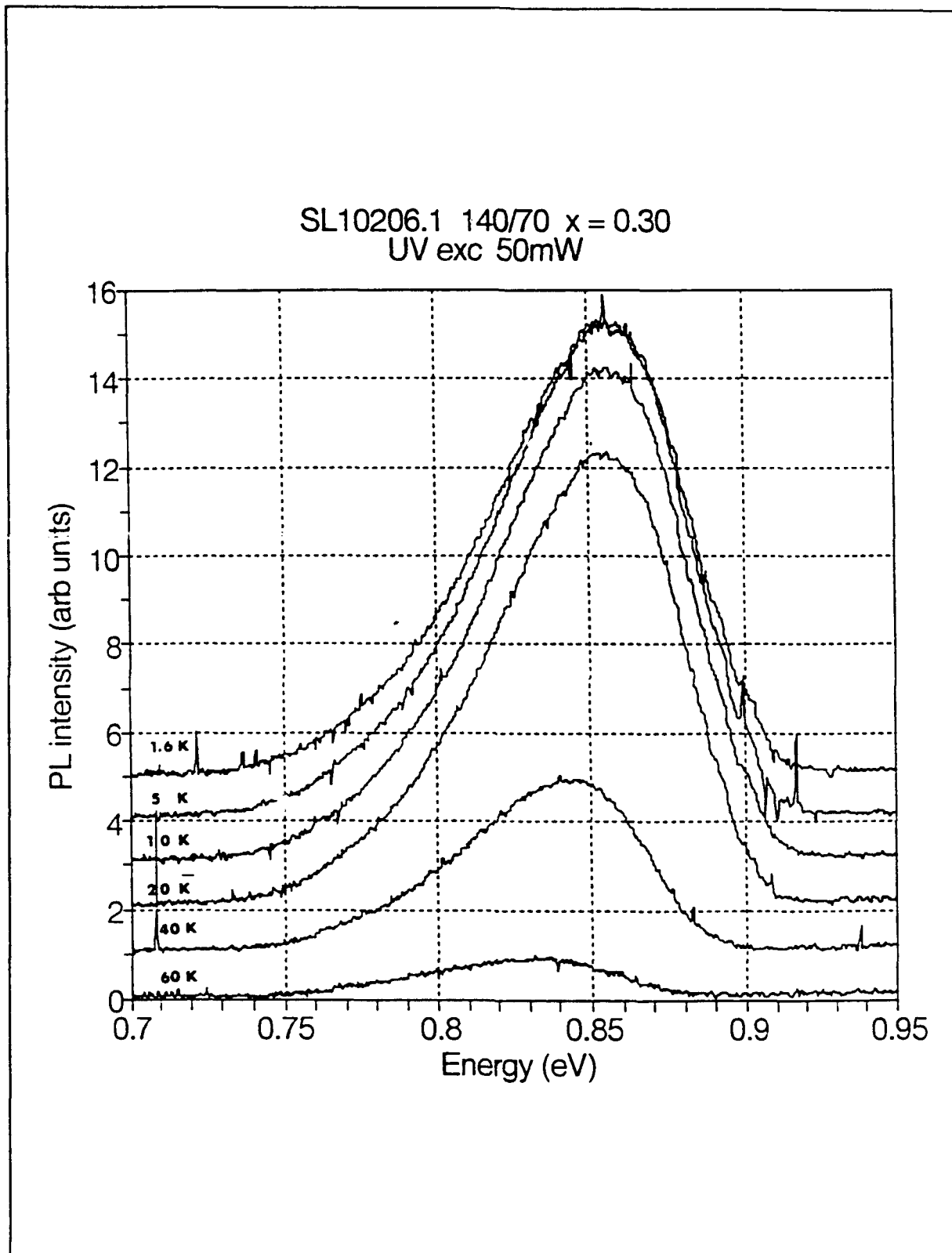


Figure 58: Temperature Dependence of Broad Band PL SL10206.1

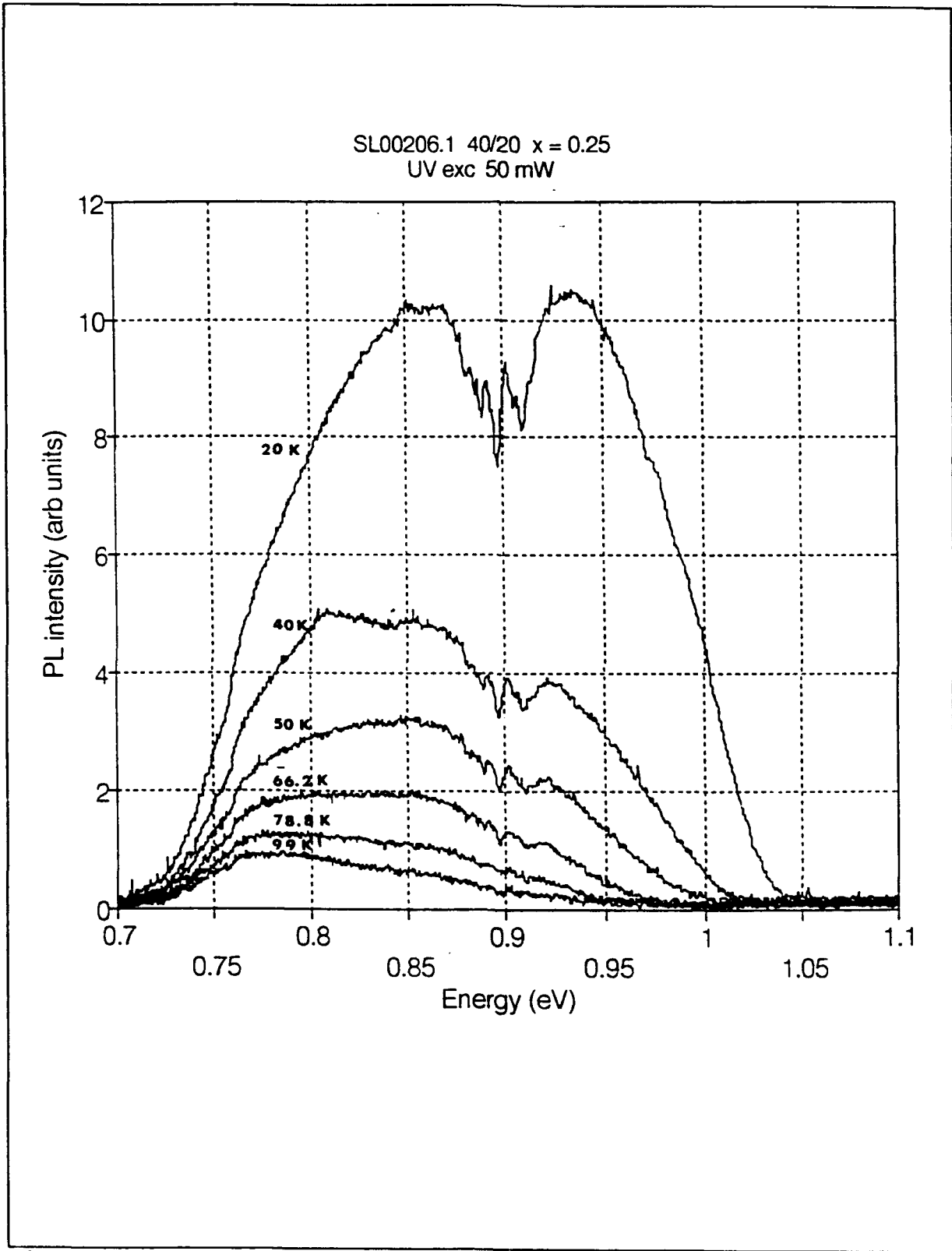


Figure 59: Temperature dependence of broad band PL - SL00206.1

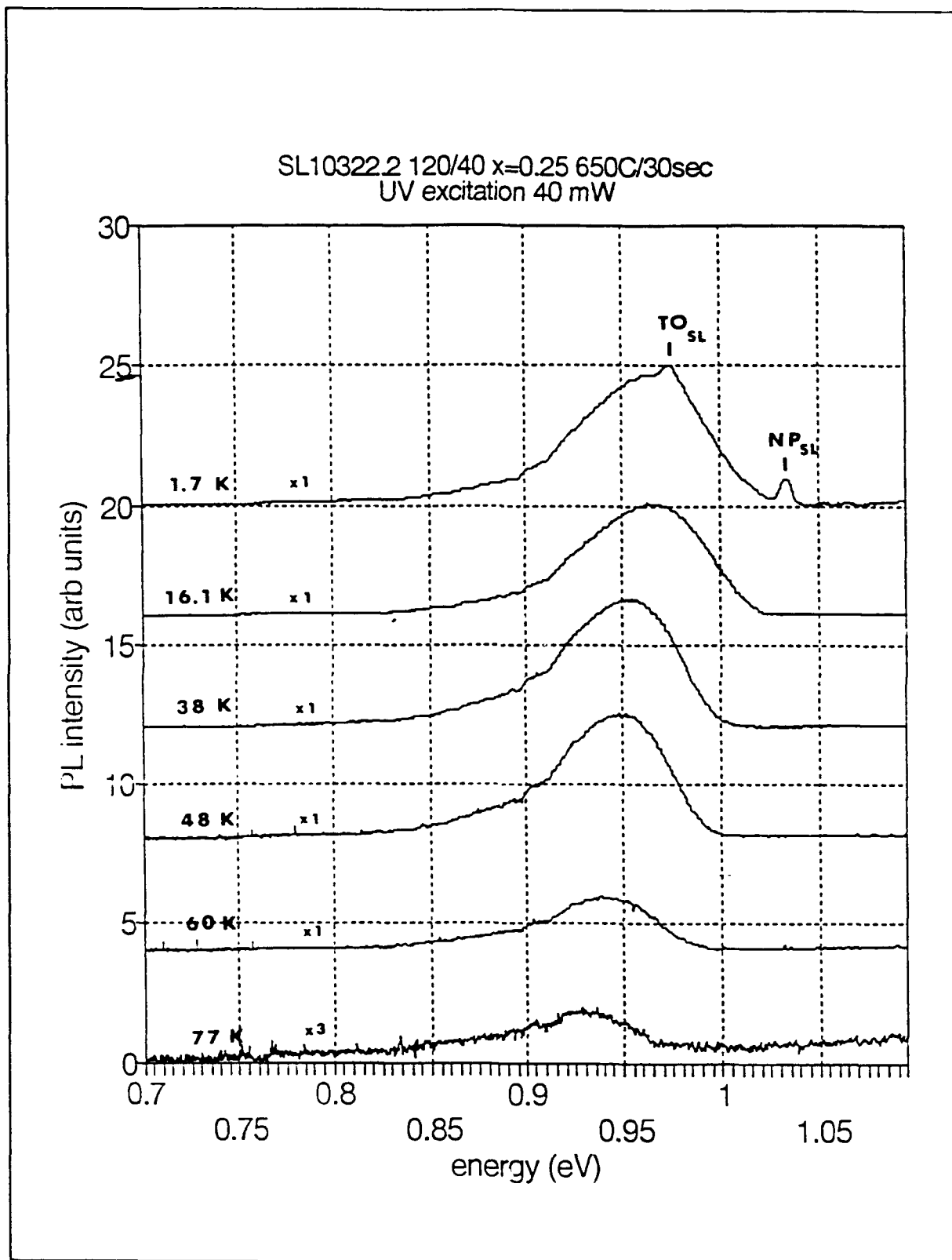


Figure 60: Temperature dependence of broad band PL - SL10322.2

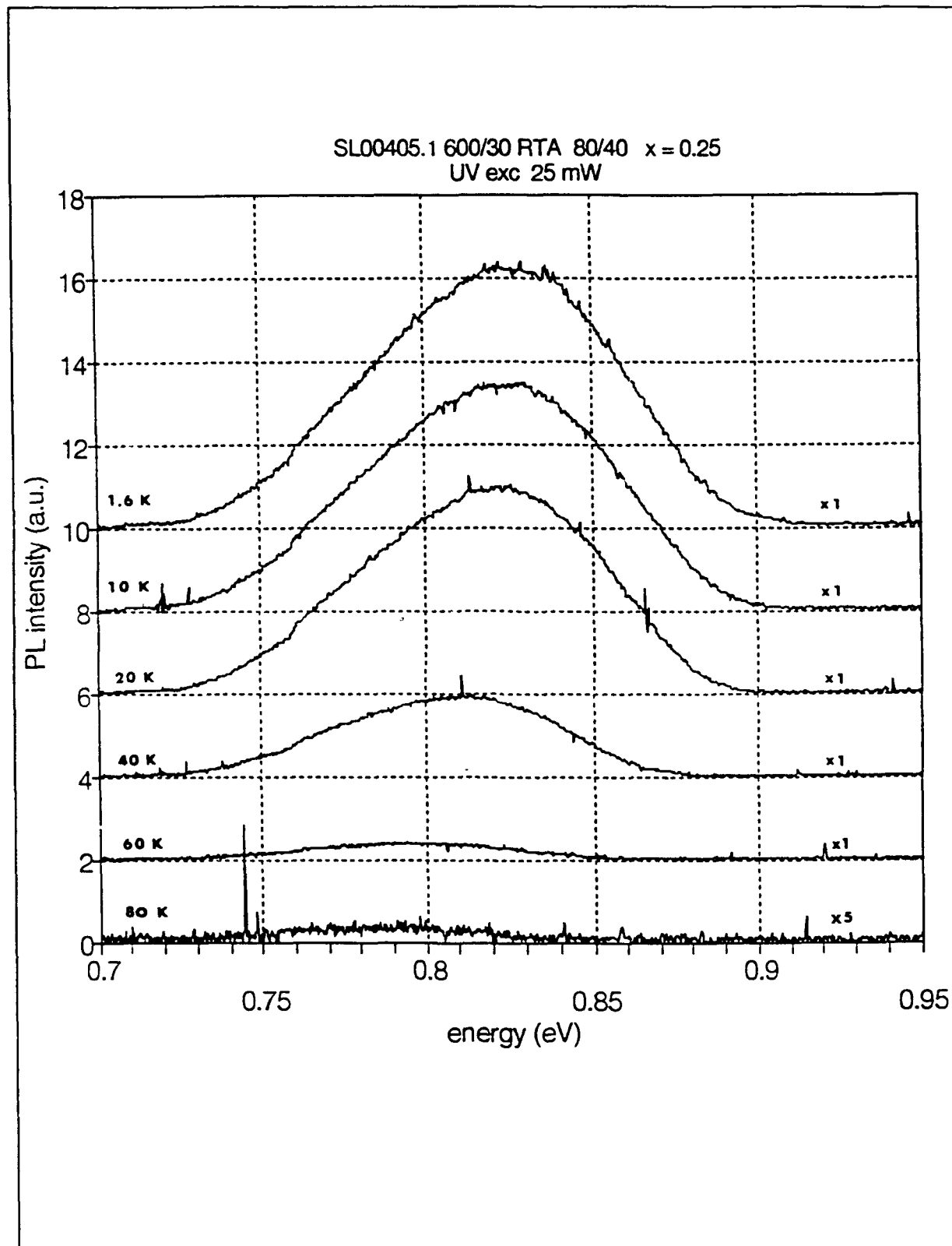


Figure 61: Temperature dependence of broad band PL - SL00405.1

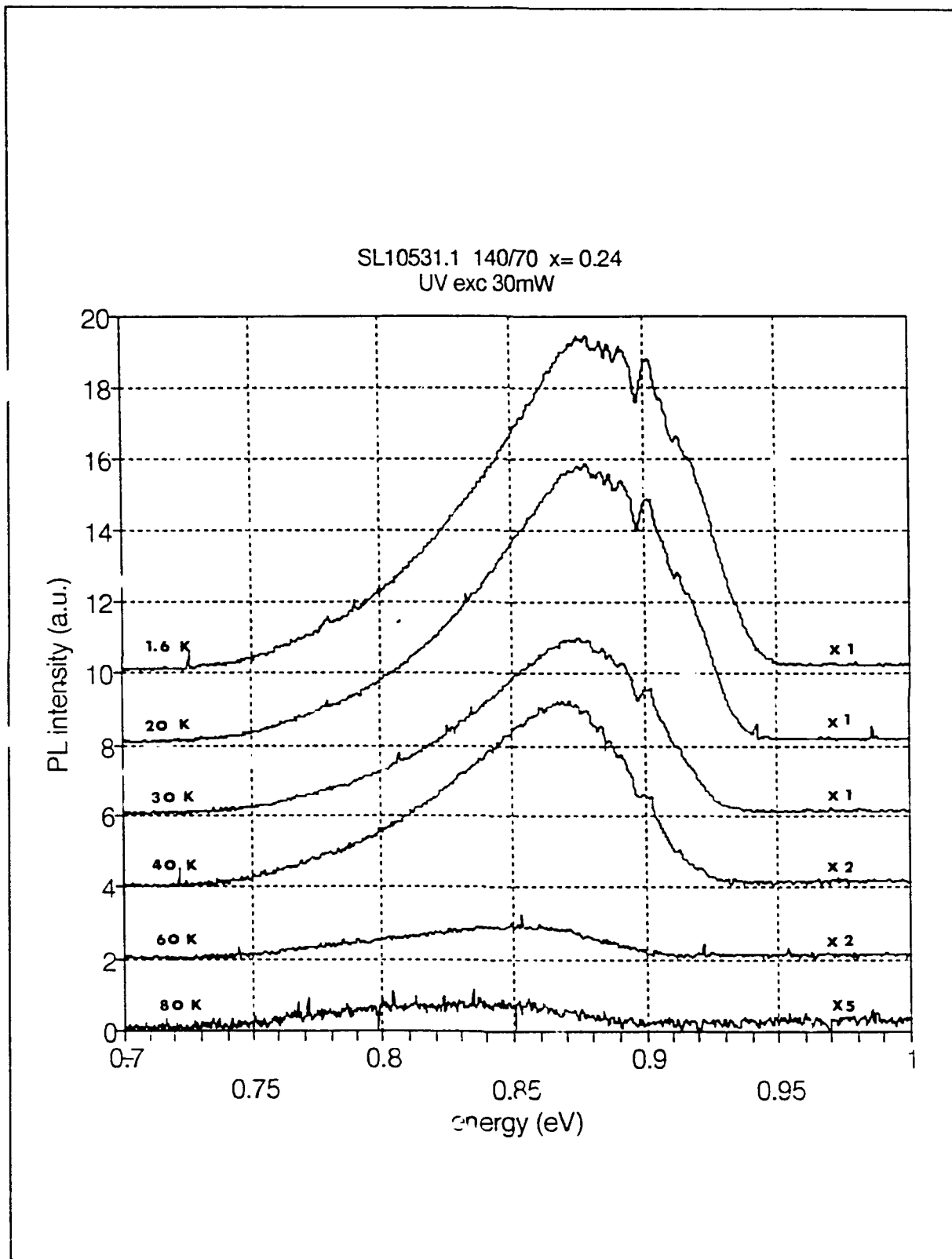


Figure 62: Temperature dependence of broad band PL - SL10531.1

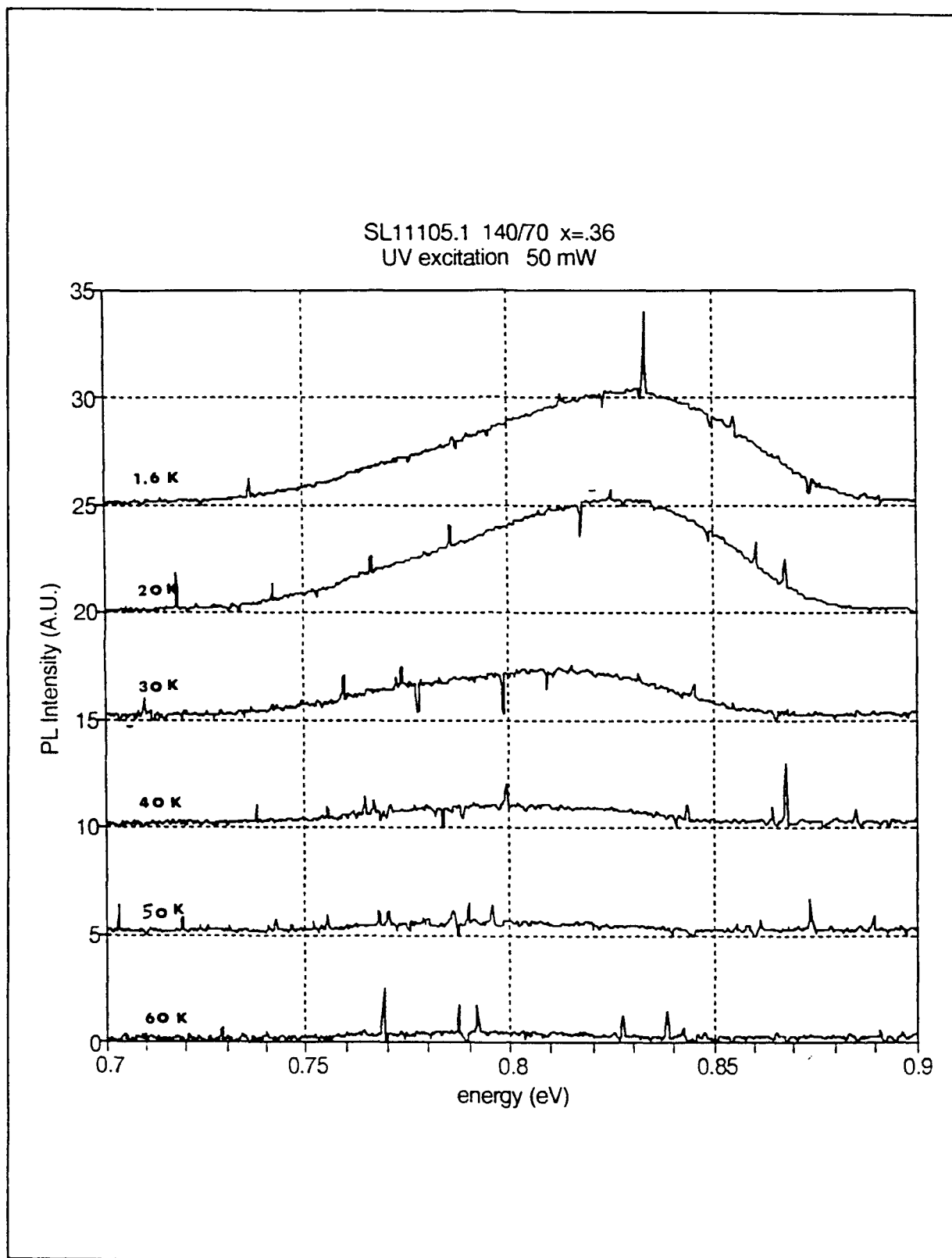


Figure 64: Temperature dependence of broad band PL - SL11105.1

SL10206.1 140/70 x = 0.3
UV exc (files 1206v10-16)

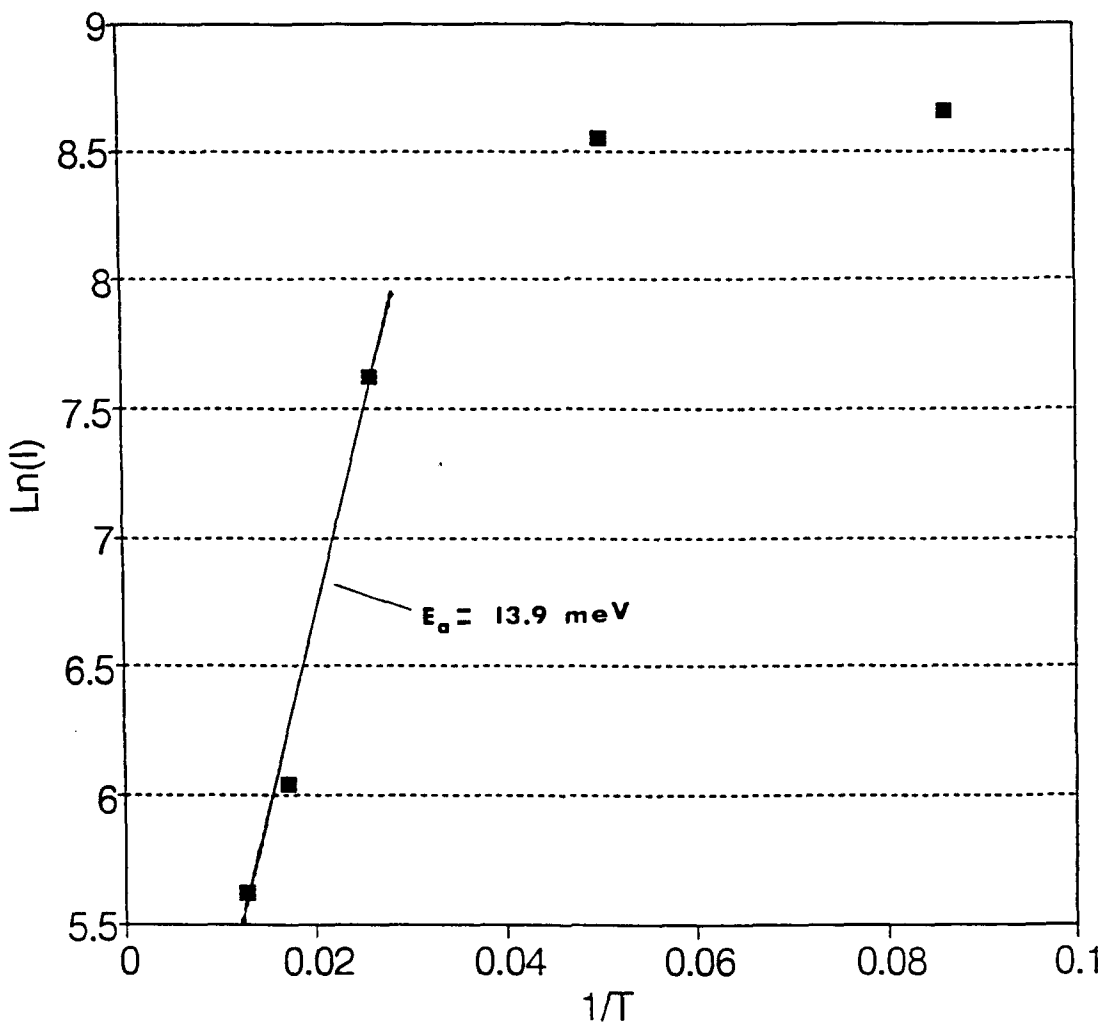


Figure 65: Ln I vs. 1/T, broad band PL - SL10206.1

SL00206.1 40/20 x = 0.25
UV exc 50mW

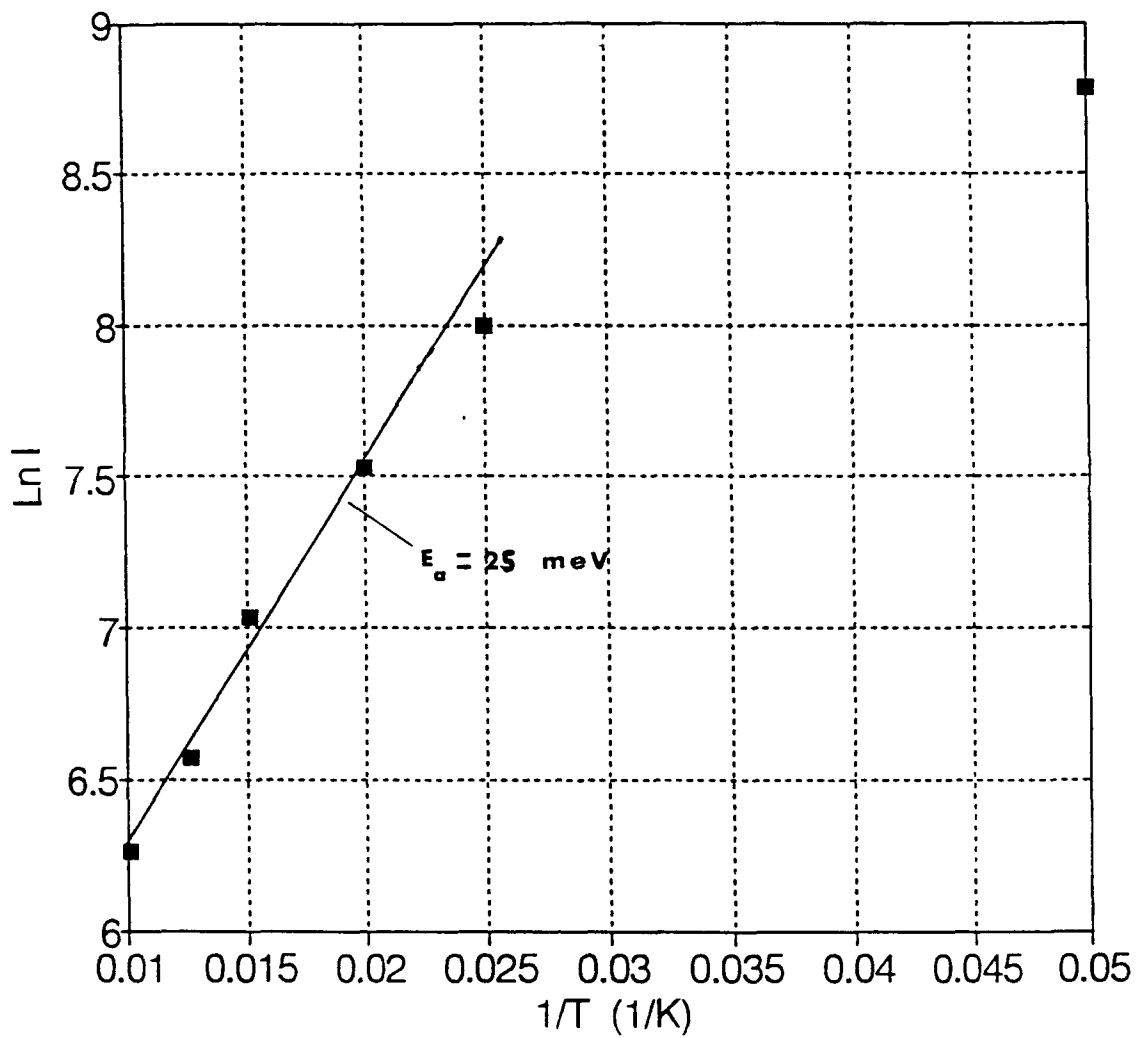


Figure 66: $\ln I$ vs. $1/T$, broad band PL - SL00206.1

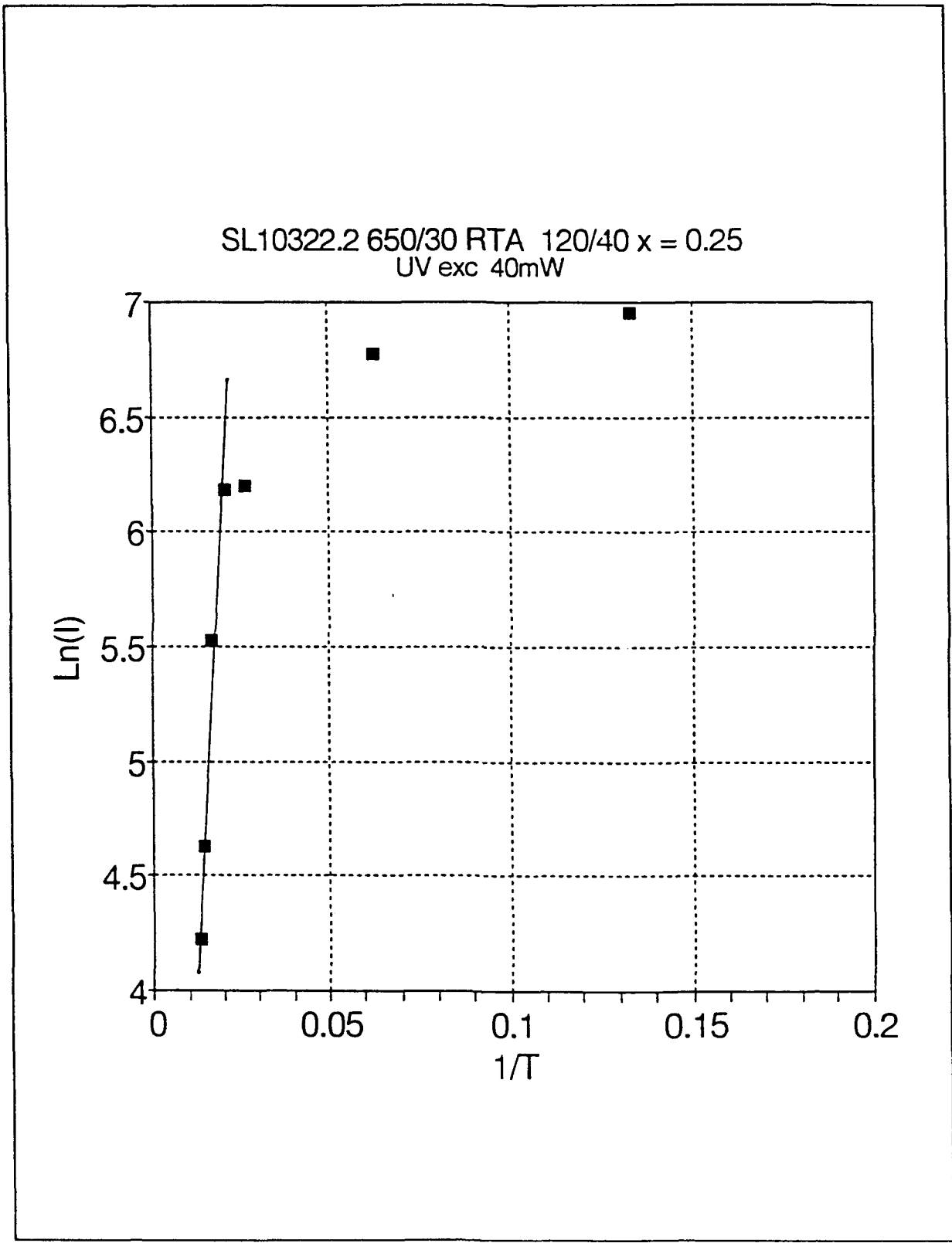


Figure 67: $\ln I$ vs. $1/T$, broad band PL - SL10322.2

SL00405.1 660C/30sec RTA 80/40 x = 0.35
UV exc 50mW

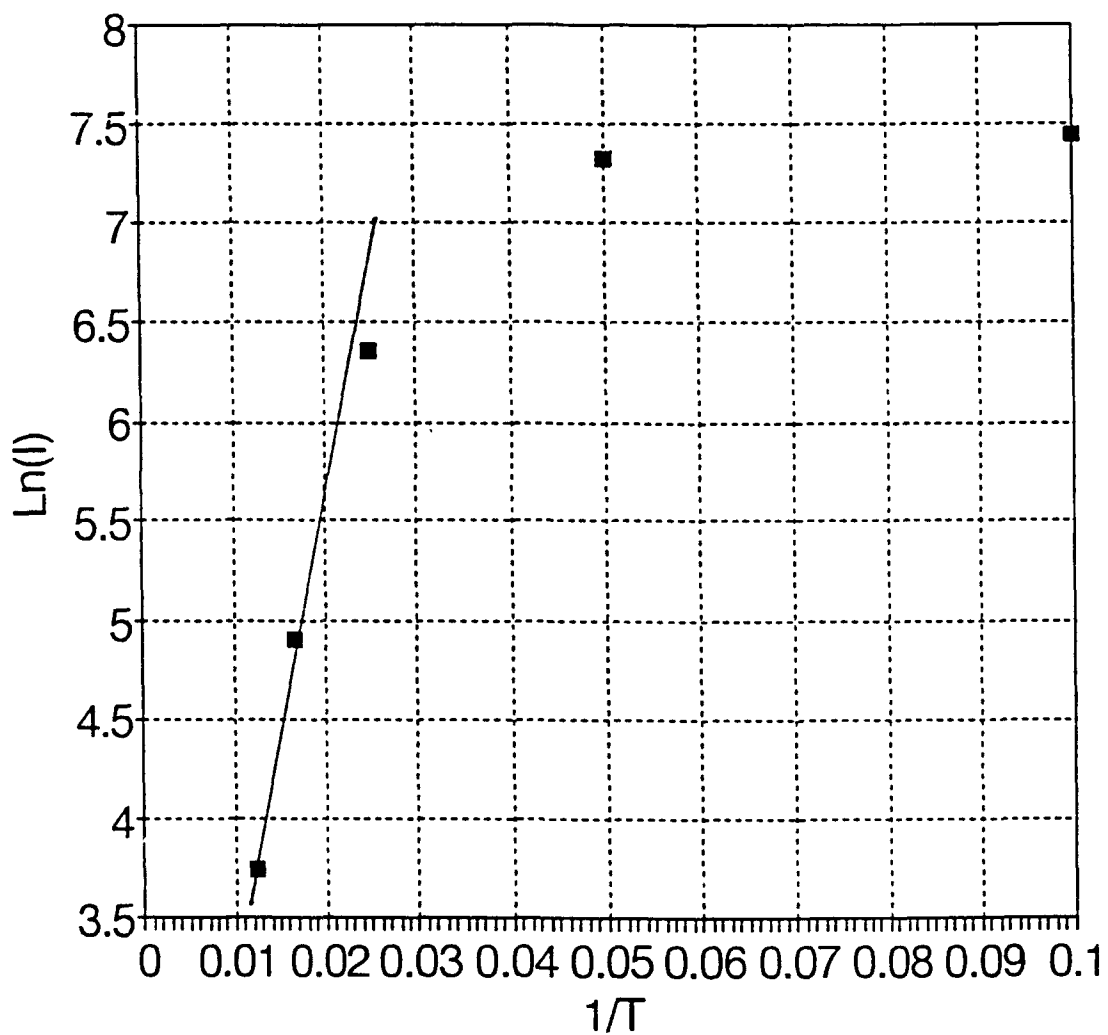


Figure 68: $\ln I$ vs. $1/T$, broad band PL - SL00405.1

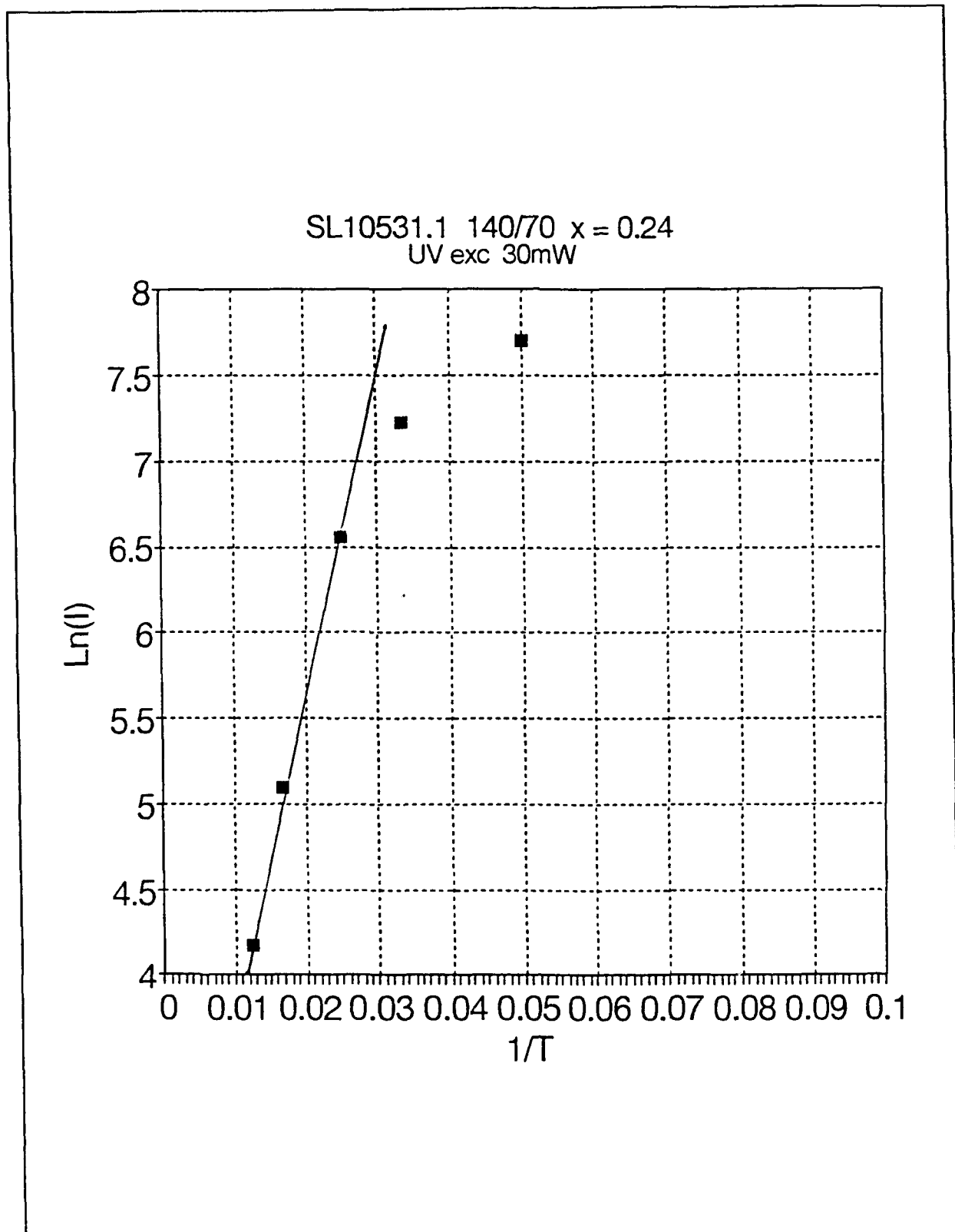


Figure 69: $\ln I$ vs. $1/T$, broad band PL - SL10531.1

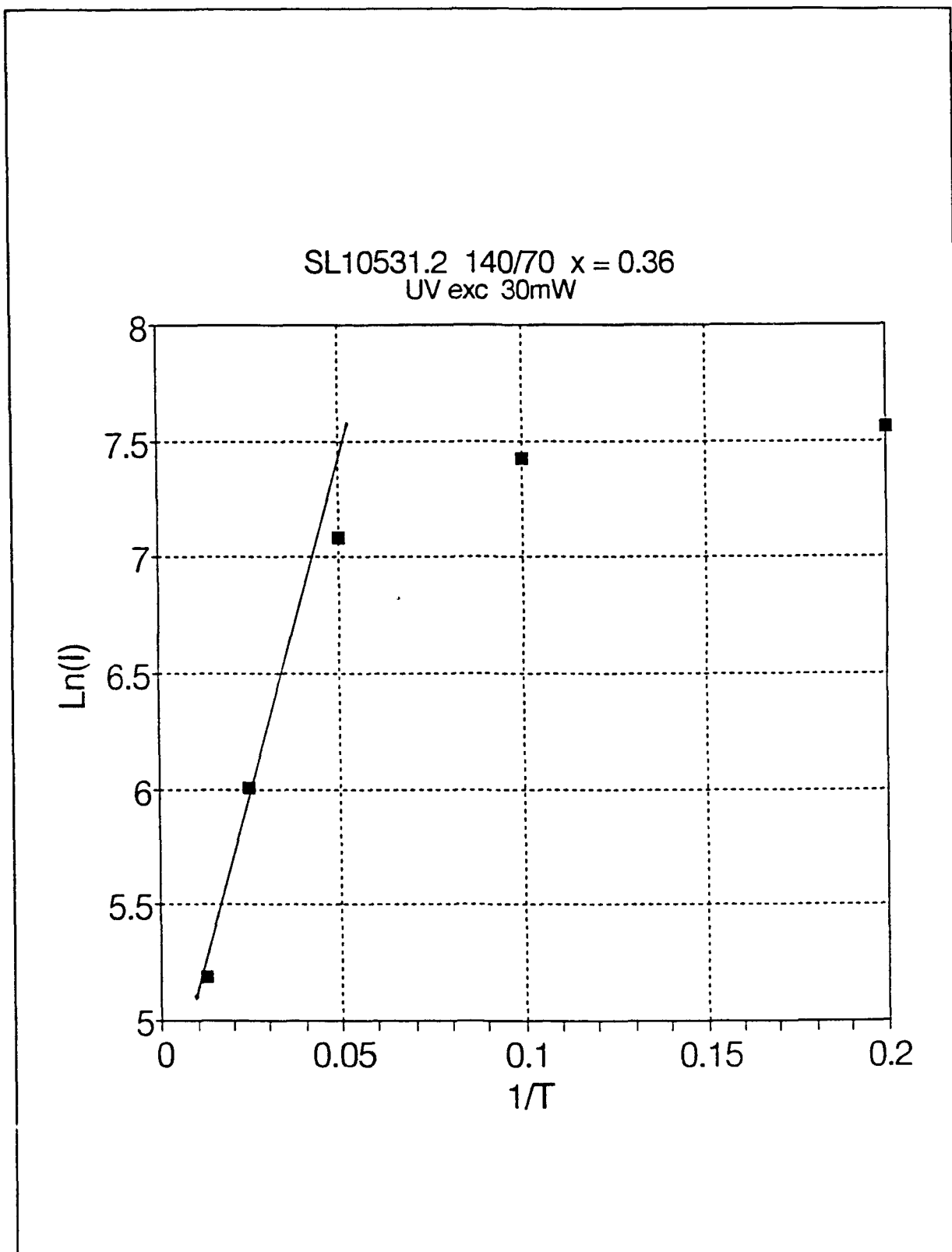


Figure 70: Ln I vs. 1/T, broad band PL - SL10531.2

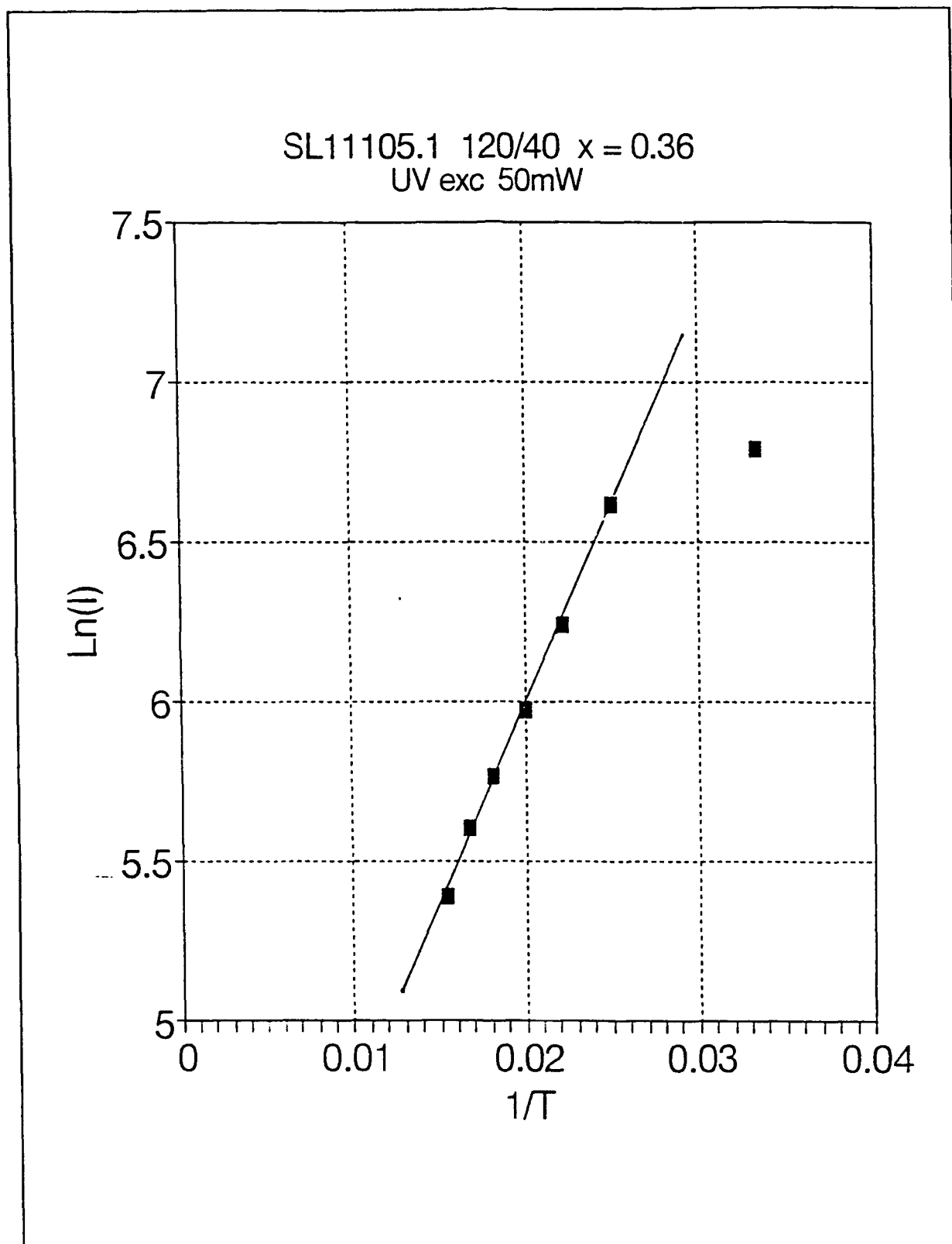


Figure 71: $\ln I$ vs. $1/T$, broad band PL - SL11105.1

Table IX: Activation Energies of broad peaks vs. annealing temperatures

Sample No.	Activation Energies (meV)				
	As grown	550/30	600/30	650/30	750/30
SL00405.1	22.3	21.4	10.9	7.75	7.7
SL10206.1	13.9	13.0	12.5	----	10.0
SL11105.1	14.0	10.7	10.4	8.1	----
SL10322.2	26.8	22.4	16.3	15.1	-----
SL00206.1	25.0	22.0	17.2	11.5	-----

the isoelectronic centers responsible for this emission are randomly distributed throughout the $\text{Si}_{1-x}\text{Ge}_x$ layers. The excitons bound to these centers, in the model proposed, are composed of a tightly bound electron and a loosely bound hole with hydrogen-like orbits. The excitons have an effective Bohr radius of approximately 20 angstroms (see Table X for the computation), comparable to the dimensions of the $\text{Si}_{1-x}\text{Ge}_x$ wells, where most of the effective Bohr radius is due to the loosely bound hole. The quantum well provided by the $\text{Si}_{1-x}\text{Ge}_x$ layer surrounded by silicon on both sides results in additional confinement of the bound exciton (due to additional hole confinement) and a higher binding energy. However, the increase in the exciton binding energy depends on the position of the center within the $\text{Si}_{1-x}\text{Ge}_x$ layer. (Meynadier 1988) Centers nearest the middle of the wells have the highest binding energies; those near the interfaces have the lowest binding energies. If we consider the hole part of the exciton as hydrogenic, then the calculations for changes in the binding energy

for a hydrogenic impurity in a quantum well can be used. In Figure 72, the result of these calculations is shown. The effective Bohr radius is calculated from

$$a_0^* = \frac{h/2\pi}{\sqrt{2m_h^* E_b^{\text{hole}}}} \quad (36)$$

where m_h^* is the effective mass of holes and E_b^{hole} is the binding energy of holes to the complex. The hole binding energies were assumed to be the activation energies determined from the PL temperature dependence. Since the holes are more loosely bound than the electrons, they have a lower binding energy; the dissociation of holes occurs at much lower temperatures than the dissociation of electrons. Thus, the reduction of PL as the temperature increases is dominated by hole dissociation. Given the effective Bohr radius of holes, the differences in the hole binding energy between complexes located at the center of the $\text{Si}_{1-x}\text{Ge}_x$ layers vs. those at the edges can be determined from Figure 72; these are labeled theoretical differences in Table X. These are compared with the experimental differences determined from the temperature dependent PL. Here it is assumed that the hole binding energy for complexes located at the edges of the $\text{Si}_{1-x}\text{Ge}_x$ layers (at the interfaces) is equal to the activation energy for the highest annealing temperature for which the broad band PL was observed, in which the complexes have diffused to the interfaces (edges of $\text{Si}_{1-x}\text{Ge}_x$ layers). Also, the binding energy for the complexes located at the center of the $\text{Si}_{1-x}\text{Ge}_x$ layers was assumed to be the binding

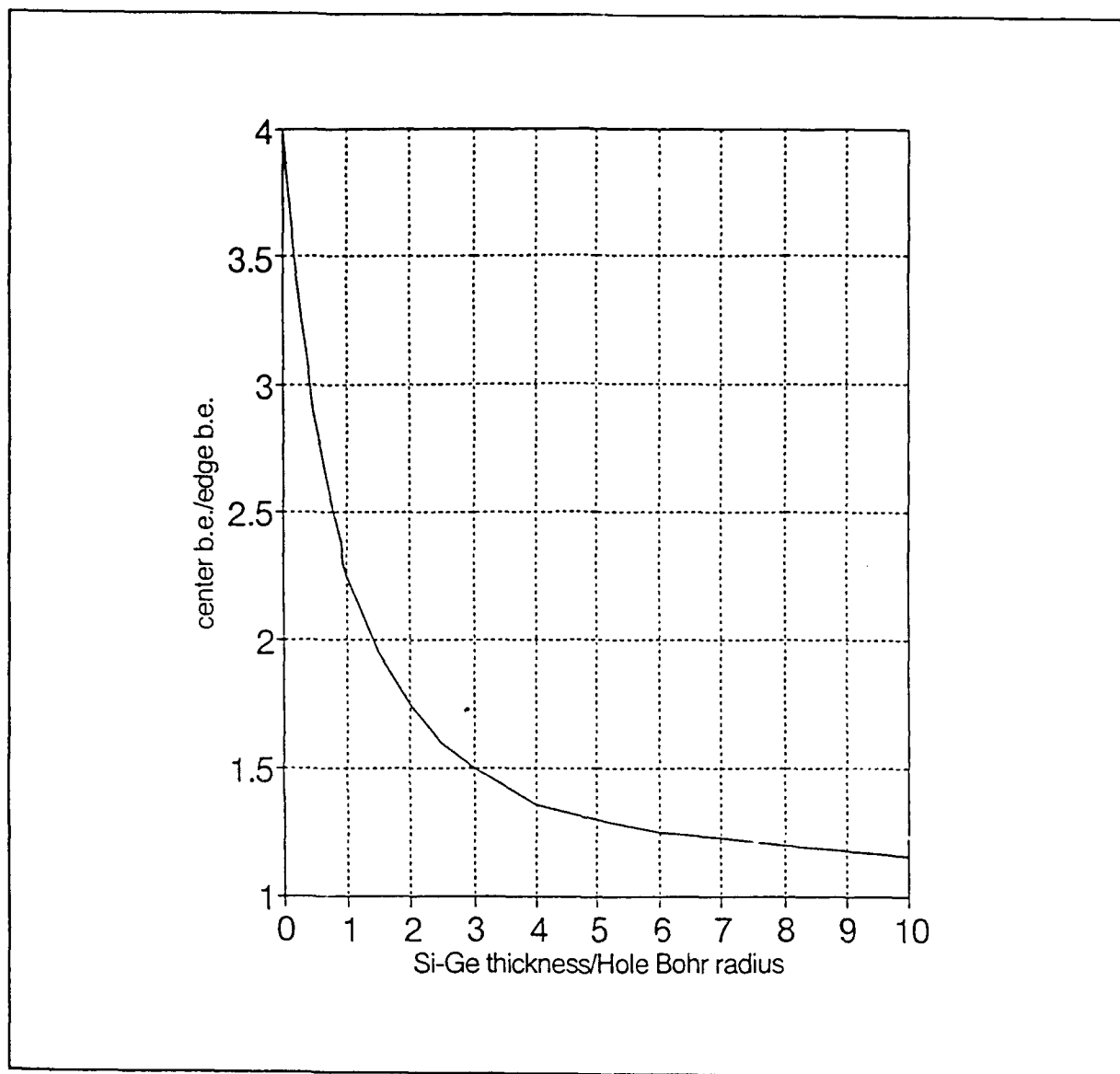


Figure 72: Hole Binding Energy vs position in $\text{Si}_{1-x}\text{Ge}_x$ layer. The ratio of the hole binding energies for on center complexes vs interface complexes is plotted vs. $t_{\text{Si-Ge}}/a_0^*$

energy of the as grown samples. Even though the as-grown samples were assumed to have a uniform distribution of complexes, the high-temperature reduction of PL would be dominated by the higher binding energy complexes, i.e., those located at the center of the $\text{Si}_{1-x}\text{Ge}_x$ layers. There is good agreement between the experimental and theoretical shifts in hole binding energy in Table X.

Table X: Hole Binding Energy vs. Well Position. The theoretical values are determined from Figure 75. The experimental values are determined from PL temperature dependences vs anneal temp.

Sample No.	As-grown	Bohr	L/a ₀	Hole Binding Energy	
	binding energy (meV)	Radius (angstroms)		Change - Center to edge (meV)	Theoretical Experimental
SL00405.1	22.3	18.3	2.2	6.2	14.6
SL10206.1	13.9	22.9	3.1	5.0	3.9
SL11105.1	14.0	23.2	1.7	7.3	5.9
SL10322.2	26.8	16.3	2.4	10.6	11.7
SL00206.1	25.0	16.9	1.2	13.8	13.5

Shifts of Broad Band with Sample Temperature. The broad PL band for both the as-grown and annealed samples shifts to lower energies as the sample temperature is increased. The shifts, shown in Table XI, range from 20 to 100 meV. The broad band peak emission is given by

$$E_{PL} = E_g - E_b \pm E_{phonon} \quad (37)$$

where E_b is the binding energy of the exciton which contains contributions from both the hole and the electron, E_g is the effective band gap, and E_{phonon} is the phonon term that accounts for the secondary low energy peak in some of the samples (SL10322.2, SL00201.1, and SL00206.1). The peak emission does not involve phonons, as was determined by Noel et al. (Noel 1990a). The broad band is a convolution of the emission from all the individual

Table XI: Shifts of Broad Band Peaks with Temperature.

Sample #	Peak Shift 1.6 K to 50K meV)	Hole bind. E diff (meV)	elect. Bohr Radius (nm)	alloy fluct Δx	ΔE_g from Δx (meV)	ΔE_g Center to edge (meV)
SL00405.1	50	14.6	1.16	0.095	61	107
SL10206.1	30	3.9	1.14	0.090	60	100
SL11105.1	30	5.9	1.16	0.096	58	105
SL10531.1	45	---	1.13	0.081	60	95
SL10531.2	20	---	1.16	0.096	63	105
SL10322.2	45	11.7	1.13	0.083	57	95
SL00206.1	100	13.5	11.3	0.083	76	104

isoelectronic centers within the $\text{Si}_{1-x}\text{Ge}_x$ layers, each with a different exciton binding energy and temperature behavior. The emission energy for a given center is the superlattice energy gap minus the exciton binding energy. The exciton binding energy is comprised of two parts, the energy to bind the electron to the center, the largest part, and the energy to bind the hole to the charged center, the smaller part that varies depending on the position of the center within the well. The higher the binding energy, the more the luminescence persists to higher temperatures. Thus centers with the highest binding energies have the lowest energy emission and persist to higher temperatures than centers with lower binding energies and higher energy emission. The result is a shift in broad peak energy to lower energy as the sample temperature is increased.

The temperature-dependent peak shifts in Table XI cannot be fully explained by the hole binding energy changes from variations in the position of the complex within the $\text{Si}_{1-x}\text{Ge}_x$ layers, though part of the shift is due to these variations. The remaining shifts, from 35 to 87 meV depending on the sample, must be due to either a reduction in the band gap or an increase in the electron binding energy. The part of the exciton binding energy due to the binding of the electron, since the electron is very tightly bound and highly localized, should depend more on the properties of the binding center and is assumed to be constant. However, the band gap, as seen by the highly localized electron, varies due to

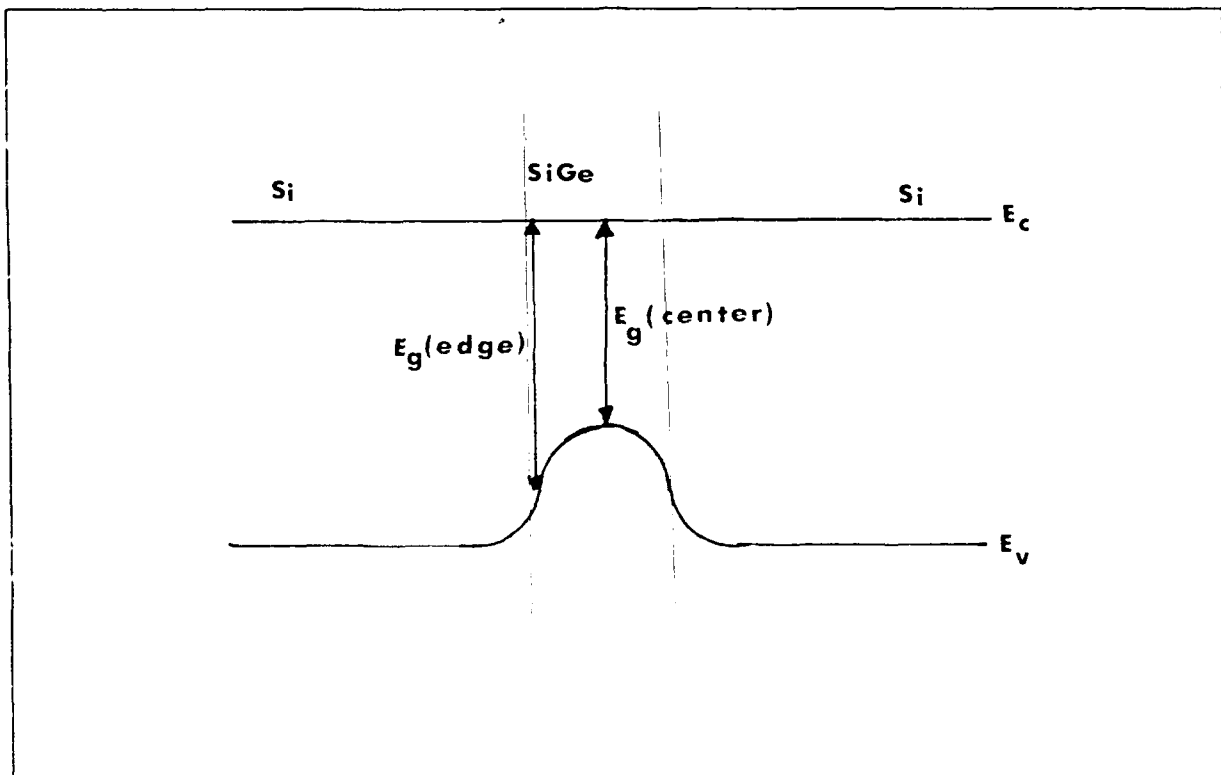


Figure 73: Local Band gap Fluctuations. The reduction in local band gap for emission centers located in well centers corresponds with temperature dependent PL peak shifts.

variations in the position of the center within the well, as shown in Figure 73. For a center located at the Si/Si_{1-x}Ge_x interface, the effective local alloy concentration is one-half the average alloy concentration in the Si_{1-x}Ge_x layers. The fluctuations of the alloy concentration also affect the local band gap. To determine the effects of alloy fluctuations, first the effective Bohr radius of the electron is determined using Equation (35). Here it is assumed that the electron is in a hydrogenic orbit, which admittedly it is not. However, this calculation will underestimate the spatial localization of the electron, providing a lower bound to the alloy fluctuations. The effective Bohr radius of electrons for the samples in Table XI were calculated using Equation (35) but substituting the electron effective mass, m_e^* , for the hole effective mass, m_h^* , and substituting the electron contribution to the exciton binding energy, estimated to be 105 meV, for the hole binding energy. The effective electron Bohr radii ranged from 11.3 to 11.6 angstroms, approximately 2 lattice constants. Assuming a random distribution of Ge atoms within the Si_{1-x}Ge_x layers, which was proven by the sharp BE linewidths, the alloy fluctuations within an effective Bohr radius sphere can be calculated from

$$\delta x = \left[\frac{x}{\frac{4}{3}\pi a^3 N} \right]^{\frac{1}{2}} \quad (38)$$

where a = Bohr radius, and N = density of lattice sites. (Mitchard and McGill 1982) The results are given in Table XI. These alloy

fluctuations were used to compute a band gap fluctuation associated with this alloy fluctuation, using the band gap curves determined using the Kronig-Penney model, Figures 40-47. The observed shifts of broad band can be explained as follows. As the temperature is raised above 1.6 K, holes begin to dissociate from the isoelectronic centers, with activation energies determined by well position. The centers located at the interfaces dissociate first, due to the lower hole binding energy of holes at the interfaces. The centers located at the middle of the $\text{Si}_{1-x}\text{Ge}_x$ layers dissociate last because of their higher binding energy. Because the local band gap for centers located near the middle of the $\text{Si}_{1-x}\text{Ge}_x$ layers is lower, on average, than those at the edges, the emission energy, in accordance with Equation (37), shifts to lower energies as the temperature increases. As the emission shifts to lower energy, corresponding to the shift in the emission from the edges to the center of the $\text{Si}_{1-x}\text{Ge}_x$ layers the emission remains broad due to the alloy fluctuation effects. The amount of the shift depends on the distribution of isoelectronic centers within the $\text{Si}_{1-x}\text{Ge}_x$ layers. In Table XI, the fluctuation in the local band gap due to both alloy fluctuations, and position within the $\text{Si}_{1-x}\text{Ge}_x$ layer is calculated. The fluctuations in the local band gap due to alloy fluctuations corresponds to the observed linewidths. These fluctuations are uniform throughout the $\text{Si}_{1-x}\text{Ge}_x$ layers and thus do not contribute to the temperature dependent peak shifts of the broad PL band. The differences in the local band gap vs the position in the $\text{Si}_{1-x}\text{Ge}_x$ layer, near 100 meV, are greater than the

observed temperature dependent peak shifts. There are two reasons for this. First, the shifts were only measured up to 50 K; the peaks continue to shift as the temperature is raised above 50 K. Second, at 1.6 K the emission is from all positions within the $\text{Si}_{1-x}\text{Ge}_x$ layers so that the overall peak position is intermediate between the edge and center peak positions (assuming they could be resolved). Thus the shift from 1.6 K to 50 K can be expected to be one half of the maximum shifts given in Table XI.

Shifts of Broad Band with Annealing Temperature. The shifts in the broad PL band to higher energy with increasing anneal temperature can be explained in terms of the results already discussed. The reduction of activation energies vs annealing temperature shows that the broad band emission centers move towards the Si/Si_{1-x}Ge_x interfaces as the annealing temperature increases. This changes the distribution of local band gaps seen by the broad band emission centers, so that Si-rich environments dominate. Thus the emission at low temperatures, is shifted to higher energies when compared to the as-grown samples that have a uniform distribution of these emission centers. The broad band from annealed samples still shifts to lower energies with increasing sample temperature consistent with the argument presented in the last section.

Photoluminescence from monolayer Si/Ge superlattices

Two samples, SL11112.1 and SL11112.2, consisted of alternating layers of pure Si and pure Ge, each with 5 nm Si layers alternating with 1 nm of Ge. SL11112.1 was grown at 470 °C while SL11112.2 was grown at 420 °C. Neither of the as grown samples have very strong emission. However, SL11112.1, when annealed by RTA above 600 °C, has a strong broad band that emerges (see Figure 74), similar to the broad bands seen in $\text{Si}_{1-x}\text{Ge}_x/\text{Si}$ superlattices. In addition, there are dislocation-related D-bands present that indicate partial strain relaxation. Using the band offsets for Si/Ge determined by van de Walle and Martin of 0.84 eV, (van de Walle and Martin 1986) and assuming for thin Ge well the confined hole states are one half the valence band offset, and the confined electron states are one-half the conduction band offset, the effective SL band gap is approximately 855 meV. Thus the broad peak at 750 meV is 105 meV below the effective band gap, and is therefore of the same nature as the broad band peaks in $\text{Si}_{1-x}\text{Ge}_x/\text{Si}$ superlattices. Since we know that the Si/Ge system has a type II band alignment, the fact that broad band peaks are not seen in as grown samples is not surprising. The as-grown samples have very little interstitial Ge in the Si layers that could form isoelectronic centers. Annealing causes some interstitial Ge to diffuse into the Si layers. The interstitial Ge forms isoelectronic complexes; those near the interfaces can bind a type II exciton by trapping electrons in the Si and loosely binding holes in the Ge regions.

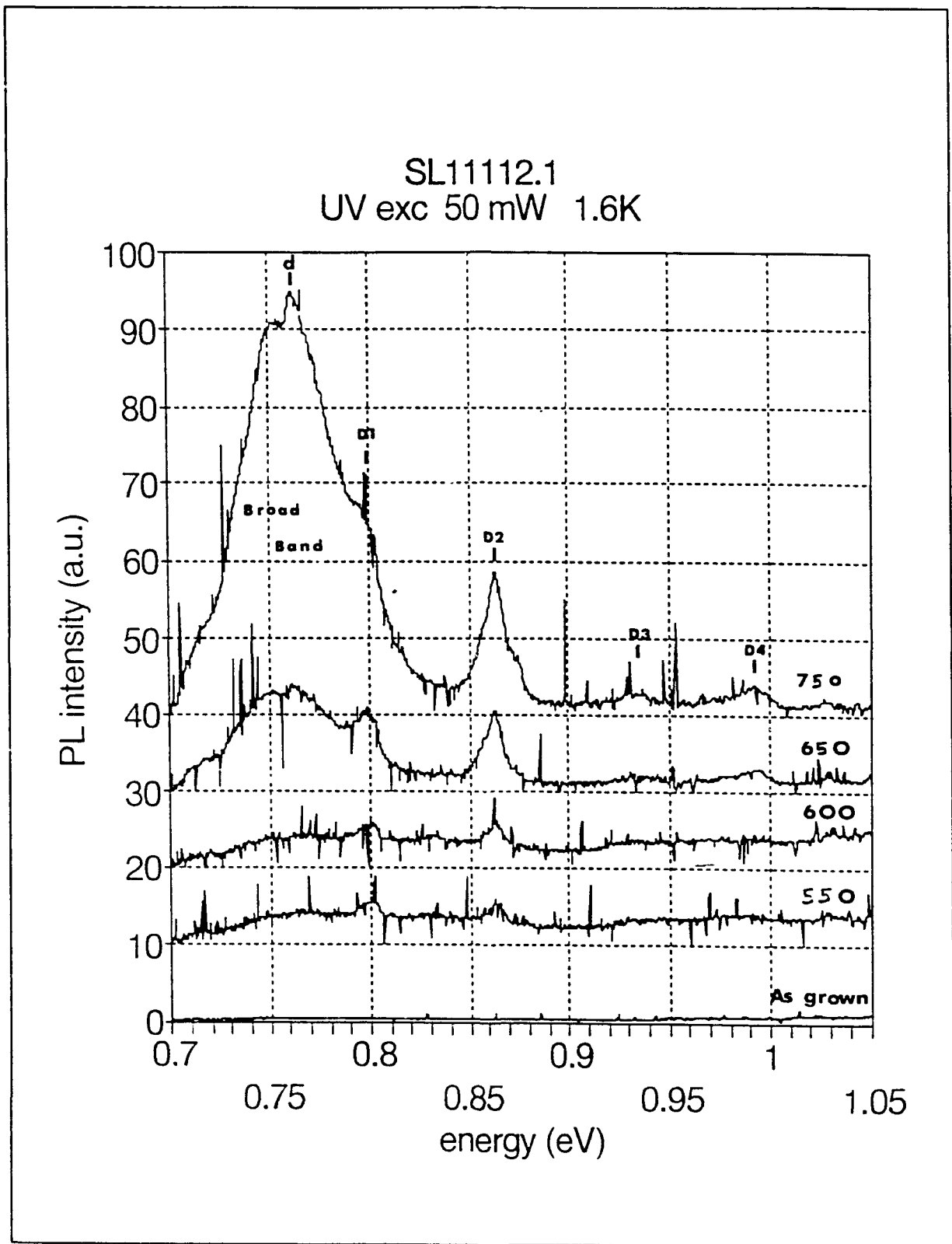


Figure 74: PL, SL11112.1, as a function of anneal temperature

PL from Deep Centers

Several samples have emission other than the sharp bound exciton emission and the broad band PL. Strong dislocation related lines, D1-D4, D5, D6, and D5', have also been seen and noted above. In addition to these, the "G" line at 969 meV, the "j" line at 990 meV, the "W" or "I1" line at 1018.9, and a line at 770-775 meV have been identified.

The "G" line is related to a monoclinic isoelectronic center involving two carbon and one Si atoms. (Davies 1989) One of the carbon atoms is interstitial and is captured by a substitutional carbon. This center has previously been seen only in bulk Si, and is formed by irradiation and annealing; the formation mechanism is believed to involve the creation of carbon interstitials by silicon interstitials formed by irradiation damage. Carbon is a common contaminant in Si-MBE, and it is reasonable that under appropriate conditions there will be centers formed with the carbon contaminants, particularly since the MBE growth at low temperatures proceeds in a nonequilibrium manner. Figure 75 shows the strong "G" lines that were found in a portion of SL00201.1.

The "j" line at 990 meV has been previously seen in MBE Si grown at 550 °C. (Lightowers 1989a and 1989b) It is believed to be associated with carbon-nitrogen-hydrogen complexes. Sample SL10322.2 has a "j" line, as shown in Figures 33 and 36, as well as

SL00201.1 40/20 $x=0.25$
UV exc 1.6 K 50 mW

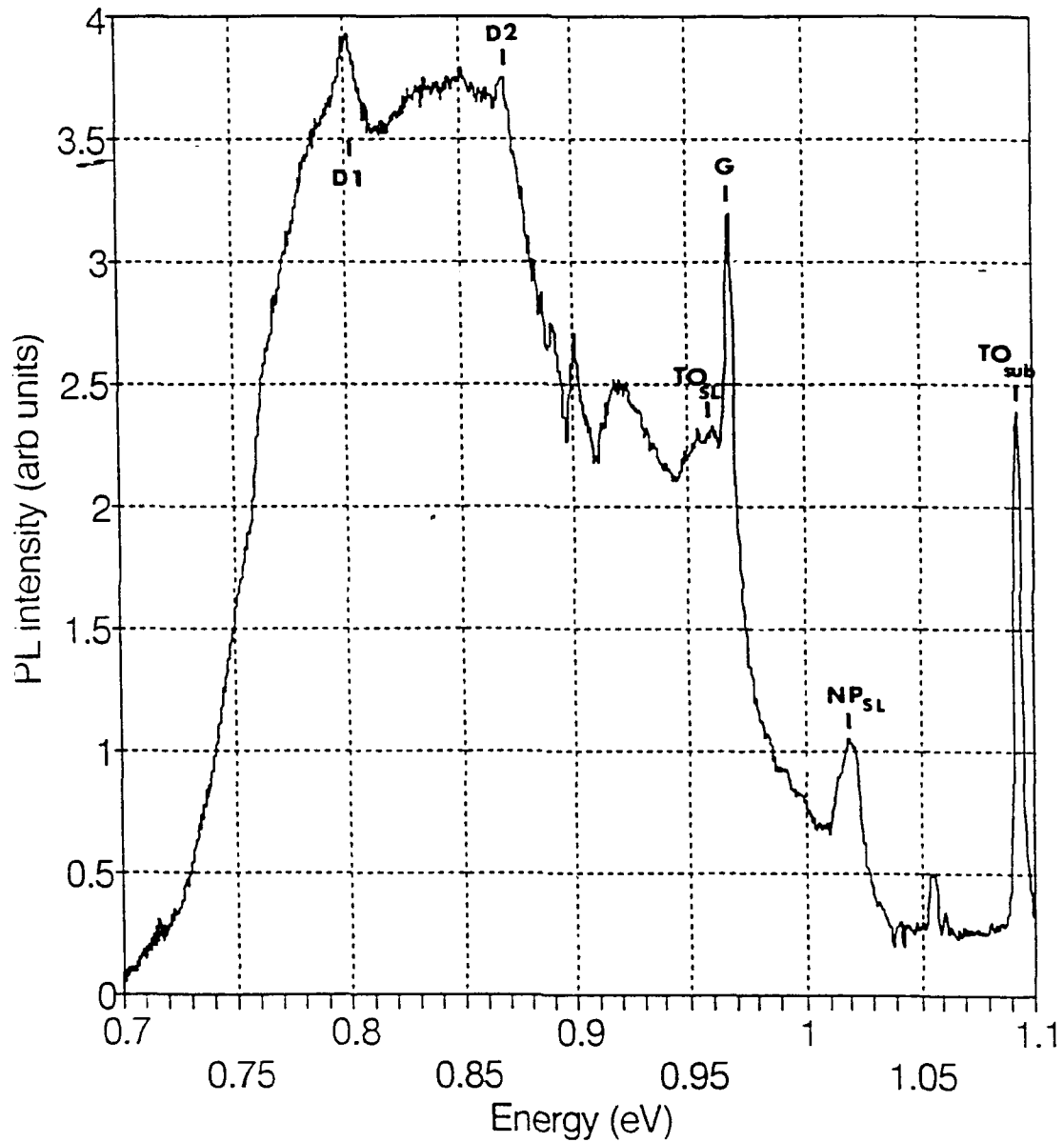


Figure 75: PL, SL00201.1, for portion of sample containing sharp "G" line at 969 meV

SL00326.1 shown in Figure 30. The line anneals out for anneal temperatures above 550 °C (see Figure 50). The Lightowlers studies found the "j" line anneals out at 300 °C, but these were for longer anneal times. In Si-Ge a rough equivalence has been found between annealing at lower temperatures for long periods and annealing at higher temperatures for shorter periods. (Houghton 1991a)

Sample SL00201.1, when annealed by RTA at 550 and 575 °C, had emission at 1018.9 meV as shown in Figure 48, that may be "W" or "I1" emission that has been previously identified in $\text{Si}_{1-x}\text{Ge}_x$ grown at low temperatures. (Noel 1990) This center has been identified as a trigonal isoelectronic center. (Davies 1989)

A line at 770-775 appears in several of the samples, including SL00206.1, SL00405.1, SL00326.1, and SL10301.1 shown in Figures 26, 27, 30, and 55 respectively. It is labeled "d" because it may be the "d" line at 767.19 meV previously identified in MBE Si with a high concentration of carbon and nitrogen. The "d" line is believed to be associated with the "N4" line seen in carbon rich CZ Si that has been implanted with nitrogen or in FZ Si that has been implanted with both nitrogen and carbon.

The presence of the "G", "j", and possibly "d" lines indicates that there is a high concentration of carbon and nitrogen in the

samples. It is unknown what roles these impurities play in the broad band PL but clearly they are available as possible constituents in the complex responsible for the broad band.

Sample characterization vs. position in wafer

In this section, the variations in the MBE-growth, as determined by PL, are discussed. For several of the wafers, the PL as a function of the position in the wafer were examined for different excitations. The changes evident were in four categories: (1) shifts of peaks due to a change in the superlattice band gap, (2) change in the intensity of peaks, (3) new peaks indicating a nonuniform distribution of defects, and (4) changes due to variations in growth temperature. As will be discussed below these categories are not mutually exclusive.

Peak shifts due to changes in SL band gap. The $\text{Si}_{1-x}\text{Ge}_x/\text{Si}$ superlattice samples with sharp bound exciton (BE) emission, SL10322.2, SL00201.1, and SL00206.1, offer the most sensitive probe of changes in the superlattice bandgap. In Figure 76, the PL for three samples from the same wafer, SL00201.1, are shown. The BE peaks shift to higher energy as the radial distance from the center of the wafer increases. These shifts are due to an increase in the superlattice bandgap as a function of radial distance from the center of the wafer. The superlattice bandgap shift could be due

SL00201.1 40/20 $x = 0.25$
UV exc 1.6K 50 mW

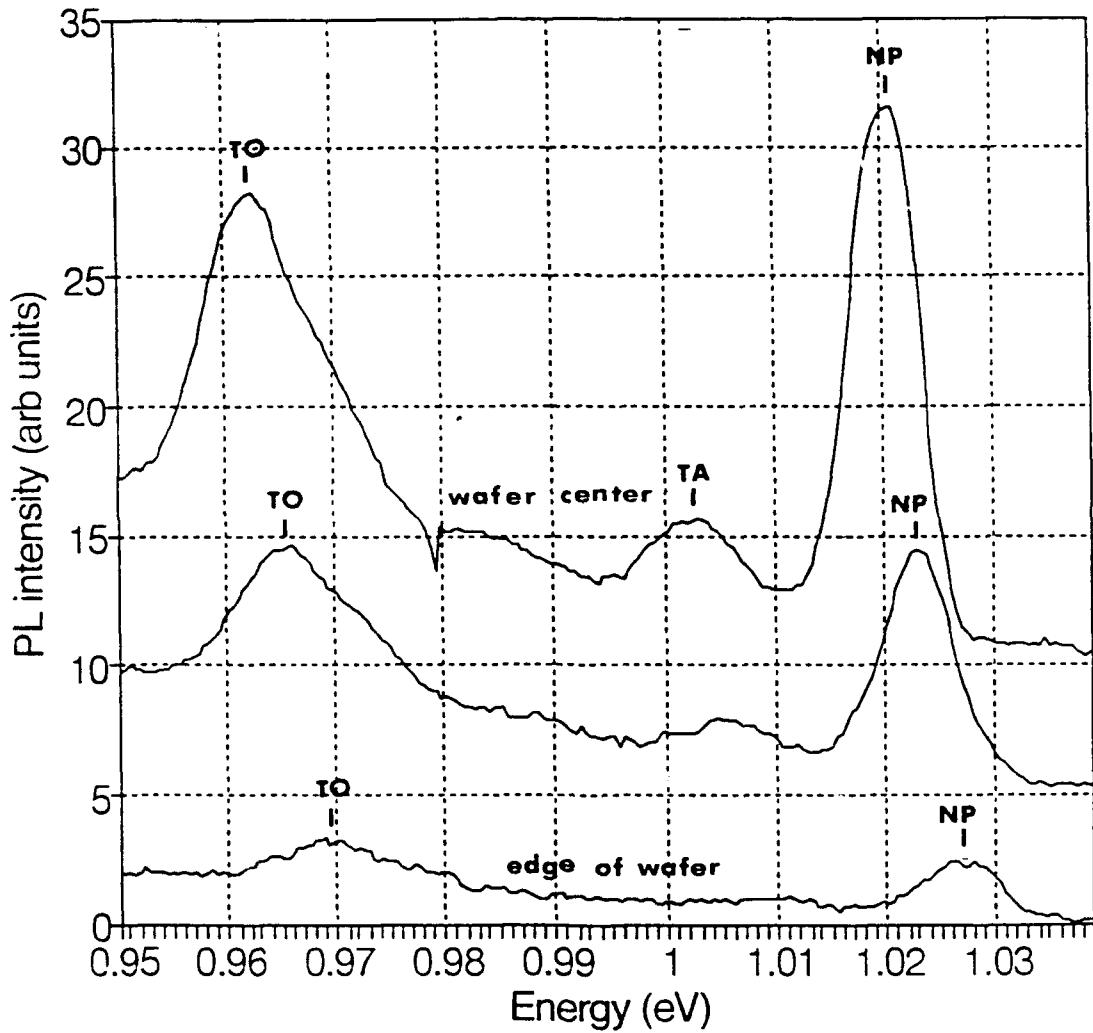


Figure 76: PL Sample SL00201.1 for three positions in wafer. The BE lines shift to higher energy as the distance from the center of the wafer increases.

to changes in either the superlattice layer thicknesses or changes in the alloy concentration, x , in the $\text{Si}_{1-x}\text{Ge}_x$ layers, or a combination of the two.

Changes in peak intensity. The intensity of the sharp BE lines are reduced as the radial distance from the center of the wafer increases (see Figure 76). In addition, the intensity of the broad PL band was found to vary as a function of the radial distance from the center of the wafer as shown in Figures 77-78. It is believed that this reduction in PL intensity is due to an increased concentration of nonradiative defects at the outer edges of the samples as compared with the center.

New PL peaks. Some of the samples have PL peaks that appear in only some of the pieces cut from the wafers. Sample SL00201.1 has one piece that had BE emission from two different impurities that had no phonon lines 10 meV apart, as shown in Figure 79. The NP lines have slightly different temperature behaviors, indicative of two different binding energies. The higher energy NP line is probably due to phosphorus or boron, both with binding energies near 2.7 meV (Thewalt 1982). The lower energy NP line may be Indium, which is found 10 meV lower than boron or phosphorus in Si. (Davies 1989).

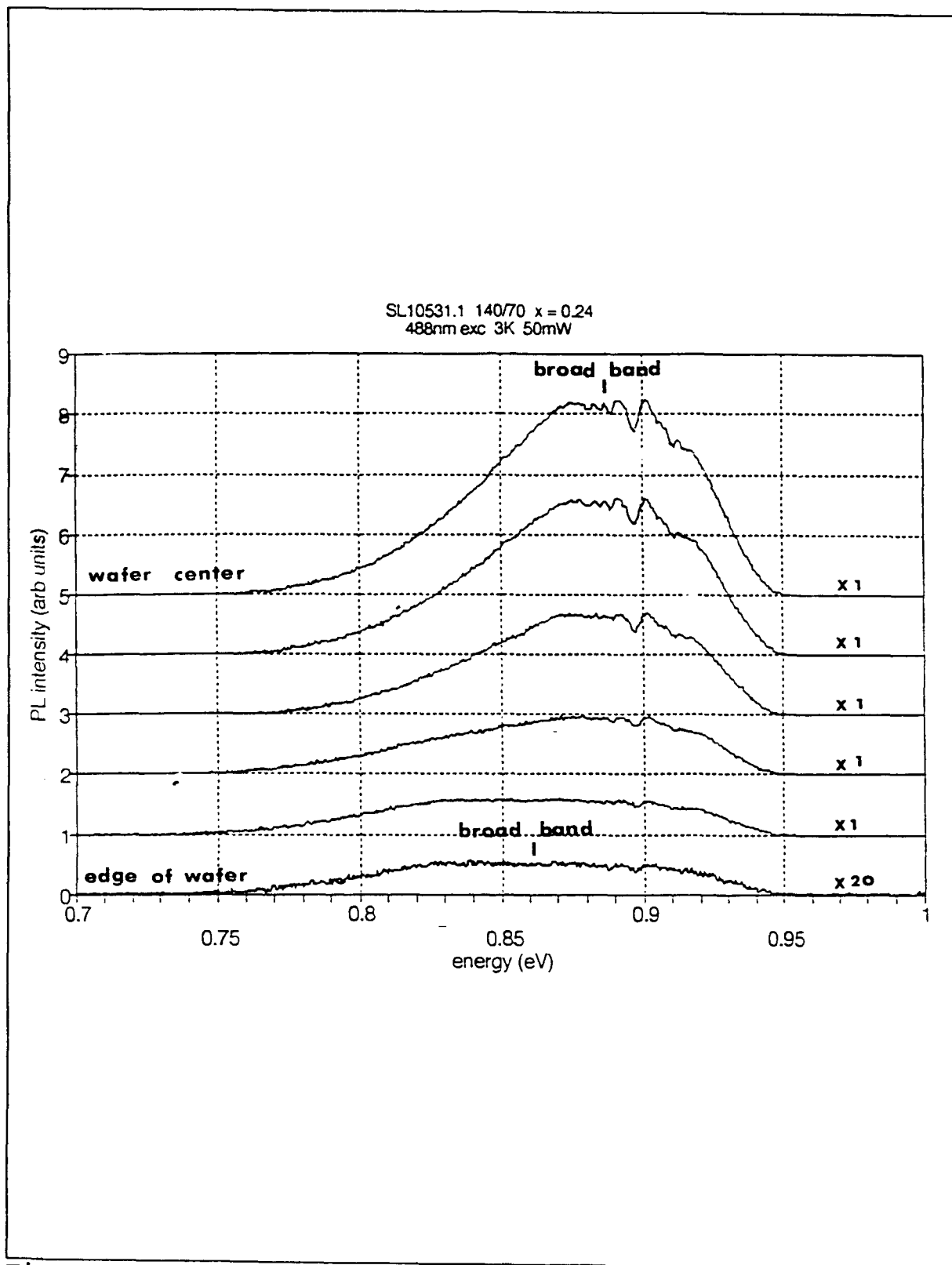


Figure 77: PL vs. sample position in wafer - SL10531.1

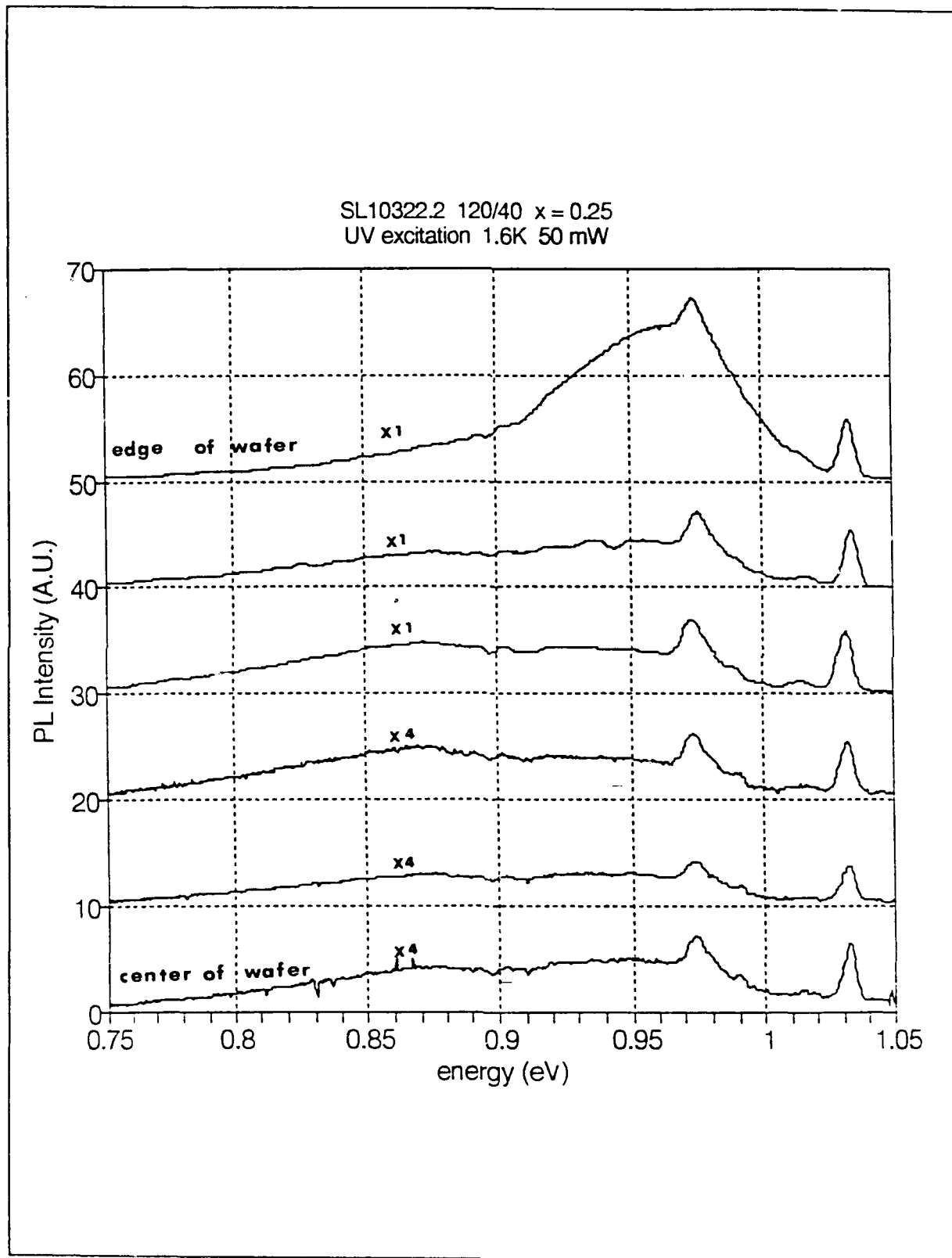


Figure 78: PL vs. sample position in wafer - SL10322.2

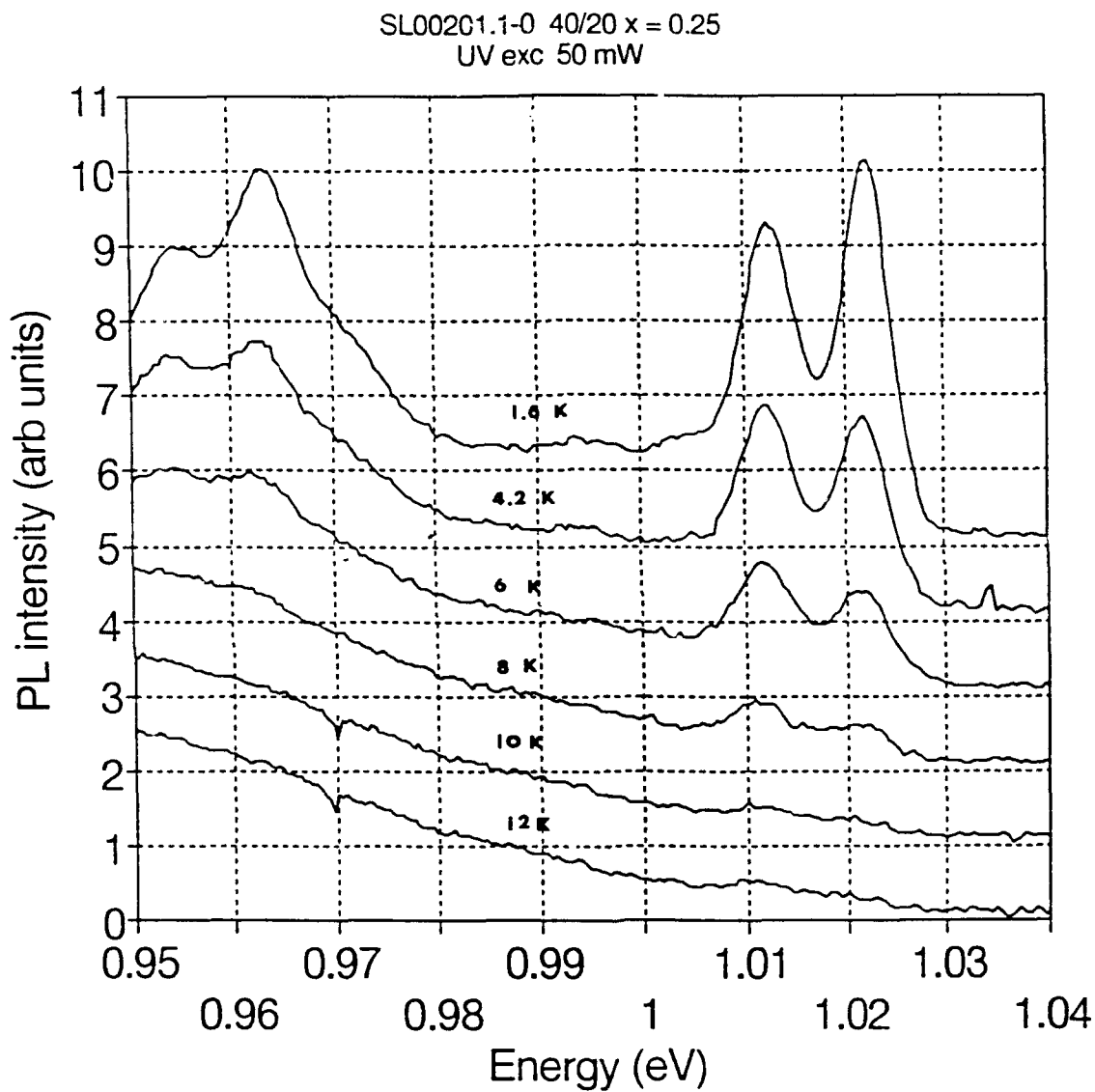


Figure 79: Temperature dependent PL - SL00201.1-0. BE emission from two different impurities is evident. The temperature behavior shows the impurities have two different binding energies

In addition, the "G" and "j" discussed in the previous section were found in only some of the portions of the wafer for SL00201.1 and SL10322.2 respectively.

Changes due to growth temperature variations. As mentioned in Chapter II, the growth temperature varies by as much as twenty degrees between the center and the outside edge of the wafer. In addition, at the extreme edge of the wafer, where the sample is held down with metal clamps, there are areas where the growth temperature may be much higher than the nominal growth temperature of 500 °C. While the outer edge of the wafer cannot be considered representative of the wafer and is normally not used for characterization studies, there is the opportunity to examine the effects of growth temperature in a rough sense as the sample position approaches the outside of the wafer. The trend for most of the samples is that the broad PL band intensity becomes considerably weaker as the distance from the center of the wafer increases. This dropoff corresponds to the gradual reduction in the growth temperature across the wafer. Thus the broad band intensity is growth temperature dependent, as well as annealing temperature dependent.

Comparing the samples examined in this study to those studied by the NRC-Canada group with similar emission provides another interesting observation. (Noel 1990a) The NRC-Canada samples were

grown at 390 °C compared to 500 °C for those in this study, but our growth temperature could be reduced to perhaps 480 °C at the edges of the samples. The weak broad band emission from the outside edge samples is similar to that from the NRC-Canada as-grown samples, which had very weak emission. Thus it appears likely that the broad PL band is very dependent on the growth temperature. In the model that has been proposed here, the broad PL band is due to isoelectronic centers related to interstitial Ge complexes. The occurrence of Ge interstitials is due to the non-equilibrium MBE growth process, so that the interstitial Ge concentration and configuration should be highly dependent on the growth temperature and the post growth annealing conditions. The fact that the broad band PL is not seen in CVD samples grown at 700 °C with comparable structure, (Sturm 1991, Houghton 1991) gives support to this model. The higher temperature CVD growth does not allow the formation of Ge interstitials.

IV. SUMMARY

Sharp Near-Band-Edge Bound Exciton Lines in $\text{Si}_{1-x}\text{Ge}_x/\text{Si}$ Superlattices

Near-band-edge excitonic features approximately 20 meV below the effective band gap have been seen in $\text{Si}_{1-x}\text{Ge}_x/\text{Si}$ superlattices grown by MBE. These features were identified as bound exciton lines, including a strong no phonon line and $\text{TO}_{\text{Si-Si}}$, $\text{TO}_{\text{Si-Ge}}$, $\text{TO}_{\text{Si-Ge}}$, and TA. The primary reason they have been found is that the excitation source for the photoluminescence (PL) measurements was UV (350-357 nm). Excitation with 488 nm or 514 nm had much weaker (or no) bound exciton lines. Temperature dependent PL measurements were used to determine the binding energy of the exciton to the shallow impurities, in the range from 1.5 to 4.2 meV. The linewidths of the BE lines, 5.9 to 7 meV, were the same as those in bulk $\text{Si}_{1-x}\text{Ge}_x$ random alloys; thus the fluctuations of the alloy concentration in the $\text{Si}_{1-x}\text{Ge}_x$ layers was statistical (there was no evidence of clustering of Ge atoms).

Broad PL Band

The broad PL band was found to be 120 meV below the effective superlattice band gap, after the effects of quantum confinement of hole was accounted for.

Temperature dependent PL on as-grown and annealed samples was used

to determine the activation energies of the broad PL band. The activation energies were determined to be 7.7 to 27, and were found to vary depending on the annealing conditions, being the highest for the as-grown samples and the lowest for the highest annealing temperature at which the broad band was seen. The broad PL band also was found to shift to lower energies as the sample temperature increased. The temperature-dependent shifts were 20 to 100 meV over the temperature range 1.6 K to 50 K, comparable to the 40 meV shifts in the L-band in bulk $\text{Si}_{1-x}\text{Ge}_x$ over the same temperature range.

A model was proposed to account for the annealing and temperature-induced shifts in the activation energies and peak positions of the broad PL band. The broad PL band is due to isoelectronic centers originating from Ge interstitial complexes in the $\text{Si}_{1-x}\text{Ge}_x$ layers. The complex binds an exciton by first tightly binding an electron with a binding energy of approximately 105 meV. The hole is then loosely bound to the charged center in a hydrogenic orbit with a binding energy of approximately 15 meV. The result is that the hole orbits are greatly affected by the superlattice potential. The emission centers are distributed throughout the $\text{Si}_{1-x}\text{Ge}_x$ layers; the position of the emission center within the well affects the binding energy of the hole to the charged complex. The difference in the hole binding energy for centers located at the center vs centers located at the edges was calculated for each sample, assuming the hole was bound

hydrogenically. These differences agree with the differences in the activation energies between as-grown and 750 °C annealed samples. Thus the activation energy changes vs annealing temperature can be explained if we assume that the centers responsible for the broad band emission diffuse to the interfaces with annealing. Under this assumption, the shift of the broad PL band with temperature is explained by the distribution of local band gaps at the emission centers. As the temperature increases and holes begin to dissociate, those with the lower dissociation energies dissociate first, leaving those with the higher binding energy. The local band gap surrounding the emission centers with higher binding energy (those located in the center of the $\text{Si}_{1-x}\text{Ge}_x$ layers) is lower than the average, which includes those near the interfaces. Thus, the broad band shifts to lower energy as temperature increases. The annealing-induced shifts in the broad PL band were due to the shifts in the centers to the interfaces. The effective alloy concentration seen by the electrons at interfaces is higher than that at the center. Thus the effective band gap seen by the isoelectronic centers located at the interfaces is higher, producing the shift of the broad band to higher energy.

Annealing Studies

The annealing studies produced results in five areas in addition to the changes in the broad band PL dissociation energy discussed above. First, the sharp bound exciton lines were found

not to shift as a function of anneal temperature for anneal temperatures below 650 °C, consistent with little or no lattice interdiffusion at low annealing temperatures. Second the broad PL bands shift to higher energy as the annealing temperature increases, with some shifts even for 550 °C annealing temperatures. These shifts are due to the diffusion of the interstitial complexes responsible for the broad band emission. Third, the intensity of BE and broad band PL features increase as the annealing temperature increases, corresponding to a reduction of nonradiative defects inherent in samples grown by MBE at low temperatures. Fourth, in the samples with both broad band and sharp BE emission, the broad band increases at a faster rate than the sharp PL band as annealing temperature increases. Fifth, annealing at high temperatures (850 °C) eliminates the broad band emission, replacing it with dislocation-related D-bands in most cases. The disappearance of the broad PL band with high temperature annealing is due to the destruction of the complexes responsible for the emission, by incorporation of interstitial Ge on substitutional sites. The D-bands in at least one case have a Si component and a $\text{Si}_{1-x}\text{Ge}_x$ component, corresponding to the propagation of dislocations through the superlattice as the annealing temperature increases.

Recommendations for future study

The broad PL band must be studied as a function of the growth temperature, to determine if stable conditions for efficient emission applicable to emitting devices can be obtained. It would also be useful to determine the components of the Ge complexes; are there other impurities such as oxygen, nitrogen, or carbon that are involved in these complexes and can intentional doping of one or more of these create more intense PL.

REFERENCES

- Abstreiter G., "Light scattering in semiconductor heterojunctions", in *Molecular Beam Epitaxy and Heterostructures*, ed by L.L. Chang and K. Ploog, 1985a.
- Abstreiter G., H. Brugger, T. Wolf, H. Jorke, and H.-J. Herzog, "Strain-induced two-dimensional electron gas in selectively doped Si/Si_{1-x}Ge_x Superlattices", *Phys. Rev. Lett.*, **54**, 2441 (1985b).
- Abstreiter G, H. Brugger, T. Wolf, R. Zachai, and Ch. Zeller, "Optical and electronic properties of Si/SiGe superlattices", in *Two-Dimensional Systems: Physics and New Devices*, edited by G Bauer, F Kuchar, and H Heinrich (Springer, Berlin), 1986, p 130.
- Abstreiter G, "Si-Ge Strained layer superlattices", *Thin Solid Films*, **183**, 1 (1989a).
- Abstreiter, et al., "Silicon/Germanium strained layer superlattices", *J Crystal Growth*, **95**, 431 (1989b).
- Aharoni H., "Measurement of the lattice constant of Si-Ge heteroepitaxial layers grown on a silicon substrate", *Vacuum*, **28**, 571 (1978).
- Ahlers E.D. and F.G. Allen, *Electrochem Soc Proc*, **88-8**, 526 (1988).
- Aitelhabti D, et al, *Can J Phys*, **68**, 268 (1990).
- Allen F.G., "Experimental issues in Si MBE homoepitaxial growth", *Electrochemical Soc Proc*, **85-7**, 3 (1985).
- Alt H.Ch. and L. Tapfer, *J. Electronic Mater*, **14a**, 833 (1985).
- Arbet V., S.J. Chang, and K.L. Wang, "Investigation of Si_mGe_n strained monolayer superlattices by RHEED, Raman, and X-ray techniques", *Thin Solid Films*, **183**, 57 (1989).
- Arhavani M R, et al, *Sol State Comm*, **71**, 599 (1989).
- Awadelkarim O.O., A. Henry, B. Monemar, J.L. Lindstrom, Y. Zhang, and J.W. Corbett, "Photoluminescence study of radiative channels in ion-implanted silicon", *Phys Rev B*, **42**, 5635 (1990).
- Bucsa W, et al, "Confined phonons in strained short-period (001) Si/Ge superlattices", *Thin Solid Films*, **183**, 65 (1989).
- Bartholomeusz B J and K Rajan, *J Elect Mat*, **19**, 943 (1990).
- Bass J M and C C Matthai, "A strain-dependent study of the [001] Si₆Ge₆ superlattice", *Semicond Sci Technol*, **5**, 707 (1990).

G Bastard, "Envelope function approach to the superlattices band structure", in *Molecular Beam Epitaxy and Heterostructures*, ed by L L Chang and K Ploog, 1985.

Bastard G and J A Brum, "Electronic States in Semiconductor Heterostructures", *J Quan Elec*, **QE-22**, 1625 (1986).

Bastard G, "Electronic states in semiconductor heterostructures", in *Physics and Applications of Quantum Wells and Superlattices*, ed E E Mendez and K von Klitzing, 1987.

Batra I P and C Y Fong, "Electronic states in heavily and ordered doped superlattice semiconductors", in *Properties of Impurity States in Superlattice Semiconductors*, 1988.

Bean J C, "Strained-Layer epitaxy of Germanium-silicon alloys", *Science*, **230**, 127 (Oct 1985).

Bean, J C, "The growth of novel silicon materials", *Physics Today*, Oct 1986.

Bean, J C, "Silicon Based Semiconductor Heterostructures", in *Silicon Molecular Beam Epitaxy*, edited by E Kaspar and JC Bean, (Boca Raton:CRC), 1988.

Bergh A.A. and P.J. Dean, *Light-Emitting Diodes*, (Oxford; Clarendon Press), 1976.

Bevk J, et al, *Materials Sci & Engineering B*, **6**, 159 (1990).

Beyer H.J., C. Metzner, J. Heitzer, and D.H. Dohler, "Temperature dependence of the tunable luminescence, absorption and gain spectra of nipi doping superlattices - theory and comparison with experiment", *Superlattices and Microstructures*, **6**, 351 (1989).

Bimberg D., M. Sondergeld, and E. Grobe, *Phys. Rev. B*, **4**, 3451 (1971).

Bradfield P.L., T.G. Brown, and D.G. Hall, "Radiative decay of excitons bound to chalcogen-related isoelectronic impurity complexes in silicon", *Phys. Rev. B*, **38**, 3533 (1988).

Bradfield P.L., et al, *Appl. Phys. Lett.*, **55**, 100 (1989).

Braunstein R, et al, "Intrinsic optical absorption in Germanium-Silicon Alloys", *Physical Review*, **109**, 695 (1958).

Brey L., and C. Tejedor, "New optical transitions in Si-Ge Strained superlattices", *Phys Rev Lett*, **59**, 1022 (1987).

Brown T.G. and D.G. Hall, "Optical emission at 1.32 μm from sulphur-doped crystalline silicon", *Appl. Phys. Lett.*, **49**, 245

(1986a).

Brown T.G. and D.G. Hall, *J. Appl. Phys.*, **59**, 1399 (1986b).

Brugger H., G. Abstreiter, H. Jorke, H.J. Herzog, and E. Kasper, "Folded acoustic phonons in Si-Si_xGe_{1-x} superlattices", *Phys Rev B*, **33**, 5928 (1986).

Brugger H., and G. Abstreiter, "Si-Ge strained layer superlattices", *J de Physique*, **48**, C5-321 (1987).

Brugger H., E. Freiss, G. Abstreiter, E. Kasper, and H. Kibbel, "Annealing effects in short period Si-Ge strained layer superlattices", *Semicond Sci Technol*, **3**, 1166 (1988).

Brya W.J., "Raman scattering in Ge-Si alloys", *Solid State Commun.*, **12**, 253 (1973).

Canham L.T., K.G. Barraclough, and D.J. Robbins, *Appl. Phys. Lett*, **51**, 1509 (1987).

Capasso F., "Band-gap engineering for new photonic and electronic devices", in *Physics and Applications of Quantum Wells and Superlattices*, ed E E Mendez, and K von Klitzing (Plenum: New York), 1987.

Cerdiera F. C.J. Buchenauer, F.H. Pollak, and M. Cardona, "Stress induced shifts of first-order Raman frequencies of diamond- and zincblende-type semiconductors", *Phys Rev B*, **5**, 580 (1972).

Cerdeira F., A. Pinczuk, J.C. Bean, B. Batlog, and B.A. Wilson, "Raman scattering from Ge_xSi_{1-x}/Si strained-layer superlattices", *Appl Phys Lett*, **45**, 1138 (1984).

Chambers S.A. and V.A. Loebis, "Elastic strain at pseudomorphic semiconductor heterojunctions studied by x-ray photoelectron diffraction: Ge/Si(001) and Si/Ge(001)", *Phys Rev B*, **42**, 5109 (1990).

Chang L.L. and E.E. Mendez, "Compositionally Modulated Superlattices", in *Synthetic Modulated Structures*, edited by L.L. Chang and B.C. Giessen (Orlando, Academic Press), 1985, p.113.

Chang S.J., C.F. Huang, M.A. Kallel, K.L. Wang, R.C. Bowman Jr., and P.M. Adams, "Growth and characterization of Ge/Si strained-layer superlattices", *Appl Phys Lett*, **53**, 1835 (1988a).

Chang S.J., M.A. Kallel, K.L. Wang, R.C. Bowman Jr., P Chow, "Study of molecular-beam-epitaxially grown Ge_xSi_{1-x}/Si layers by Raman Scattering", *J. Appl. Phys*, **64**, 3634 (1988b).

Chi M.M., Masters Thesis, Air Force Institute of Technology, 1991.

Ciraci S and I P Batra, "Structure and Electronic Properties of strained Si/Ge semiconductor superlattices", in *Properties of Impurity States in Superlattice Semiconductors*, ed Fong, Batra, and Ciraci, 1988.

Daembkes H., H.J. Herzog, H. Jorke, H. Kibbel, and E. Kasper, "The n-channel SiGe/Si modulation-doped field-effect transistor", *IEEE Trans on Electron Devices*, **ED-33**, 633 (1986).

Daembkes H., "SiGe/Si: High speed devices", in *Proc 2nd Int Symp on Silicon Molecular Beam Epitaxy*, edited by J.C. Bean and L.J. Schowalter (Pennington NJ: Electrochemical Society (1987), p15.

Davies G., "The optical properties of luminescent centres in silicon", *Physics Reports*, **176**, 83 (1989).

Dean P.J., J.R. Haynes, and W.F. Flood, "New radiative processes involving neutral donors and acceptors in silicon and germanium", *Physical Review*, **161**, 711 (1967).

de Mello N., G. Davies, E. C. Lightowers, V. Higgs, C. J. Gibbings, and C. G. Tuppen, "The 698 meV optical band in MBE silicon", *Thin Solid Films*, **183**, 273 (1989).

Dietrich H.B., et al, *SPIE Vol 530*, 195 (1985).

Dismukes J.P., L. Ekstrom, and R.J. Paff, "Lattice parameter and density in germanium-silicon alloys", *J. Phys. Chem.*, **68**, 3021 (1964).

Dohler G.H., "Electron states in crystals with 'nipi-superstructure'", *Phys Stat Sol*, **52**, 79 (1972a).

Dohler G.H., "Electrical and optical properties of crystals with 'nipi-superstructure'", *Phys Stat Sol*, **52**, 533 (1972b).

Dohler G.H., "Physics and applications of doping superlattices", in *Two-Dimensional Systems: Physics and New Devices*, ed by G Bauer, F Kuchar, and H Heinrich, 1985.

Dohler G.H., "Properties of impurity states in n-i-p-i superlattice structures", in *Properties of Impurity States in Superlattice Semiconductors*, 1988.

Dresselhaus G., A.F. Kip, H.-Y. Ku, G. Wagoner, and S.M. Christian, "Cyclotron resonance in Ge-Si alloys", *Phys Rev*, **100**, 1218 (1955).

Duarte D., G. Bremond, A. Souifi, and T. Benyattou. "Excitonic photoluminescence from Si-capped strained Si_{1-x}Ge_x layers", *Phys. Rev. B*, **44**, 11525 (1991).

Eberl K., G. Krotz, R. Zachai, and G. Abstreiter, "Structural, compositional, and optical properties of ultrathin Si/Ge superlattices", *J de Physique*, **C-5**, 329 (1987).

Eberl K., W. Wegscheider, E. Friess, and G. Abstreiter, "Realization of short period Si/Ge strained-layer superlattices", in *Heterostructures on Si: One step further with Silicon*, 1988.

Eccleston W., "Prospects and challenges for molecular beam epitaxy in silicon very-large-scale-integration", *Thin Solid Films*, **184**, 447 (1990).

Efeoglu H., et al, Spring Meeting of the Materials Research Society, (1991).

Ekenberg U., W. Batty, and E.P.O'Reilly, "Valence band structure of strained-layer Si-Si_{0.5}Ge_{0.5} superlattices", *J de Physique*, **48**, C5-553 (1987).

Enck R.C. and A. Honig, "Radiative spectra from shallow donor-acceptor electron transfer in silicon", *Phys Rev*, **177**, 1182 (1969).

Ennen H., J. Schneider, G. Pomrenke, and A. Axeman, *Appl. Phys. Lett.*, **43**, 943 (1983).

Ennen H., G. Pomrenke, A. Axmann, K. Eisele, W. Haydle, and J. Schneider, *Appl Phys Lett*, **46**, 382 (1985).

Esaki L. and R. Tsu, IBM Res. Note, **RC-2418** (1969).

Esaki L. and R. Tsu, IBM Journal of Research and Development, **14**, 61 (1970).

Esaki L., "Semiconductor superlattices and quantum wells through development of molecular beam epitaxy", in *Molecular Beam Epitaxy and Heterostructures*, ed by L L Chang and K Ploog, 1985a.

Esaki L., "History and perspective of semiconductor superlattices", in *Synthetic Modulated Structures*, edited by L.L. Chang and B.C. Giessen (Academic Press; Orlando), 1985b, p3.

Esaki L., "A bird's eye view on the evolution of semiconductor superlattices and quantum wells", *IEEE J Quan Elec*, **QE-22**, 1611 (1986).

Esaki L., "A perspective in quantum-structure development", in *Physics and Applications of Quantum Wells and Superlattices*, ed E E Mendez and K von Klitzing, 1987a.

Esaki L., "The evolution of quantum structures", *J de Physique*, **48**, C5-1 (1987b).

Fasolino A. and E. Molinari, "Calculated phonon spectra of Si/Ge superlattices: Analogies with other systems and new features", *J de Physique*, **48**, C5-569 (1987).

Fitzgerald E.A., et al, *J Elect Mat*, **19**, 949 (1990).

Fong C.Y., et al, *Superlattices and Microstructures*, **7**, 147 (1990).

Friess E., R. Schorer, K. Eberl, and G. Abstreiter, "Stability and interdiffusion of short-period Si/Ge strained layer superlattices", *J. Vac. Sci. Technol. B*, **4**, 2045 (1991).

Froyen S., D.M. Wood, and A. Zunger, "New optical transitions in strained Si-Ge superlattices", *Phys Rev B*, **36**, 4547 (1987).

Froyen S., D.M. Wood, and A. Zunger, "Structural and electronic properties of epitaxial thin-layer Si_nGe_n superlattices", *Phys Rev B*, **37**, 6893 (1988).

Froyen S., D.M. Wood, and A. Zunger, "Electronic structure of ultrathin Si_nGe_n strained superlattices: The possibility of direct band gaps", *Thin Solid Films*, **183**, 33 (1989).

Gallup R.F. and C.Y. Fong, "Electronic properties of n-i-p-i structures in elemental Si/Ge strained-layer superlattices", *Phys Review B*, **41**, 5104 (1990).

Gell M.A., "Effect of buffer-layer composition on new optical transitions in Si/Ge short-period superlattices", *Phys Rev B*, **38**, 7535 (1988).

Gell M., "Optical window in strained-layer Si/Ge superlattices", *Appl Phys Lett*, **44**, 484 (1989).

Gell M.A., et al, *Vacuum*, **41**, 947 (1990a).

Gell M., "Buffer-induced spectral skew in short-period Si/Ge superlattices", *Semicond Sci Technol*, **5**, 449 (1990b).

Ghanbari R.A., *Phys Rev B*, **42**, 7033 (1990).

Ghahramani E., D.J. Moss, and J.E. Sipe, "Linear optical properties of strained $(\text{Si})_n/(\text{Ge})_n$ superlattices on (001) substrates", *Phys Rev B*, **41**, 5112 (1990).

Gibson J.M., "Principles of Epitaxy", in *Silicon MBE*, ed E Kaspar & J C Bean, 1988.

Glaser E., J.M. Trombetta, T.A. Kennedy, S.M. Prokes, O.J. Glembocki, K.L. Wang, and C.H. Chern, "Detection of magnetic resonance on photoluminescence from a $\text{SiSi}_{1-x}\text{Ge}_x$ strained-layer

superlattice", *Phys Rev Lett*, **65**, 1247 (1990a).

Glaser E., J.M. Trombetta, T.A. Kennedy, S.M. Prokes, O.J. Glembocki, K.L. Wang, and C.H. Chern, "Electronic structure and defects in Si/Si_{1-x}Ge_x superlattices from magnetic resonance detected on photoluminescence", International Conference on the Physics of Semiconductors, Thessaloniki, Greece, 1990b.

Glickman M, "Magnetoresistance of germanium-silicon alloys", *Phys Rev*, **100**, 1146 (1955).

Glicksman M, "Mobility of electrons in germanium-silicon alloys", *Phys Rev*, **111**, 125 (1958).

Gnutzmann U and K Clausecker, "Theory of direct optical transitions in an optical indirect semiconductor with a superlattice structure", *Applied Physics*, **3**, 9 (1974).

Gossard A.C., "Modulation doping of semiconductor heterostructures", in *Molecular Beam Epitaxy and Heterostructures*, edited by Chang and K. Ploog, 1985.

Gossard A C, "Growth of Microstructures by Molecular Beam Epitaxy", *IEEE J Quan Elec*, **QE-22**, 1649 (1986).

Green M.L., D. Brasen, H. Temkin, R.D. Yadvish, T. Boone, L.C. Feldman, M. Geva, and B.E. Spear, "High gain Si-Ge heterojunction bipolar transistors grown by rapid thermal chemical vapor deposition", *Thin Solid Films*, **184**, 107 (1990).

Gross E.F., N.S. Sokolov, and A.N. Titkov, "Zero-phonon radiative annihilation of indirect excitons in germanium crystals with isoelectronic substitutional impurities", *Sov Phys Solid State*, **14**, 1732 (1973).

Grundmann M., et al, *Superlattices and Microstruct*, **9**, 65 (1991).

Harame D.L., J.M.C. Stork, G.L. Patton, S.S Iyer, B.S. Meyerson, G.J. Scilla, E.F. Crabbe, and E. Ganin, "High performance Si and SiGe-base pnp transistors", *IEDM Tech. Digest* 889 (1988).

Harris C., W.D. Sawyer, M. Konuma, and J. Weber, *Materials Sci and Engineering B*, **4**, 457 (1989).

Hamilton B., E.C. Sidebottom, A.R. Peaker, E.H.C. Parker, G. Patel, and T.E. Whall, "Photoluminescence analysis of MBE silicon", *Electrochemical Soc Proc* **88-8**, 355(1988).

Hayes T., *Physics World*, July 1990.

Heckingbottom R., "The application of thermodynamics to molecular beam epitaxy", in *Molecular Beam Epitaxy and Heterostructures*, ed

by L L Chang and K Ploog, 1985.

Heitman D, "Electronic excitations in microstructured two-dimensional systems", in *Two-Dimensional Systems: Physics and New Devices*, ed by G. Bauer, F. Kuchar, and H. Heinrich, 1986.

Henry A., J. Svensson, E. Janzen, and B. Monemar, "New Photoluminescence Lines in Selenium-doped Silicon", *Materials Sci and Engineering B*, **4**, 261 (1989).

Henry M.O., E.C. Lightowers, N. Killoran, D.J. Dunstan, and B.E. Cavenett, "Bound exciton recombination in beryllium-doped silicon", *J. Phys. C*, **14**, L255 (1981).

Henry M.O., J.D. Champion, K.G. McGuigan, M.L.W. Thewalt, E.C. Lightowers, "A Photoluminescence study of Zinc-implanted Silicon", *Materials Sci and Engineering B*, **4**, 201 (1989).

Herman F, et al, "Semiconductor Alloys", *Progress in Semiconductors*, **2**, 3 (1957).

Herzog H.-J., H. Jorke, and F. Schaffler, "Two-dimensional electron gas properties of symmetrically strained Si/Si_{1-x}Ge_x Quantum well", *Thin Solid Films*, **184**, 237 (1990).

Higashi G.S., J.C. Bean, C. Buescher, R. Yadvish, and H. Temkin, "Improved minority-carrier lifetime in Si/SiGe heterojunction bipolar transistors grown by molecular beam epitaxy", *Appl Phys Lett*, **56**, 2560 (1990).

Higgs V., E.C. Lightowers, G. Davies, F. Schaffler, and E. Kasper, "Photoluminescence from MBE Si grown at low temperatures; donor bound excitons and decorated dislocations", *Semicond Sci Technol*, **4**, 593 (1989).

Higgs V., E.C. Lightowers, G.F.A. Van de Walle, D.J. Gravesseijn, and E.A. Montie, "New deep level luminescence bands observed from both a SiGe alloy layer and Si/Ge superlattice structures", *Appl. Phys. Lett.*, **59**, 2579 (1991).

Hinckley J.M., V. Sankaran, and J. Singh, "Charged carrier transport in Si_{1-x}Ge_x pseudomorphic alloys matched to Si-strain-related transport improvements", *Appl Phys Lett*, **55**, 2008 (1989).

Hinkley J.M. and J. Singh, "Hole transport theory in pseudomorphic Si_{1-x}Ge_x alloys grown on Si (001) substrates", *Phys Rev B*, **41**, 2912 (1990a).

Hinckley J.M. and J. Singh, "Influence of substrate composition and crystallographic orientation on the band structure of pseudomorphic Si-Ge alloy films", *Phys Rev B*, **42**, 3546 (1990b).

Hirayama H., M. Hiroi, K. Koyama, and T. Tatsumi, "Heterojunction

bipolar transistor fabrication using $\text{Si}_{1-x}\text{Ge}_x$ selective epitaxial growth by gas source silicon molecular beam epitaxy", *Appl Phys Lett*, **56**, 2645 (1990a).

Hirayama H., et al, *J Crystal Growth*, **105**, 46 (1990b).

Houghton D.C., *Appl Phys Lett*, **57**, 2124 (1990).

Houghton D.C., "Strain relaxation kinetics in $\text{Si}_{1-x}\text{Ge}_x/\text{Si}$ heterostructures", *J Appl Phys*, **70**, 2136 (1991a).

Houghton D.C., J-P Noel, and N.L. Rowell, "Si-based photonic devices by MBE", Spring Meeting of the Materials Research Society, Anaheim, CA, 1991b.

Huang C., R.P.G. Karunasiri, J.S. Park, K.L. Wang, and T.W. Kang, *Material Research Society Symposium Proceedings*, **102**, 425 (1988).

Hughes D.T. and S. Brand, "Calculation of bound states in a strained $\text{Ge}_{0.5}\text{Si}_{0.75}/\text{Si}/\text{Ge}_{0.5}\text{Si}_{0.75}$ quantum well", *J de Physique*, **48**, C5-565 (1987).

Humlicek J, et al, *Solid State Comm*, **76**, 243 (1990).

Hybertson M.S. and M. Schlüter, "Theory of optical transitions in $\text{Si}/\text{Ge}(001)$ strained-layer superlattices", *Phys Rev B*, **36**, 9683 (1987).

Hybertson M.S. and M. Schluter, *Mat Res Soc Symp Proc*, **102**, 413 (1988a).

Hybertson M.S., P. Freidel, and M. Schluter, "Theory of low energy optical transitions in Si/Ge strained layer superlattices", in *19th Int Conf Phys Semicond*, edited by W. Zawadski (Polish Academy of Sciences, Warsaw), 1988b.

Ikeda M., T. Oguchi, K. Terakura, "Electronic structure calculations of Si_m/Ge_n strained layer superlattices", in *19th Int Conf on Phys Semicond*, edited by W. Zawadski (Polish Academy of Sciences, Warsaw), 1988.

Ito T., K.E. Khor, and S. Das Sarma, "Empirical potential-based Si-Ge interatomic potential and its application to superlattice stability", *Phys Rev B*, **40**, 9715 (1989).

Iyer S.S., G.L. Patton, S.L. Delage, S. Tiwari, and J.M.C. Stork, "Silicon-Germanium base heterojunction bipolar transistors by molecular beam epitaxy", in *Proc 2nd Int Symp on Si MBE*, edited by J.C. Bean and L.J. Schowalter (Electrochemical Society, Pennignton, NJ), 1987.

Iyer S.S., R.A.A. Kubiak, and E.H.C. Parker, "Homoepitaxy", in

Silicon-MBE, edited by E. Kasper and J.C. Bean (CRC Press, Boca Raton), 1988.

Iyer S.S., G.L. Patton, D.L. Harame, J.M.C. Stork, E.F. Crabbe, and B.S. Meyerson, "Narrow band gap base heterojunction bipolar transistors using Si-Ge alloys", *Thin Solid Films*, **184**, 153 (1990).

Jain S.C. and W. Hayes, "Structure, properties and applications of $\text{Ge}_x\text{Si}_{1-x}$ strained layers and superlattices", *Semicond Sci Technol*, **6**, 547 (1991).

Jaros M., K.B. Wong, and R.J. Turton, "Optical properties of Si-Ge superlattices", *J Electronic Materials*, **19**, 35 (1990).

Jian Z., et al, *Phys Rev B*, **41**, 12862 (1990).

Johnson E.R. and S.M. Christian, "Some properties of germanium-silicon alloys", *Phys Rev*, **95**, 560 (1954).

Jorke H. and H.-J. Herzog, "Mobility enhancement in modulation-doped Si- $\text{Si}_{1-x}\text{Ge}_x$ superlattices grown by molecular beam epitaxy", in *Proc. 1st Int. Symp. Si-MBE*, Electrochemical Soc Proc **85-7**, 352 (1985).

Jorke H. and H.J. Herzog, "Boron delta doping in Si and $\text{Si}_{0.8}\text{Ge}_{0.2}$ layers", *Appl. Phys. Lett.*, **57**, 1762 (1990).

Joyce B.A., "Kinetic and surface aspects of MBE", in *Molecular Beam Epitaxy and Heterostructures*, edited by L.L. Chang and K. Ploog, 1985.

Kallel M.A., V. Arbet, R.P.G. Karunasiri, and K.L. Wang, "Photoluminescence characterization of Si_mGe_n superlattices", *J. Vac. Sci. Technol. B*, **8**, 214 (1990).

Kamins T.I., K. Nauka, L.H. Camnitz, J.B. Kruger, J.E. Turner, S.J. Rosner, M.P. Scott, J.L. Hoyt, C.A. King, D.B. Noble, and J.F. Gibbons, "High frequency Si/ $\text{Si}_{1-x}\text{Ge}_x$ heterojunction Bipolar transistors", *IEEE Proceedings IEDM-89*, **647** (1989).

Karlsteen M. and M. Willander, *Solid State Elect*, **33**, 199 (1990).

Karunasiri R.P.G., "Intersubband infrared absorption in $\text{Ge}_x\text{Si}_{1-x}/\text{Si}$ superlattice by photocurrent measurement", *Appl Phys Lett*, **56**, 1342 (1990a).

Karunasiri R.P.G., et al, *Appl Phys Lett*, **57**, 2585 (1990b).

Kasper E. and H.J. Herzog, "Elastic Strain and Misfit Dislocation Density in $\text{Ge}_{0.92}\text{Si}_{0.08}$ films on Silicon Substrates", *Thin Solid Films*, **44**, 357 (1977).

Kasper E., H.-J. Herzog, H. Daembkes, and G. Abstreiter, "Equally strained Si/SiGe superlattices on Si substrates, *Proc. Mat. Res. Soc*, Fall 1985, Boston.

Kasper E., "Strained layer superlattices", in *Physics and Applications of Quantum Wells and Superlattices*, edited by E.E. Mendez and K. von Klitzing, 1987a.

Kasper E., H.J. Herzog, H. Jorke, and G. Abstreiter, "Strained Layer Si/Ge Superlattices", *Superlattices and Microstructures*, **3**, 141 (1987b).

Kasper E., H. Kibbel, H. Jorke, H. Brugger, E. Friess, G. Abstreiter, "Symmetrically strained Si/Ge superlattices on Si substrate", *Phys Rev B*, **38**, 3599 (1988).

Kasper E., "SiGe/Si superlattices: Strain influences and devices", in *Heterostructures on Si: One step further with Si*, 1989.

Kasper E., et al, Spring Meeting of the Materials Research Society, 1991.

Katalsky A., S. Luryi, J.C. Bean, and T.T. Sheng, "Single-crystal Ge/Si infrared photodetector for fiber-optics communications", *Electrochemical Soc Proc 85-7*, **406** (1985).

Kelly M.J., "Quantum semiconductor devices", *Science Progress*, **72**, 99 (1988).

Kennedy T.A., March Meeting of the American Physical Society, Indianapolis IN, 1992, and subsequent private discussions.

Khurgin J., *IEEE J Quan Elec*, **26**, 876 (1990).

Kibbel H. and E. Kasper, *Vacuum*, **41**, 929 (1990a).

Kibbel H., E. Kasper, and P. Narozny, "Boron doping of Si-Ge base of heterobipolar transistors", *Thin Solid Films*, **184**, 163 (1990b).

King C.A., J.L. Hoyt, and J.F. Gibbons, "Bandgap and transport properties of $\text{Si}_{1-x}\text{Ge}_x$ by analysis of nearly ideal Si/ $\text{Si}_{1-x}\text{Ge}_x$ /Si heterojunction bipolar transistors", *IEEE Trans. Electronic Devices*, **36**, 2093 (1989).

Kittel C., *Introduction to Solid State Physics*, 6th edition (Wiley, New York), 1985.

Klein P.B. and G.S. Pomrenke, *Electronics Letters*, (1988).

Kline J.S., F.H. Pollak, and M. Cardona, *Helv. Phys. Acta*, **41**, 968 (1968).

Kriechbaum M., "Envelope function calculations for superlattices", in *Two-Dimensional Systems: Physics and New Devices*, edited by G. Bauer, F. Kuchar, and H. Heinrich, 1986.

Kroemer H., *Surface Science*, **132**, 543 (1983).

Kroemer H., "Theory of heterojunctions: A critical review", in *Molecular Beam Epitaxy and Heterostructures*, edited by L.L. Chang and K. Ploog (Nijhoff, Dordrecht), 1985.

Kuan T.S. and S.S. Iyer, "Strain relaxation and ordering in SiGe layers grown on (100), (111), and (110) Si surfaces by molecular-beam epitaxy", *Appl. Phys. Lett.*, **59**, 2242 (1991).

Kubiak R.A.A., E.H.C. Parker, and S.S. Iyer, "Si-MBE growth systems - Technology and practice", in *Silicon-MBE*, (Boca Raton, CRC Press), 1985, p5.

Lannin J.S., "Vibrational and Raman-scattering properties of crystalline $\text{Ge}_x\text{Si}_{1-x}$ alloys", *Phys Rev B*, **16**, 1510 (1977).

Lang D.V., R. People, J.C. Bean, and A.M. Sergent, "Measurement of the band gap of $\text{Ge}_x\text{Si}_{1-x}/\text{Si}$ strained-layer heterostructures", *Appl Phys Lett*, **47**, 1333 (1985).

Lee I., and C.Y. Fong, *Superlattices and Microstructures*, **7**, 153 (1990).

Levitas A., C.C. Wang, B.H. Alexander, *Phys Rev*, **95**, 846 (1954).

Lightowers E.C., L. Canham, G. Davies, M.L.W. Thewalt, and S.P. Watkins, *Phys Rev B.*, **29**, 4517 (1984).

Lightowers E.C., and G. Davies, "Spectroscopy of excitons bound to isoelectronic defect complexes in silicon", *Solid State Communications*, **53**, 1055 (1985).

Lightowers E. C., M. J. Gregson, V. Higgs, S. T. Davey, C. J. Gibbings, and C. G. Tuppen, *Material Science Forum*, **38**, 379 (1989a).

Lightowers E. C., V. Higgs, M. J. Gregson, G. Davies, S. T. Davey, C. J. Gibbings, C. G. Tuppen, F. Schaffler, and E. Kasper, "Photoluminescence characterization of molecular beam epitaxial silicon", *Thin Solid Films*, **183**, 235 (1989b).

Lin T.L., R.W. Fauthier, and P.J. Grunthaner, "Heavily boron-doped Si layers grown below 700°C by molecular beam epitaxy using a HBO_2 source", *Appl. Phys. Lett.*, **55**, 795 (1989).

Lin T.L., Spring Meeting of the Materials Research Society, 1991.

Lockwood D.J., M.W.C. Dharma-Wardana, J.M. Baribeau, and D.C. Houghton, "Folded acoustic phonons in Si/Ge_xSi_{1-x} strained-layer superlattices", *Phys Rev B*, **35**, 2243 (1987).

Luryi S., A. Katalisky, and J.C. Bean, "New infrared detector on a silicon chip", *IEEE Trans. Electronic Devices*, **31**, 1135 (1984).

Luryi S., and S.M. Sze, "Possible device applications of silicon molecular beam epitaxy", in *Silicon MBE*, edited by E. Kasper and J.C. Bean (CRC, Boca Raton), 1988.

Ma Q.M. and K.L. Wang, *Appl Phys Lett*, **58**, 1184 (1991).

Makhov A.F., *Sov Phys Sol State*, **2**, 1934 (1960).

Malhiot C. and D.L. Smith, "Full-zone k'p theory of semiconductor superlattice electronic structure", *J Vac Sci Technol B*, **8**, 793 (1989).

Malhiot C. and D.L. Smith, "Strained-layer Semiconductor superlattices", *Cr Rev Sol St& Mat Sci*, **16**, 131 (1990).

Manesevit H.M., I.S. Gergis, and A.B. Jones, "Electron mobility enhancement in epitaxial multilayer Si-Si_{1-x}Ge_x alloy films", *Appl Phys Lett*, **41**, 464 (1982).

Mattey N.L., M. Hopkinson, R.F. Houghton, M.G. Dowsett, D.S. McPhail, T.E. Whall, E.H.C. Parker, G.R. Booker, and J. Whitehurst, "P-type delta doping in silicon MBE", *Thin Solid Films*, **184**, 15 (1990).

Matthai C.C., J.M. Bass, and M. Oloumi, "Band offsets and electron localization in semiconductor interfaces and superlattices", *J Vac Sci Technol B*, **8**, 916 (1990).

McGill T.C., R.H. Miles, R.J. Haunstein, and O.J. Marsh, "Opportunities in devices and physics", in *Proc 2nd Int Symp on Si MBE*, edited by J.C. Bean and L.J. Schowalter (Electrochemical Society, Pennington NJ), 1987.

McGuigan K.G., M.O. Henry, M.C. Carmo, G. Davies, and E.C. Lightowers, "A uniaxial stress study of a copper-related photoluminescence band in silicon", *Materials Sci and Engineering B*, **4**, 259 (1989).

Menz P.M., S. Luryi, J.C. Bean, and C.J. Buescher, "Evidence for a real-space transfer of hot holes in strained GeSi/Si heterostructures", *Appl Phys Lett*, **56**, 2663 (1990).

Merle J.C., M. Capizzi, P. Fiorini, and A. Frova, *Phys. Rev. B*, **17**, 4821 (1978).

- Meynadier M.H., R.E. Nahory, J.M. Warlock, M.C. Tamargo, and J.L. deMiguel, "Indirect-Direct anticrossing in GaAs-AlAs superlattices induced by an Electric field: Evidence of Gamma-X mixing", *Phys Rev Lett*, **60**, 1338 (1988a).
- Meynadier M.H., in *Properties of Impurity States in Superlattice Semiconductors*, edited by Fong, Batra, and Ciraci (Plenum, New York), 1988b, p11.
- Mishima T, et al, *Appl Phys Lett*, **57**, 2567 (1990).
- Mitchard G.S., S.A. Lyon, K.R. Elliot, and T.C. McGill, *Solid State Communications*, **29**, 425 (1979).
- Mitchard G.S. and T.C. McGill, "Photoluminescence of Si-rich Si-Ge alloys", *Phys Rev B*, **25**, 5351 (1982).
- Modavis R.A., D.G. Hall, J. Bevk, B.S. Freer, L.C. Feldman, and B.E. Weir, "Isoelectronic bound exciton emission from Si-rich silicon-germanium alloys", *Appl Phys Lett*, **57**, 954 (1990).
- Modavis R.A., D.G. Hall, J. Bevk, and B.S. Freer, "Cooperative confinement of excitons bound to isoelectronic impurity complexes in $\text{Si}_{1-x}\text{Ge}_x\text{Si}$ superlattices", *Appl. Phys. Lett.*, **59**, 1230 (1991).
- Monch W., "Some aspects of surface science related to MBE", in *Molecular Beam Epitaxy and Heterostructures*, edited by L.L. Chang and K. Ploog (Nijhoff, Dordrecht), 1985.
- Montie E.A., G.F.A. van de Walle, D.J. Gravesteijn, A.A. van Gorkum, E.C. Cosman, C.W. Fredriksz, and C.W.T. Bulle-Lieuwma, "Phonons in Si/Ge superlattices: Theory and Experiment", *Thin Solid Films*, **183**, 105 (1989a).
- Montie E.A., G.F.A. van de Walle, D.J. Gravesteijn, A.A. van Gorkum, E.C. Cosman, C.W. Fredriksz, and C.W.T. Bulle-Lieuwma, "A photoluminescence study of Si/Ge superlattices", *Thin Solid Films*, **183**, 111 (1989b).
- Montie E.A., G.F.A. van de Walle, D.J. Gravesteijn, A.A. van Gorkum, and W.J.O. Tesselink, "Longitudinal phonons in Si/Ge superlattices", *Semicond Sci Technol*, **4**, 889 (1989c).
- Montie E.A., G.F.A. van de Walle, D.J. Gravesteijn, A.A. van Gorkum, and C.W.T. Bulle-Lieuwma, "Photoluminescence from Si/Ge superlattices", *Appl. Phys. Lett.*, **56**, 340 (1990).
- Moriarty J.A. and S. Krishnamurthy, "Theory of silicon superlattices: Electronic structure and enhanced mobility", *J Appl Phys*, **54**, 1892 (1983).
- Morrison I., M. Jaros, and K.B. Wong, "Strain-induced electron

states in $\text{Si}_{0.75}\text{Ge}_{0.5}$ (Si/Si_{0.5}Ge_{0.5}) (001) superlattices", *J Phys C: Sol State Phys*, **19**, L239 (1986).

Morrison I., M. Jaros, and K.B. Wong, "Strain-induced confinement in $\text{Si}_{0.75}\text{Ge}_{0.5}$ (Si/Si_{0.5}Ge_{0.5}) (001) superlattice systems", *Phys Rev B*, **35**, 9693 (1987).

Moutonnet D., H. L'Haridon, P.N. Favennec, M. Salvi, M. Gauneau, F. Arnaud D'avitaya, and J. Chroboczek, "1.54 μm Photoluminescence of Erbium-implanted Silicon", *Materials Science and Engineering B*, **4**, 75 (1989).

Murakami E., et al, *Jap J Appl Phys*, **29**, L1059 (1990).

Nazare M.H., M.C. Carmo, and A.J. Duarte, "Luminescence from transition metal centres in silicon doped with silver and nickel", *Materials Sci and Engineering B*, **4**, 273 (1989).

Ni W-X, J. Knall, and G.V. Hansson, "Band offsets at Si/Si_{1-x}Ge_x heterojunction interfaces studied with x-ray photomission: influence of strain and crystal orientation", in *Proc 2nd Int Symp on Si MBE*, edited by J.C. Bean and L.J. Schowalter (Electrochemical Society, Pennington NJ), 1987a.

Ni W.X., J. Knall, and G.V. Hansson, "New Method to study band offsets applied to strained Si/Si_{1-x}Ge_x(100) heterojunction interfaces", *Phys Rev B*, **36**, 7744 (1987b).

Ni W.-X., J. Knall, M.A. Hasan, G.V. Hansson, J.-E. Sundgren, S.A. Barnett, L.C. Markert, and J.E. Greene, "Kinetics of dopant incorporation using a low-energy antimony ion beam during growth of Si(100) films by molecular beam epitaxy", *Phys. Rev B*, **40**, 10449 (1989).

Ni W.-X. and G.V. Hansson, "Band offsets in pseudomorphically grown Si/Si_{1-x}Ge_x heterostructures studied with core-level x-ray photoelectron spectroscopy", *Phys Rev B*, **42**, 3030 (1990).

Noel J.-P., J.E. Greene, N.L. Rowell, S. Kechang, and D.C. Houghton, "Photoluminescence studies of Si(100) doped with low-energy (<1000 eV) As⁺ ions during molecular beam epitaxy", *Appl Phys Lett*, **55**, 1525 (1989).

Noel J.-P., N.L. Rowell, D.C. Houghton, and D.D. Perovic, "Intense photoluminescence between 1.3 and 1.8 μm from strained Si_{1-x}Ge_x alloys", *Appl. Phys. Lett.*, **57**, 1037 (1990a).

Noel J.-P., J.E. Greene, N.L. Rowell, and D.C. Houghton, "Photoluminescence studies of Si(100) doped with low-energy (100-1000 eV) B⁻ ions during molecular beam epitaxy", *Appl. Phys. Lett.*, **56**, 265 (1990b).

Northrop G.A., S.S. Iyer, D.J. Wolford, and S.L. Delage,

"Luminescence from Si_{1-x}Ge_x alloy layers grown by molecular beam epitaxy", in *19th Int Conf Phys Semicond*, edited by W. Zawadski (Polish Academy of Sciences, Warsaw),, 1988.

Northrup G.A., D.J. Wolford, and S.S. Iyer, "Photoluminescence from epitaxial Si/Si_{0.95}Ge_{0.05} heterostructures as probed by optically active deep levels", *J. Vac. Sci. Technol B*, **9**, 2388 (1991).

Okada Y., et al, *Solid State Electronics*, **32**, 797 (1989).

Okumura H., K. Miki, S. Misawa, K. Sakamoto, T. Sakamoto, and S. Yoshida, "Observation of Direct band Gap Properties in GenSim Strained-Layer Superlattices", *Japanese J Appl Phys*, **28**, L1893 (1989).

Osbourne G.C., "Strained-layer superlattices: A brief review", *IEEE J Quan Elec*, **QE-22**, 1677 (1986).

Panish M.B. and H. Temkin, *Ann Rev Mater Sci*, **19**, 209 (1989).

Park J.S., R.P.G. Karunasiri, and K.L. Wang, "Study of hole transport through minibands in symmetrically strained GeSi_{1-x}/Si superlattices", *Thin Solid Films*, **183**, 25 (1989).

Parry C.P, S.M. Newstead, R.D. Barlow, P. Augustus, R.A.A. Kubiak, M.G. Dowsett, T.E. Whall, and E.H.C. Parker, "Elemental boron doping behavior in silicon molecular beam epitaxy", *Appl. Phys. Lett.*, **58**, 481 (1991).

Parker J.H., D.W. Feldman, and M. Ashkin, "Raman scattering by silicon and germanium", *Phys Rev.*, **155**, 712 (1967).

Patton G.L., S.S. Iyer, S.L. Delage, S. Tiwari, and J.M.C. Stork, "Silicon-germanium-base heterojunction bipolar transistors by molecular beam epitaxy", *IEEE Trans. Electronic Devices Lett.*, **9**, 165 (1988).

Patton G.L., D.L. Harame, J.M.C. Stork, B.S. Meyerson, G.J Scilla, and E. Ganin, "Graded-SiGe-base polyemitter heterojunction bipolar transistors", *IEEE Trans. Electron. Devices Lett*, **10**, 534 (1989).

Patton G.L., J.H. Comfort, B.S. Meyerson, E.F. Crabbe, G.J. Scilla, E. de Fresart, J.M.C. Stork, J.Y.C. Sun, D.L. Harame, and J.N. Burghartz, "75-Ghz f_T SiGe-base heterojunction bipolar transistors", *IEEE Trans. Electronic Device Lett.*, **11**, 171 (1990).

Pawlik M., "Assessment of layers", in *Silicon-MBE*, edited by E. Kasper and J.C. Bean (Boca Raton; CRC Press), 1988, p111.

Peacock D.C., D.A. Ritchie, J.E.F. Frost, E.H. Linfield, A.G. Davies, C. Smith, D.A. Wharam, C.J.B. Ford, T.J. Thornton, R.

Newbury, D.G. Hasko, H. Ahmed, G.A.C. Jones, and M. Pepper, *Physica Scripta*, **T29**, 141 (1989).

Pearce C.W., in *VLSI Technology*, edited by S.M. Sze (Singapore, McGraw Hill), 1983, Chapter 1.

Pearsall T.P., J.C. Bean, R. People, and A.T. Fiory, in *Proc. 1st Int. Symp. Si-MBE*, Electrochemical Soc Proc **85-7**, 400 (1985).

Pearsall, T.P., F.H. Pollak, J.C. Bean, and R. Hull, "Electroreflectance spectroscopy of Si-GexSi1-x quantum well structures", *Phys Rev B*, **33**, 6621 (1986a).

Pearsall T.P. and J.C. Bean, "Enhancement- and depletion-mode p-channel GexSi1-x modulation doped FET's", *IEEE Electr Dev Lett*, **EDL-7**, 308 (1986b).

Pearsall T.P., H. Temkin, J.C. Bean, and S. Luryi, "Avalanche Gain in Ge_xSi_{1-x}/Si infrared waveguide detectors", *IEEE Trans. Electronic Devices*, **7**, 330 (1986c).

Pearsall, T.P., J. Bevkj, L.C. JFeldman, M.Bonar, J.P.Mannaerts, and A. Ourmazd, "Structurally Induced Optical Transitions in Ge-Si Superlattices", *Phys Rev Lett*, **58**, 729 (1987).

Pearsall T.P., E.A. Beam, H. Temkin, J.C. Bean, "Ge-Si/Si infra-red, zone-folded superlattice detectors", *Electronics Letters*, **24**, 685 (1988).

Pearsall T.P., "Silicon-Germanium alloys and heterostructures: Optical and Electronic properties", *Critical Rev Sol. State and Mat Sci*, **15**, 551 (1989a).

Pearsall T.P., "Optical Properties of Ge-Si alloys and Superlattices", *J Luminescence*, **44**, 367 (1989b).

Pearsall T.P., "Direct band-gap Si-based semiconductors, Principles and Prospects", in *Heterostructures on Si: One step further with Si*, 1989c.

Pearsall T.P., J.M. Vandenberg, R. Hull, and J.M. Bonar, "Structure and optical properties of strained Ge-Si superlattices grown on (001) Ge", *Phys Rev Lett*, **63**, 2104 (1989d).

Pearsall T.P., R. Hull, J.C. Bean, and J.M. Bonar, "Optical properties of strained Ge-Si superlattices", *Thin Solid Films*, **183**, 9 (1989e).

Pearsall T. P., "Prospects and challenges for Si-Ge strained-layer epitaxy", *Thin Solid Films*, **184**, 451 (1990).

People R., J.C. Bean, D.V. Lang, A.M. Sargent, H.L. Stormer, K.W.

Wecht, R.T. Lynch, and K. Baldwin, "Modulation doping in $\text{Ge}_x\text{Si}_{1-x}/\text{Si}$ strained layer heterostructures", *Appl. Phys. Lett.*, **45**, 1231 (1984).

People R., "Indirect band gap of coherently strained $\text{Ge}_x\text{Si}_{1-x}/\text{Si}$ bulk alloys on (001) silicon substrates", *Phys. Rev. B.*, **32**, 1405 (1985a).

People R., J.C. Bean, D.V. Lang, "Modulation doping in $\text{Ge}(x)\text{Si}(1-x)/\text{Si}$ strained layer heterostructures: Effects of alloy layer thickness, doping setback, and cladding layer dopant concentration", *J. Vac. Sci. Technol.*, **3**, 846 (1985b).

People R., J.C. Bean, and D.V. Lang, in *Proc. 1st Int. Symp. Si-MBE*, Electrochemical Soc Proc **85-7**, 360 (1985c).

People R. and J.C. Bean, "Calculation of critical layer thickness versus lattice mismatch for $\text{Ge}_x\text{Si}_{1-x}/\text{Si}$ strained layer heterostructures", *Appl Phys Lett*, **47**, 322 (1985d).

People R., "Physics and Applications of $\text{Ge}_x\text{Si}_{1-x}/\text{Si}$ Strained Layer Heterostructures", *IEEE J Quan Elec*, **QE-22**, 1696 (1986a).

People R., "Indirect band gap and band alignment for coherently strained $\text{Si}_x\text{Ge}_{1-x}$ bulk alloys on germanium (001) substrates", *Phys Rev B*, **34**, 2508 (1986b).

People R., and S.A. Jackson, "Indirect, quasidirect, and direct optical transitions in the pseudomorphic (4x4) -monolayer Si-Ge strained-layer superlattice on Si(001)", *Phys Rev B*, **36**, 1310 (1987).

Ploog K., et al, *J Electrochemical Soc*, **128**, 400 (1981).

Ploog K., "Doping superlattices", in *Properties of Impurity States in Superlattice Semiconductors*, 1988a.

Pollard W., *J Appl Phys*, **69**, 3154 (1991).

Presting H., et al, Spring Meeting of the Materials Research Society, 1991.

Prokes S.M., O.J. Glembocki, and K.L. Wang, "Optical and structural studies of relaxation in $\text{Si}_{1-x}\text{Ge}_x/\text{Si}$ strained-layer superlattices", *Superlattices and Microstructures*, **10**, 113 (1991a).

Prokes S.M., O.J. Glembocki, M.E. Twigg, "The study of relaxation in asymmetrically strained $\text{Si}_{1-x}\text{Ge}_x/\text{Si}$ superlattices", *Journal of Electronic Materials*, **20**, 389 (1991b).

Rajakarunanayake Y. and T.C. McGill, "Band structure and optical properties of $\text{Si}-\text{Si}_{1-x}\text{Ge}_x$ superlattices", *Phys Rev B*, **40**, 3051

(1989a).

Rajakarunanayake Y. and T.C. McGill, *J Vac Sci Technol B*, **7**, 799 (1989b).

Rajakarunanayake Y. and T.C. McGill, "Intersubband absorption in Si_{1-x}Ge_x/Si superlattices for long wavelength infrared detectors", *J Vac Sci Tech B*, **8**, 929 (1990).

Rajan K., *J Electronic Mat*, **19**, 1009 (1990).

Rentzsch R. and I.S. Shlimak, "Influence of the composition on the interimpurity radiative recombination in germanium-silicon alloys", *Soviet Phys. Semicond.*, **12**, 416 (1978).

Rhee S.S., J.S. Park, R.P.G. Karunasiri, "Resonant tunneling through a Si/GeSi_{1-x}/Si heterostructure on a GeSi buffer layer", *Appl Phys Lett*, **53**, 204 (1988).

Rhee S.S., G.K. Chang, T.K. Carns, and K.L. Wang, "SiGe resonant tunneling hot carrier transistor", *IEEE Proceedings IEDM-89*, 651 (1989).

Rhee S.S., G.K. Chang, T.K. Carns, and K.L. Wang, "SiGe resonant tunneling hot-carrier transistor", *Appl Phys Lett*, **56**, 1061 (1990).

Ridley B.K., *J Appl Phys*, **68**, 4667 (1990).

Robbins D.J., R.A.A. Kubiak, and E.H.C. Parker, "Photoluminescence studies of silicon molecular beam epitaxy layers", *J Vac Sci Technol B*, **3**, 588 (1985a).

Robbins D.J., D.B. Gasson, R.W. Hardeman, N.G. Chew, A.G. Cullis, and C.A. Warwick, "Luminescence and TEM of defects in silicon MBE layers", *Electrochemical Soc Proc*, **85-7**, (1985b).

Robbins D.J., P. Calcott, and W.Y. Leong, "Electroluminescence from a pseudomorphic Si_{0.8}Ge_{0.2} alloy", *Appl. Phys. Lett.*, **59**, 1350 (1991).

Robbins D.J., L.T. Canham, S.J. Barnett, A.D. Pitt, and P. Calcott, "Near-band-gap photoluminescence from pseudomorphic Si_{1-x}Ge_x single layers on silicon", *J. Appl. Phys.*, **71**, 1407 (1992).

Rosencher E., "Device application: Work to date", in *Silicon MBE*, edited by E. Kasper and J.C. Bean (CRC, Boca Raton), 1988. (1988).

Rowell N.L., J.M. Baribeau, and D.C. Houghton, "Photoluminescence of MBE grown Si_{1-x}Ge_x films", in *Proceedings of the 2nd International Symposium on Silicon Molecular Beam Epitaxy*, edited by J.C. Bean and L.J. Schowalter (Pennington NJ; Electrochemical Society), 1987, p48.

- Rowell N. L., D. C. Houghton, J.-P. Noel, J. E. Greene, "Effect of growth temperature on photoluminescence from ion-beam-doped molecular beam epitaxial Si:As", *Thin Solid Films*, **184**, 69 (1990).
- Rowell N.L., J-P Noel, D.C. Houghton, and M. Buchanan, "Electroluminescence and photoluminescence from $\text{Si}_{1-x}\text{Ge}_x$ alloys", *Appl Phys Lett*, **58**, 957 (1991).
- Sakamoto T., K. Sakamoto, H. Oyanagi, T. Yao, T. Ishiguro, S. Nagao, G. Hashiguchi, K. Kuniyoshi, and Y. Bando, "Growth control of $\text{Ge}_x\text{Si}_{1-x}/\text{Si}$ strained-layer superlattice by the RHEED intensity oscillations", *Journal de Physique*, **C5**, 333 (1987).
- Sandhu A., B. Hamilton, R.A.A. Kubiak, W.Y. Leong, and E.H.C. Parker, "Photoluminescence spectroscopy of shallow states in MBE silicon", *Electrochemical Soc Proc*, **85-7**, (1985).
- Saris F.W. and T. de Jong, "Silicon Molecular Beam Epitaxy", in *Molecular Beam Epitaxy and Heterostructures*, edited by L.L. Chang and K Ploog, 1985.
- Satpathy S., R. M. Martin, and C. G. van de Walle, "Electronic properties of the (100) (Si/Ge) strained-layer superlattices", *Phys Rev B*, **38**, 13237 (1988).
- Sauer R., "Dislocation-related photoluminescence in silicon", *Appl Phys A*, **36**, 1 (1985).
- Schaffler F., M. Asom, R. People, D.V. Lang, L.C. Kimerling, and J.C. Bean, "New photoluminescence defect at 1.0192 eV in silicon molecular beam epitaxy layers ascribed to Cu", *Appl. Phys. Lett.*, **51**, 1185 (1987).
- Schaffler F. and H. Jorke, "Gallium doping of silicon molecular beam epitaxial layers at low growth temperatures and under Si⁺ ion bombardment", *Thin Solid Films*, **184**, 75 (1990).
- Schaffler F. and H. Jorke, *Appl Phys Lett*, **58**, 397 (1991).
- Schmid U., N.E. Christensen, and M. Cardona, "Direct transition energies in strained ten-monolayer Ge/Si superlattices", *Phys Rev Lett*, **65**, 1933 (1990a).
- Schmid U., et al. *Phys Rev Lett*, **65**, 2610 (1990b).
- Schowalter L.J., F.M. Steranka, M.B. Salamon, and J.P. Wolfe, "Long lifetimes of excitons in stressed Ge", *Sol State Comm*, **37**, 319 (1981).
- Schowalter L.J., *Mat Res Soc Symp Proc*, **116**, 3 (1988).
- Schreiber H.-U. and B.G. Bosch, "Si/SiGe heterojunction bipolar

transistors with current gains up to 5000", *IEEE Proceedings, IEDM-89*, 643 (1989).

Schorer R., E. Friess, K. Eberl, and G. Abstreiter, "Structural stability of short-period Si/Ge superlattices studied with Raman spectroscopy", *Phys. Rev. B*, **44**, 1772 (1991).

Schwartz G.P., M.S. Hybertson, J. Bevk, B.A. Davidson, H.-J. Gossman, J.P. Mannaerts, G.J. Gualtieri, *Phys Rev B*, **39**, 1235 (1989).

Schwartz P.V. and J.C. Sturm, *Appl Phys Lett*, **57**, 2004 (1990).

Sham L.J., and Y.T. Lu, "Theory of electronic structure in superlattices", *J Luminescence*, **44**, 207 (1989).

Shen D., K. Zhang, and X. Xie, "Electronic structure of strained-layer superlattices", *Appl Phys Lett*, **52**, 717 (1988).

Shen G.D., D.X. Xu, M. Willander, J. Knall, M.A. Hasan, and G. V. Hansson, "Novel transport phenomena in Si/SiGe/Si double heterojunction bipolar transistors", *Semicond Sci and Technol*, **4**, 370 (1989).

Shigekawa H., et al, *Jap J Appl Phys*, **29**, L736 (1990).

Singh M., E.C. Lightowers, G. Davies, C. Jeynes, and K.J. Reeson, "Isoelectronic bound exciton photoluminescence from a metastable defect in sulphur-doped silicon", *Materials Sci and Engineering B*, **4**, 303 (1989).

Smith D.L. and C. Mailhiot, "Theory of semiconductor superlattice electronic structure", *Rev Mod Phys*, **62**, 173 (1990).

Stroud D. and H. Ehrenreich, *Phys Rev B*, **2**, 3197 (1970).

Sturm J.C., H. Manoharan, L.C. Lenchyshyn, M.L.W. Thewalt, N.L. Rowell, J.-P. Noel, and D.C. Houghton, "Well-resolved band-edge photoluminescence of excitons confined in strained Si_{1-x}Ge_x quantum wells", *Phys. Rev. Lett.*, **66**, 1362 (1991).

Sze S.M., *Physics of Semiconductor Devices* (Wiley, New York), 1981, p21.

Taft R.C. and J.C. Plummer, "Advanced Heterojunction Ge_xSi_{1-x}/Si Bipolar devices", *IEDM Tech. Digest*, 655 (1989a).

Taft R.C., J.D. Plummer, and S.S. Iyer, "Demonstration of a p-channel BICFET in the Ge_xSi_{1-x}/Si system", *IEEE Electron. Device Lett.*, **10**, 14 (1989b).

Tang T.S., *Phys Stat Solidi B*, **153**, K153 (1989).

Tatsumi T., H. Hirayama, and N. Aizaki, "Si/Ge_{0.3}Si_{0.7}/Si heterojunction bipolar transistor made with Si molecular beam epitaxy", *Appl. Phys. Lett.*, **52**, 897 (1988).

Tatsumi T., "Boron doping using compound source", *Thin Solid Films*, **184**, 1 (1990).

Tauc J. and A. Abraham, "Optical Investigation of the Band Structure of Ge-Si Alloys", *J Phys Chem Sol*, **20**, 190 (1961).

Taylor G.W. and J.G. Simmons, "The bipolar inversion channel field-effect transistor (BICFET) - A new field-effect solid state device: Theory and structure", *IEEE Trans. Electronic Device* **32**, 2345 (1985).

Taylor G.W., M.S. Leiby, P.A. Kiely, P. Cooke, A. Isabelle, T.Y. Chang, B. Tell, D.L. Crawford, K. Brown-Goebeler, and J.G. Simmons, "Performance advantages of BICFETs versus HBTs", *IEEE Proc. Bipolar Circuits and Technology Meeting*, Minneapolis, 1988.

Tejedor C. and L. Brey, "Electronic structure of Si-Ge strained superlattices", *J de Physique*, **48**, C5-557 (1987).

Temkin H., T.P. Pearsall, J.C. Bean, R.A. Logan, and S. Luryi, "GexSil-x strained layer superlattice waveguide photodetectors operating near 1.3 microns", *Appl Phys Lett*, **48**, 963 (1986).

Temkin H., "GexSil-x Optoelectronic devices", in *Proceedings of the 2nd International Symposium on Silicon Molecular Beam Epitaxy*, edited by J.C. Bean and L.J. Schowalter (Pennington NJ; Electrochemical Society), 1987, p 28.

Temkin H., J.C. Bean, A. Antreasyan, and R. Leibenguth, "GexSil-x strained-layer heterostructure bipolar transistors", *Appl Phys Lett*, **52**, 1089 (1988).

Terashima K., M. Tajima, T. Tatsumi, "Near-band-gap photoluminescence of Si_{1-x}Ge_x alloys grown on Si(100) by molecular beam epitaxy", *Appl. Phys. Lett.*, **57**, 1925 (1990).

Thewalt M.L.W., in *Excitons*, edited by E.I. Rashba and M.D. Sturge (North Holland: Amsterdam), 1982, p 393.

Thewalt M.L.W., T. Steiner, J.I. Pankove, "Photoluminescence studies of Si implanted with In and/or Tl: The effects of thermal treatment and atomic H", *J Appl Phys*, **57**, 498 (1985).

Thomas D.G., M. Gershenson, and J.J. Hopfield, *Phys Rev*, **131**, 2397 (1953).

Thompson P.E., private discussions, August 1991.

Tsao J.Y. and B.W. Dodson, "Time, temperature and excess stress: Relaxation in strained heterostructures", *Surface Science*, **228**, 260 (1990).

Tuppen C.G. and C.J. Gibbings, *J Appl Phys*, **68**, 1526 (1990).

Turton R.J. and M. Jaros, *Mat Sci and Eng B*, **7**, 37 (1990a).

Turton R.J. and M. Jaros, *Superlattices and Microstructures*, **8**, 25 (1990b).

Turton R.J. and M. Jaros, "Optimum Si-Si_{1-x}Ge_x structures with strong infrared spectra", *Appl Phys Lett*, **56**, 767 (1989).

Van de Walle C. and R.M. Martin, "Theoretical calculations of heterojunction discontinuities in the Si/Ge system", *Phys Rev B*, **34**, 5621 (1986).

Van De Walle C.G., *Mat Res Soc Symp Proc*, **102**, 565 (1988).

Voronkova G.I., M.I. Iglitsyn, and A.R. Salmonov, "Behavior of holmium in silicon", *Sov. Phys. Semicond.*, **8**, 1043 (1975).

Wang P.J., B.S. Meyerson, F.F. Fang, J. Nocera, and B. Parker, *Appl Phys Lett*, **55**, 2333 (1989).

Watkins S.P., M.L.W. Thewalt, and T. Steiner, *Phys Rev B.*, **29**, 5727 (1984).

Weber J., W. Schmid, and R. Sauer, *Phys. Rev. B*, **21**, 2401 (1980).

Weber J., H. Bauch, and R. Sauer, *Phys Rev B*, **25**, 7688 (1982).

Weber J. and M.I. Alonso, "Near-band-gap photoluminescence of Si-Ge alloys", *Phys Rev B*, **40**, 5683 (1989).

Wegscheider W., et al, *Appl Phys Lett*, **57**, 1496 (1990).

Weisbuch C., "Optical properties of quantum wells", in *Physics and Applications of Quantum Wells and Superlattices*, edited by E.E. Mendez and K. von Klitzing, 1987.

White J.D., G. Fasol, R.A. Ghanbari, C.J. Gibbings, and C.G. Tuppen, "Calculation of energies and Raman intensities of confined phonons in Si-Ge strained layer superlattices", *Thin Solid Films*, **183**, 71 (1989).

White J.D., et al, *Appl Phys Lett*, **57**, 1523 (1990).

White J.D., M. Gell, G. Fasol, C.J. Gibbings, and C.G. Tuppen, "Vibrational properties of Si/Ge superlattices incorporating diatomic sheets of silicon and germanium", *Phys Rev B*, **43**, 1689

(1991).

Wilke S., *Solid State Comm*, **73**, 399 (1990a).

Wilke S., et al, *Phys Rev B*, **41**, 3769 (1990b).

Wong K.B., M. Jaros, I. Morrison, and J.P. Hagon, "Electronic structure and optical properties of Si-Ge superlattices", *Phys Rev Lett*, **60**, 2221 (1988).

Wong K.B., R.J. Turton, and M. Jaros, "Optical properties of perfect and imperfect Si-Ge superlattices", *Thin Solid Films*, **183**, 49 (1989).

Xu D.-X., G.D. Shen, M. Willander, W.-X. Ni, and G.V. Hansson, "n-Si/p-Si_{1-x}Ge_x/n-Si double-heterojunction bipolar transistor", *Appl. Phys. Lett*, **52**, 2239 (1988).

Yang L.H., et al, *Mat Res Soc Symp Proc*, **116**, 513 (1988).

Yang L.H., R.F. Gallup, and C.Y. Fong, "Electronic properties of micro-n-i-p-i structures in silicon", *Phys Rev B*, **39**, 3795 (1989).

Yu E.T., E.T. Croke, and T.Ç. McGill, "Measurement of the valence band offset in strained Si/Ge(100) heterojunctions by x-ray photoelectron spectroscopy", *Appl Phys Lett*, **56**, 569 (1990a).

Yu E.T., E.T. Croke, D.H. Chow, D.A. Collins, M.C. Phillips, T.C. McGill, J.O. McCaldin, R.H. Miles, "Measurement of the valence band offset in novel heterojunction systems: Si/Ge (100) and AlSb/ZnTe (100)", *J Vac Sci Technol B*, **8**, 908 (1990b).

Zachai R., K. Eberl, G. Abstreiter, E. Kasper, and H. Kibbel, *Phys Rev Lett*, **65**, 2610 (1990a).

Zachai R., E. Friess, G. Abstreiter, E. Kasper, and H. Kibbel, "Band structure and optical properties of strain symmetrized short period Si/Ge superlattices on Si(100) Substrates", *Proc 19th Int Conf on Physics of Semiconductors*, Warsaw, 1988, W. Zawadski, ed., Institute of Physics, Polish Academy of Sciences, Warsaw, 1988, p. 487.

Zachai R., K. Eberl, G. Abstreiter, E. Kasper, and H. Kibbel, "Photoluminescence in short-period Si/Ge strained-layer superlattices", *Phys. Rev. Lett.*, **64**, 1055 (1990a).

Zachai R., K. Eberl, G. Abstreiter, E. Kasper, and H. Kibbel, "Photoluminescence in short period Si/Ge strained layer superlattices grown on Si and Ge substrates", *Surface Science*, **228**, 267 (1990b).

Zachai R., K. Eberl, G. Abstreiter, E. Kasper, and H. Kibbel,

"Reply to Schmid et al PRL 65 2610 (1990)", *Phys. Rev. Lett.*, **65**, 2611 (1990c).

Ziemelis U.O. and R.R. Parsons, "Sharp donor-acceptor pair luminescence in silicon", *Can J Phys*, **59**, 784 (1981).

Ziemelis U.O., M.L.W. Thewalt, and R.R. Parsons, "Sharp-line, donor-acceptor pair recombination luminescence in Si(In,Li), Si(Ga,Li), Si(Al,Li), and Si(B,Li)", *Can J Phys*, **60**, 1041 (1982).

VITA

Captain Todd D. Steiner was born on 6 December 1960 in Omaha, Nebraska. He graduated from Richmond Senior High School in Rockingham, North Carolina in 1978 and attended Georgia Institute of Technology on an AFROTC scholarship, graduating with a Bachelor of Science in Physics in June of 1982. He was also commissioned in June, 1982, and began his first tour at the Air Force Weapons Laboratory at Kirtland AFB in Albuquerque, New Mexico where he was an instrumentation engineer for field tests of the effects of blast and shock on structures. After his first tour, he served as a Nuclear Systems Evaluator at the Air Force Technical Applications Center, Patrick AFB, Cocoa Beach, Florida. While at Patrick AFB he completed the requirements for a Masters in Physics at the Florida Institute of Technology at Melbourne, Florida, graduating in June 1988. He entered the School of Engineering, Air Force Institute of Technology, in July 1989 to pursue a PhD in Physics. Captain Steiner is married to the former Kimbree D. Samora they have two children, Westley and Madison. Captain Steiner is a member of Sigma Pi Sigma, Tau Beta Pi, and the American Physical Society. After completion of his studies Captain Steiner will be assigned to the Wright Laboratory Armament Directorate, Eglin AFB, Fort Walton Beach, FL.

Permanent Address: 612A 35th Avenue N.

Myrtle Beach SC 29577

REPORT DOCUMENTATION PAGE

Form Approved
OMB No. 0704-0188

Public reporting burden for this collection of information is estimated to average 1 hour per response, including the time for reviewing instructions, searching existing data sources, gathering and maintaining the data needed, and completing and reviewing the collection of information. Send comments regarding this burden estimate or any other aspect of this collection of information, including suggestions for reducing this burden, to Washington Headquarters Services, Directorate for Information Operations and Reports, 1215 Jefferson Davis Highway, Suite 1204, Arlington, VA 22202-4302, and to the Office of Management and Budget, Paperwork Reduction Project (0704-0188), Washington, DC 20503.

1. AGENCY USE ONLY (Leave blank)	2. REPORT DATE 13 July 1992	3. REPORT TYPE AND DATES COVERED Final	
4. TITLE AND SUBTITLE Photoluminescence Study of Si _{1-x} Ge _x /Si and Si/Ge Strained Layer Superlattices		5. FUNDING NUMBERS	
6. AUTHOR(S) Todd D. Steiner, Capt, USAF		8. PERFORMING ORGANIZATION REPORT NUMBER AFIT/DS/ENP/92-002	
7. PERFORMING ORGANIZATION NAME(S) AND ADDRESS(ES) Air Force Institute of Technology Wright-Patterson AFB OH 45433		10. SPONSORING / MONITORING AGENCY REPORT NUMBER	
9. SPONSORING / MONITORING AGENCY NAME(S) AND ADDRESS(ES) LT COL GERNOT POMRENKE AFOSR/NE (Bldg 410) BOLLING AFB DC 20332-6448		10. SPONSORING / MONITORING AGENCY REPORT NUMBER	
11. SUPPLEMENTARY NOTES			
12a. DISTRIBUTION / AVAILABILITY STATEMENT Approved for public release; distribution unlimited		12b. DISTRIBUTION CODE	
13. ABSTRACT (Maximum 200 words) In this dissertation, long-period Si _{1-x} Ge _x /Si superlattices grown by MBE at 500 °C and annealed post-growth using rapid thermal annealing were investigated using photoluminescence (PL). The as-grown samples have broad PL bands from isoelectronic centers related to Ge complexes as well as sharp near-edge bound exciton lines. The broad PL band was found to be 120 meV below the band gap, after accounting for the effects of confinement of holes. Annealing resulted in a reduction in the broad PL band activation energies and a shift of the broad band to higher energies. The reduction in the activation energies of the broad band were found to be due to the position of the emission centers within the Si _{1-x} Ge _x layers. The emission centers in the middle of the Si _{1-x} Ge _x were deactivated at higher temperatures than those at the edges, which caused the shift of the broad band to lower energies as the sample temperature increased. The shifts of the broad PL band as the annealing temperature increased were found to be due to a net shift of the emission centers towards the interfaces.			
14. SUBJECT TERMS Silicon-Germanium alloys, superlattices, heterostructures, photoluminescence, Si/Ge, semiconductor alloys, optical properties		15. NUMBER OF PAGES 209	
17. SECURITY CLASSIFICATION OF REPORT U		16. PRICE CODE	
18. SECURITY CLASSIFICATION OF THIS PAGE U		19. SECURITY CLASSIFICATION OF ABSTRACT U	
20. LIMITATION OF ABSTRACT SAR			